

G-41-606

GEORGIA INSTITUTE OF TECHNOLOGY
OFFICE OF RESEARCH ADMINISTRATION

Date: 3 February 1970

RESEARCH PROJECT INITIATION

Project Title: Optical Interactions in Solids Relating to Solid State Detectors and Corrosion Control

Project No.: E-2018 (See G-41-606)

Project Director: Dr. James R. Stevenson

Sponsor: Air Force Office of Scientific Research, Arlington, Va.

Agreement Period: From 1 February 1970 until 31 January 1972

Type Agreement: Grant No. AFOSR-70-1832

Amount: \$72,600 AFOSR Funds (E-2018)
 30,599 GIT Contribution (E-2012)
 \$103,199 Total Budget

Project Scientist

Roger J. Austin, Captain USAF
Attention: SRPS
Air Force Office of Scientific Research
1400 Wilson Boulevard
Arlington, Virginia 22209

Reports Required

Publications - As generated
AFOSR Scientific - As generated
Final Scientific - Within thirty
(30) days after completion of
the research.

Assigned to: School of Physics

COPIES TO:

- ☒ Project Director
- ☒ School Director
- ☒ Dean of the College
- ☒ Administrator of Research
- ☒ Associate Controller (2)
- ☒ Security-Reports-Property Office
- ☒ Patent Coordinator

- ☒ Library
- ☒ Rich Electronic Computer Center
- ☒ Photographic Laboratory
- ☐ EES Machine Shop
- ☐ EES Accounting Office

File: E-2018

Other: _____

GEORGIA INSTITUTE OF TECHNOLOGY

OFFICE OF RESEARCH ADMINISTRATION

RESEARCH PROJECT TERMINATION

Date: December 10, 1974

Project Title: **Optical Interactions in Solids Relating to Solid State Detectors and Corrosion Control**

Project No: **G-41-606 (formerly B-2018)**

Principal Investigator: **Dr. J. R. Stevenson**

Sponsor: **Air Force Office of Scientific Research ; Arlington, Va.**

Effective Termination Date: 9-30-74 (Grant Expiration)

Clearance of Accounting Charges: 9-30-74

Grant Closeout Actions Remaining: **Final Fiscal Report**
Final Patent Report

NOTE: Companion account is G-41-632

Assigned to School of Physics

COPIES TO:

Principal Investigator
School Director
Dean of the College
Director of Research Administration
Associate Controller (2)
Security-Reports-Property Office ✓
Patent and Inventions Coordinator

Library, Technical Reports Section
Rich Electronic Computer Center
Photographic Laboratory
Terminated Project File No. _____
Other _____

Interim Scientific Report

Optical Interactions in Solids Relating to
Solid State Detectors and Corrosion Control

James R. Stevenson

May 8, 1973

Grant No. AFOSR 70-1892

This research was supported by the Air Force Office of Scientific Research (AFSC) under grant No. AFOSR 70-1892.

Approved for public release; distribution unlimited.

Qualified requestors may obtain additional copies from the Defense Documentation Center. All others should apply to the Clearinghouse for Federal Scientific and Technical Information.

OBJECTIVES

The purpose of the research is a study of optical interactions in solids and related physical properties of solid surfaces. Particular emphasis in the study is being given to some complex tertiary semiconductor alloy systems. Although complex in nature, evidence exists for believing the semiconductor alloys will have important device applications in the future e.g. the variation in band gap with alloy composition. The research concentrates on the determination and analysis of data related to surface characterization such as that obtained from optical reflectivity and auger spectroscopy. The techniques and data are directly related to factors contributing to an understanding of surface stability and corrosion control in semiconductor devices. Synchrotron radiation from the electron storage ring at the Physical Sciences Laboratory of the University of Wisconsin is utilized to provide a continuum source in a compatible high vacuum environment. In addition the infrared characteristics of existing of proposed synchrotron radiation sources are being investigated as possible infrared sources for application to infrared solid state spectroscopy.

ACHIEVEMENTS

A. Equipment and Technique Development

A necessary prerequisite to the current research was a parallel development of equipment and techniques beyond the state of the art at the time of the initiation of the research. The combination of the use of synchrotron radiation with well characterized surfaces imposed severe vacuum constraints

on the system. An ion pumped sample chamber is shown in the drawing in Figure 1. The sample chamber can be operated in the 10^{-10} to 10^{-11} torr range which is necessary for Auger spectroscopy and at the same time includes the necessary elements to measure optical reflectivity. The sample chamber developed at Georgia Tech represents the first time a system combines these measurements for in situ determination.

Figure 2 shows a block diagram of the electronics associated with the optical measurements using the synchrotron radiation source. As noted in the block diagram the experiment is controlled by a PDP-12 computer. Although the PDP-12 computer is part of the University of Wisconsin PSL, the Georgia Tech group has made significant contributions to the development of soft-wave both for our use as well as other users. The contributions of Dr. Wrege of Georgia Tech as a consultant on soft-wave development accelerated the effective utilization of the computer.

Other techniques relating to data handling and sample preparation have also been developed and are being described in two Ph.D. theses under preparation.

B. Infrared Properties of Synchrotron Radiation

For the first time the characteristics of synchrotron radiation in the infrared have been experimentally investigated. These experiments were done at the electron storage ring of the University of Wisconsin using a NaCl prism monochromator. The experiments confirmed our theoretical estimates of the importance of proposed storage rings as continuum sources in the far-infrared. A paper has been submitted for publication and a report was made to the American Physical Society at San Diego. The paper presented at San Diego was one of

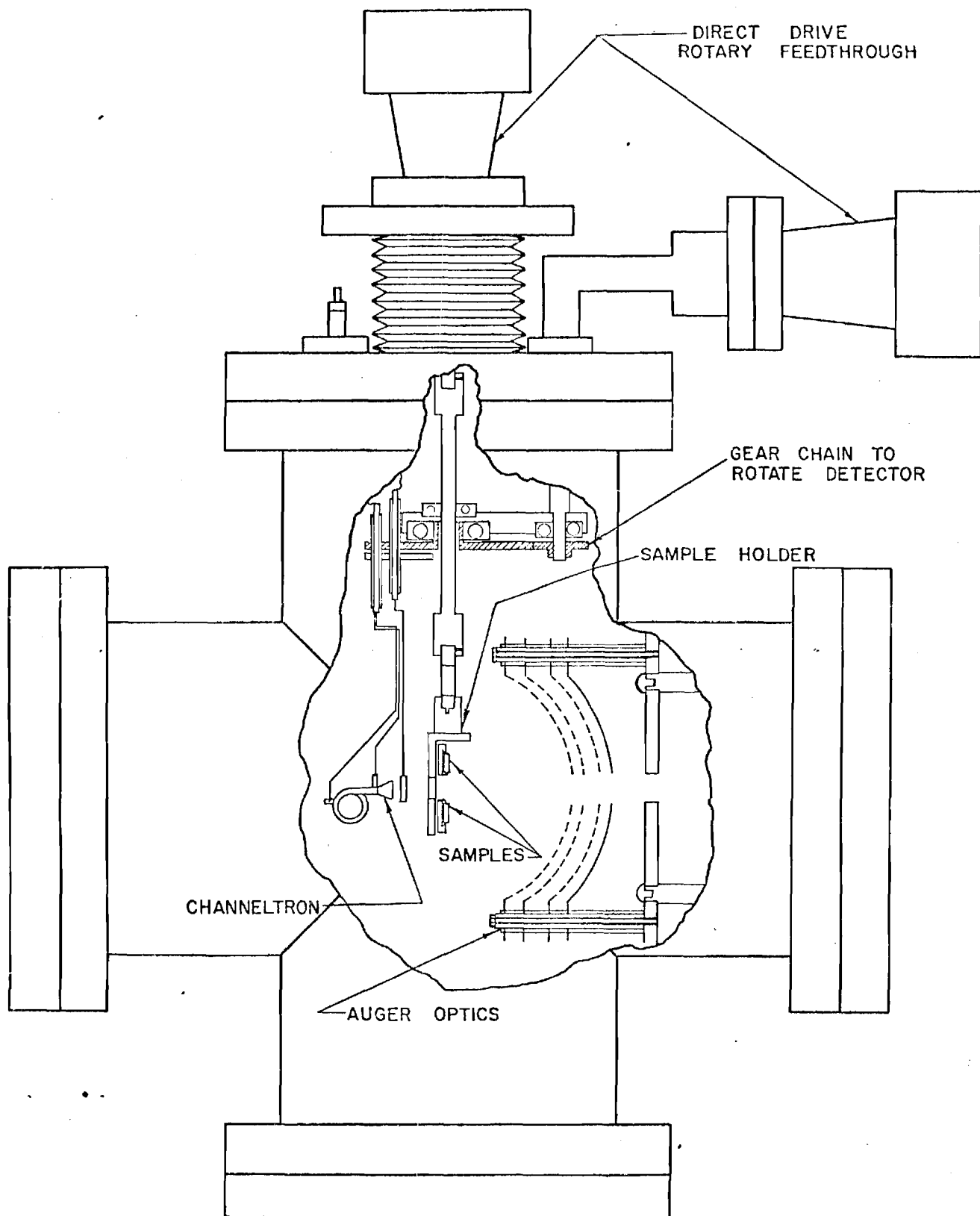


Figure 1. Ultra High Vacuum Sample Chamber for Optical Reflectivity and Auger Spectroscopy Studies.

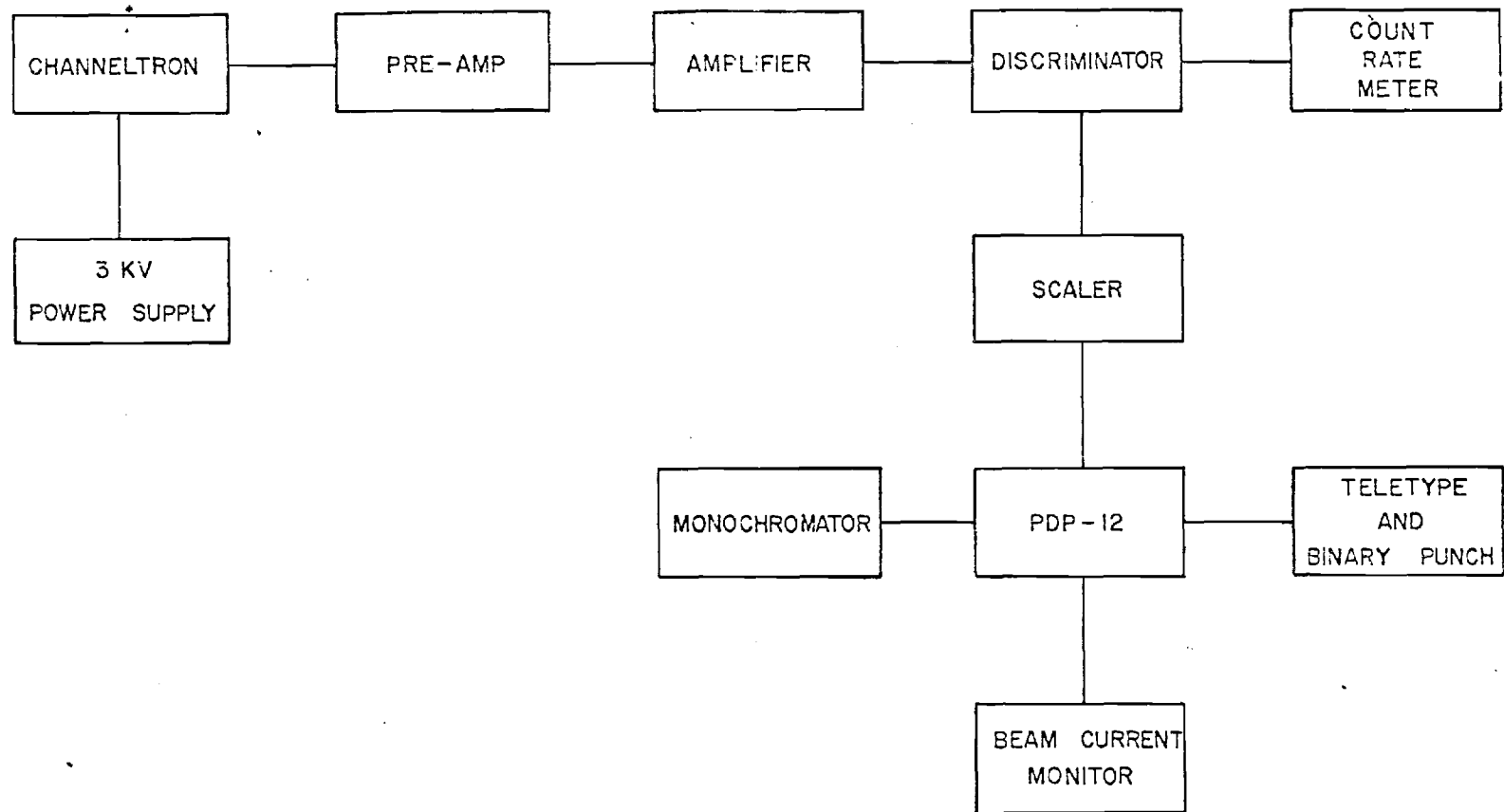


Figure 2. Block Diagram of Electronics Used for Optical Reflectivity Studies at the University of Wisconsin Electron Storage Ring.

a few selected for a press release to the news media. A copy of the press release from the American Institute of Physics is included as Appendix A of this report.

C. Tertiary Semiconductor Alloy Systems

Optical reflectivity data have been obtained on both the $\text{Cd}_x\text{Zn}_{3-x}\text{As}_2$ and the $\text{Cd}_3\text{P}_x\text{As}_{2-x}$ systems. These data cover the wavelength region from 15 microns in the near infrared to 300 Angstroms in the vacuum ultraviolet. Limited Auger spectroscopy data are now available on the $\text{Cd}_x\text{Zn}_{3-x}\text{As}_2$ system. The results of these investigations are currently being analyzed in terms of the theoretically calculated band structure and will be presented in two Ph.D. theses as well as several papers to scientific journals.

PROFESSIONAL PERSONNEL

The following individuals have participated in the research described above.

1. Dr. James R. Stevenson	-	Principal Investigator
2. Dr. Roger Bartlett	-	Postdoctoral Research Associate
3. Mr. Maury Zivitz	-	Graduate Research Assistant
4. Mr. Harry Ellis	-	Graduate Research Assistant
5. Mr. Abdol Gholamnezhad	-	Graduate Research Assistant
6. Mr. Stephen Zehner	-	Graduate Research Assistant
7. Dr. Douglas Wrege	-	Computer Consultant
8. Dr. L. N. Tharp	-	Auger Spectroscopy Consultant
9. Mr. James House	-	Electronics Technician

PAPERS PRESENTED

1. "Visible and Vacuum Ultraviolet Reflectance Study of the Semiconductor Alloy System $\text{Cd}_{3-x}\text{Zn}_x\text{As}_2$," Bull. Am. Phys. Soc. 15, 1343 (1970).
2. "Optical Reflectivity Studies in the Vacuum Ultraviolet," Synchrotron Radiation Users Meeting, Physical Sciences Laboratory, University of Wisconsin, Stoughton, Wisconsin, November 19, 1970.

3. "Infrared Reflectance Study of the Semiconductor Alloy System $\text{Cd}_{3-x}\text{Zn}_x\text{As}_2$," Bull. Am. Phys. Soc. 15, 1343 (1970).
4. "Auger Spectroscopy and Optical Reflectivity of the $\text{Cd}_{3-x}\text{Zn}_x\text{As}_2$ System," Synchrotron Radiation Users Meeting, Physical Sciences Laboratory, University of Wisconsin, Stoughton, Wisconsin, November 29, 1971.
5. "Reflectivity of $\text{Cd}_x\text{Zn}_{3-x}\text{As}_2$ Semiconductor Alloy Systems," Conference Digest - 3rd International Conference on Vacuum Ultraviolet Physics, Tokyo, Japan (1971).
6. "Ultrahigh Vacuum Reflectometer", Bull. Am. Phys. Soc. 17, 193 (1972).
7. "Optical Properties of $\text{Cd}_x\text{Zn}_{3-x}\text{As}_2$," Seminar - Group F41 - DESY, Hamburg, W. Germany, August 10, 1972.
8. "A Preliminary Study of the Utility of Synchrotron Radiation for Studies in the Infrared", Physical Sciences Laboratory, University of Wisconsin, Stoughton, Wisconsin, November 27, 1972.
9. "Synchrotron Radiation as a Spectroscopy Source in the Infrared," Bull. Am. Phys. Soc. 18, 464 (1973).

PAPERS PUBLISHED

1. James R. Stevenson, Maury Zivitz, Harry Ellis and Roger J. Bartlett, "Reflectivity of $\text{Cd}_x\text{Zn}_{3-x}\text{As}_2$ Semiconductor Alloy Systems," Conference Digest - 3rd International Conference on Vacuum Ultraviolet Physics, Tokyo, Japan (1971).

SUBMITTED FOR PUBLICATION

1. H. W. Ellis, R. J. Bartlett and J. R. Stevenson, "Vacuum Ultraviolet Spectroscopy of Solids Using Synchrotron Radiation with Auger Analysis of Sample Surface".

2. James R. Stevenson, H. W. Ellis and R. J. Bartlett, "Synchrotron Radiation as an Infrared Source".

PH.D. THESES IN PREPARATION

1. M. Zivitz, "The Optical Properties of the $\text{Cd}_{3-x}\text{As}_2\text{P}_x$ Alloy System".
2. H. Ellis, "Extreme Vacuum Ultraviolet and Auger Spectroscopic Surface Studies of the $\text{Cd}_{3-x}\text{Zn}_x\text{As}_2$ Alloy System".

RESEARCH GROUP INTERACTIONS

1. Physical Sciences Laboratory, University of Wisconsin, Madison, Wisconsin.
2. Solid State Division, U. S. Naval Research Laboratory, Washington, D.C.
3. F-41 Group, DESY, Hamburg, W. Germany.
4. T. C. Collins, Wright Patterson Air Force Base, Dayton, Ohio.
5. F. C. Brown, Physics Department, University of Illinois.
6. G. J. Lapeyre, Physics Department, Montana State University.
7. D. W. Lynch, Physics Department, Iowa State University.
8. E. T. Arakawa, Health Physics Division, Oak Ridge National Laboratory.

APPENDIX A



AUDREY ARMSTRONG
Director, Press Relations

NEWS FROM THE AMERICAN INSTITUTE OF PHYSICS
335 EAST 45 STREET, NEW YORK 10017 (212) 685-1940

FROM: PRESS ROOM, MARCH MEETING
THE AMERICAN PHYSICAL SOCIETY

Town and Country Hotel
San Diego, California
Telephone: (714) 291-7131
Meeting Dates: March 19-22, 1973

RELEASED FOR FRIDAY MORNING, MARCH 23, 1973

Authors' Popular Version of Paper: HE-1

"SYNCHROTRON RADIATION AS A
SPECTROSCOPY SOURCE IN THE INFRARED"

Presented by: H.W. Ellis, R.J. Bartlett, and J.R. Stevenson
School of Physics
Georgia Institute of Technology
.. Atlanta, Georgia 30332

A Giant Lightbulb

Between radio waves and visible light is the infrared region. Scientists have bridged this gap for a number of years but strong continuous sources of light have not been found.

Recently a group of physicists headed by Prof. James Stevenson at Georgia Tech has demonstrated the availability of a strong continuous source as a by-product of electron and positron storage rings. These facilities are being built in various sections of the world by experimental high energy physicists for a different purpose. The machines are in the shape of a tube bent into a circle, and while some could be squeezed into a good-sized living room, others would crowd the fences at a major league baseball park.

The ring is evacuated and then electrons or positrons are injected.

Electrons are the negatively charged particles giving rise to the chemical properties of atoms, and from a more realistic set of values, the electron beam as it scans the face of a TV picture tube leaves the transmitted studio image in its wake.

Positrons are more rare but are frequent products of nuclear radioactive decay. Although similar to electrons they have a positive charge.

By the use of proper size magnets, these electrons or positrons can be bent into a circle having the same diameter as the storage ring tube. If the vacuum is very good, the electrons or positrons will continue to circulate for a long time and hence the name storage ring.

These circulating charged particles give off light (synchrotron radiation in the scientific vernacular). Scientists have used this fact to exploit regions of the ultraviolet, or "blacklight", but no effort has been made to utilize the facilities as a giant infrared light bulb.

The group at Georgia Tech, working with a grant from the Air Force Office of Scientific Research, used some theoretical calculations published in 1949 by an eminent physicist, Julian Schwinger. The analysis of these results, with a knowledge of present day technology, showed the feasibility of using the infrared radiation. On the basis of this analysis, they were able to design an experiment and then demonstrate the effect at the electron storage ring located at the University of Wisconsin.

Although not many facilities in operation today are brilliant infrared sources, some of the ones under construction should be quite intense infrared light bulbs. Applications of infrared light to scientific investigations are of importance in providing information on the structure of molecules and the properties of solids. Laser research as well as the chemical and electronics industry continue to benefit from data gathered using available infrared sources. The future availability of new continuous infrared sources should provide a valuable scientific tool for these and possibly other new investigations.

Source of information:

Abstract of a talk (HE-1) to be presented at the March meeting of the American Physical Society in San Diego, California.

"Synchrotron Radiation as a Spectroscopy Source in the Infrared"

H. W. Ellis, R. J. Bartlett, and J. R. Stevenson

School of Physics, Georgia Institute of Technology, Atlanta, Georgia 30332.

Interim Scientific Report

Optical Interactions in Solids Relating to
Solid State Detectors and Corrosion Control

James R. Stevenson

January 23, 1974

Grant No. AFOSR 70-1892

This research was supported by the Air Force Office of Scientific Research (AFSC) under grant No. AFOSR 70-1892.

Approved for public release; distribution unlimited.

Qualified requestors may obtain additional copies from the Defense Documentation center. All others should apply to the Clearinghouse for Federal Scientific and Technical Information.

OBJECTIVES

The purpose of the research is a study of optical interactions in solids and related physical properties of solid surfaces. Particular emphasis in the study is being given to some complex tertiary semiconductor alloy systems. Although complex in nature, evidence exists for believing the semiconductor alloys will have important device applications in the future e.g. the variation in band gap with alloy composition. The research concentrates on the determination and analysis of data related to surface characterization such as that obtained from optical reflectivity and auger spectroscopy. The techniques and data are directly related to factors contributing to an understanding of surface stability and corrosion control in semiconductor devices. Synchrotron radiation from the electron storage ring at the Physical Sciences Laboratory of the University of Wisconsin is utilized to provide a continuum source in a compatible high vacuum environment. In addition the infrared characteristics of existing and proposed synchrotron radiation sources have been investigated as possible infrared sources for application to infrared solid state spectroscopy.

ACHIEVEMENTS

1. An exhaustive study of the optical properties of the $\text{Cd}_{\frac{1}{3}}\text{As}_{\frac{2}{3}}\text{-Cd}_{\frac{1}{3}}\text{P}_{\frac{2}{3}}$ alloy system has been completed in the form of a PhD thesis by Dr. Maury Zivitz. The thesis is appended as a part of this report (Appendix A) and additional comments on this phase of the work will not be made. The thesis is available as a report of the School of Physics of Georgia Institute of Technology.
2. A supplement to the recently published paper "Synchrotron Radiation as an Infrared Source" has been prepared and is also appended (Appendix B) to this report. The supplement is entitled "Computer Calculations and

Numerical Tabulations of Some MacDonald Functions". Tabulations of these functions are not available in the current literature. This supplement is also available as a report of the School of Physics of Georgia Institute of Technology.

3. Dr. John Carden, a physical chemist, has joined our research effort and is concentrating on the Auger spectroscopy for surface characterization. During the Fall of 1973, Dr. Carden and Dr. Stevenson spent four weeks at the storage ring facility in Stoughton, Wisconsin. Both optical and Auger data were obtained on semiconductor alloys. In addition the surfaces were etched by argon bombardment and the effects of this bombardment on both Auger and optical reflectivity were measured. The data is being analyzed at this time.
4. Mr. Harry Ellis has completed the experimental work for his PhD thesis and is currently writing the final draft. Of particular significance is his computer analysis concerning the reliability of optical data generated from Kramers-Kronig analysis. Mr. Ellis has used an analytically described classical model to investigate the effect of high energy extrapolations of reflectivity data. The convergence of sum rules and the effects on peak height have been investigated. The results show the need for measurements in the vacuum ultraviolet.

CURRENT STATUS

1. The results of our research as well as other investigators indicate that surface characterization is essential for the generation of good reliable optical data. We plan to use magnesium metal and magnesium oxide as a control system in the evaluation of Auger spectroscopy a tool for characterization of an optical surface.

2. Our work on semiconductor alloys will continue with plans for attempting flash evaporations to obtain thin films for both reflection and transmission measurements.

PROFESSIONAL PERSONNEL

The following individuals have participated in the research described above.

- | | | |
|---------------------------|---|--|
| 1. Dr. James R. Stevenson | - | Principal Investigator |
| 2. Dr. Roger Bartlett | - | Postdoctoral Research Associate |
| 3. Mr. Maury Zivitz | - | Graduate Research Assistant |
| 4. Mr. Harry Ellis | - | Graduate Research Assistant |
| 5. Mr. Abdol Gholamnezhad | - | Graduate Research Assistant |
| 6. Mr. Stephen Zehner | - | Graduate Research Assistant |
| 7. Dr. Douglas Wrege | - | Computer Consultant |
| 8. Dr. L. N. Tharp | - | Auger Spectroscopy Consultant |
| 9. Mr. James House | - | Electronics Technician |
| 10. Dr. John Carden | - | Auger Spectroscopy Consultant and Research Scientist |

PAPERS PRESENTED

1. "Visible and Vacuum Ultraviolet Reflectance Study of the Semiconductor Alloy System $\text{Cd}_{3-x}\text{Zn}_x\text{As}_2$," Bull. Am. Phys. Soc. 15, 1343 (1970).
2. "Optical Reflectivity Studies in the Vacuum Ultraviolet." Synchrotron Radiation Users Meeting, Physical Sciences Laboratory, University of Wisconsin, Stoughton, Wisconsin, November 19, 1970.
3. "Infrared Reflectance Study of the Semiconductor Alloy System $\text{Cd}_{3-x}\text{Zn}_x\text{As}_2$," Bull. Am. Phys. Soc. 15, 1343 (1970).
4. "Auger Spectroscopy and Optical Reflectivity of the $\text{Cd}_{3-x}\text{Zn}_x\text{As}_2$ System," Synchrotron Radiation Users Meeting, Physical Sciences Laboratory, University of Wisconsin, Stoughton, Wisconsin, November 29, 1971
5. "Reflectivity of $\text{Cd}_x\text{Zn}_{3-x}\text{As}_2$ Semiconductor Alloy Systems," Conference Digest - 3rd. International Conference on Vacuum Ultraviolet Physics, Tokyo, Japan (1971).
6. "Ultrahigh Vacuum Reflectometer", Bull. Am. Phys. Soc. 17, 193 (1972).

7. "Optical Properties of $\text{Cd}_{1-x}\text{Zn}_x\text{As}_2$," Seminar - Group F41 - DESY, Hamburg, W. Germany, August 10, 1972.
8. "A Preliminary Study of the Utility of Synchrotron Radiation for Studies in the Infrared", Physical Sciences Laboratory, University of Wisconsin, Stoughton, Wisconsin, November 27, 1972.
9. "Synchrotron Radiation as a Spectroscopy Source in the Infrared," Bull. Am. Phys. Soc. 18, 464 (1973).
10. "The Optical Properties of Cd_3As_2 - Cd_3P_2 Alloy Systems," Sixth Annual Synchrotron Radiation Users Group Conference - Physical Sciences Laboratory - University of Wisconsin, October 22, 1973.
11. "Use of Synchrotron Radiation for Optical Excitation of Solids," Seminar - Georgia State University, November 26, 1973.

PAPERS PUBLISHED

1. James R. Stevenson, Maury Zivitz, Harry Ellis and Roger J. Bartlett, "Reflectivity of $\text{Cd}_{1-x}\text{Zn}_x\text{As}_2$ Semiconductor Alloy Systems," Conference Digest - 3rd International Conference on Vacuum Ultraviolet Physics, Tokyo, Japan (1971).
2. "Synchrotron Radiation as an Infrared Source," with H. Ellis and Roger Bartlett, Applied Optics 12, 2884 (1973).
3. "Computer Calculations and Numerical Tabulations of Some MacDonald Functions as a Supplement to "Synchrotron Radiation as an Infrared Source" with H. Ellis, A Report of the School of Physics Georgia Institute of Technology (1973).

SUBMITTED FOR PUBLICATION

"Optical Properties of the Cd_3As_2 - Cd_3P_2 Semiconductor Alloy System", with M. Zivitz.

PH.D. THESIS

M. Zivitz, "The Optical Properties of the $\text{Cd}_{3-x}\text{As}_2\text{P}_x$ Alloy System", (1973).

PH.D. THESIS IN PREPARATION

H. Ellis, "Extreme Vacuum Ultraviolet and Auger Spectroscopic Surface Studies of the $\text{Cd}_{3-x}\text{Zn}_x\text{As}_2$ Alloy System".

RESEARCH GROUP INTERACTIONS

1. Physical Sciences Laboratory, University of Wisconsin, Madison, Wisconsin.
2. Solid State Division, U. S. Naval Research Laboratory, Washington, D.C.
3. F-41 Group, DESY, Hamburg, W. Germany.
4. T. C. Collins, Wright Patterson Air Force Base, Dayton, Ohio.
5. F. C. Brown Physics Department, University of Illinois.
6. G. J. Lapeyre, Physics Department, Montana State University.
7. D. W. Lynch, Physics Department, Iowa State University.
8. E. T. Arakawa, Health Physics Division, Oak Ridge National Laboratory.
9. T. F. Connally, Research Material Information Center, Oak Ridge National Laboratory.

**Computer Calculations and Numerical Tabulations of Some MacDonald Functions
as a Supplement to "Synchrotron Radiation as an Infrared Source"**

**H. Ellis and J. R. Stevenson
School of Physics
Georgia Institute of Technology
Atlanta, Georgia 30332**

Appendix B
Interim Scientific Report -
James R. Stevenson
Grant No. AFOSR 70-1892
January 23, 1974



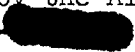
**This research sponsored by the Air Force Office of Scientific Research, under
AFOSR grant number AFOSR-██████████**

70-1892

Computer Calculations and Numerical Tabulations of Some MacDonald Functions
as a Supplement to "Synchrotron Radiation as an Infrared Source"

H. Ellis and J. R. Stevenson

School of Physics, Georgia Institute of Technology, Atlanta, Georgia 30332

This research sponsored by the Air Force Office of Scientific Research, under
AFOSR grant number AFOSR-

70-1892

INTRODUCTION

The authors⁽¹⁾ have made a theoretical and experimental investigation into the nature of infrared radiation emitted by an electron moving in a magnetic field. The distribution of the intensity over wavelength is dependent on the environmental parameter λ_c , the critical wavelength, which is defined in terms of the electron energy E and the orbital radius R :

$$\lambda_c = \frac{2\pi c}{\omega_c} \quad \omega_c = \frac{3c}{2R} \left(\frac{E}{m_0 c^2} \right)^3$$

An expression for the power radiated per unit wavelength and integrated over all angular dependence is⁽²⁾

$$P(\lambda) = F(E, R) \eta^3 \int_{\eta}^{\infty} K_{5/3}(x) dx \quad \eta = \frac{\lambda_c}{\lambda}$$

where F is a function independent of λ . The wavelength-dependent part is, then

$$G(\eta) = \eta^3 \int_{\eta}^{\infty} K_{5/3}(x) dx$$

The geometrical nature of the radiation was also of interest. The distribution of intensity per unit frequency in an angle θ measured from the plane of the electron orbit is

$$\frac{dI(\omega)}{d\Omega} = F'(E, R) \left(\frac{1}{\gamma^2} + \theta^2 \right)^2 \left\{ K_{2/3}^2(\xi) + \frac{\theta^2}{\frac{1}{\gamma^2} + \theta^2} K_{1/3}^2(\xi) \right\}$$

where

$$\xi = \frac{\omega R}{3c} \left(\frac{1}{\gamma^2} + \theta^2 \right)^{3/2}$$

$$\gamma = \frac{E}{m_0 c^2}$$

and F' is a function independent of θ . The two terms represent radiation which is plane-polarized (parallel and perpendicular respectively) relative to the electron orbital plane.

Of particular interest to us was a knowledge of the radiation characteristics at long wavelengths, $\lambda \gg \lambda_c$. Thus $G(\eta)$ was required for $\eta \ll 1$, and $dI(\omega)/d\Omega$ was required for small values of ξ , as well as larger values (as the angle θ was increased from zero until $dI/d\Omega$ was vanishingly small).

MacDonald Functions

The desire for numerical results moved us to a study of the functions denoted by $K_{1/3}$, $K_{2/3}$, $K_{5/3}$, etc. The functions $K_\mu(x)$ are defined by MacDonald for unrestricted values of μ , and are thus called "MacDonald" functions⁽³⁾. They are defined in terms of Bessel functions of imaginary argument $I_\mu(x)$ via

$$K_\mu(x) \equiv \frac{\pi}{2} \frac{I_{-\mu}(x) - I_\mu(x)}{\sin(\pi\mu)} \quad (1)$$

where

$$I_{\mu}(x) = \sum_{m=0}^{\infty} \frac{(x/2)^{\mu + 2m}}{m! \Gamma(\mu + m + 1)}$$

For asymptotic values of the argument, the MacDonald function may be approximated by well-known function:

$$x \gg 1 \quad K_{\mu}(x) = \sqrt{\frac{\pi}{2}} \sqrt{x} e^{-x}$$

$$x \ll 1 \quad K_{\mu}(x) = 2^{\mu - 1} \Gamma(\mu) x^{-\mu}$$

A search through mathematical tables showed that the integer-order and half-integer order MacDonald function are well tabulated. For the third-order functions, however, only one table was found. that of $K_{1/3}(x)$ for increments of 0.02 to an upper limit of 16.00⁽³⁾. The third-order functions are closely related to Airy functions, which are well-tabulated, and a short hand calculation will yield the value of $K_{1/3}(x)$ for a particular value of x . Nevertheless, we feel that the lack of tables of MacDonald function of one-third order presents a difficulty for the researcher who wishes to quickly find values for hand calculations. The person using an asymptotic approximation generally wishes to know the accuracy of the approximation and over what range of argument it has validity.

In the course of our investigation, computer programs were written which calculate these functions. For large arguments, it was found that the BESK subroutine in the MATHPACK⁽⁴⁾ series calculates $K_{\mu}(x)$ correct to six places via

$$e^x K_\mu(x) = \int_0^\infty \exp [x(1 - \cosh y)] \cosh (\mu y) dy \quad (2)$$

Using a Simpson Rule integration procedure with $\Delta y = 0.2$. Obviously this procedure is not valid for arguments small compared to 0.2. A second subroutine was written which employed equation (1), and was called instead of BESK for small arguments.

With the increasing interest in synchrotron radiation as a source of light for spectroscopy, we think it worthwhile to make available tabulated results of these calculations.

The MacDonald functions are "even" in the order, i.e.

$$K_{-\mu}(x) = K_\mu(x). \quad (3)$$

In addition, there exists a recurrence relation

$$K_{\mu-1}(x) - K_{\mu+1}(x) = -\frac{2\mu}{x} K_\mu(x) \quad (4)$$

Thus a knowledge of $K_{1/3}(x)$ and $K_{2/3}(x)$ is sufficient to find all third-order function $K_\mu(x)$. For example

$$K_{4/3}(x) = \frac{2(1/3)}{x} K_{1/3}(x) + K_{-2/3}(x) = \frac{2}{3x} K_{1/3}(x) + K_{2/3}(x)$$

$$K_{5/3}(x) = \frac{2(2/3)}{x} K_{2/3}(x) + K_{-1/3}(x) = \frac{4}{3x} K_{2/3}(x) + K_{1/3}(x)$$

etc.

The following tables contain $K_{1/3}(x)$, $K_{2/3}(x)$, $K_{5/3}(x)$ and $G(x)$, where $G(x) = x^3 \int_x^{40.0} K_{5/3}(y) dy$. The values for $K_{1/3}$, $K_{2/3}$ and $K_{5/3}$ may be inaccurate in the last digit. The integration procedure for G was a Simpson Rule program. The computer programs used to generate the tables are given on the following pages.

C / THIS PROGRAM GENERATES ITS OWN INPUT. IT PRODUCES VALUES
C / OF THE INTEGRAL OF $K5/3(X)$ FROM A LOWER LIMIT Y TO THE UPPER
C / LIMIT OF 40.0, WHICH IS NAMED GS. IT ALSO PRINTS OUT
C / THE PRODUCT OF THIS INTEGRAL TIMES $Y^{**3.0}$, NAMED GT.
C /

C / OUTPUT FILE NAME: GINTANS.....COLUMNS Y,GS,GT

```

      IMPLICIT DOUBLE PRECISION (F-G)
      DIMENSION G(6000), T(6000)
101  FORMAT(2X,F7.3,2X,2(1PE15.6))
      FP=0.0
      DEL=0.100
      U=9.900
40   U=U+DEL
      V=U+DEL
      W=(U+V)*0.5
      GR=(DEL/6.0)*(B(U)+4.0*B(W)+B(V))
      FP=FP+GR
      IF((40.0-U).GT.0.001) GO TO 40
      G(0)=0.0
      D=0.001
      DO 77 J=1,999
      T(J)=0.001*J
      X=T(J)
      Z=X+D
      Y=(X+Z)*0.5
      IF(X.LT.0.15) F1=A(X)
      IF(X.GE.0.15) F1=B(X)
      IF(Y.LT.0.15) F2=A(Y)
      IF(Y.GE.0.15) F2=B(Y)
      IF(Z.LT.0.15) F3=A(Z)
      IF(Z.GE.0.15) F3=B(Z)
      F=(F1+4.0*F2+F3)*(D/6.0)
      G(J)=G(J-1)+F
77   CONTINUE
      D=0.005
      DO 88 J=1000,1799
      T(J)=-4.000+0.005*J
      X=T(J)
      Z=X+D
      Y=(X+Z)/2.0
      IF(X.LT.0.15) F1=A(X)
      IF(X.GE.0.15) F1=B(X)
      IF(Y.LT.0.15) F2=A(Y)
      IF(Y.GE.0.15) F2=B(Y)
      IF(Z.LT.0.15) F3=A(Z)
      IF(Z.GE.0.15) F3=B(Z)
      F=(F1+4.0*F2+F3)*(D/6.0)
      G(J)=G(J-1)+F
88   CONTINUE
      D=0.01
      DO 55 J=1800,2300
      T(J)=-13.000+0.010*J
      X=T(J)
      Z=X+D
      Y=(X+Z)/2.0
      IF(X.LT.0.15) F1=A(X)
      IF(X.GE.0.15) F1=B(X)
      IF(Y.LT.0.15) F2=A(Y)
      IF(Y.GE.0.15) F2=B(Y)
      IF(Z.LT.0.15) F3=A(Z)
      IF(Z.GE.0.15) F3=B(Z)
      F=(F1+4.0*F2+F3)*(D/6.0)
      G(J)=G(J-1)+F
55   CONTINUE
      GP=G(2299)+FP
      DO 99 K=1,2300
      GS=GP-G(K-1)
      S=T(K)
      GT=GS*(S**3.0)
      WRITE(9,101) S,GS,GT
99   CONTINUE
      STOP
      END

```

SCAN: 73

E0F: 73

0: GINT.CAL 03 APRIL 1973

```

C / THIS FUNCTION CALCULATES  $K_{1/3}(X)$  WHEN CALLED, FROM THE
C / MACDONALD DEFINING RELATION:
C /
C /  $K_{1/3}(X) = (PI/2) * (I(-1/3)(X) - I_{1/3}(X)) / SIN(PI/3)$ 
C /
      FUNCTION A1(X)
      ORDER=1.0/3.0
      G1=2.6789385
      G2=1.3541179
      PI=3.1415927
      ARG=PI*ORDER
      COEF=(0.5*PI)/SIN(ARG)
      Z=X/2.0
      YNEG=Z**(-ORDER)
      YPOS=Z**(ORDER)
      OUTNEG=YNEG/G2
      OUTPOS=YPOS/((1.0/3.0)*G1)
C THE FOLLOWING COMPUTES  $I(-1/3)$ 
      TERMN=1.0
      SUMNEG=1.0
      DO 22 K=1,20
      TERMN=(3.0)*(Z**2.0)/(K*((3.0)*K-(1.0)))*TERMN
      SUMNEG=SUMNEG+TERMN
      FIRST=OUTNEG*SUMNEG
      22 CONTINUE
C THE FOLLOWING COMPUTES  $I(+1/3)$ 
      TERMP=1.0
      SUMPOS=1.0
      DO 33 J=1,20
      TERMP=(3.0)*(Z**2.0)/(J*((3.0)*J+(1.0)))*TERMP
      SUMPOS=SUMPOS+TERMP
      SECOND=OUTPOS*SUMPOS
      33 CONTINUE
      A1=COEF*(FIRST-SECOND)
      END
SCAN:35
EOF:35
0:      TABL1.A1      03 APRIL 1973

```

```

C / THIS FUNCTION CALCULATES  $K_{2/3}(X)$  WHEN CALLED, FROM THE
C / MACDONALD DEFINING RELATION:
C /
C /  $K_{2/3}(X) = (\pi/2) * (I(-2/3)(X) - I_{2/3}(X)) / \sin(2\pi/3)$ 
C /
      FUNCTION A2(X)
      ORDER=2.0/3.0
      G1=2.6789385
      G2=1.3541179
      PI=3.1415927
      ARG=PI*ORDER
      COEF=(0.5*PI)/SIN(ARG)
      Z=X/2.0
      YNEG=Z**(-ORDER)
      YPOS=Z**(ORDER)
      OUTNEG=YNEG/G1
      OUTPOS=YPOS/((2.0/3.0)*G2)
C THE FOLLOWING COMPUTES  $I(-2/3)$ 
      TERMN=1.0
      SUMNEG=1.0
      DO 22 K=1,20
      TERMN=(3.0)*(Z**2.0)/(K*((3.0)*K-(2.0)))*TERMN
      SUMNEG=SUMNEG+TERMN
      FIRST=OUTNEG*SUMNEG
      22 CONTINUE
C THE FOLLOWING COMPUTES  $I(+2/3)$ 
      TERMP=1.0
      SUMP0S=1.0
      DO 33 J=1,20
      TERMP=(3.0)*(Z**2.0)/(J*((3.0)*J+(2.0)))*TERMP
      SUMP0S=SUMP0S+TERMP
      SEC0ND=OUTPOS*SUMP0S
      33 CONTINUE
      A2=COEF*(FIRST-SEC0ND)
      END
SCAN:35
EOF:35
0:      TABL2.A2      03 APRIL 1973

```



```

C / THIS FUNCTION CALCULATES K5/3(X) WHEN CALLED, FROM THE
C / MACDONALD DEFINING RELATION:
C /
C /    $K_{5/3}(X) = (\pi/2) * (I_{-5/3}(X) - I_{5/3}(X)) / \sin(5\pi/3)$ 
C /
      FUNCTION A(X)
      ORDER=5.0/3.0
      G1=2.6789385
      G2=1.3541179
      PI=3.14159
      ARG=PI*ORDER
      COEF=(0.5)*PI/SIN(ARG)
      Z=X/2.0
      YNEG=Z**(-ORDER)
      YPOS=Z**(ORDER)
      OUTNEG=YNEG/G1
      OUTPOS=YPOS*(0.9)/G2
C THE FOLLOWING COMPUTES I(-5/3)
      TERMN=Z**(2.0)
      SUMNEG=(-2.0/3.0)+TERMN
      DO 66 K=1,25
      TERMN=((3.0*(Z**2.0))/((K+1.0)*(3.0*K-2.0)))*TERMN
      SUMNEG=SUMNEG+TERMN
      BOSS=OUTNEG*SUMNEG
      66 CONTINUE
C THE FOLLOWING COMPUTES I(+5/3)
      TERMP=1.0
      SUMP0S=1.0
      DO 55 J=2,25
      TERMP=((3.0*(Z**2.0))/((J-1.0)*(3.0*J+2.0)))*TERMP
      SUMP0S=SUMP0S+TERMP
      H0SS=OUTPOS*SUMP0S
      55 CONTINUE
      A=COEF*(BOSS-H0SS)
      11 CONTINUE
      END
SCAN:36
EOF:36
01      SUPER.A      03 APRIL 1973

```

```

C / THIS PROGRAM READS THE OUTPUT OF GINT. AS INPUT. IT THEN
C / PRODUCES A TABLE CONSISTING OF Y,K1/3(Y),K2/3(Y),K5/3(Y),AND
C / GT (FROM GINTANS.), THE INTEGRAL OF K5/3(X) FROM Y TO 40.0
C / MULTIPLIED BY Y**3.0.
101 FORMAT(2X,F7.3,4(1PE15.6))
102 FORMAT(1H0)
103 FORMAT(1H1,4X,'X',9X,'K1/3(X)',9X,'K2/3(X)',9X,'K5/3(X)',10X,'G')
104 FORMAT(2X,F7.3,2X,2(1PE15.6))
  WRITE(6,103)
  WRITE(6,102)
  DO 2 J=1,2300
    READ(9,104) X,GS,GT
    IF(X.LE.0.15) Z=A1(X)
    IF(X.GT.0.15) Z=B1(X)
    IF(X.LE.0.15) T=A2(X)
    IF(X.GT.0.15) T=B2(X)
    IF(X.LE.0.15) S=A(X)
    IF(X.GT.0.15) S=B(X)
    WRITE(6,101) X,Z,T,S,GT
    RJ=FLOAT(J)
    TR1=RJ/5.0
    TR2=RJ/40.0
    Y=TR1-AINT(TR1)
    YY=TR2-AINT(TR2)
    IF(YY.LE.0.001) GO TO 4
    IF(Y.LE.0.001) GO TO 3
    GO TO 2
  3  WRITE(6,102)
    GO TO 2
  4  WRITE(6,103)
    GO TO 3
  2  CONTINUE
  STOP
  END
SCAN: 34
EOF: 34
0:          LIST.CAL

```

REFERENCES

1. J. R. Stevenson, H. W. Ellis, and R. J. Bartlett, "Synchrotron Radiation as an Infrared Source", to be published.
2. J. Schwinger, "On the Classical Radiation of Accelerated Electrons", Phys. Rev. 75, 1912 (1949).
3. G. N. Watson, A Treatise on the Theory of Bessel Functions, 2nd ed., Cambridge Univ. Press, Cambridge, England, 1958.
4. UP-7542 Rev. 1, LARGE SCALE SYSTEMS MATHPACK, Sperry Rand, Univac Division, 1970.

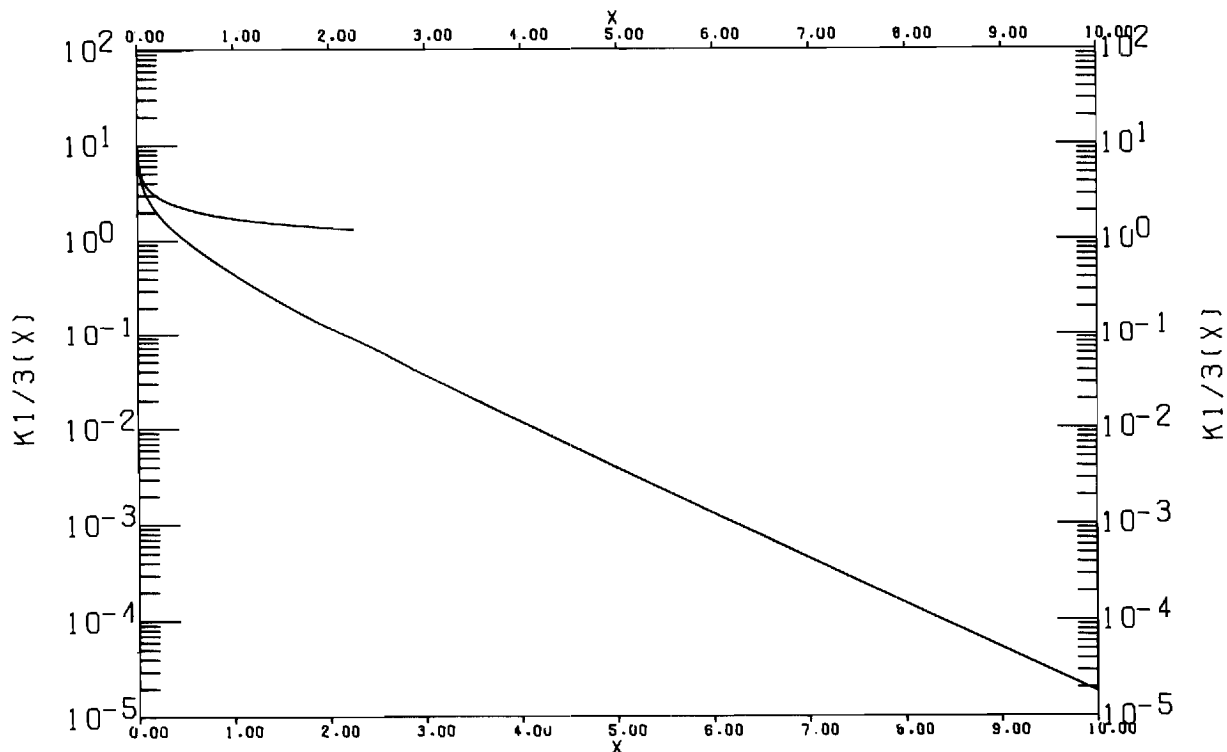


Figure 1. Plot of $K_{1/3}(x)$ versus x . The approximation for small arguments is plotted for arguments less than 2.5, and the large-argument approximation for arguments greater than 3.5. The large-argument approximation is not resolved from the plot of $K_{1/3}(x)$.

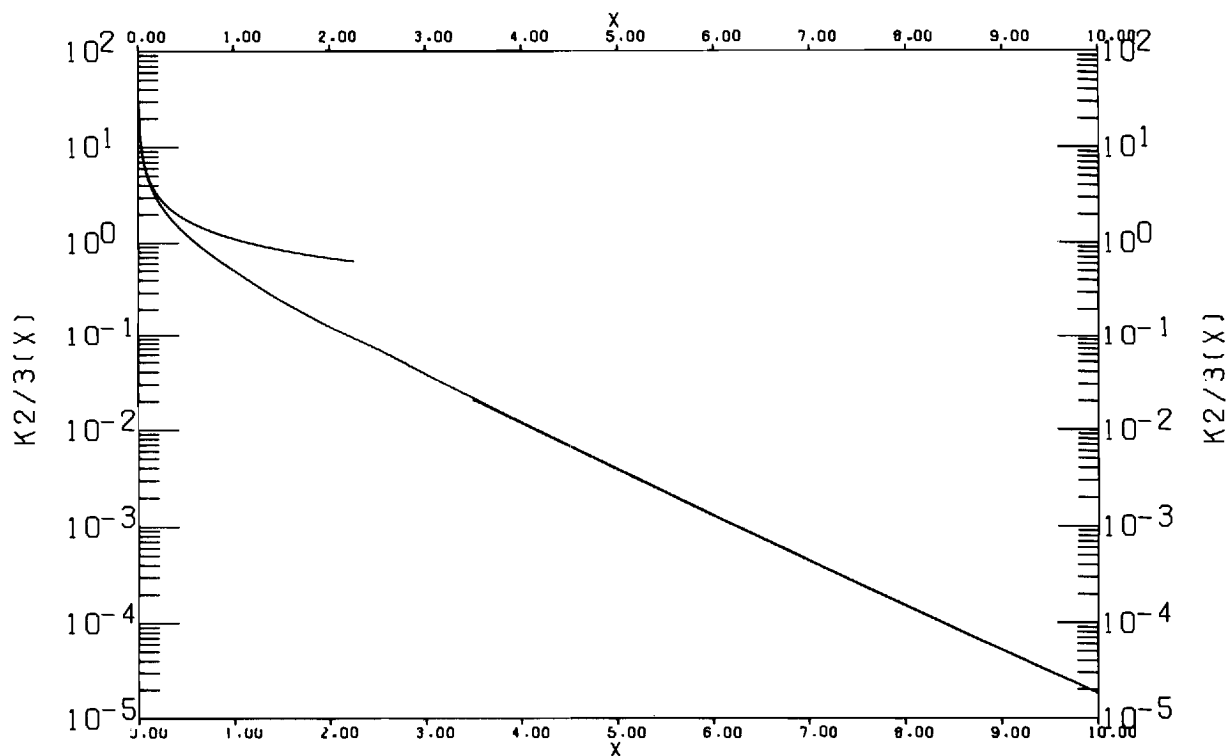


Figure 2. Plot of $K_{2/3}(x)$ versus x . The approximation for small arguments is plotted for arguments less than 2.5, and the large-argument approximation for arguments greater than 3.5. The large-argument approximation is not well-resolved from the plot of $K_{2/3}(x)$.

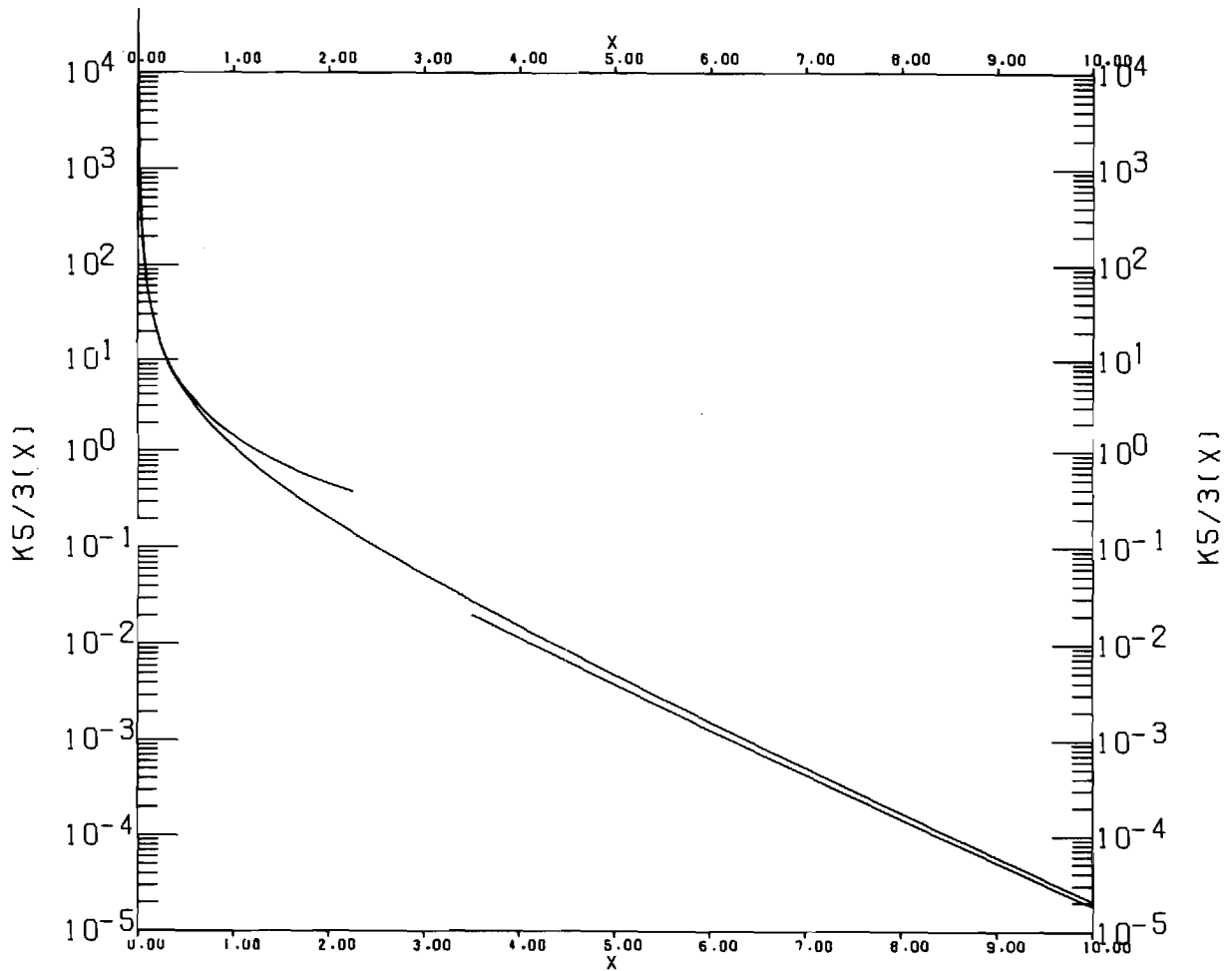


Figure 3. Plot of $K_{5/3}(x)$ versus x . The approximations for small and large arguments are plotted for arguments less than 2.5 and greater than 3.5 respectively.

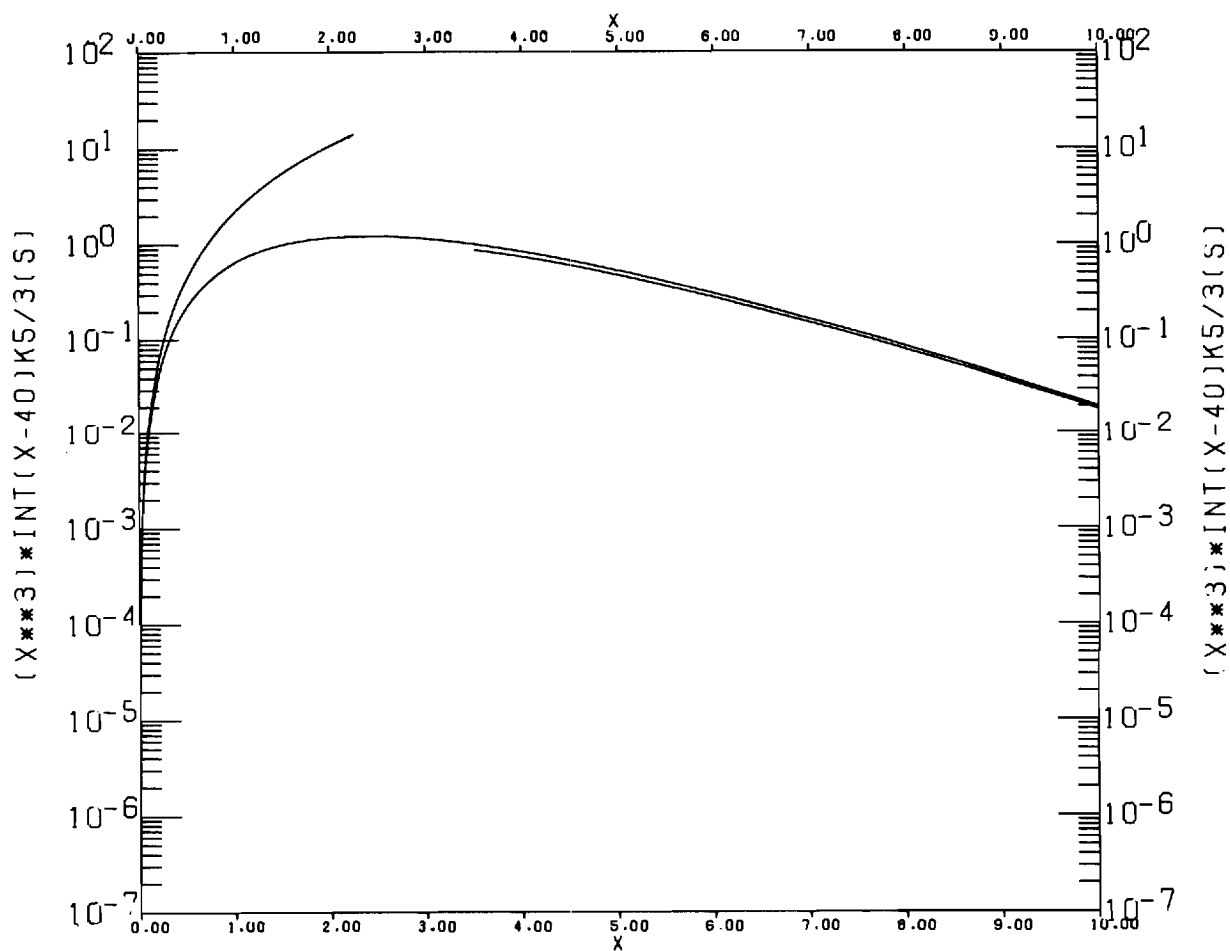


Figure 4. Plot of the function $G(x)$ versus x . The approximations for small and large arguments are plotted for arguments less than 2.5 and greater than 3.5 respectively.

X	K1/3(X)	K2/3(X)	K5/3(X)	G
.001	1.671505+01	1.074638+02	1.433013+05	2.136353-07
.002	1.319159+01	6.768601+01	4.513704+04	1.068998-06
.003	1.146887+01	5.164329+01	2.296397+04	2.741284-06
.004	1.037553+01	4.262066+01	1.421721+04	5.343455-06
.005	9.593712+00	3.672010+01	9.801586+03	8.962448-06
.006	8.994538+00	3.250869+01	7.233122+03	1.366974-05
.007	8.513964+00	2.932547+01	5.594299+03	1.952633-05
.008	8.115897+00	2.681976+01	4.478061+03	2.658557-05
.009	7.778159+00	2.478674+01	3.679875+03	3.489492-05
.010	7.486225+00	2.309808+01	3.087219+03	4.449714-05
.011	7.230110+00	2.166895+01	2.633760+03	5.543114-05
.012	7.002682+00	2.044083+01	2.278199+03	6.773264-05
.013	6.798682+00	1.937195+01	1.993658+03	8.143457-05
.014	6.614133+00	1.843158+01	1.761997+03	9.656751-05
.015	6.445958+00	1.759664+01	1.570586+03	1.131600-04
.016	6.291734+00	1.684935+01	1.410400+03	1.312386-04
.017	6.149524+00	1.617584+01	1.274839+03	1.508286-04
.018	6.017752+00	1.556508+01	1.158983+03	1.719533-04
.019	5.895123+00	1.500818+01	1.059097+03	1.946352-04
.020	5.780562+00	1.449790+01	9.723042+02	2.188952-04
.021	5.673166+00	1.402829+01	8.963550+02	2.447533-04
.022	5.572170+00	1.359436+01	8.294702+02	2.722286-04
.023	5.476922+00	1.319197+01	7.702261+02	3.013390-04
.024	5.386861+00	1.281758+01	7.174720+02	3.321017-04
.025	5.301501+00	1.246818+01	6.702690+02	3.645330-04
.026	5.220420+00	1.214121+01	6.278443+02	3.986488-04
.027	5.143247+00	1.183443+01	5.895574+02	4.344638-04
.028	5.069655+00	1.154590+01	5.548727+02	4.719924-04
.029	4.999358+00	1.127396+01	5.233404+02	5.112484-04
.030	4.932099+00	1.101710+01	4.945794+02	5.522448-04
.031	4.867650+00	1.077403+01	4.682654+02	5.949942-04
.032	4.805806+00	1.054360+01	4.441212+02	6.395087-04
.033	4.746384+00	1.032478+01	4.219080+02	6.857999-04
.034	4.689217+00	1.011666+01	4.014197+02	7.338790-04
.035	4.634157+00	9.918416+00	3.824773+02	7.837566-04
.036	4.581068+00	9.729316+00	3.649249+02	8.354432-04
.037	4.529825+00	9.548700+00	3.486259+02	8.889486-04
.038	4.480316+00	9.375970+00	3.334606+02	9.442822-04
.039	4.432438+00	9.210587+00	3.193232+02	1.001453-03
.040	4.386096+00	9.052058+00	3.061203+02	1.060471-03

X	K1/3(X)	K2/3(X)	K5/3(X)	G
.041	4.341205+00	8.899937+00	2.937690+02	1.121343-03
.042	4.297682+00	8.753817+00	2.821957+02	1.184079-03
.043	4.255456+00	8.613324+00	2.713343+02	1.248686-03
.044	4.214458+00	8.478117+00	2.611262+02	1.315171-03
.045	4.174624+00	8.347882+00	2.515184+02	1.383542-03
.046	4.135897+00	8.222331+00	2.424635+02	1.453806-03
.047	4.098222+00	8.101197+00	2.339186+02	1.525970-03
.048	4.061548+00	7.984234+00	2.258451+02	1.600041-03
.049	4.025828+00	7.871216+00	2.182078+02	1.676024-03
.050	3.991018+00	7.761932+00	2.109752+02	1.753926-03
.051	3.957077+00	7.656187+00	2.041181+02	1.833753-03
.052	3.923966+00	7.553798+00	1.976104+02	1.915511-03
.053	3.891650+00	7.454597+00	1.914280+02	1.999204-03
.054	3.860095+00	7.358427+00	1.855490+02	2.084839-03
.055	3.829268+00	7.265140+00	1.799533+02	2.172420-03
.056	3.799139+00	7.174600+00	1.746223+02	2.261953-03
.057	3.769682+00	7.086677+00	1.695393+02	2.353441-03
.058	3.740868+00	7.001251+00	1.646886+02	2.446890-03
.059	3.712672+00	6.918210+00	1.600559+02	2.542303-03
.060	3.685072+00	6.837448+00	1.556278+02	2.639686-03
.061	3.658045+00	6.758865+00	1.513923+02	2.739042-03
.062	3.631569+00	6.682367+00	1.473379+02	2.840375-03
.063	3.605625+00	6.607866+00	1.434542+02	2.943689-03
.064	3.580192+00	6.535280+00	1.397314+02	3.048987-03
.065	3.555255+00	6.464529+00	1.361605+02	3.156273-03
.066	3.530794+00	6.395540+00	1.327332+02	3.265550-03
.067	3.506794+00	6.328242+00	1.294415+02	3.376822-03
.068	3.483239+00	6.262569+00	1.262783+02	3.490091-03
.069	3.460114+00	6.198459+00	1.232367+02	3.605360-03
.070	3.437406+00	6.135853+00	1.203104+02	3.722633-03
.071	3.415101+00	6.074693+00	1.174934+02	3.841911-03
.072	3.393186+00	6.014926+00	1.147803+02	3.963198-03
.073	3.371649+00	5.956502+00	1.121658+02	4.086495-03
.074	3.350478+00	5.899373+00	1.096451+02	4.211806-03
.075	3.329662+00	5.843492+00	1.072136+02	4.339132-03
.076	3.309190+00	5.788815+00	1.048670+02	4.468476-03
.077	3.289053+00	5.735302+00	1.026013+02	4.599839-03
.078	3.269240+00	5.682912+00	1.004127+02	4.733224-03
.079	3.249742+00	5.631607+00	9.829763+01	4.868631-03
.080	3.230550+00	5.581352+00	9.625276+01	5.006064-03

X	K1/3(X)	K2/3(X)	K5/3(X)	G
.081	3.211655+00	5.532112+00	9.427491+01	5.145524-03
.082	3.193049+00	5.483854+00	9.236110+01	5.287012-03
.083	3.174725+00	5.436547+00	9.050851+01	5.430529-03
.084	3.156674+00	5.390161+00	8.871449+01	5.576077-03
.085	3.138889+00	5.344667+00	8.697650+01	5.723658-03
.086	3.121364+00	5.300036+00	8.529218+01	5.873272-03
.087	3.104090+00	5.256244+00	8.365927+01	6.024920-03
.088	3.087063+00	5.213264+00	8.207564+01	6.178604-03
.089	3.070275+00	5.171073+00	8.053926+01	6.334324-03
.090	3.053720+00	5.129647+00	7.904822+01	6.492082-03
.091	3.037394+00	5.088964+00	7.760070+01	6.651878-03
.092	3.021289+00	5.049002+00	7.619497+01	6.813712-03
.093	3.005400+00	5.009740+00	7.482938+01	6.977586-03
.094	2.989724+00	4.971160+00	7.350239+01	7.143500-03
.095	2.974253+00	4.933242+00	7.221249+01	7.311455-03
.096	2.958983+00	4.895967+00	7.095829+01	7.481450-03
.097	2.943911+00	4.859319+00	6.973843+01	7.653487-03
.098	2.929030+00	4.823279+00	6.855164+01	7.827565-03
.099	2.914337+00	4.787832+00	6.739670+01	8.003685-03
.100	2.899828+00	4.752963+00	6.627244+01	8.181847-03
.101	2.885498+00	4.718655+00	6.517775+01	8.362051-03
.102	2.871343+00	4.684894+00	6.411158+01	8.544297-03
.103	2.857360+00	4.651667+00	6.307290+01	8.728585-03
.104	2.843544+00	4.618960+00	6.206076+01	8.914916-03
.105	2.829893+00	4.586758+00	6.107424+01	9.103287-03
.106	2.816402+00	4.555051+00	6.011244+01	9.293701-03
.107	2.803069+00	4.523825+00	5.917452+01	9.486156-03
.108	2.789889+00	4.493069+00	5.825968+01	9.680652-03
.109	2.776860+00	4.462772+00	5.736715+01	9.877189-03
.110	2.763978+00	4.432921+00	5.649617+01	1.007577-02
.111	2.751242+00	4.403508+00	5.564604+01	1.027638-02
.112	2.738646+00	4.374521+00	5.481609+01	1.047904-02
.113	2.726190+00	4.345950+00	5.400565+01	1.068374-02
.114	2.713870+00	4.317786+00	5.321410+01	1.089047-02
.115	2.701683+00	4.290019+00	5.244085+01	1.109924-02
.116	2.689627+00	4.262640+00	5.168531+01	1.131005-02
.117	2.677699+00	4.235641+00	5.094693+01	1.152289-02
.118	2.665897+00	4.209012+00	5.022519+01	1.173777-02
.119	2.654219+00	4.182747+00	4.951956+01	1.195468-02
.120	2.642662+00	4.156836+00	4.882956+01	1.217363-02

X	K1/3(X)	K2/3(X)	K5/3(X)	G
.121	2.631223+00	4.131272+00	4.815471+01	1.239461-02
.122	2.619901+00	4.106047+00	4.749457+01	1.261762-02
.123	2.608694+00	4.081155+00	4.684869+01	1.284266-02
.124	2.597599+00	4.056587+00	4.621666+01	1.306973-02
.125	2.586615+00	4.032338+00	4.559806+01	1.329883-02
.126	2.575738+00	4.008400+00	4.499252+01	1.352996-02
.127	2.564969+00	3.984767+00	4.439965+01	1.376311-02
.128	2.554304+00	3.961433+00	4.381909+01	1.399829-02
.129	2.543742+00	3.938392+00	4.325049+01	1.423549-02
.130	2.533281+00	3.915637+00	4.269351+01	1.447471-02
.131	2.522919+00	3.893163+00	4.214784+01	1.471596-02
.132	2.512654+00	3.870964+00	4.161316+01	1.495922-02
.133	2.502486+00	3.849035+00	4.108917+01	1.520450-02
.134	2.492412+00	3.827371+00	4.057556+01	1.545180-02
.135	2.482431+00	3.805966+00	4.007208+01	1.570112-02
.136	2.472541+00	3.784814+00	3.957843+01	1.595245-02
.137	2.462740+00	3.763913+00	3.909436+01	1.620579-02
.138	2.453028+00	3.743256+00	3.861962+01	1.646114-02
.139	2.443403+00	3.722838+00	3.815395+01	1.671850-02
.140	2.433863+00	3.702657+00	3.769713+01	1.697786-02
.141	2.424407+00	3.682706+00	3.724892+01	1.723924-02
.142	2.415034+00	3.662982+00	3.680910+01	1.750261-02
.143	2.405743+00	3.643480+00	3.637746+01	1.776799-02
.144	2.396531+00	3.624197+00	3.595379+01	1.803537-02
.145	2.387399+00	3.605128+00	3.553788+01	1.830475-02
.146	2.378344+00	3.586270+00	3.512955+01	1.857613-02
.147	2.369366+00	3.567619+00	3.472861+01	1.884950-02
.148	2.360463+00	3.549171+00	3.433486+01	1.912486-02
.149	2.351635+00	3.530922+00	3.394814+01	1.940222-02
.150	2.342879+00	3.512870+00	3.356828+01	1.968156-02
.151	2.334195+00	3.495010+00	3.319521+01	1.996289-02
.152	2.325583+00	3.477339+00	3.282856+01	2.024621-02
.153	2.317041+00	3.459855+00	3.246828+01	2.053151-02
.154	2.308567+00	3.442553+00	3.211422+01	2.081879-02
.155	2.300161+00	3.425431+00	3.176623+01	2.110805-02
.156	2.291823+00	3.408486+00	3.142418+01	2.139929-02
.157	2.283550+00	3.391714+00	3.108791+01	2.169250-02
.158	2.275342+00	3.375113+00	3.075731+01	2.198769-02
.159	2.267199+00	3.358680+00	3.043223+01	2.228484-02
.160	2.259118+00	3.342413+00	3.011256+01	2.258397-02

X	K1/3(X)	K2/3(X)	K5/3(X)	G
.161	2.251101+00	3.326308+00	2.979816+01	2.288506-02
.162	2.243144+00	3.310363+00	2.948893+01	2.318811-02
.163	2.235249+00	3.294575+00	2.918474+01	2.349313-02
.164	2.227413+00	3.278942+00	2.888548+01	2.380011-02
.165	2.219636+00	3.263461+00	2.859104+01	2.410904-02
.166	2.211917+00	3.248130+00	2.830132+01	2.441993-02
.167	2.204256+00	3.232947+00	2.801621+01	2.473277-02
.168	2.196652+00	3.217909+00	2.773561+01	2.504756-02
.169	2.189103+00	3.203014+00	2.745943+01	2.536430-02
.170	2.181610+00	3.188260+00	2.718757+01	2.568299-02
.171	2.174171+00	3.173644+00	2.691994+01	2.600362-02
.172	2.166786+00	3.159165+00	2.665644+01	2.632618-02
.173	2.159454+00	3.144820+00	2.639699+01	2.665069-02
.174	2.152175+00	3.130608+00	2.614151+01	2.697713-02
.175	2.144947+00	3.116526+00	2.588991+01	2.730551-02
.176	2.137770+00	3.102572+00	2.564211+01	2.763581-02
.177	2.130644+00	3.088745+00	2.539803+01	2.796805-02
.178	2.123567+00	3.075043+00	2.515760+01	2.830220-02
.179	2.116540+00	3.061464+00	2.492074+01	2.863829-02
.180	2.109562+00	3.048005+00	2.468738+01	2.897629-02
.181	2.102631+00	3.034666+00	2.445745+01	2.931621-02
.182	2.095747+00	3.021445+00	2.423087+01	2.965804-02
.183	2.088911+00	3.008339+00	2.400759+01	3.000179-02
.184	2.082121+00	2.995348+00	2.378754+01	3.034745-02
.185	2.075376+00	2.982469+00	2.357065+01	3.069501-02
.186	2.068677+00	2.969701+00	2.335686+01	3.104448-02
.187	2.062022+00	2.957043+00	2.314611+01	3.139585-02
.188	2.055411+00	2.944492+00	2.293834+01	3.174912-02
.189	2.048844+00	2.932048+00	2.273349+01	3.210428-02
.190	2.042320+00	2.919710+00	2.253151+01	3.246134-02
.191	2.035839+00	2.907474+00	2.233234+01	3.282029-02
.192	2.029399+00	2.895341+00	2.213593+01	3.318113-02
.193	2.023001+00	2.883308+00	2.194223+01	3.354385-02
.194	2.016644+00	2.871375+00	2.175118+01	3.390845-02
.195	2.010328+00	2.859540+00	2.156274+01	3.427493-02
.196	2.004052+00	2.847802+00	2.137685+01	3.464329-02
.197	1.997816+00	2.836159+00	2.119348+01	3.501353-02
.198	1.991619+00	2.824610+00	2.101256+01	3.538563-02
.199	1.985461+00	2.813154+00	2.083407+01	3.575960-02
.200	1.979341+00	2.801790+00	2.065794+01	3.613544-02

X	K1/3(X)	K2/3(X)	K5/3(X)	G
.201	1.973259+00	2.790516+00	2.048415+01	3.651314-02
.202	1.967215+00	2.779332+00	2.031264+01	3.689269-02
.203	1.961208+00	2.768236+00	2.014338+01	3.727411-02
.204	1.955238+00	2.757227+00	1.997633+01	3.765737-02
.205	1.949304+00	2.746304+00	1.981145+01	3.804249-02
.206	1.943406+00	2.735466+00	1.964869+01	3.842946-02
.207	1.937543+00	2.724712+00	1.948802+01	3.881827-02
.208	1.931716+00	2.714040+00	1.932941+01	3.920892-02
.209	1.925924+00	2.703450+00	1.917282+01	3.960140-02
.210	1.920166+00	2.692941+00	1.901820+01	3.999573-02
.211	1.914442+00	2.682512+00	1.886554+01	4.039188-02
.212	1.908752+00	2.672161+00	1.871480+01	4.078987-02
.213	1.903095+00	2.661888+00	1.856593+01	4.118968-02
.214	1.897472+00	2.651692+00	1.841891+01	4.159131-02
.215	1.891881+00	2.641571+00	1.827372+01	4.199476-02
.216	1.886322+00	2.631526+00	1.813031+01	4.240003-02
.217	1.880795+00	2.621554+00	1.798866+01	4.280712-02
.218	1.875301+00	2.611656+00	1.784873+01	4.321601-02
.219	1.869837+00	2.601830+00	1.771051+01	4.362672-02
.220	1.864405+00	2.592075+00	1.757395+01	4.403922-02
.221	1.859003+00	2.582391+00	1.743904+01	4.445353-02
.222	1.853632+00	2.572777+00	1.730575+01	4.486963-02
.223	1.848291+00	2.563232+00	1.717404+01	4.528753-02
.224	1.842980+00	2.553754+00	1.704390+01	4.570723-02
.225	1.837698+00	2.544345+00	1.691529+01	4.612871-02
.226	1.832446+00	2.535001+00	1.678820+01	4.655197-02
.227	1.827223+00	2.525724+00	1.666260+01	4.697702-02
.228	1.822028+00	2.516511+00	1.653847+01	4.740385-02
.229	1.816862+00	2.507363+00	1.641577+01	4.783245-02
.230	1.811724+00	2.498278+00	1.629450+01	4.826282-02
.231	1.806614+00	2.489256+00	1.617462+01	4.869497-02
.232	1.801532+00	2.480297+00	1.605611+01	4.912888-02
.233	1.796477+00	2.471399+00	1.593896+01	4.956455-02
.234	1.791449+00	2.462561+00	1.582314+01	5.000198-02
.235	1.786448+00	2.453784+00	1.570862+01	5.044117-02
.236	1.781473+00	2.445066+00	1.559540+01	5.088211-02
.237	1.776525+00	2.436407+00	1.548345+01	5.132480-02
.238	1.771603+00	2.427806+00	1.537275+01	5.176924-02
.239	1.766707+00	2.419262+00	1.526329+01	5.221542-02
.240	1.761836+00	2.410775+00	1.515503+01	5.266334-02

X	K1/3(X)	K2/3(X)	K5/3(X)	G
.241	1.756991+00	2.402345+00	1.504797+01	5.311300-02
.242	1.752171+00	2.393970+00	1.494209+01	5.356439-02
.243	1.747376+00	2.385651+00	1.483737+01	5.401751-02
.244	1.742606+00	2.377385+00	1.473378+01	5.447235-02
.245	1.737860+00	2.369174+00	1.463132+01	5.492892-02
.246	1.733139+00	2.361016+00	1.452997+01	5.538721-02
.247	1.728441+00	2.352911+00	1.442971+01	5.584721-02
.248	1.723768+00	2.344858+00	1.433053+01	5.630893-02
.249	1.719118+00	2.336856+00	1.423240+01	5.677236-02
.250	1.714491+00	2.328906+00	1.413532+01	5.723749-02
.251	1.709888+00	2.321006+00	1.403927+01	5.770433-02
.252	1.705308+00	2.313157+00	1.394423+01	5.817286-02
.253	1.700750+00	2.305357+00	1.385019+01	5.864309-02
.254	1.696215+00	2.297605+00	1.375714+01	5.911502-02
.255	1.691703+00	2.289903+00	1.366505+01	5.958863-02
.256	1.687213+00	2.282249+00	1.357392+01	6.006393-02
.257	1.682744+00	2.274642+00	1.348374+01	6.054091-02
.258	1.678298+00	2.267082+00	1.339448+01	6.101957-02
.259	1.673874+00	2.259569+00	1.330615+01	6.149991-02
.260	1.669470+00	2.252102+00	1.321871+01	6.198192-02
.261	1.665089+00	2.244680+00	1.313217+01	6.246560-02
.262	1.660728+00	2.237304+00	1.304650+01	6.295094-02
.263	1.656388+00	2.229973+00	1.296170+01	6.343795-02
.264	1.652069+00	2.222686+00	1.287776+01	6.392661-02
.265	1.647771+00	2.215443+00	1.279465+01	6.441693-02
.266	1.643493+00	2.208244+00	1.271238+01	6.490890-02
.267	1.639235+00	2.201087+00	1.263093+01	6.540252-02
.268	1.634998+00	2.193973+00	1.255029+01	6.589778-02
.269	1.630780+00	2.186902+00	1.247044+01	6.639468-02
.270	1.626582+00	2.179872+00	1.239138+01	6.689322-02
.271	1.622404+00	2.172884+00	1.231310+01	6.739340-02
.272	1.618245+00	2.165936+00	1.223558+01	6.789520-02
.273	1.614106+00	2.159030+00	1.215882+01	6.839863-02
.274	1.609985+00	2.152163+00	1.208280+01	6.890369-02
.275	1.605884+00	2.145337+00	1.200752+01	6.941037-02
.276	1.601802+00	2.138550+00	1.193296+01	6.991866-02
.277	1.597738+00	2.131802+00	1.185912+01	7.042857-02
.278	1.593693+00	2.125093+00	1.178598+01	7.094008-02
.279	1.589666+00	2.118422+00	1.171355+01	7.145320-02
.280	1.585657+00	2.111789+00	1.164180+01	7.196793-02

X	K1/3(X)	K2/3(X)	K5/3(X)	G
.281	1.581667+00	2.105194+00	1.157073+01	7.248425-02
.282	1.577694+00	2.098637+00	1.150033+01	7.300217-02
.283	1.573740+00	2.092116+00	1.143059+01	7.352168-02
.284	1.569803+00	2.085632+00	1.136150+01	7.404278-02
.285	1.565884+00	2.079185+00	1.129306+01	7.456546-02
.286	1.561982+00	2.072773+00	1.122526+01	7.508973-02
.287	1.558097+00	2.066398+00	1.115809+01	7.561557-02
.288	1.554229+00	2.060057+00	1.109153+01	7.614299-02
.289	1.550379+00	2.053752+00	1.102559+01	7.667198-02
.290	1.546545+00	2.047481+00	1.096025+01	7.720253-02
.291	1.542729+00	2.041245+00	1.089551+01	7.773465-02
.292	1.538929+00	2.035043+00	1.083136+01	7.826833-02
.293	1.535145+00	2.028874+00	1.076779+01	7.880356-02
.294	1.531378+00	2.022740+00	1.070480+01	7.934035-02
.295	1.527627+00	2.016638+00	1.064238+01	7.987869-02
.296	1.523892+00	2.010570+00	1.058051+01	8.041857-02
.297	1.520174+00	2.004534+00	1.051920+01	8.096000-02
.298	1.516471+00	1.998530+00	1.045844+01	8.150296-02
.299	1.512784+00	1.992559+00	1.039822+01	8.204746-02
.300	1.509113+00	1.986619+00	1.033853+01	8.259349-02
.301	1.505457+00	1.980711+00	1.027937+01	8.314105-02
.302	1.501817+00	1.974834+00	1.022073+01	8.369013-02
.303	1.498192+00	1.968988+00	1.016261+01	8.424073-02
.304	1.494583+00	1.963173+00	1.010499+01	8.479285-02
.305	1.490988+00	1.957389+00	1.004788+01	8.534648-02
.306	1.487409+00	1.951634+00	9.991261+00	8.590163-02
.307	1.483844+00	1.945910+00	9.935136+00	8.645828-02
.308	1.480295+00	1.940215+00	9.879494+00	8.701643-02
.309	1.476760+00	1.934550+00	9.824332+00	8.757608-02
.310	1.473239+00	1.928914+00	9.769643+00	8.813723-02
.311	1.469734+00	1.923307+00	9.715423+00	8.869987-02
.312	1.466242+00	1.917729+00	9.661664+00	8.926399-02
.313	1.462765+00	1.912179+00	9.608363+00	8.982961-02
.314	1.459302+00	1.906657+00	9.555512+00	9.039670-02
.315	1.455854+00	1.901164+00	9.503109+00	9.096527-02
.316	1.452419+00	1.895699+00	9.451146+00	9.153531-02
.317	1.448998+00	1.890260+00	9.399620+00	9.210683-02
.318	1.445591+00	1.884850+00	9.348525+00	9.267981-02
.319	1.442198+00	1.879466+00	9.297856+00	9.325425-02
.320	1.438818+00	1.874110+00	9.247608+00	9.383016-02

X	K1/3(X)	K2/3(X)	K5/3(X)	G
.321	1.435452+00	1.868780+00	9.197777+00	9.440752-02
.322	1.432099+00	1.863476+00	9.148357+00	9.498633-02
.323	1.428760+00	1.858199+00	9.099345+00	9.556659-02
.324	1.425434+00	1.852948+00	9.050735+00	9.614829-02
.325	1.422121+00	1.847723+00	9.002523+00	9.673144-02
.326	1.418821+00	1.842523+00	8.954704+00	9.731602-02
.327	1.415534+00	1.837349+00	8.907275+00	9.790204-02
.328	1.412261+00	1.832201+00	8.860231+00	9.848949-02
.329	1.409000+00	1.827077+00	8.813566+00	9.907837-02
.330	1.405751+00	1.821978+00	8.767278+00	9.966866-02
.331	1.402516+00	1.816904+00	8.721362+00	1.002604-01
.332	1.399293+00	1.811854+00	8.675815+00	1.008535-01
.333	1.396082+00	1.806829+00	8.630631+00	1.014481-01
.334	1.392884+00	1.801827+00	8.585807+00	1.020440-01
.335	1.389698+00	1.796850+00	8.541339+00	1.026414-01
.336	1.386525+00	1.791896+00	8.497224+00	1.032401-01
.337	1.383363+00	1.786966+00	8.453456+00	1.038403-01
.338	1.380214+00	1.782059+00	8.410033+00	1.044419-01
.339	1.377077+00	1.777176+00	8.366952+00	1.050448-01
.340	1.373952+00	1.772315+00	8.324207+00	1.056491-01
.341	1.370838+00	1.767478+00	8.281796+00	1.062548-01
.342	1.367737+00	1.762663+00	8.239715+00	1.068619-01
.343	1.364647+00	1.757870+00	8.197960+00	1.074704-01
.344	1.361568+00	1.753100+00	8.156529+00	1.080803-01
.345	1.358502+00	1.748352+00	8.115417+00	1.086915-01
.346	1.355447+00	1.743626+00	8.074621+00	1.093040-01
.347	1.352403+00	1.738922+00	8.034138+00	1.099180-01
.348	1.349370+00	1.734239+00	7.993965+00	1.105333-01
.349	1.346349+00	1.729578+00	7.954098+00	1.111499-01
.350	1.343339+00	1.724939+00	7.914535+00	1.117679-01
.351	1.340341+00	1.720320+00	7.875271+00	1.123873-01
.352	1.337353+00	1.715723+00	7.836304+00	1.130080-01
.353	1.334376+00	1.711147+00	7.797631+00	1.136300-01
.354	1.331411+00	1.706591+00	7.759249+00	1.142534-01
.355	1.328456+00	1.702056+00	7.721154+00	1.148781-01
.356	1.325512+00	1.697541+00	7.683345+00	1.155041-01
.357	1.322578+00	1.693047+00	7.645817+00	1.161314-01
.358	1.319656+00	1.688573+00	7.608568+00	1.167601-01
.359	1.316744+00	1.684119+00	7.571595+00	1.173901-01
.360	1.313842+00	1.679685+00	7.534896+00	1.180214-01

X	K1/3(X)	K2/3(X)	K5/3(X)	G
.361	1.310951+00	1.675270+00	7.498467+00	1.186540-01
.362	1.308071+00	1.670875+00	7.462307+00	1.192880-01
.363	1.305201+00	1.666500+00	7.426411+00	1.199232-01
.364	1.302341+00	1.662143+00	7.390778+00	1.205597-01
.365	1.299491+00	1.657806+00	7.355405+00	1.211975-01
.366	1.296652+00	1.653488+00	7.320289+00	1.218367-01
.367	1.293822+00	1.649190+00	7.285428+00	1.224771-01
.368	1.291003+00	1.644909+00	7.250819+00	1.231188-01
.369	1.288194+00	1.640648+00	7.216459+00	1.237617-01
.370	1.285394+00	1.636404+00	7.182347+00	1.244060-01
.371	1.282605+00	1.632180+00	7.148480+00	1.250515-01
.372	1.279825+00	1.627973+00	7.114855+00	1.256983-01
.373	1.277055+00	1.623785+00	7.081470+00	1.263464-01
.374	1.274295+00	1.619615+00	7.048323+00	1.269957-01
.375	1.271544+00	1.615462+00	7.015411+00	1.276463-01
.376	1.268804+00	1.611328+00	6.982732+00	1.282981-01
.377	1.266072+00	1.607211+00	6.950284+00	1.289512-01
.378	1.263350+00	1.603111+00	6.918064+00	1.296056-01
.379	1.260638+00	1.599029+00	6.886071+00	1.302612-01
.380	1.257935+00	1.594965+00	6.854302+00	1.309180-01
.381	1.255241+00	1.590917+00	6.822755+00	1.315761-01
.382	1.252556+00	1.586887+00	6.791428+00	1.322354-01
.383	1.249881+00	1.582873+00	6.760318+00	1.328959-01
.384	1.247215+00	1.578876+00	6.729425+00	1.335577-01
.385	1.244558+00	1.574896+00	6.698745+00	1.342207-01
.386	1.241910+00	1.570933+00	6.668277+00	1.348849-01
.387	1.239271+00	1.566986+00	6.638018+00	1.355503-01
.388	1.236641+00	1.563056+00	6.607967+00	1.362170-01
.389	1.234020+00	1.559142+00	6.578122+00	1.368848-01
.390	1.231408+00	1.555244+00	6.548480+00	1.375539-01
.391	1.228805+00	1.551362+00	6.519041+00	1.382241-01
.392	1.226210+00	1.547496+00	6.489801+00	1.388956-01
.393	1.223625+00	1.543646+00	6.460760+00	1.395682-01
.394	1.221047+00	1.539811+00	6.431915+00	1.402421-01
.395	1.218479+00	1.535993+00	6.403264+00	1.409171-01
.396	1.215919+00	1.532189+00	6.374806+00	1.415933-01
.397	1.213367+00	1.528402+00	6.346539+00	1.422707-01
.398	1.210824+00	1.524630+00	6.318461+00	1.429493-01
.399	1.208290+00	1.520873+00	6.290571+00	1.436290-01
.400	1.205764+00	1.517131+00	6.262866+00	1.443100-01

X	K1/3(X)	K2/3(X)	K5/3(X)	G
.401	1.203246+00	1.513404+00	6.235345+00	1.449920-01
.402	1.200737+00	1.509692+00	6.208007+00	1.456753-01
.403	1.198235+00	1.505995+00	6.180849+00	1.463597-01
.404	1.195742+00	1.502313+00	6.153871+00	1.470453-01
.405	1.193258+00	1.498645+00	6.127070+00	1.477320-01
.406	1.190781+00	1.494993+00	6.100445+00	1.484198-01
.407	1.188312+00	1.491354+00	6.073993+00	1.491088-01
.408	1.185852+00	1.487730+00	6.047715+00	1.497990-01
.409	1.183399+00	1.484121+00	6.021608+00	1.504903-01
.410	1.180955+00	1.480525+00	5.995671+00	1.511827-01
.411	1.178518+00	1.476944+00	5.969901+00	1.518763-01
.412	1.176089+00	1.473377+00	5.944298+00	1.525709-01
.413	1.173668+00	1.469824+00	5.918861+00	1.532667-01
.414	1.171255+00	1.466284+00	5.893587+00	1.539637-01
.415	1.168849+00	1.462759+00	5.868476+00	1.546617-01
.416	1.166452+00	1.459247+00	5.843525+00	1.553609-01
.417	1.164061+00	1.455749+00	5.818733+00	1.560611-01
.418	1.161679+00	1.452264+00	5.794100+00	1.567625-01
.419	1.159304+00	1.448793+00	5.769624+00	1.574650-01
.420	1.156937+00	1.445335+00	5.745302+00	1.581685-01
.421	1.154577+00	1.441891+00	5.721135+00	1.588732-01
.422	1.152225+00	1.438459+00	5.697120+00	1.595789-01
.423	1.149880+00	1.435041+00	5.673256+00	1.602858-01
.424	1.147542+00	1.431636+00	5.649543+00	1.609937-01
.425	1.145212+00	1.428244+00	5.625978+00	1.617027-01
.426	1.142889+00	1.424865+00	5.602561+00	1.624128-01
.427	1.140574+00	1.421499+00	5.579289+00	1.631240-01
.428	1.138266+00	1.418145+00	5.556163+00	1.638362-01
.429	1.135965+00	1.414804+00	5.533180+00	1.645495-01
.430	1.133671+00	1.411476+00	5.510340+00	1.652639-01
.431	1.131384+00	1.408160+00	5.487641+00	1.659793-01
.432	1.129105+00	1.404857+00	5.465082+00	1.666958-01
.433	1.126832+00	1.401566+00	5.442662+00	1.674133-01
.434	1.124566+00	1.398287+00	5.420380+00	1.681319-01
.435	1.122308+00	1.395021+00	5.398234+00	1.688515-01
.436	1.120056+00	1.391767+00	5.376224+00	1.695722-01
.437	1.117812+00	1.388525+00	5.354348+00	1.702939-01
.438	1.115574+00	1.385295+00	5.332605+00	1.710166-01
.439	1.113343+00	1.382076+00	5.310994+00	1.717404-01
.440	1.111119+00	1.378870+00	5.289514+00	1.724652-01

X	K1/3(X)	K2/3(X)	K5/3(X)	G
.441	1.108902+00	1.375676+00	5.268164+00	1.731910-01
.442	1.106691+00	1.372493+00	5.246942+00	1.739179-01
.443	1.104488+00	1.369322+00	5.225848+00	1.746458-01
.444	1.102291+00	1.366163+00	5.204882+00	1.753746-01
.445	1.100100+00	1.363015+00	5.184040+00	1.761045-01
.446	1.097917+00	1.359879+00	5.163323+00	1.768354-01
.447	1.095739+00	1.356754+00	5.142730+00	1.775673-01
.448	1.093569+00	1.353640+00	5.122259+00	1.783002-01
.449	1.091405+00	1.350538+00	5.101910+00	1.790342-01
.450	1.089247+00	1.347447+00	5.081682+00	1.797690-01
.451	1.087096+00	1.344367+00	5.061573+00	1.805049-01
.452	1.084952+00	1.341298+00	5.041583+00	1.812418-01
.453	1.082813+00	1.338240+00	5.021710+00	1.819797-01
.454	1.080682+00	1.335193+00	5.001955+00	1.827185-01
.455	1.078556+00	1.332158+00	4.982315+00	1.834583-01
.456	1.076437+00	1.329133+00	4.962790+00	1.841991-01
.457	1.074324+00	1.326118+00	4.943379+00	1.849408-01
.458	1.072217+00	1.323115+00	4.924080+00	1.856836-01
.459	1.070117+00	1.320122+00	4.904894+00	1.864273-01
.460	1.068023+00	1.317140+00	4.885820+00	1.871719-01
.461	1.065935+00	1.314168+00	4.866855+00	1.879175-01
.462	1.063853+00	1.311207+00	4.848000+00	1.886640-01
.463	1.061777+00	1.308256+00	4.829254+00	1.894115-01
.464	1.059708+00	1.305316+00	4.810616+00	1.901600-01
.465	1.057644+00	1.302386+00	4.792084+00	1.909094-01
.466	1.055587+00	1.299466+00	4.773659+00	1.916597-01
.467	1.053535+00	1.296557+00	4.755339+00	1.924110-01
.468	1.051489+00	1.293657+00	4.737123+00	1.931631-01
.469	1.049450+00	1.290768+00	4.719011+00	1.939163-01
.470	1.047416+00	1.287889+00	4.701002+00	1.946703-01
.471	1.045388+00	1.285020+00	4.683094+00	1.954253-01
.472	1.043366+00	1.282160+00	4.665289+00	1.961811-01
.473	1.041350+00	1.279311+00	4.647583+00	1.969379-01
.474	1.039340+00	1.276471+00	4.629977+00	1.976957-01
.475	1.037336+00	1.273642+00	4.612470+00	1.984543-01
.476	1.035337+00	1.270822+00	4.595061+00	1.992138-01
.477	1.033344+00	1.268011+00	4.577750+00	1.999742-01
.478	1.031357+00	1.265210+00	4.560535+00	2.007355-01
.479	1.029375+00	1.262419+00	4.543416+00	2.014977-01
.480	1.027399+00	1.259638+00	4.526393+00	2.022608-01

X	K1/3(X)	K2/3(X)	K5/3(X)	G
.481	1.025429+00	1.256866+00	4.509464+00	2.030248-01
.482	1.023464+00	1.254103+00	4.492628+00	2.037897-01
.483	1.021505+00	1.251349+00	4.475886+00	2.045555-01
.484	1.019551+00	1.248605+00	4.459236+00	2.053221-01
.485	1.017603+00	1.245871+00	4.442677+00	2.060896-01
.486	1.015661+00	1.243145+00	4.426210+00	2.068580-01
.487	1.013724+00	1.240429+00	4.409833+00	2.076272-01
.488	1.011792+00	1.237722+00	4.393545+00	2.083973-01
.489	1.009866+00	1.235023+00	4.377347+00	2.091683-01
.490	1.007946+00	1.232334+00	4.361236+00	2.099401-01
.491	1.006030+00	1.229654+00	4.345213+00	2.107128-01
.492	1.004120+00	1.226983+00	4.329278+00	2.114863-01
.493	1.002216+00	1.224321+00	4.313428+00	2.122607-01
.494	1.000316+00	1.221667+00	4.297664+00	2.130359-01
.495	9.984224-01	1.219023+00	4.281985+00	2.138120-01
.496	9.965336-01	1.216387+00	4.266391+00	2.145889-01
.497	9.946501-01	1.213760+00	4.250880+00	2.153666-01
.498	9.927719-01	1.211141+00	4.235453+00	2.161452-01
.499	9.908989-01	1.208532+00	4.220108+00	2.169246-01
.500	9.890310-01	1.205930+00	4.204845+00	2.177048-01
.501	9.871683-01	1.203338+00	4.189664+00	2.184858-01
.502	9.853107-01	1.200754+00	4.174563+00	2.192677-01
.503	9.834583-01	1.198178+00	4.159543+00	2.200503-01
.504	9.816109-01	1.195611+00	4.144602+00	2.208338-01
.505	9.797686-01	1.193052+00	4.129740+00	2.216181-01
.506	9.779314-01	1.190501+00	4.114956+00	2.224032-01
.507	9.760991-01	1.187959+00	4.100251+00	2.231891-01
.508	9.742719-01	1.185425+00	4.085623+00	2.239757-01
.509	9.724497-01	1.182899+00	4.071071+00	2.247632-01
.510	9.706325-01	1.180381+00	4.056596+00	2.255515-01
.511	9.688201-01	1.177871+00	4.042197+00	2.263405-01
.512	9.670128-01	1.175370+00	4.027872+00	2.271304-01
.513	9.652103-01	1.172877+00	4.013623+00	2.279210-01
.514	9.634127-01	1.170391+00	3.999447+00	2.287124-01
.515	9.616199-01	1.167914+00	3.985345+00	2.295046-01
.516	9.598320-01	1.165444+00	3.971316+00	2.302975-01
.517	9.580489-01	1.162983+00	3.957359+00	2.310912-01
.518	9.562707-01	1.160529+00	3.943475+00	2.318857-01
.519	9.544972-01	1.158083+00	3.929662+00	2.326809-01
.520	9.527284-01	1.155645+00	3.915920+00	2.334769-01

X	K1/3(X)	K2/3(X)	K5/3(X)	G
.521	9.509644-01	1.153214+00	3.902248+00	2.342737-01
.522	9.492051-01	1.150791+00	3.888647+00	2.350712-01
.523	9.474506-01	1.148376+00	3.875115+00	2.358694-01
.524	9.457007-01	1.145969+00	3.861652+00	2.366684-01
.525	9.439554-01	1.143569+00	3.848258+00	2.374682-01
.526	9.422149-01	1.141177+00	3.834931+00	2.382686-01
.527	9.404789-01	1.138792+00	3.821673+00	2.390698-01
.528	9.387476-01	1.136414+00	3.808481+00	2.398718-01
.529	9.370208-01	1.134045+00	3.795356+00	2.406745-01
.530	9.352986-01	1.131682+00	3.782298+00	2.414779-01
.531	9.335809-01	1.129327+00	3.769305+00	2.422820-01
.532	9.318678-01	1.126979+00	3.756377+00	2.430868-01
.533	9.301592-01	1.124639+00	3.743514+00	2.438924-01
.534	9.284551-01	1.122305+00	3.730716+00	2.446986-01
.535	9.267555-01	1.119980+00	3.717982+00	2.455056-01
.536	9.250603-01	1.117661+00	3.705311+00	2.463133-01
.537	9.233696-01	1.115349+00	3.692703+00	2.471217-01
.538	9.216833-01	1.113045+00	3.680158+00	2.479308-01
.539	9.200014-01	1.110747+00	3.667675+00	2.487405-01
.540	9.183239-01	1.108457+00	3.655255+00	2.495510-01
.541	9.166507-01	1.106174+00	3.642895+00	2.503622-01
.542	9.149819-01	1.103897+00	3.630597+00	2.511740-01
.543	9.133175-01	1.101628+00	3.618359+00	2.519866-01
.544	9.116573-01	1.099366+00	3.606181+00	2.527998-01
.545	9.100015-01	1.097110+00	3.594063+00	2.536137-01
.546	9.083500-01	1.094862+00	3.582005+00	2.544283-01
.547	9.067027-01	1.092620+00	3.570005+00	2.552435-01
.548	9.050596-01	1.090385+00	3.558064+00	2.560594-01
.549	9.034209-01	1.088157+00	3.546182+00	2.568760-01
.550	9.017863-01	1.085935+00	3.534357+00	2.576933-01
.551	9.001559-01	1.083721+00	3.522589+00	2.585112-01
.552	8.985297-01	1.081513+00	3.510879+00	2.593297-01
.553	8.969077-01	1.079311+00	3.499225+00	2.601489-01
.554	8.952898-01	1.077116+00	3.487628+00	2.609688-01
.555	8.936761-01	1.074928+00	3.476086+00	2.617893-01
.556	8.920665-01	1.072747+00	3.464600+00	2.626104-01
.557	8.904610-01	1.070572+00	3.453170+00	2.634322-01
.558	8.888595-01	1.068403+00	3.441794+00	2.642546-01
.559	8.872622-01	1.066241+00	3.430472+00	2.650777-01
.560	8.856689-01	1.064085+00	3.419205+00	2.659014-01

X	K1/3(X)	K2/3(X)	K5/3(X)	G
.561	8.840797-01	1.061936+00	3.407992+00	2.667257-01
.562	8.824944-01	1.059793+00	3.396832+00	2.675507-01
.563	8.809132-01	1.057657+00	3.385725+00	2.683762-01
.564	8.793360-01	1.055527+00	3.374671+00	2.692024-01
.565	8.777628-01	1.053403+00	3.363669+00	2.700292-01
.566	8.761935-01	1.051285+00	3.352719+00	2.708566-01
.567	8.746281-01	1.049174+00	3.341821+00	2.716846-01
.568	8.730667-01	1.047069+00	3.330974+00	2.725133-01
.569	8.715093-01	1.044970+00	3.320179+00	2.733425-01
.570	8.699557-01	1.042877+00	3.309434+00	2.741723-01
.571	8.684060-01	1.040790+00	3.298740+00	2.750027-01
.572	8.668602-01	1.038710+00	3.288095+00	2.758338-01
.573	8.653183-01	1.036635+00	3.277501+00	2.766654-01
.574	8.637802-01	1.034567+00	3.266955+00	2.774976-01
.575	8.622459-01	1.032505+00	3.256459+00	2.783304-01
.576	8.607155-01	1.030448+00	3.246012+00	2.791637-01
.577	8.591888-01	1.028398+00	3.235614+00	2.799977-01
.578	8.576660-01	1.026353+00	3.225263+00	2.808322-01
.579	8.561469-01	1.024315+00	3.214961+00	2.816673-01
.580	8.546315-01	1.022282+00	3.204706+00	2.825029-01
.581	8.531199-01	1.020256+00	3.194498+00	2.833392-01
.582	8.516121-01	1.018235+00	3.184338+00	2.841760-01
.583	8.501080-01	1.016220+00	3.174224+00	2.850133-01
.584	8.486076-01	1.014210+00	3.164156+00	2.858512-01
.585	8.471109-01	1.012207+00	3.154135+00	2.866897-01
.586	8.456178-01	1.010209+00	3.144160+00	2.875287-01
.587	8.441284-01	1.008217+00	3.134230+00	2.883683-01
.588	8.426427-01	1.006231+00	3.124345+00	2.892084-01
.589	8.411605-01	1.004250+00	3.114505+00	2.900490-01
.590	8.396821-01	1.002275+00	3.104710+00	2.908902-01
.591	8.382072-01	1.000306+00	3.094960+00	2.917319-01
.592	8.367359-01	9.983419-01	3.085254+00	2.925742-01
.593	8.352682-01	9.963837-01	3.075591+00	2.934170-01
.594	8.338041-01	9.944310-01	3.065972+00	2.942603-01
.595	8.323436-01	9.924839-01	3.056397+00	2.951042-01
.596	8.308865-01	9.905423-01	3.046865+00	2.959485-01
.597	8.294330-01	9.886061-01	3.037375+00	2.967934-01
.598	8.279831-01	9.866754-01	3.027928+00	2.976388-01
.599	8.265367-01	9.847502-01	3.018524+00	2.984847-01
.600	8.250937-01	9.828304-01	3.009161+00	2.993312-01

X	K1/3(X)	K2/3(X)	K5/3(X)	G
.601	8.236542-01	9.809159-01	2.999840+00	3.001781-01
.602	8.222182-01	9.790069-01	2.990561+00	3.010255-01
.603	8.207857-01	9.771032-01	2.981323+00	3.018735-01
.604	8.193566-01	9.752047-01	2.972126+00	3.027219-01
.605	8.179309-01	9.733117-01	2.962970+00	3.035708-01
.606	8.165086-01	9.714239-01	2.953855+00	3.044202-01
.607	8.150898-01	9.695413-01	2.944780+00	3.052701-01
.608	8.136743-01	9.676640-01	2.935744+00	3.061205-01
.609	8.122623-01	9.657919-01	2.926749+00	3.069714-01
.610	8.108536-01	9.639249-01	2.917793+00	3.078228-01
.611	8.094482-01	9.620632-01	2.908877+00	3.086746-01
.612	8.080463-01	9.602066-01	2.900000+00	3.095269-01
.613	8.066476-01	9.583552-01	2.891161+00	3.103797-01
.614	8.052523-01	9.565088-01	2.882361+00	3.112330-01
.615	8.038602-01	9.546675-01	2.873600+00	3.120867-01
.616	8.024715-01	9.528313-01	2.864877+00	3.129409-01
.617	8.010861-01	9.510002-01	2.856192+00	3.137955-01
.618	7.997039-01	9.491740-01	2.847544+00	3.146506-01
.619	7.983251-01	9.473529-01	2.838934+00	3.155062-01
.620	7.969494-01	9.455368-01	2.830362+00	3.163622-01
.621	7.955771-01	9.437256-01	2.821826+00	3.172186-01
.622	7.942079-01	9.419194-01	2.813328+00	3.180755-01
.623	7.928420-01	9.401181-01	2.804866+00	3.189329-01
.624	7.914793-01	9.383216-01	2.796440+00	3.197906-01
.625	7.901197-01	9.365301-01	2.788051+00	3.206489-01
.626	7.887634-01	9.347435-01	2.779697+00	3.215075-01
.627	7.874102-01	9.329617-01	2.771380+00	3.223666-01
.628	7.860602-01	9.311847-01	2.763098+00	3.232261-01
.629	7.847134-01	9.294125-01	2.754851+00	3.240861-01
.630	7.833697-01	9.276451-01	2.746640+00	3.249464-01
.631	7.820291-01	9.258825-01	2.738463+00	3.258072-01
.632	7.806917-01	9.241246-01	2.730322+00	3.266684-01
.633	7.793574-01	9.223715-01	2.722215+00	3.275300-01
.634	7.780261-01	9.206230-01	2.714142+00	3.283921-01
.635	7.766980-01	9.188793-01	2.706103+00	3.292545-01
.636	7.753730-01	9.171402-01	2.698099+00	3.301173-01
.637	7.740510-01	9.154058-01	2.690128+00	3.309806-01
.638	7.727320-01	9.136761-01	2.682191+00	3.318442-01
.639	7.714162-01	9.119509-01	2.674287+00	3.327083-01
.640	7.701033-01	9.102303-01	2.666416+00	3.335727-01

X	K1/3(X)	K2/3(X)	K5/3(X)	G
.641	7.687935-01	9.085144-01	2.658579+00	3.344375-01
.642	7.674867-01	9.068030-01	2.650774+00	3.353028-01
.643	7.661829-01	9.050961-01	2.643002+00	3.361684-01
.644	7.648821-01	9.033938-01	2.635263+00	3.370344-01
.645	7.635843-01	9.016959-01	2.627555+00	3.379007-01
.646	7.622895-01	9.000026-01	2.619880+00	3.387675-01
.647	7.609977-01	8.983138-01	2.612237+00	3.396346-01
.648	7.597087-01	8.966294-01	2.604625+00	3.405021-01
.649	7.584228-01	8.949494-01	2.597045+00	3.413700-01
.650	7.571398-01	8.932739-01	2.589497+00	3.422382-01
.651	7.558597-01	8.916028-01	2.581979+00	3.431068-01
.652	7.545825-01	8.899361-01	2.574493+00	3.439758-01
.653	7.533083-01	8.882737-01	2.567037+00	3.448451-01
.654	7.520369-01	8.866157-01	2.559612+00	3.457148-01
.655	7.507684-01	8.849620-01	2.552218+00	3.465848-01
.656	7.495028-01	8.833127-01	2.544854+00	3.474552-01
.657	7.482401-01	8.816677-01	2.537520+00	3.483260-01
.658	7.469802-01	8.800270-01	2.530216+00	3.491970-01
.659	7.457232-01	8.783905-01	2.522942+00	3.500685-01
.660	7.444690-01	8.767583-01	2.515698+00	3.509402-01
.661	7.432177-01	8.751303-01	2.508483+00	3.518123-01
.662	7.419692-01	8.735065-01	2.501298+00	3.526848-01
.663	7.407235-01	8.718871-01	2.494141+00	3.535575-01
.664	7.394806-01	8.702717-01	2.487014+00	3.544306-01
.665	7.382405-01	8.686605-01	2.479916+00	3.553040-01
.666	7.370032-01	8.670536-01	2.472846+00	3.561778-01
.667	7.357686-01	8.654507-01	2.465805+00	3.570518-01
.668	7.345369-01	8.638520-01	2.458792+00	3.579262-01
.669	7.333079-01	8.622573-01	2.451808+00	3.588009-01
.670	7.320816-01	8.606668-01	2.444852+00	3.596759-01
.671	7.308581-01	8.590804-01	2.437923+00	3.605513-01
.672	7.296373-01	8.574980-01	2.431022+00	3.614269-01
.673	7.284193-01	8.559197-01	2.424149+00	3.623028-01
.674	7.272039-01	8.543455-01	2.417304+00	3.631791-01
.675	7.259913-01	8.527752-01	2.410486+00	3.640556-01
.676	7.247813-01	8.512090-01	2.403695+00	3.649324-01
.677	7.235741-01	8.496468-01	2.396931+00	3.658096-01
.678	7.223695-01	8.480885-01	2.390193+00	3.666870-01
.679	7.211676-01	8.465342-01	2.383483+00	3.675647-01
.680	7.199684-01	8.449839-01	2.376799+00	3.684427-01

X	K1/3(X)	K2/3(X)	K5/3(X)	G
.681	7.187718-01	8.434374-01	2.370142+00	3.693210-01
.682	7.175778-01	8.418949-01	2.363511+00	3.701995-01
.683	7.163865-01	8.403563-01	2.356906+00	3.710784-01
.684	7.151979-01	8.388216-01	2.350328+00	3.719575-01
.685	7.140118-01	8.372908-01	2.343775+00	3.728369-01
.686	7.128284-01	8.357638-01	2.337248+00	3.737166-01
.687	7.116475-01	8.342407-01	2.330746+00	3.745965-01
.688	7.104693-01	8.327214-01	2.324271+00	3.754767-01
.689	7.092936-01	8.312059-01	2.317820+00	3.763571-01
.690	7.081206-01	8.296943-01	2.311395+00	3.772379-01
.691	7.069501-01	8.281865-01	2.304994+00	3.781189-01
.692	7.057822-01	8.266824-01	2.298619+00	3.790001-01
.693	7.046168-01	8.251820-01	2.292269+00	3.798816-01
.694	7.034540-01	8.236855-01	2.285943+00	3.807633-01
.695	7.022937-01	8.221926-01	2.279642+00	3.816453-01
.696	7.011359-01	8.207035-01	2.273365+00	3.825275-01
.697	6.999807-01	8.192182-01	2.267113+00	3.834100-01
.698	6.988280-01	8.177364-01	2.260884+00	3.842927-01
.699	6.976777-01	8.162584-01	2.254680+00	3.851757-01
.700	6.965300-01	8.147841-01	2.248500+00	3.860588-01
.701	6.953848-01	8.133134-01	2.242343+00	3.869423-01
.702	6.942421-01	8.118463-01	2.236210+00	3.878259-01
.703	6.931018-01	8.103829-01	2.230101+00	3.887098-01
.704	6.919640-01	8.089231-01	2.224015+00	3.895939-01
.705	6.908287-01	8.074670-01	2.217953+00	3.904782-01
.706	6.896958-01	8.060144-01	2.211914+00	3.913628-01
.707	6.885654-01	8.045653-01	2.205897+00	3.922475-01
.708	6.874374-01	8.031199-01	2.199904+00	3.931325-01
.709	6.863118-01	8.016780-01	2.193934+00	3.940177-01
.710	6.851887-01	8.002396-01	2.187986+00	3.949031-01
.711	6.840680-01	7.988048-01	2.182061+00	3.957887-01
.712	6.829497-01	7.973735-01	2.176159+00	3.966745-01
.713	6.818338-01	7.959457-01	2.170278+00	3.975605-01
.714	6.807203-01	7.945214-01	2.164420+00	3.984467-01
.715	6.796091-01	7.931005-01	2.158585+00	3.993331-01
.716	6.785004-01	7.916832-01	2.152771+00	4.002197-01
.717	6.773940-01	7.902693-01	2.146979+00	4.011065-01
.718	6.762900-01	7.888588-01	2.141209+00	4.019935-01
.719	6.751883-01	7.874518-01	2.135461+00	4.028807-01
.720	6.740891-01	7.860482-01	2.129734+00	4.037680-01

X	K1/3(X)	K2/3(X)	K5/3(X)	G
.721	6.729921-01	7.846479-01	2.124029+00	4.046556-01
.722	6.718975-01	7.832511-01	2.118345+00	4.055433-01
.723	6.708052-01	7.818577-01	2.112682+00	4.064312-01
.724	6.697152-01	7.804676-01	2.107041+00	4.073192-01
.725	6.686276-01	7.790809-01	2.101420+00	4.082075-01
.726	6.675422-01	7.776976-01	2.095821+00	4.090959-01
.727	6.664592-01	7.763176-01	2.090242+00	4.099845-01
.728	6.653784-01	7.749409-01	2.084684+00	4.108732-01
.729	6.643000-01	7.735675-01	2.079147+00	4.117621-01
.730	6.632238-01	7.721974-01	2.073630+00	4.126512-01
.731	6.621499-01	7.708307-01	2.068134+00	4.135404-01
.732	6.610783-01	7.694672-01	2.062658+00	4.144298-01
.733	6.600089-01	7.681069-01	2.057202+00	4.153194-01
.734	6.589418-01	7.667500-01	2.051766+00	4.162090-01
.735	6.578769-01	7.653962-01	2.046351+00	4.170989-01
.736	6.568142-01	7.640457-01	2.040955+00	4.179889-01
.737	6.557539-01	7.626984-01	2.035579+00	4.188790-01
.738	6.546957-01	7.613544-01	2.030223+00	4.197693-01
.739	6.536397-01	7.600135-01	2.024886+00	4.206597-01
.740	6.525860-01	7.586759-01	2.019570+00	4.215502-01
.741	6.515345-01	7.573414-01	2.014272+00	4.224409-01
.742	6.504852-01	7.560100-01	2.008994+00	4.233317-01
.743	6.494380-01	7.546819-01	2.003735+00	4.242226-01
.744	6.483931-01	7.533569-01	1.998495+00	4.251137-01
.745	6.473503-01	7.520350-01	1.993274+00	4.260049-01
.746	6.463097-01	7.507162-01	1.988072+00	4.268962-01
.747	6.452713-01	7.494006-01	1.982889+00	4.277876-01
.748	6.442350-01	7.480881-01	1.977725+00	4.286792-01
.749	6.432009-01	7.467786-01	1.972580+00	4.295708-01
.750	6.421690-01	7.454723-01	1.967453+00	4.304626-01
.751	6.411391-01	7.441690-01	1.962345+00	4.313545-01
.752	6.401115-01	7.428688-01	1.957255+00	4.322465-01
.753	6.390859-01	7.415716-01	1.952183+00	4.331386-01
.754	6.380625-01	7.402775-01	1.947130+00	4.340308-01
.755	6.370412-01	7.389865-01	1.942094+00	4.349231-01
.756	6.360220-01	7.376984-01	1.937077+00	4.358155-01
.757	6.350050-01	7.364134-01	1.932078+00	4.367080-01
.758	6.339900-01	7.351313-01	1.927097+00	4.376006-01
.759	6.329771-01	7.338522-01	1.922133+00	4.384933-01
.760	6.319663-01	7.325762-01	1.917188+00	4.393860-01

X	K1/3(X)	K2/3(X)	K5/3(X)	G
.761	6.309576-01	7.313031-01	1.912260+00	4.402789-01
.762	6.299509-01	7.300330-01	1.907349+00	4.411719-01
.763	6.289464-01	7.287658-01	1.902456+00	4.420649-01
.764	6.279439-01	7.275016-01	1.897580+00	4.429580-01
.765	6.269434-01	7.262403-01	1.892722+00	4.438512-01
.766	6.259450-01	7.249819-01	1.887880+00	4.447445-01
.767	6.249487-01	7.237265-01	1.883056+00	4.456378-01
.768	6.239544-01	7.224739-01	1.878249+00	4.465312-01
.769	6.229621-01	7.212242-01	1.873459+00	4.474247-01
.770	6.219719-01	7.199775-01	1.868686+00	4.483182-01
.771	6.209837-01	7.187336-01	1.863930+00	4.492118-01
.772	6.199974-01	7.174925-01	1.859190+00	4.501055-01
.773	6.190133-01	7.162544-01	1.854467+00	4.509992-01
.774	6.180311-01	7.150191-01	1.849761+00	4.518930-01
.775	6.170509-01	7.137866-01	1.845071+00	4.527869-01
.776	6.160727-01	7.125569-01	1.840397+00	4.536808-01
.777	6.150965-01	7.113301-01	1.835740+00	4.545747-01
.778	6.141223-01	7.101061-01	1.831099+00	4.554687-01
.779	6.131501-01	7.088849-01	1.826475+00	4.563628-01
.780	6.121798-01	7.076665-01	1.821866+00	4.572569-01
.781	6.112115-01	7.064508-01	1.817274+00	4.581510-01
.782	6.102451-01	7.052380-01	1.812697+00	4.590451-01
.783	6.092808-01	7.040279-01	1.808136+00	4.599394-01
.784	6.083183-01	7.028206-01	1.803591+00	4.608336-01
.785	6.073578-01	7.016160-01	1.799062+00	4.617279-01
.786	6.063993-01	7.004142-01	1.794549+00	4.626222-01
.787	6.054427-01	6.992150-01	1.790051+00	4.635165-01
.788	6.044880-01	6.980186-01	1.785569+00	4.644109-01
.789	6.035352-01	6.968250-01	1.781102+00	4.653053-01
.790	6.025844-01	6.956340-01	1.776650+00	4.661997-01
.791	6.016354-01	6.944457-01	1.772214+00	4.670941-01
.792	6.006884-01	6.932601-01	1.767793+00	4.679886-01
.793	5.997433-01	6.920772-01	1.763387+00	4.688830-01
.794	5.988001-01	6.908970-01	1.758997+00	4.697775-01
.795	5.978587-01	6.897195-01	1.754621+00	4.706720-01
.796	5.969193-01	6.885445-01	1.750260+00	4.715665-01
.797	5.959817-01	6.873723-01	1.745914+00	4.724610-01
.798	5.950460-01	6.862026-01	1.741583+00	4.733555-01
.799	5.941122-01	6.850356-01	1.737267+00	4.742500-01
.800	5.931802-01	6.838713-01	1.732966+00	4.751445-01

X	K1/3(X)	K2/3(X)	K5/3(X)	G
.801	5.922501-01	6.827095-01	1.728679+00	4.760390-01
.802	5.913219-01	6.815503-01	1.724406+00	4.769336-01
.803	5.903955-01	6.803938-01	1.720149+00	4.778281-01
.804	5.894709-01	6.792398-01	1.715905+00	4.787226-01
.805	5.885482-01	6.780884-01	1.711676+00	4.796170-01
.806	5.876273-01	6.769395-01	1.707461+00	4.805115-01
.807	5.867083-01	6.757933-01	1.703261+00	4.814060-01
.808	5.857911-01	6.746496-01	1.699074+00	4.823004-01
.809	5.848757-01	6.735084-01	1.694902+00	4.831948-01
.810	5.839621-01	6.723698-01	1.690744+00	4.840893-01
.811	5.830503-01	6.712337-01	1.686599+00	4.849836-01
.812	5.821403-01	6.701001-01	1.682469+00	4.858780-01
.813	5.812322-01	6.689691-01	1.678352+00	4.867723-01
.814	5.803258-01	6.678406-01	1.674250+00	4.876666-01
.815	5.794212-01	6.667145-01	1.670161+00	4.885609-01
.816	5.785184-01	6.655910-01	1.666085+00	4.894551-01
.817	5.776173-01	6.644699-01	1.662024+00	4.903493-01
.818	5.767181-01	6.633513-01	1.657975+00	4.912435-01
.819	5.758206-01	6.622352-01	1.653941+00	4.921376-01
.820	5.749249-01	6.611216-01	1.649919+00	4.930317-01
.821	5.740309-01	6.600104-01	1.645911+00	4.939257-01
.822	5.731388-01	6.589016-01	1.641917+00	4.948197-01
.823	5.722483-01	6.577953-01	1.637935+00	4.957137-01
.824	5.713596-01	6.566914-01	1.633967+00	4.966076-01
.825	5.704727-01	6.555900-01	1.630012+00	4.975014-01
.826	5.695875-01	6.544910-01	1.626070+00	4.983952-01
.827	5.687040-01	6.533943-01	1.622141+00	4.992889-01
.828	5.678222-01	6.523001-01	1.618225+00	5.001826-01
.829	5.669422-01	6.512083-01	1.614322+00	5.010762-01
.830	5.660639-01	6.501188-01	1.610431+00	5.019698-01
.831	5.651873-01	6.490318-01	1.606554+00	5.028633-01
.832	5.643124-01	6.479471-01	1.602689+00	5.037567-01
.833	5.634392-01	6.468648-01	1.598837+00	5.046501-01
.834	5.625677-01	6.457848-01	1.594997+00	5.055434-01
.835	5.616979-01	6.447072-01	1.591171+00	5.064366-01
.836	5.608298-01	6.436320-01	1.587356+00	5.073297-01
.837	5.599634-01	6.425590-01	1.583554+00	5.082228-01
.838	5.590987-01	6.414884-01	1.579764+00	5.091158-01
.839	5.582357-01	6.404201-01	1.575987+00	5.100087-01
.840	5.573743-01	6.393542-01	1.572222+00	5.109015-01

X	K1/3(X)	K2/3(X)	K5/3(X)	G
.841	5.565146-01	6.382905-01	1.568469+00	5.117943-01
.842	5.556566-01	6.372292-01	1.564729+00	5.126869-01
.843	5.548002-01	6.361702-01	1.561001+00	5.135795-01
.844	5.539455-01	6.351134-01	1.557284+00	5.144720-01
.845	5.530924-01	6.340589-01	1.553580+00	5.153644-01
.846	5.522410-01	6.330067-01	1.549888+00	5.162567-01
.847	5.513912-01	6.319568-01	1.546207+00	5.171489-01
.848	5.505431-01	6.309091-01	1.542539+00	5.180409-01
.849	5.496966-01	6.298637-01	1.538882+00	5.189329-01
.850	5.488517-01	6.288206-01	1.535237+00	5.198249-01
.851	5.480085-01	6.277796-01	1.531604+00	5.207166-01
.852	5.471668-01	6.267409-01	1.527982+00	5.216083-01
.853	5.463268-01	6.257045-01	1.524372+00	5.224999-01
.854	5.454884-01	6.246702-01	1.520774+00	5.233914-01
.855	5.446517-01	6.236382-01	1.517187+00	5.242828-01
.856	5.438165-01	6.226084-01	1.513611+00	5.251740-01
.857	5.429829-01	6.215808-01	1.510048+00	5.260651-01
.858	5.421509-01	6.205553-01	1.506495+00	5.269562-01
.859	5.413206-01	6.195321-01	1.502954+00	5.278471-01
.860	5.404918-01	6.185111-01	1.499424+00	5.287378-01
.861	5.396645-01	6.174922-01	1.495905+00	5.296285-01
.862	5.388389-01	6.164755-01	1.492397+00	5.305190-01
.863	5.380149-01	6.154610-01	1.488901+00	5.314094-01
.864	5.371924-01	6.144486-01	1.485416+00	5.322997-01
.865	5.363714-01	6.134384-01	1.481941+00	5.331899-01
.866	5.355521-01	6.124303-01	1.478478+00	5.340799-01
.867	5.347343-01	6.114243-01	1.475026+00	5.349697-01
.868	5.339181-01	6.104205-01	1.471584+00	5.358595-01
.869	5.331034-01	6.094188-01	1.468153+00	5.367491-01
.870	5.322903-01	6.084193-01	1.464734+00	5.376385-01
.871	5.314787-01	6.074218-01	1.461325+00	5.385279-01
.872	5.306686-01	6.064264-01	1.457926+00	5.394171-01
.873	5.298601-01	6.054332-01	1.454539+00	5.403061-01
.874	5.290531-01	6.044421-01	1.451162+00	5.411950-01
.875	5.282477-01	6.034530-01	1.447795+00	5.420837-01
.876	5.274437-01	6.024660-01	1.444439+00	5.429723-01
.877	5.266413-01	6.014811-01	1.441094+00	5.438607-01
.878	5.258405-01	6.004983-01	1.437759+00	5.447490-01
.879	5.250411-01	5.995175-01	1.434434+00	5.456371-01
.880	5.242432-01	5.985388-01	1.431120+00	5.465251-01

X	K1/3(X)	K2/3(X)	K5/3(X)	G
.881	5.234469-01	5.975621-01	1.427816+00	5.474129-01
.882	5.226520-01	5.965875-01	1.424523+00	5.483006-01
.883	5.218586-01	5.956149-01	1.421239+00	5.491880-01
.884	5.210667-01	5.946444-01	1.417966+00	5.500754-01
.885	5.202764-01	5.936759-01	1.414703+00	5.509625-01
.886	5.194875-01	5.927094-01	1.411451+00	5.518495-01
.887	5.187000-01	5.917450-01	1.408208+00	5.527363-01
.888	5.179141-01	5.907825-01	1.404975+00	5.536229-01
.889	5.171297-01	5.898221-01	1.401752+00	5.545094-01
.890	5.163467-01	5.888636-01	1.398539+00	5.553957-01
.891	5.155652-01	5.879072-01	1.395337+00	5.562818-01
.892	5.147851-01	5.869527-01	1.392143+00	5.571677-01
.893	5.140065-01	5.860003-01	1.388960+00	5.580534-01
.894	5.132294-01	5.850498-01	1.385787+00	5.589390-01
.895	5.124537-01	5.841013-01	1.382623+00	5.598244-01
.896	5.116794-01	5.831547-01	1.379469+00	5.607095-01
.897	5.109067-01	5.822101-01	1.376325+00	5.615945-01
.898	5.101353-01	5.812675-01	1.373190+00	5.624793-01
.899	5.093654-01	5.803268-01	1.370065+00	5.633639-01
.900	5.085969-01	5.793880-01	1.366950+00	5.642484-01
.901	5.078299-01	5.784512-01	1.363844+00	5.651326-01
.902	5.070643-01	5.775164-01	1.360747+00	5.660166-01
.903	5.063001-01	5.765834-01	1.357660+00	5.669004-01
.904	5.055373-01	5.756524-01	1.354582+00	5.677841-01
.905	5.047760-01	5.747233-01	1.351514+00	5.686675-01
.906	5.040160-01	5.737961-01	1.348455+00	5.695507-01
.907	5.032575-01	5.728708-01	1.345405+00	5.704337-01
.908	5.025004-01	5.719474-01	1.342364+00	5.713165-01
.909	5.017447-01	5.710260-01	1.339333+00	5.721991-01
.910	5.009903-01	5.701064-01	1.336311+00	5.730815-01
.911	5.002374-01	5.691887-01	1.333298+00	5.739637-01
.912	4.994859-01	5.682728-01	1.330294+00	5.748456-01
.913	4.987357-01	5.673589-01	1.327299+00	5.757274-01
.914	4.979870-01	5.664468-01	1.324313+00	5.766089-01
.915	4.972396-01	5.655366-01	1.321337+00	5.774902-01
.916	4.964936-01	5.646282-01	1.318369+00	5.783712-01
.917	4.957490-01	5.637217-01	1.315410+00	5.792521-01
.918	4.950058-01	5.628171-01	1.312460+00	5.801327-01
.919	4.942639-01	5.619143-01	1.309519+00	5.810131-01
.920	4.935234-01	5.610133-01	1.306586+00	5.818933-01

X	K1/3(X)	K2/3(X)	K5/3(X)	G
.921	4.927843-01	5.601141-01	1.303662+00	5.827732-01
.922	4.920465-01	5.592168-01	1.300748+00	5.836529-01
.923	4.913100-01	5.583213-01	1.297841+00	5.845324-01
.924	4.905750-01	5.574277-01	1.294944+00	5.854117-01
.925	4.898412-01	5.565358-01	1.292055+00	5.862906-01
.926	4.891089-01	5.556458-01	1.289175+00	5.871694-01
.927	4.883778-01	5.547575-01	1.286303+00	5.880479-01
.928	4.876481-01	5.538711-01	1.283440+00	5.889262-01
.929	4.869197-01	5.529864-01	1.280585+00	5.898042-01
.930	4.861927-01	5.521036-01	1.277739+00	5.906820-01
.931	4.854670-01	5.512225-01	1.274901+00	5.915596-01
.932	4.847426-01	5.503432-01	1.272072+00	5.924369-01
.933	4.840196-01	5.494657-01	1.269251+00	5.933139-01
.934	4.832978-01	5.485899-01	1.266438+00	5.941907-01
.935	4.825774-01	5.477160-01	1.263634+00	5.950673-01
.936	4.818583-01	5.468437-01	1.260838+00	5.959435-01
.937	4.811405-01	5.459733-01	1.258050+00	5.968196-01
.938	4.804241-01	5.451045-01	1.255271+00	5.976953-01
.939	4.797089-01	5.442376-01	1.252499+00	5.985708-01
.940	4.789950-01	5.433723-01	1.249736+00	5.994461-01
.941	4.782824-01	5.425088-01	1.246981+00	6.003211-01
.942	4.775711-01	5.416471-01	1.244234+00	6.011958-01
.943	4.768611-01	5.407870-01	1.241495+00	6.020702-01
.944	4.761524-01	5.399287-01	1.238764+00	6.029444-01
.945	4.754450-01	5.390721-01	1.236041+00	6.038183-01
.946	4.747389-01	5.382172-01	1.233325+00	6.046920-01
.947	4.740340-01	5.373640-01	1.230618+00	6.055653-01
.948	4.733304-01	5.365126-01	1.227919+00	6.064384-01
.949	4.726281-01	5.356628-01	1.225228+00	6.073113-01
.950	4.719271-01	5.348147-01	1.222544+00	6.081838-01
.951	4.712273-01	5.339683-01	1.219868+00	6.090561-01
.952	4.705288-01	5.331236-01	1.217201+00	6.099280-01
.953	4.698316-01	5.322806-01	1.214540+00	6.107997-01
.954	4.691356-01	5.314392-01	1.211888+00	6.116712-01
.955	4.684409-01	5.305996-01	1.209243+00	6.125423-01
.956	4.677474-01	5.297616-01	1.206606+00	6.134131-01
.957	4.670551-01	5.289252-01	1.203976+00	6.142837-01
.958	4.663642-01	5.280905-01	1.201354+00	6.151539-01
.959	4.656744-01	5.272575-01	1.198740+00	6.160239-01
.960	4.649859-01	5.264261-01	1.196133+00	6.168936-01

X	K1/3(X)	K2/3(X)	K5/3(X)	G
.961	4.642987-01	5.255964-01	1.193534+00	6.177630-01
.962	4.636126-01	5.247683-01	1.190942+00	6.186321-01
.963	4.629278-01	5.239418-01	1.188358+00	6.195009-01
.964	4.622443-01	5.231170-01	1.185781+00	6.203693-01
.965	4.615619-01	5.222938-01	1.183211+00	6.212375-01
.966	4.608808-01	5.214722-01	1.180649+00	6.221054-01
.967	4.602009-01	5.206522-01	1.178094+00	6.229730-01
.968	4.595222-01	5.198339-01	1.175547+00	6.238403-01
.969	4.588448-01	5.190172-01	1.173007+00	6.247072-01
.970	4.581685-01	5.182020-01	1.170474+00	6.255739-01
.971	4.574935-01	5.173885-01	1.167948+00	6.264402-01
.972	4.568196-01	5.165766-01	1.165430+00	6.273063-01
.973	4.561470-01	5.157663-01	1.162918+00	6.281720-01
.974	4.554756-01	5.149575-01	1.160414+00	6.290374-01
.975	4.548053-01	5.141504-01	1.157917+00	6.299025-01
.976	4.541363-01	5.133448-01	1.155427+00	6.307673-01
.977	4.534684-01	5.125408-01	1.152944+00	6.316317-01
.978	4.528018-01	5.117384-01	1.150468+00	6.324959-01
.979	4.521363-01	5.109375-01	1.147999+00	6.333597-01
.980	4.514720-01	5.101383-01	1.145538+00	6.342232-01
.981	4.508089-01	5.093405-01	1.143083+00	6.350864-01
.982	4.501470-01	5.085444-01	1.140635+00	6.359492-01
.983	4.494862-01	5.077498-01	1.138194+00	6.368117-01
.984	4.488266-01	5.069567-01	1.135760+00	6.376739-01
.985	4.481682-01	5.061652-01	1.133333+00	6.385357-01
.986	4.475110-01	5.053752-01	1.130912+00	6.393973-01
.987	4.468549-01	5.045867-01	1.128499+00	6.402584-01
.988	4.462000-01	5.037998-01	1.126092+00	6.411193-01
.989	4.455462-01	5.030145-01	1.123692+00	6.419798-01
.990	4.448936-01	5.022306-01	1.121298+00	6.428400-01
.991	4.442422-01	5.014483-01	1.118912+00	6.436998-01
.992	4.435919-01	5.006674-01	1.116532+00	6.445593-01
.993	4.429427-01	4.998881-01	1.114159+00	6.454185-01
.994	4.422947-01	4.991103-01	1.111792+00	6.462773-01
.995	4.416478-01	4.983341-01	1.109432+00	6.471357-01
.996	4.410021-01	4.975593-01	1.107079+00	6.479938-01
.997	4.403575-01	4.967860-01	1.104732+00	6.488516-01
.998	4.397141-01	4.960142-01	1.102392+00	6.497090-01
.999	4.390718-01	4.952439-01	1.100058+00	6.505661-01
1.000	4.384306-01	4.944750-01	1.097731+00	6.514228-01

X	K1/3(X)	K2/3(X)	K5/3(X)	G
1.005	4.352416-01	4.906531-01	1.086191+00	6.557010-01
1.010	4.320804-01	4.868677-01	1.074810+00	6.599702-01
1.015	4.289468-01	4.831185-01	1.063585+00	6.642303-01
1.020	4.258404-01	4.794049-01	1.052514+00	6.684809-01
1.025	4.227610-01	4.757265-01	1.041592+00	6.727220-01
1.030	4.197082-01	4.720830-01	1.030819+00	6.769535-01
1.035	4.166818-01	4.684738-01	1.020191+00	6.811750-01
1.040	4.136814-01	4.648985-01	1.009705+00	6.853866-01
1.045	4.107068-01	4.613567-01	9.993597-01	6.895879-01
1.050	4.077577-01	4.578480-01	9.891520-01	6.937789-01
1.055	4.048337-01	4.543720-01	9.790796-01	6.979594-01
1.060	4.019348-01	4.509283-01	9.691402-01	7.021294-01
1.065	3.990604-01	4.475165-01	9.593315-01	7.062884-01
1.070	3.962105-01	4.441362-01	9.496513-01	7.104365-01
1.075	3.933847-01	4.407871-01	9.400973-01	7.145735-01
1.080	3.905827-01	4.374687-01	9.306676-01	7.186992-01
1.085	3.878044-01	4.341807-01	9.213599-01	7.228136-01
1.090	3.850494-01	4.309228-01	9.121721-01	7.269164-01
1.095	3.823176-01	4.276945-01	9.031023-01	7.310075-01
1.100	3.796086-01	4.244956-01	8.941487-01	7.350868-01
1.105	3.769222-01	4.213256-01	8.853091-01	7.391541-01
1.110	3.742582-01	4.181843-01	8.765817-01	7.432094-01
1.115	3.716164-01	4.150713-01	8.679647-01	7.472524-01
1.120	3.689965-01	4.119863-01	8.594563-01	7.512832-01
1.125	3.663983-01	4.089289-01	8.510548-01	7.553014-01
1.130	3.638215-01	4.058989-01	8.427583-01	7.593070-01
1.135	3.612660-01	4.028959-01	8.345651-01	7.632998-01
1.140	3.587315-01	3.999196-01	8.264737-01	7.672797-01
1.145	3.562178-01	3.969698-01	8.184825-01	7.712467-01
1.150	3.537247-01	3.940460-01	8.105896-01	7.752006-01
1.155	3.512520-01	3.911481-01	8.027938-01	7.791412-01
1.160	3.487994-01	3.882757-01	7.950934-01	7.830685-01
1.165	3.463668-01	3.854285-01	7.874868-01	7.869824-01
1.170	3.439540-01	3.826063-01	7.799727-01	7.908826-01
1.175	3.415608-01	3.798088-01	7.725495-01	7.947692-01
1.180	3.391869-01	3.770357-01	7.652160-01	7.986420-01
1.185	3.368322-01	3.742867-01	7.579706-01	8.025010-01
1.190	3.344965-01	3.715616-01	7.508120-01	8.063459-01
1.195	3.321796-01	3.688601-01	7.437390-01	8.101766-01
1.200	3.298812-01	3.661819-01	7.367501-01	8.139931-01

X	K1/3(X)	K2/3(X)	K5/3(X)	G
1.205	3.276013-01	3.635269-01	7.298441-01	8.177953-01
1.210	3.253397-01	3.608946-01	7.230197-01	8.215831-01
1.215	3.230961-01	3.582850-01	7.162758-01	8.253564-01
1.220	3.208704-01	3.556977-01	7.096110-01	8.291150-01
1.225	3.186624-01	3.531325-01	7.030243-01	8.328590-01
1.230	3.164719-01	3.505892-01	6.965143-01	8.365881-01
1.235	3.142988-01	3.480675-01	6.900801-01	8.403023-01
1.240	3.121428-01	3.455672-01	6.837205-01	8.440015-01
1.245	3.100039-01	3.430881-01	6.774343-01	8.476858-01
1.250	3.078819-01	3.406299-01	6.712205-01	8.513547-01
1.255	3.057766-01	3.381925-01	6.650781-01	8.550085-01
1.260	3.036878-01	3.357756-01	6.590059-01	8.586468-01
1.265	3.016153-01	3.333790-01	6.530029-01	8.622698-01
1.270	2.995592-01	3.310024-01	6.470683-01	8.658772-01
1.275	2.975190-01	3.286458-01	6.412009-01	8.694691-01
1.280	2.954948-01	3.263088-01	6.353998-01	8.730453-01
1.285	2.934864-01	3.239912-01	6.296640-01	8.766058-01
1.290	2.914935-01	3.216929-01	6.239927-01	8.801504-01
1.295	2.895162-01	3.194137-01	6.183849-01	8.836791-01
1.300	2.875541-01	3.171534-01	6.128396-01	8.871919-01
1.305	2.856073-01	3.149117-01	6.073562-01	8.906887-01
1.310	2.836755-01	3.126885-01	6.019335-01	8.941694-01
1.315	2.817585-01	3.104836-01	5.965708-01	8.976339-01
1.320	2.798564-01	3.082968-01	5.912673-01	9.010821-01
1.325	2.779688-01	3.061279-01	5.860220-01	9.045140-01
1.330	2.760957-01	3.039768-01	5.808344-01	9.079296-01
1.335	2.742370-01	3.018432-01	5.757034-01	9.113287-01
1.340	2.723925-01	2.997270-01	5.706284-01	9.147113-01
1.345	2.705621-01	2.976280-01	5.656085-01	9.180774-01
1.350	2.687457-01	2.955461-01	5.606431-01	9.214268-01
1.355	2.669430-01	2.934810-01	5.557313-01	9.247595-01
1.360	2.651541-01	2.914327-01	5.508724-01	9.280756-01
1.365	2.633788-01	2.894008-01	5.460658-01	9.313748-01
1.370	2.616169-01	2.873854-01	5.413107-01	9.346573-01
1.375	2.598684-01	2.853861-01	5.366065-01	9.379228-01
1.380	2.581330-01	2.834030-01	5.319523-01	9.411714-01
1.385	2.564108-01	2.814357-01	5.273477-01	9.444030-01
1.390	2.547015-01	2.794841-01	5.227918-01	9.476175-01
1.395	2.530051-01	2.775482-01	5.182841-01	9.508149-01
1.400	2.513214-01	2.756276-01	5.138239-01	9.539952-01

X	K1/3(X)	K2/3(X)	K5/3(X)	G
1.405	2.496504-01	2.737224-01	5.094107-01	9.571583-01
1.410	2.479919-01	2.718323-01	5.050437-01	9.603042-01
1.415	2.463458-01	2.699571-01	5.007224-01	9.634328-01
1.420	2.447120-01	2.680969-01	4.964461-01	9.665441-01
1.425	2.430903-01	2.662513-01	4.922144-01	9.696380-01
1.430	2.414808-01	2.644203-01	4.880265-01	9.727146-01
1.435	2.398832-01	2.626037-01	4.838820-01	9.757738-01
1.440	2.382975-01	2.608014-01	4.797803-01	9.788154-01
1.445	2.367235-01	2.590133-01	4.757208-01	9.818396-01
1.450	2.351613-01	2.572392-01	4.717030-01	9.848462-01
1.455	2.336105-01	2.554789-01	4.677264-01	9.878352-01
1.460	2.320712-01	2.537324-01	4.637904-01	9.908067-01
1.465	2.305433-01	2.519996-01	4.598945-01	9.937604-01
1.470	2.290267-01	2.502802-01	4.560382-01	9.966966-01
1.475	2.275212-01	2.485742-01	4.522210-01	9.996150-01
1.480	2.260267-01	2.468815-01	4.484424-01	1.002516+00
1.485	2.245432-01	2.452018-01	4.447020-01	1.005399+00
1.490	2.230706-01	2.435352-01	4.409992-01	1.008264+00
1.495	2.216088-01	2.418814-01	4.373336-01	1.011111+00
1.500	2.201577-01	2.402404-01	4.337047-01	1.013941+00
1.505	2.187171-01	2.386121-01	4.301121-01	1.016753+00
1.510	2.172871-01	2.369962-01	4.265553-01	1.019546+00
1.515	2.158675-01	2.353928-01	4.230339-01	1.022322+00
1.520	2.144582-01	2.338017-01	4.195474-01	1.025080+00
1.525	2.130591-01	2.322228-01	4.160954-01	1.027821+00
1.530	2.116702-01	2.306559-01	4.126776-01	1.030543+00
1.535	2.102914-01	2.291010-01	4.092934-01	1.033247+00
1.540	2.089225-01	2.275579-01	4.059424-01	1.035933+00
1.545	2.075636-01	2.260266-01	4.026243-01	1.038601+00
1.550	2.062144-01	2.245070-01	3.993387-01	1.041251+00
1.555	2.048750-01	2.229988-01	3.960852-01	1.043884+00
1.560	2.035452-01	2.215021-01	3.928633-01	1.046498+00
1.565	2.022250-01	2.200168-01	3.896728-01	1.049094+00
1.570	2.009143-01	2.185426-01	3.865131-01	1.051672+00
1.575	1.996130-01	2.170796-01	3.833841-01	1.054232+00
1.580	1.983210-01	2.156276-01	3.802852-01	1.056774+00
1.585	1.970383-01	2.141865-01	3.772163-01	1.059298+00
1.590	1.957648-01	2.127563-01	3.741768-01	1.061803+00
1.595	1.945003-01	2.113368-01	3.711664-01	1.064291+00
1.600	1.932449-01	2.099279-01	3.681848-01	1.066760+00

X	K1/3(X)	K2/3(X)	K5/3(X)	G
1.605	1.919984-01	2.085296-01	3.652317-01	1.069212+00
1.610	1.907608-01	2.071417-01	3.623068-01	1.071645+00
1.615	1.895320-01	2.057642-01	3.594096-01	1.074060+00
1.620	1.883120-01	2.043970-01	3.565399-01	1.076457+00
1.625	1.871006-01	2.030399-01	3.536974-01	1.078836+00
1.630	1.858977-01	2.016930-01	3.508818-01	1.081197+00
1.635	1.847034-01	2.003560-01	3.480927-01	1.083540+00
1.640	1.835176-01	1.990290-01	3.453298-01	1.085864+00
1.645	1.823401-01	1.977117-01	3.425928-01	1.088171+00
1.650	1.811710-01	1.964043-01	3.398815-01	1.090459+00
1.655	1.800101-01	1.951065-01	3.371955-01	1.092729+00
1.660	1.788573-01	1.938182-01	3.345346-01	1.094982+00
1.665	1.777127-01	1.925395-01	3.318985-01	1.097216+00
1.670	1.765761-01	1.912701-01	3.292868-01	1.099432+00
1.675	1.754475-01	1.900101-01	3.266994-01	1.101630+00
1.680	1.743268-01	1.887594-01	3.241359-01	1.103809+00
1.685	1.732140-01	1.875178-01	3.215961-01	1.105971+00
1.690	1.721090-01	1.862853-01	3.190797-01	1.108115+00
1.695	1.710117-01	1.850618-01	3.165864-01	1.110240+00
1.700	1.699221-01	1.838473-01	3.141160-01	1.112348+00
1.705	1.688400-01	1.826416-01	3.116683-01	1.114438+00
1.710	1.677655-01	1.814447-01	3.092429-01	1.116509+00
1.715	1.666985-01	1.802565-01	3.068397-01	1.118563+00
1.720	1.656389-01	1.790770-01	3.044583-01	1.120598+00
1.725	1.645867-01	1.779060-01	3.020986-01	1.122616+00
1.730	1.635418-01	1.767435-01	2.997604-01	1.124615+00
1.735	1.625042-01	1.755895-01	2.974433-01	1.126597+00
1.740	1.614737-01	1.744438-01	2.951471-01	1.128561+00
1.745	1.604504-01	1.733064-01	2.928717-01	1.130507+00
1.750	1.594341-01	1.721772-01	2.906167-01	1.132435+00
1.755	1.584249-01	1.710561-01	2.883820-01	1.134345+00
1.760	1.574226-01	1.699431-01	2.861674-01	1.136237+00
1.765	1.564273-01	1.688381-01	2.839726-01	1.138111+00
1.770	1.554388-01	1.677411-01	2.817975-01	1.139967+00
1.775	1.544571-01	1.666519-01	2.796417-01	1.141806+00
1.780	1.534822-01	1.655706-01	2.775051-01	1.143627+00
1.785	1.525140-01	1.644970-01	2.753875-01	1.145430+00
1.790	1.515524-01	1.634310-01	2.732888-01	1.147216+00
1.795	1.505975-01	1.623727-01	2.712086-01	1.148983+00
1.800	1.496490-01	1.613220-01	2.691468-01	1.150733+00

X	K1/3(X)	K2/3(X)	K5/3(X)	G
1.805	1.487071-01	1.602787-01	2.671032-01	1.152465+00
1.810	1.477716-01	1.592429-01	2.650776-01	1.154180+00
1.815	1.468425-01	1.582145-01	2.630698-01	1.155877+00
1.820	1.459197-01	1.571933-01	2.610797-01	1.157557+00
1.825	1.450033-01	1.561794-01	2.591070-01	1.159218+00
1.830	1.440931-01	1.551728-01	2.571516-01	1.160863+00
1.835	1.431891-01	1.541732-01	2.552132-01	1.162489+00
1.840	1.422912-01	1.531807-01	2.532918-01	1.164099+00
1.845	1.413995-01	1.521953-01	2.513870-01	1.165690+00
1.850	1.405138-01	1.512168-01	2.494989-01	1.167265+00
1.855	1.396341-01	1.502452-01	2.476271-01	1.168822+00
1.860	1.387604-01	1.492804-01	2.457715-01	1.170361+00
1.865	1.378926-01	1.483225-01	2.439320-01	1.171883+00
1.870	1.370307-01	1.473713-01	2.421083-01	1.173388+00
1.875	1.361746-01	1.464268-01	2.403004-01	1.174876+00
1.880	1.353244-01	1.454889-01	2.385080-01	1.176346+00
1.885	1.344798-01	1.445576-01	2.367310-01	1.177799+00
1.890	1.336410-01	1.436328-01	2.349692-01	1.179235+00
1.895	1.328078-01	1.427146-01	2.332226-01	1.180654+00
1.900	1.319802-01	1.418027-01	2.314908-01	1.182056+00
1.905	1.311582-01	1.408972-01	2.297739-01	1.183440+00
1.910	1.303417-01	1.399980-01	2.280716-01	1.184808+00
1.915	1.295307-01	1.391051-01	2.263837-01	1.186158+00
1.920	1.287252-01	1.382184-01	2.247102-01	1.187491+00
1.925	1.279250-01	1.373379-01	2.230509-01	1.188808+00
1.930	1.271303-01	1.364635-01	2.214056-01	1.190107+00
1.935	1.263408-01	1.355952-01	2.197742-01	1.191390+00
1.940	1.255567-01	1.347329-01	2.181566-01	1.192656+00
1.945	1.247777-01	1.338766-01	2.165526-01	1.193905+00
1.950	1.240040-01	1.330263-01	2.149622-01	1.195137+00
1.955	1.232355-01	1.321818-01	2.133851-01	1.196352+00
1.960	1.224721-01	1.313431-01	2.118212-01	1.197551+00
1.965	1.217138-01	1.305103-01	2.102704-01	1.198733+00
1.970	1.209605-01	1.296832-01	2.087326-01	1.199898+00
1.975	1.202123-01	1.288618-01	2.072076-01	1.201047+00
1.980	1.194690-01	1.280461-01	2.056953-01	1.202179+00
1.985	1.187307-01	1.272360-01	2.041956-01	1.203295+00
1.990	1.179972-01	1.264314-01	2.027084-01	1.204394+00
1.995	1.172687-01	1.256324-01	2.012336-01	1.205477+00
2.000	1.165450-01	1.248389-01	1.997709-01	1.206544+00

X	K1/3(X)	K2/3(X)	K5/3(X)	G
2.005	1.158260-01	1.240508-01	1.983204-01	1.207594+00
2.010	1.151119-01	1.232682-01	1.968818-01	1.208627+00
2.015	1.144024-01	1.224909-01	1.954551-01	1.209645+00
2.020	1.136977-01	1.217189-01	1.940402-01	1.210646+00
2.025	1.129976-01	1.209522-01	1.926369-01	1.211631+00
2.030	1.123022-01	1.201907-01	1.912451-01	1.212600+00
2.035	1.116113-01	1.194344-01	1.898648-01	1.213553+00
2.040	1.109250-01	1.186833-01	1.884958-01	1.214490+00
2.045	1.102432-01	1.179373-01	1.871379-01	1.215410+00
2.050	1.095659-01	1.171964-01	1.857912-01	1.216315+00
2.055	1.088931-01	1.164605-01	1.844554-01	1.217204+00
2.060	1.082247-01	1.157296-01	1.831306-01	1.218077+00
2.065	1.075606-01	1.150037-01	1.818165-01	1.218934+00
2.070	1.069010-01	1.142827-01	1.805130-01	1.219775+00
2.075	1.062457-01	1.135666-01	1.792202-01	1.220601+00
2.080	1.055946-01	1.128554-01	1.779378-01	1.221411+00
2.085	1.049479-01	1.121489-01	1.766658-01	1.222205+00
2.090	1.043054-01	1.114473-01	1.754041-01	1.222984+00
2.095	1.036670-01	1.107504-01	1.741526-01	1.223747+00
2.100	1.030329-01	1.100582-01	1.729111-01	1.224494+00
2.105	1.024029-01	1.093707-01	1.716797-01	1.225226+00
2.110	1.017770-01	1.086878-01	1.704581-01	1.225943+00
2.115	1.011552-01	1.080095-01	1.692463-01	1.226644+00
2.120	1.005375-01	1.073357-01	1.680443-01	1.227330+00
2.125	9.992378-02	1.066666-01	1.668518-01	1.228000+00
2.130	9.931407-02	1.060019-01	1.656689-01	1.228656+00
2.135	9.870834-02	1.053416-01	1.644955-01	1.229296+00
2.140	9.810654-02	1.046858-01	1.633314-01	1.229921+00
2.145	9.750865-02	1.040344-01	1.621765-01	1.230531+00
2.150	9.691466-02	1.033874-01	1.610309-01	1.231125+00
2.155	9.632452-02	1.027447-01	1.598943-01	1.231705+00
2.160	9.573821-02	1.021063-01	1.587668-01	1.232270+00
2.165	9.515570-02	1.014722-01	1.576482-01	1.232820+00
2.170	9.457697-02	1.008423-01	1.565384-01	1.233355+00
2.175	9.400199-02	1.002166-01	1.554374-01	1.233875+00
2.180	9.343073-02	9.959504-02	1.543451-01	1.234381+00
2.185	9.286317-02	9.897767-02	1.532614-01	1.234872+00
2.190	9.229928-02	9.836442-02	1.521863-01	1.235348+00
2.195	9.173903-02	9.775524-02	1.511196-01	1.235810+00
2.200	9.118240-02	9.715011-02	1.500613-01	1.236257+00

X	K1/3(X)	K2/3(X)	K5/3(X)	G
2.205	9.062936-02	9.654901-02	1.490112-01	1.236689+00
2.210	9.007990-02	9.595190-02	1.479694-01	1.237107+00
2.215	8.953397-02	9.535875-02	1.469358-01	1.237511+00
2.220	8.899156-02	9.476954-02	1.459102-01	1.237900+00
2.225	8.845265-02	9.418424-02	1.448926-01	1.238275+00
2.230	8.791720-02	9.360280-02	1.438830-01	1.238636+00
2.235	8.738519-02	9.302522-02	1.428812-01	1.238982+00
2.240	8.685661-02	9.245146-02	1.418872-01	1.239315+00
2.245	8.633142-02	9.188149-02	1.409010-01	1.239633+00
2.250	8.580960-02	9.131529-02	1.399224-01	1.239937+00
2.255	8.529114-02	9.075282-02	1.389514-01	1.240228+00
2.260	8.477599-02	9.019407-02	1.379878-01	1.240504+00
2.265	8.426415-02	8.963900-02	1.370318-01	1.240766+00
2.270	8.375558-02	8.908758-02	1.360831-01	1.241015+00
2.275	8.325027-02	8.853979-02	1.351417-01	1.241250+00
2.280	8.274820-02	8.799561-02	1.342076-01	1.241471+00
2.285	8.224934-02	8.745501-02	1.332807-01	1.241678+00
2.290	8.175366-02	8.691795-02	1.323609-01	1.241872+00
2.295	8.126115-02	8.638443-02	1.314482-01	1.242052+00
2.300	8.077178-02	8.585440-02	1.305424-01	1.242219+00
2.305	8.028553-02	8.532785-02	1.296437-01	1.242372+00
2.310	7.980239-02	8.480474-02	1.287517-01	1.242512+00
2.315	7.932233-02	8.428507-02	1.278666-01	1.242638+00
2.320	7.884532-02	8.376879-02	1.269883-01	1.242751+00
2.325	7.837135-02	8.325589-02	1.261167-01	1.242851+00
2.330	7.790039-02	8.274634-02	1.252517-01	1.242937+00
2.335	7.743243-02	8.224012-02	1.243932-01	1.243011+00
2.340	7.696745-02	8.173721-02	1.235414-01	1.243071+00
2.345	7.650542-02	8.123757-02	1.226959-01	1.243118+00
2.350	7.604632-02	8.074119-02	1.218569-01	1.243153+00
2.355	7.559013-02	8.024805-02	1.210243-01	1.243174+00
2.360	7.513683-02	7.975811-02	1.201979-01	1.243182+00
2.365	7.468641-02	7.927136-02	1.193778-01	1.243178+00
2.370	7.423885-02	7.878778-02	1.185639-01	1.243161+00
2.375	7.379412-02	7.830734-02	1.177561-01	1.243131+00
2.380	7.335220-02	7.783002-02	1.169545-01	1.243088+00
2.385	7.291308-02	7.735580-02	1.161588-01	1.243033+00
2.390	7.247673-02	7.688466-02	1.153692-01	1.242965+00
2.395	7.204314-02	7.641657-02	1.145854-01	1.242885+00
2.400	7.161229-02	7.595151-02	1.138076-01	1.242792+00

X	K1/3(X)	K2/3(X)	K5/3(X)	G
2.405	7.118416-02	7.548946-02	1.130356-01	1.242687+00
2.410	7.075873-02	7.503040-02	1.122693-01	1.242570+00
2.415	7.033598-02	7.457431-02	1.115088-01	1.242440+00
2.420	6.991590-02	7.412117-02	1.107540-01	1.242298+00
2.425	6.949846-02	7.367096-02	1.100048-01	1.242144+00
2.430	6.908365-02	7.322365-02	1.092612-01	1.241977+00
2.435	6.867145-02	7.277922-02	1.085232-01	1.241799+00
2.440	6.826185-02	7.233767-02	1.077906-01	1.241609+00
2.445	6.785481-02	7.189896-02	1.070635-01	1.241406+00
2.450	6.745034-02	7.146307-02	1.063418-01	1.241192+00
2.455	6.704841-02	7.102999-02	1.056255-01	1.240966+00
2.460	6.664900-02	7.059969-02	1.049144-01	1.240728+00
2.465	6.625209-02	7.017216-02	1.042086-01	1.240478+00
2.470	6.585768-02	6.974738-02	1.035081-01	1.240217+00
2.475	6.546574-02	6.932533-02	1.028127-01	1.239944+00
2.480	6.507625-02	6.890598-02	1.021225-01	1.239659+00
2.485	6.468921-02	6.848933-02	1.014373-01	1.239363+00
2.490	6.430458-02	6.807535-02	1.007572-01	1.239055+00
2.495	6.392236-02	6.766402-02	1.000822-01	1.238736+00
2.500	6.354253-02	6.725532-02	9.941204-02	1.238406+00
2.505	6.316508-02	6.684924-02	9.874685-02	1.238064+00
2.510	6.278998-02	6.644575-02	9.808654-02	1.237711+00
2.515	6.241723-02	6.604485-02	9.743107-02	1.237347+00
2.520	6.204680-02	6.564650-02	9.678040-02	1.236971+00
2.525	6.167869-02	6.525070-02	9.613451-02	1.236585+00
2.530	6.131287-02	6.485743-02	9.549333-02	1.236187+00
2.535	6.094933-02	6.446667-02	9.485684-02	1.235779+00
2.540	6.058805-02	6.407840-02	9.422501-02	1.235359+00
2.545	6.022903-02	6.369260-02	9.359778-02	1.234929+00
2.550	5.987224-02	6.330925-02	9.297511-02	1.234487+00
2.555	5.951767-02	6.292835-02	9.235699-02	1.234035+00
2.560	5.916530-02	6.254988-02	9.174336-02	1.233573+00
2.565	5.881512-02	6.217381-02	9.113419-02	1.233100+00
2.570	5.846712-02	6.180013-02	9.052944-02	1.232616+00
2.575	5.812128-02	6.142882-02	8.992909-02	1.232121+00
2.580	5.777759-02	6.105987-02	8.933308-02	1.231616+00
2.585	5.743603-02	6.069326-02	8.874139-02	1.231101+00
2.590	5.709659-02	6.032897-02	8.815398-02	1.230575+00
2.595	5.675926-02	5.996700-02	8.757082-02	1.230038+00
2.600	5.642401-02	5.960732-02	8.699187-02	1.229492+00

X	K1/3(X)	K2/3(X)	K5/3(X)	G
2.605	5.609084-02	5.924992-02	8.641709-02	1.228935+00
2.610	5.575973-02	5.889477-02	8.584646-02	1.228368+00
2.615	5.543067-02	5.854188-02	8.527994-02	1.227791+00
2.620	5.510365-02	5.819122-02	8.471750-02	1.227204+00
2.625	5.477865-02	5.784277-02	8.415911-02	1.226607+00
2.630	5.445566-02	5.749653-02	8.360472-02	1.226000+00
2.635	5.413466-02	5.715247-02	8.305431-02	1.225383+00
2.640	5.381565-02	5.681058-02	8.250786-02	1.224756+00
2.645	5.349860-02	5.647084-02	8.196531-02	1.224119+00
2.650	5.318351-02	5.613325-02	8.142665-02	1.223473+00
2.655	5.287037-02	5.579779-02	8.089185-02	1.222817+00
2.660	5.255915-02	5.546444-02	8.036087-02	1.222151+00
2.665	5.224986-02	5.513318-02	7.983369-02	1.221476+00
2.670	5.194247-02	5.480401-02	7.931026-02	1.220791+00
2.675	5.163696-02	5.447691-02	7.879057-02	1.220096+00
2.680	5.133335-02	5.415187-02	7.827458-02	1.219393+00
2.685	5.103160-02	5.382887-02	7.776226-02	1.218679+00
2.690	5.073170-02	5.350790-02	7.725358-02	1.217957+00
2.695	5.043365-02	5.318894-02	7.674852-02	1.217225+00
2.700	5.013743-02	5.287198-02	7.624705-02	1.216484+00
2.705	4.984302-02	5.255701-02	7.574913-02	1.215734+00
2.710	4.955043-02	5.224401-02	7.525474-02	1.214975+00
2.715	4.925964-02	5.193298-02	7.476386-02	1.214206+00
2.720	4.897062-02	5.162389-02	7.427645-02	1.213429+00
2.725	4.868338-02	5.131674-02	7.379249-02	1.212643+00
2.730	4.839790-02	5.101151-02	7.331194-02	1.211847+00
2.735	4.811416-02	5.070819-02	7.283479-02	1.211043+00
2.740	4.783217-02	5.040676-02	7.236100-02	1.210230+00
2.745	4.755190-02	5.010722-02	7.189056-02	1.209409+00
2.750	4.727335-02	4.980954-02	7.142343-02	1.208578+00
2.755	4.699650-02	4.951373-02	7.095959-02	1.207739+00
2.760	4.672135-02	4.921976-02	7.049901-02	1.206892+00
2.765	4.644788-02	4.892762-02	7.004167-02	1.206036+00
2.770	4.617607-02	4.863731-02	6.958753-02	1.205171+00
2.775	4.590593-02	4.834880-02	6.913659-02	1.204298+00
2.780	4.563744-02	4.806209-02	6.868880-02	1.203417+00
2.785	4.537059-02	4.777717-02	6.824415-02	1.202527+00
2.790	4.510536-02	4.749401-02	6.780262-02	1.201629+00
2.795	4.484175-02	4.721262-02	6.736417-02	1.200722+00
2.800	4.457975-02	4.693298-02	6.692879-02	1.199808+00

X	K1/3(X)	K2/3(X)	K5/3(X)	G
2.805	4.431935-02	4.665508-02	6.649645-02	1.198885+00
2.810	4.406053-02	4.637890-02	6.606712-02	1.197955+00
2.815	4.380329-02	4.610443-02	6.564079-02	1.197016+00
2.820	4.354762-02	4.583167-02	6.521744-02	1.196069+00
2.825	4.329350-02	4.556060-02	6.479702-02	1.195115+00
2.830	4.304092-02	4.529122-02	6.437954-02	1.194152+00
2.835	4.278988-02	4.502350-02	6.396495-02	1.193182+00
2.840	4.254037-02	4.475744-02	6.355325-02	1.192203+00
2.845	4.229238-02	4.449303-02	6.314440-02	1.191218+00
2.850	4.204589-02	4.423025-02	6.273840-02	1.190224+00
2.855	4.180090-02	4.396910-02	6.233521-02	1.189223+00
2.860	4.155739-02	4.370957-02	6.193481-02	1.188214+00
2.865	4.131536-02	4.345164-02	6.153718-02	1.187198+00
2.870	4.107480-02	4.319530-02	6.114230-02	1.186174+00
2.875	4.083570-02	4.294055-02	6.075016-02	1.185143+00
2.880	4.059805-02	4.268737-02	6.036072-02	1.184104+00
2.885	4.036183-02	4.243575-02	5.997397-02	1.183059+00
2.890	4.012705-02	4.218569-02	5.958988-02	1.182005+00
2.895	3.989369-02	4.193716-02	5.920844-02	1.180945+00
2.900	3.966174-02	4.169017-02	5.882964-02	1.179877+00
2.905	3.943120-02	4.144470-02	5.845344-02	1.178803+00
2.910	3.920205-02	4.120075-02	5.807982-02	1.177721+00
2.915	3.897428-02	4.095829-02	5.770877-02	1.176632+00
2.920	3.874790-02	4.071733-02	5.734028-02	1.175536+00
2.925	3.852287-02	4.047785-02	5.697431-02	1.174433+00
2.930	3.829921-02	4.023984-02	5.661085-02	1.173324+00
2.935	3.807690-02	4.000329-02	5.624989-02	1.172207+00
2.940	3.785593-02	3.976820-02	5.589139-02	1.171084+00
2.945	3.763629-02	3.953455-02	5.553536-02	1.169954+00
2.950	3.741799-02	3.930234-02	5.518175-02	1.168817+00
2.955	3.720099-02	3.907155-02	5.483057-02	1.167674+00
2.960	3.698530-02	3.884218-02	5.448178-02	1.166524+00
2.965	3.677091-02	3.861421-02	5.413537-02	1.165367+00
2.970	3.655782-02	3.838764-02	5.379133-02	1.164204+00
2.975	3.634601-02	3.816246-02	5.344963-02	1.163034+00
2.980	3.613547-02	3.793866-02	5.311026-02	1.161858+00
2.985	3.592620-02	3.771623-02	5.277320-02	1.160676+00
2.990	3.571818-02	3.749516-02	5.243843-02	1.159487+00
2.995	3.551142-02	3.727545-02	5.210594-02	1.158293+00
3.000	3.530590-02	3.705707-02	5.177571-02	1.157091+00

X	K1/3(X)	K2/3(X)	K5/3(X)	G
3.005	3.510162-02	3.684004-02	5.144772-02	1.155884+00
3.010	3.489856-02	3.662432-02	5.112196-02	1.154670+00
3.015	3.469673-02	3.640993-02	5.079841-02	1.153451+00
3.020	3.449610-02	3.619684-02	5.047704-02	1.152225+00
3.025	3.429668-02	3.598506-02	5.015786-02	1.150994+00
3.030	3.409846-02	3.577457-02	4.984084-02	1.149756+00
3.035	3.390142-02	3.556536-02	4.952596-02	1.148513+00
3.040	3.370557-02	3.535743-02	4.921321-02	1.147263+00
3.045	3.351089-02	3.515077-02	4.890257-02	1.146008+00
3.050	3.331737-02	3.494536-02	4.859403-02	1.144747+00
3.055	3.312502-02	3.474120-02	4.828757-02	1.143481+00
3.060	3.293381-02	3.453829-02	4.798318-02	1.142208+00
3.065	3.274376-02	3.433662-02	4.768084-02	1.140930+00
3.070	3.255484-02	3.413617-02	4.738053-02	1.139647+00
3.075	3.236705-02	3.393694-02	4.708225-02	1.138358+00
3.080	3.218038-02	3.373892-02	4.678597-02	1.137063+00
3.085	3.199483-02	3.354210-02	4.649168-02	1.135763+00
3.090	3.181038-02	3.334648-02	4.619937-02	1.134457+00
3.095	3.162704-02	3.315205-02	4.590902-02	1.133147+00
3.100	3.144480-02	3.295880-02	4.562063-02	1.131830+00
3.105	3.126364-02	3.276672-02	4.533416-02	1.130509+00
3.110	3.108357-02	3.257581-02	4.504961-02	1.129182+00
3.115	3.090457-02	3.238605-02	4.476697-02	1.127850+00
3.120	3.072663-02	3.219745-02	4.448622-02	1.126513+00
3.125	3.054976-02	3.200999-02	4.420735-02	1.125171+00
3.130	3.037394-02	3.182366-02	4.393035-02	1.123824+00
3.135	3.019918-02	3.163846-02	4.365519-02	1.122472+00
3.140	3.002545-02	3.145439-02	4.338187-02	1.121115+00
3.145	2.985275-02	3.127142-02	4.311038-02	1.119752+00
3.150	2.968109-02	3.108957-02	4.284069-02	1.118385+00
3.155	2.951045-02	3.090881-02	4.257281-02	1.117013+00
3.160	2.934082-02	3.072915-02	4.230671-02	1.115637+00
3.165	2.917221-02	3.055057-02	4.204238-02	1.114255+00
3.170	2.900459-02	3.037308-02	4.177981-02	1.112869+00
3.175	2.883797-02	3.019665-02	4.151898-02	1.111478+00
3.180	2.867235-02	3.002129-02	4.125989-02	1.110083+00
3.185	2.850770-02	2.984699-02	4.100252-02	1.108683+00
3.190	2.834404-02	2.967374-02	4.074685-02	1.107278+00
3.195	2.818135-02	2.950153-02	4.049289-02	1.105869+00
3.200	2.801962-02	2.933036-02	4.024060-02	1.104455+00

X	K1/3(X)	K2/3(X)	K5/3(X)	G
3.205	2.785885-02	2.916023-02	3.998999-02	1.103037+00
3.210	2.769904-02	2.899112-02	3.974104-02	1.101614+00
3.215	2.754018-02	2.882302-02	3.949374-02	1.100188+00
3.220	2.738226-02	2.865594-02	3.924807-02	1.098756+00
3.225	2.722527-02	2.848987-02	3.900403-02	1.097321+00
3.230	2.706922-02	2.832480-02	3.876160-02	1.095881+00
3.235	2.691408-02	2.816071-02	3.852076-02	1.094438+00
3.240	2.675987-02	2.799762-02	3.828153-02	1.092990+00
3.245	2.660658-02	2.783550-02	3.804386-02	1.091537+00
3.250	2.645419-02	2.767436-02	3.780777-02	1.090081+00
3.255	2.630270-02	2.751419-02	3.757323-02	1.088621+00
3.260	2.615211-02	2.735498-02	3.734024-02	1.087157+00
3.265	2.600241-02	2.719673-02	3.710878-02	1.085689+00
3.270	2.585359-02	2.703942-02	3.687884-02	1.084217+00
3.275	2.570566-02	2.688306-02	3.665041-02	1.082741+00
3.280	2.555859-02	2.672764-02	3.642349-02	1.081261+00
3.285	2.541240-02	2.657315-02	3.619806-02	1.079777+00
3.290	2.526708-02	2.641959-02	3.597410-02	1.078290+00
3.295	2.512261-02	2.626695-02	3.575162-02	1.076799+00
3.300	2.497899-02	2.611521-02	3.553059-02	1.075304+00
3.305	2.483622-02	2.596439-02	3.531101-02	1.073806+00
3.310	2.469429-02	2.581448-02	3.509287-02	1.072304+00
3.315	2.455321-02	2.566546-02	3.487616-02	1.070798+00
3.320	2.441295-02	2.551733-02	3.466087-02	1.069289+00
3.325	2.427352-02	2.537009-02	3.444699-02	1.067777+00
3.330	2.413491-02	2.522372-02	3.423450-02	1.066261+00
3.335	2.399712-02	2.507824-02	3.402340-02	1.064741+00
3.340	2.386014-02	2.493362-02	3.381368-02	1.063218+00
3.345	2.372397-02	2.478987-02	3.360533-02	1.061692+00
3.350	2.358860-02	2.464697-02	3.339834-02	1.060163+00
3.355	2.345403-02	2.450493-02	3.319270-02	1.058630+00
3.360	2.332025-02	2.436374-02	3.298840-02	1.057094+00
3.365	2.318725-02	2.422338-02	3.278542-02	1.055555+00
3.370	2.305504-02	2.408387-02	3.258377-02	1.054012+00
3.375	2.292361-02	2.394519-02	3.238344-02	1.052467+00
3.380	2.279295-02	2.380733-02	3.218440-02	1.050918+00
3.385	2.266306-02	2.367030-02	3.198666-02	1.049367+00
3.390	2.253393-02	2.353408-02	3.179020-02	1.047812+00
3.395	2.240556-02	2.339868-02	3.159502-02	1.046255+00
3.400	2.227794-02	2.326408-02	3.140111-02	1.044694+00

X	K1/3(X)	K2/3(X)	K5/3(X)	G
3.405	2.215107-02	2.313028-02	3.120845-02	1.043131+00
3.410	2.202495-02	2.299728-02	3.101704-02	1.041564+00
3.415	2.189957-02	2.286507-02	3.082688-02	1.039995+00
3.420	2.177492-02	2.273365-02	3.063794-02	1.038423+00
3.425	2.165101-02	2.260300-02	3.045023-02	1.036848+00
3.430	2.152782-02	2.247314-02	3.026373-02	1.035271+00
3.435	2.140535-02	2.234404-02	3.007844-02	1.033691+00
3.440	2.128361-02	2.221572-02	2.989435-02	1.032108+00
3.445	2.116257-02	2.208815-02	2.971144-02	1.030522+00
3.450	2.104225-02	2.196135-02	2.952972-02	1.028934+00
3.455	2.092263-02	2.183529-02	2.934917-02	1.027344+00
3.460	2.080371-02	2.170998-02	2.916979-02	1.025751+00
3.465	2.068548-02	2.158542-02	2.899156-02	1.024155+00
3.470	2.056795-02	2.146160-02	2.881448-02	1.022557+00
3.475	2.045111-02	2.133851-02	2.863854-02	1.020956+00
3.480	2.033495-02	2.121615-02	2.846374-02	1.019353+00
3.485	2.021947-02	2.109451-02	2.829006-02	1.017748+00
3.490	2.010466-02	2.097360-02	2.811750-02	1.016140+00
3.495	1.999053-02	2.085340-02	2.794604-02	1.014530+00
3.500	1.987706-02	2.073391-02	2.777569-02	1.012918+00
3.505	1.976426-02	2.061514-02	2.760644-02	1.011304+00
3.510	1.965211-02	2.049706-02	2.743827-02	1.009687+00
3.515	1.954062-02	2.037968-02	2.727118-02	1.008068+00
3.520	1.942978-02	2.026300-02	2.710516-02	1.006447+00
3.525	1.931959-02	2.014701-02	2.694021-02	1.004824+00
3.530	1.921004-02	2.003170-02	2.677631-02	1.003199+00
3.535	1.910113-02	1.991707-02	2.661347-02	1.001572+00
3.540	1.899286-02	1.980312-02	2.645166-02	9.999426-01
3.545	1.888522-02	1.968985-02	2.629089-02	9.983115-01
3.550	1.877820-02	1.957724-02	2.613116-02	9.966784-01
3.555	1.867181-02	1.946530-02	2.597244-02	9.950433-01
3.560	1.856604-02	1.935402-02	2.581474-02	9.934065-01
3.565	1.846089-02	1.924340-02	2.565804-02	9.917677-01
3.570	1.835634-02	1.913342-02	2.550235-02	9.901271-01
3.575	1.825241-02	1.902410-02	2.534765-02	9.884847-01
3.580	1.814908-02	1.891542-02	2.519393-02	9.868405-01
3.585	1.804636-02	1.880738-02	2.504120-02	9.851947-01
3.590	1.794423-02	1.869998-02	2.488944-02	9.835471-01
3.595	1.784269-02	1.859321-02	2.473865-02	9.818978-01
3.600	1.774175-02	1.848708-02	2.458881-02	9.802469-01

X	K1/3(X)	K2/3(X)	K5/3(X)	G
3.605	1.764139-02	1.838156-02	2.443994-02	9.785944-01
3.610	1.754162-02	1.827667-02	2.429201-02	9.769403-01
3.615	1.744243-02	1.817239-02	2.414502-02	9.752846-01
3.620	1.734381-02	1.806873-02	2.399896-02	9.736275-01
3.625	1.724577-02	1.796568-02	2.385383-02	9.719688-01
3.630	1.714830-02	1.786323-02	2.370963-02	9.703086-01
3.635	1.705139-02	1.776139-02	2.356634-02	9.686470-01
3.640	1.695505-02	1.766014-02	2.342396-02	9.669840-01
3.645	1.685926-02	1.755949-02	2.328248-02	9.653196-01
3.650	1.676403-02	1.745943-02	2.314190-02	9.636539-01
3.655	1.666936-02	1.735996-02	2.300222-02	9.619868-01
3.660	1.657523-02	1.726107-02	2.286341-02	9.603185-01
3.665	1.648165-02	1.716276-02	2.272549-02	9.586489-01
3.670	1.638861-02	1.706503-02	2.258844-02	9.569780-01
3.675	1.629611-02	1.696788-02	2.245226-02	9.553059-01
3.680	1.620415-02	1.687129-02	2.231693-02	9.536327-01
3.685	1.611272-02	1.677527-02	2.218247-02	9.519583-01
3.690	1.602182-02	1.667981-02	2.204885-02	9.502827-01
3.695	1.593145-02	1.658492-02	2.191608-02	9.486060-01
3.700	1.584160-02	1.649058-02	2.178415-02	9.469283-01
3.705	1.575227-02	1.639679-02	2.165305-02	9.452495-01
3.710	1.566346-02	1.630355-02	2.152277-02	9.435697-01
3.715	1.557516-02	1.621085-02	2.139332-02	9.418889-01
3.720	1.548737-02	1.611870-02	2.126468-02	9.402071-01
3.725	1.540009-02	1.602709-02	2.113686-02	9.385244-01
3.730	1.531332-02	1.593602-02	2.100984-02	9.368408-01
3.735	1.522705-02	1.584548-02	2.088362-02	9.351562-01
3.740	1.514127-02	1.575546-02	2.075819-02	9.334708-01
3.745	1.505600-02	1.566598-02	2.063356-02	9.317846-01
3.750	1.497121-02	1.557701-02	2.050971-02	9.300976-01
3.755	1.488692-02	1.548857-02	2.038663-02	9.284098-01
3.760	1.480311-02	1.540065-02	2.026433-02	9.267212-01
3.765	1.471979-02	1.531323-02	2.014280-02	9.250318-01
3.770	1.463695-02	1.522633-02	2.002203-02	9.233418-01
3.775	1.455458-02	1.513994-02	1.990202-02	9.216510-01
3.780	1.447269-02	1.505405-02	1.978276-02	9.199597-01
3.785	1.439128-02	1.496866-02	1.966425-02	9.182676-01
3.790	1.431033-02	1.488377-02	1.954649-02	9.165750-01
3.795	1.422985-02	1.479937-02	1.942946-02	9.148817-01
3.800	1.414984-02	1.471547-02	1.931316-02	9.131879-01

X	K1/3(X)	K2/3(X)	K5/3(X)	G
3.805	1.407029-02	1.463206-02	1.919759-02	9.114936-01
3.810	1.399119-02	1.454913-02	1.908275-02	9.097988-01
3.815	1.391255-02	1.446669-02	1.896862-02	9.081034-01
3.820	1.383437-02	1.438472-02	1.885521-02	9.064076-01
3.825	1.375663-02	1.430324-02	1.874251-02	9.047114-01
3.830	1.367935-02	1.422223-02	1.863051-02	9.030147-01
3.835	1.360250-02	1.414169-02	1.851921-02	9.013176-01
3.840	1.352610-02	1.406162-02	1.840861-02	8.996202-01
3.845	1.345015-02	1.398201-02	1.829870-02	8.979224-01
3.850	1.337462-02	1.390287-02	1.818947-02	8.962243-01
3.855	1.329954-02	1.382419-02	1.808093-02	8.945258-01
3.860	1.322488-02	1.374597-02	1.797306-02	8.928271-01
3.865	1.315065-02	1.366820-02	1.786586-02	8.911282-01
3.870	1.307686-02	1.359089-02	1.775933-02	8.894290-01
3.875	1.300348-02	1.351402-02	1.765347-02	8.877296-01
3.880	1.293053-02	1.343760-02	1.754826-02	8.860300-01
3.885	1.285800-02	1.336163-02	1.744371-02	8.843302-01
3.890	1.278588-02	1.328609-02	1.733981-02	8.826303-01
3.895	1.271418-02	1.321100-02	1.723655-02	8.809302-01
3.900	1.264289-02	1.313634-02	1.713394-02	8.792301-01
3.905	1.257201-02	1.306211-02	1.703197-02	8.775299-01
3.910	1.250154-02	1.298832-02	1.693063-02	8.758296-01
3.915	1.243147-02	1.291495-02	1.682992-02	8.741292-01
3.920	1.236180-02	1.284201-02	1.672983-02	8.724289-01
3.925	1.229253-02	1.276949-02	1.663036-02	8.707286-01
3.930	1.222367-02	1.269739-02	1.653152-02	8.690283-01
3.935	1.215519-02	1.262571-02	1.643328-02	8.673280-01
3.940	1.208711-02	1.255445-02	1.633566-02	8.656278-01
3.945	1.201942-02	1.248360-02	1.623863-02	8.639277-01
3.950	1.195212-02	1.241316-02	1.614221-02	8.622277-01
3.955	1.188520-02	1.234313-02	1.604639-02	8.605279-01
3.960	1.181867-02	1.227350-02	1.595116-02	8.588282-01
3.965	1.175252-02	1.220428-02	1.585652-02	8.571286-01
3.970	1.168674-02	1.213545-02	1.576246-02	8.554293-01
3.975	1.162135-02	1.206703-02	1.566899-02	8.537301-01
3.980	1.155633-02	1.199900-02	1.557610-02	8.520312-01
3.985	1.149168-02	1.193137-02	1.548377-02	8.503326-01
3.990	1.142740-02	1.186412-02	1.539202-02	8.486342-01
3.995	1.136349-02	1.179727-02	1.530083-02	8.469361-01
4.000	1.129995-02	1.173080-02	1.521021-02	8.452383-01

X	K1/3(X)	K2/3(X)	K5/3(X)	G
4.005	1.123677-02	1.166472-02	1.512015-02	8.435409-01
4.010	1.117395-02	1.159902-02	1.503064-02	8.418437-01
4.015	1.111149-02	1.153369-02	1.494169-02	8.401470-01
4.020	1.104938-02	1.146875-02	1.485328-02	8.384506-01
4.025	1.098764-02	1.140418-02	1.476542-02	8.367547-01
4.030	1.092624-02	1.133998-02	1.467810-02	8.350592-01
4.035	1.086520-02	1.127616-02	1.459131-02	8.333641-01
4.040	1.080450-02	1.121270-02	1.450506-02	8.316695-01
4.045	1.074416-02	1.114961-02	1.441935-02	8.299753-01
4.050	1.068415-02	1.108688-02	1.433415-02	8.282817-01
4.055	1.062449-02	1.102452-02	1.424949-02	8.265885-01
4.060	1.056517-02	1.096251-02	1.416534-02	8.248959-01
4.065	1.050619-02	1.090086-02	1.408171-02	8.232039-01
4.070	1.044755-02	1.083957-02	1.399860-02	8.215124-01
4.075	1.038924-02	1.077863-02	1.391599-02	8.198215-01
4.080	1.033126-02	1.071804-02	1.383389-02	8.181313-01
4.085	1.027362-02	1.065781-02	1.375230-02	8.164416-01
4.090	1.021630-02	1.059791-02	1.367121-02	8.147526-01
4.095	1.015931-02	1.053837-02	1.359061-02	8.130642-01
4.100	1.010265-02	1.047916-02	1.351051-02	8.113765-01
4.105	1.004631-02	1.042030-02	1.343089-02	8.096895-01
4.110	9.990287-03	1.036178-02	1.335177-02	8.080033-01
4.115	9.934586-03	1.030359-02	1.327313-02	8.063177-01
4.120	9.879203-03	1.024574-02	1.319497-02	8.046330-01
4.125	9.824135-03	1.018822-02	1.311730-02	8.029489-01
4.130	9.769382-03	1.013103-02	1.304009-02	8.012656-01
4.135	9.714940-03	1.007417-02	1.296336-02	7.995832-01
4.140	9.660808-03	1.001764-02	1.288710-02	7.979015-01
4.145	9.606985-03	9.961430-03	1.281130-02	7.962206-01
4.150	9.553467-03	9.905545-03	1.273597-02	7.945406-01
4.155	9.500255-03	9.849982-03	1.266110-02	7.928615-01
4.160	9.447345-03	9.794737-03	1.258668-02	7.911832-01
4.165	9.394737-03	9.739810-03	1.251272-02	7.895058-01
4.170	9.342427-03	9.685200-03	1.243921-02	7.878293-01
4.175	9.290416-03	9.630902-03	1.236615-02	7.861537-01
4.180	9.238700-03	9.576916-03	1.229354-02	7.844791-01
4.185	9.187279-03	9.523240-03	1.222137-02	7.828054-01
4.190	9.136150-03	9.469872-03	1.214963-02	7.811327-01
4.195	9.085312-03	9.416811-03	1.207834-02	7.794610-01
4.200	9.034762-03	9.364054-03	1.200748-02	7.777903-01

X	K1/3(X)	K2/3(X)	K5/3(X)	G
4.205	8.984500-03	9.311599-03	1.193705-02	7.761205-01
4.210	8.934524-03	9.259446-03	1.186705-02	7.744518-01
4.215	8.884831-03	9.207591-03	1.179747-02	7.727842-01
4.220	8.835420-03	9.156033-03	1.172832-02	7.711176-01
4.225	8.786291-03	9.104771-03	1.165959-02	7.694521-01
4.230	8.737440-03	9.053803-03	1.159128-02	7.677876-01
4.235	8.688867-03	9.003127-03	1.152338-02	7.661243-01
4.240	8.640570-03	8.952741-03	1.145590-02	7.644621-01
4.245	8.592546-03	8.902644-03	1.138882-02	7.628010-01
4.250	8.544796-03	8.852834-03	1.132215-02	7.611411-01
4.255	8.497316-03	8.803309-03	1.125589-02	7.594823-01
4.260	8.450105-03	8.754067-03	1.119003-02	7.578246-01
4.265	8.403163-03	8.705108-03	1.112457-02	7.561682-01
4.270	8.356486-03	8.656428-03	1.105951-02	7.545129-01
4.275	8.310074-03	8.608027-03	1.099484-02	7.528589-01
4.280	8.263926-03	8.559903-03	1.093056-02	7.512061-01
4.285	8.218038-03	8.512054-03	1.086667-02	7.495545-01
4.290	8.172412-03	8.464479-03	1.080317-02	7.479041-01
4.295	8.127043-03	8.417176-03	1.074006-02	7.462551-01
4.300	8.081932-03	8.370143-03	1.067733-02	7.446073-01
4.305	8.037076-03	8.323379-03	1.061497-02	7.429608-01
4.310	7.992475-03	8.276882-03	1.055299-02	7.413156-01
4.315	7.948126-03	8.230651-03	1.049139-02	7.396717-01
4.320	7.904028-03	8.184684-03	1.043016-02	7.380292-01
4.325	7.860180-03	8.138980-03	1.036931-02	7.363880-01
4.330	7.816580-03	8.093536-03	1.030882-02	7.347481-01
4.335	7.773227-03	8.048352-03	1.024869-02	7.331096-01
4.340	7.730119-03	8.003426-03	1.018893-02	7.314725-01
4.345	7.687254-03	7.958756-03	1.012953-02	7.298368-01
4.350	7.644633-03	7.914341-03	1.007048-02	7.282025-01
4.355	7.602253-03	7.870180-03	1.001180-02	7.265696-01
4.360	7.560112-03	7.826271-03	9.953466-03	7.249381-01
4.365	7.518210-03	7.782612-03	9.895486-03	7.233080-01
4.370	7.476544-03	7.739202-03	9.837856-03	7.216795-01
4.375	7.435114-03	7.696039-03	9.780574-03	7.200524-01
4.380	7.393919-03	7.653123-03	9.723636-03	7.184267-01
4.385	7.352956-03	7.610451-03	9.667042-03	7.168026-01
4.390	7.312224-03	7.568022-03	9.610788-03	7.151799-01
4.395	7.271723-03	7.525836-03	9.554873-03	7.135588-01
4.400	7.231450-03	7.483889-03	9.499295-03	7.119391-01

X	K1/3(X)	K2/3(X)	K5/3(X)	G
4.405	7.191405-03	7.442182-03	9.444052-03	7.103210-01
4.410	7.151586-03	7.400711-03	9.389140-03	7.087044-01
4.415	7.111992-03	7.359477-03	9.334559-03	7.070894-01
4.420	7.072621-03	7.318478-03	9.280306-03	7.054760-01
4.425	7.033473-03	7.277712-03	9.226380-03	7.038641-01
4.430	6.994545-03	7.237178-03	9.172778-03	7.022538-01
4.435	6.955838-03	7.196875-03	9.119497-03	7.006451-01
4.440	6.917348-03	7.156801-03	9.066538-03	6.990380-01
4.445	6.879076-03	7.116955-03	9.013895-03	6.974325-01
4.450	6.841020-03	7.077336-03	8.961570-03	6.958287-01
4.455	6.803178-03	7.037942-03	8.909558-03	6.942265-01
4.460	6.765550-03	6.998772-03	8.857858-03	6.926259-01
4.465	6.728134-03	6.959825-03	8.806468-03	6.910270-01
4.470	6.690928-03	6.921098-03	8.755386-03	6.894298-01
4.475	6.653932-03	6.882592-03	8.704611-03	6.878342-01
4.480	6.617145-03	6.844305-03	8.654140-03	6.862403-01
4.485	6.580565-03	6.806235-03	8.603972-03	6.846482-01
4.490	6.544192-03	6.768382-03	8.554104-03	6.830577-01
4.495	6.508023-03	6.730744-03	8.504535-03	6.814690-01
4.500	6.472058-03	6.693319-03	8.455263-03	6.798820-01
4.505	6.436295-03	6.656107-03	8.406286-03	6.782967-01
4.510	6.400734-03	6.619105-03	8.357602-03	6.767131-01
4.515	6.365373-03	6.582315-03	8.309209-03	6.751314-01
4.520	6.330211-03	6.545732-03	8.261105-03	6.735513-01
4.525	6.295247-03	6.509358-03	8.213290-03	6.719731-01
4.530	6.260480-03	6.473189-03	8.165760-03	6.703966-01
4.535	6.225908-03	6.437226-03	8.118513-03	6.688219-01
4.540	6.191531-03	6.401466-03	8.071550-03	6.672490-01
4.545	6.157347-03	6.365910-03	8.024867-03	6.656780-01
4.550	6.123356-03	6.330555-03	7.978463-03	6.641087-01
4.555	6.089555-03	6.295400-03	7.932336-03	6.625413-01
4.560	6.055945-03	6.260445-03	7.886484-03	6.609757-01
4.565	6.022524-03	6.225688-03	7.840906-03	6.594119-01
4.570	5.989290-03	6.191128-03	7.795600-03	6.578500-01
4.575	5.956244-03	6.156763-03	7.750564-03	6.562900-01
4.580	5.923382-03	6.122593-03	7.705796-03	6.547318-01
4.585	5.890706-03	6.088617-03	7.661296-03	6.531755-01
4.590	5.858213-03	6.054833-03	7.617060-03	6.516211-01
4.595	5.825903-03	6.021240-03	7.573088-03	6.500686-01
4.600	5.793774-03	5.987838-03	7.529379-03	6.485180-01

X	K1/3(X)	K2/3(X)	K5/3(X)	G
4.605	5.761826-03	5.954624-03	7.485929-03	6.469693-01
4.610	5.730057-03	5.921598-03	7.442738-03	6.454225-01
4.615	5.698466-03	5.888760-03	7.399804-03	6.438776-01
4.620	5.667053-03	5.856107-03	7.357127-03	6.423347-01
4.625	5.635816-03	5.823639-03	7.314702-03	6.407937-01
4.630	5.604755-03	5.791354-03	7.272530-03	6.392546-01
4.635	5.573867-03	5.759252-03	7.230609-03	6.377175-01
4.640	5.543153-03	5.727331-03	7.188938-03	6.361824-01
4.645	5.512611-03	5.695591-03	7.147513-03	6.346492-01
4.650	5.482241-03	5.664030-03	7.106335-03	6.331180-01
4.655	5.452041-03	5.632648-03	7.065402-03	6.315888-01
4.660	5.422010-03	5.601442-03	7.024711-03	6.300616-01
4.665	5.392148-03	5.570414-03	6.984263-03	6.285364-01
4.670	5.362453-03	5.539560-03	6.944054-03	6.270132-01
4.675	5.332924-03	5.508881-03	6.904084-03	6.254919-01
4.680	5.303561-03	5.478375-03	6.864351-03	6.239728-01
4.685	5.274363-03	5.448041-03	6.824854-03	6.224556-01
4.690	5.245328-03	5.417878-03	6.785592-03	6.209405-01
4.695	5.216456-03	5.387886-03	6.746561-03	6.194274-01
4.700	5.187745-03	5.358063-03	6.707763-03	6.179163-01
4.705	5.159195-03	5.328408-03	6.669194-03	6.164073-01
4.710	5.130806-03	5.298921-03	6.630854-03	6.149004-01
4.715	5.102575-03	5.269600-03	6.592741-03	6.133955-01
4.720	5.074502-03	5.240444-03	6.554853-03	6.118927-01
4.725	5.046586-03	5.211452-03	6.517189-03	6.103919-01
4.730	5.018827-03	5.182624-03	6.479749-03	6.088933-01
4.735	4.991223-03	5.153959-03	6.442531-03	6.073967-01
4.740	4.963773-03	5.125455-03	6.405533-03	6.059022-01
4.745	4.936477-03	5.097112-03	6.368753-03	6.044099-01
4.750	4.909334-03	5.068929-03	6.332191-03	6.029196-01
4.755	4.882343-03	5.040904-03	6.295845-03	6.014315-01
4.760	4.855502-03	5.013038-03	6.259714-03	5.999455-01
4.765	4.828812-03	4.985328-03	6.223796-03	5.984616-01
4.770	4.802271-03	4.957774-03	6.188091-03	5.969798-01
4.775	4.775878-03	4.930376-03	6.152597-03	5.955001-01
4.780	4.749633-03	4.903132-03	6.117312-03	5.940226-01
4.785	4.723534-03	4.876041-03	6.082235-03	5.925473-01
4.790	4.697581-03	4.849102-03	6.047366-03	5.910740-01
4.795	4.671774-03	4.822316-03	6.012702-03	5.896030-01
4.800	4.646110-03	4.795680-03	5.978243-03	5.881341-01

X	K1/3(X)	K2/3(X)	K5/3(X)	G
4.805	4.620590-03	4.769194-03	5.943987-03	5.866674-01
4.810	4.595213-03	4.742857-03	5.909933-03	5.852028-01
4.815	4.569977-03	4.716668-03	5.876081-03	5.837404-01
4.820	4.544882-03	4.690626-03	5.842427-03	5.822802-01
4.825	4.519927-03	4.664731-03	5.808972-03	5.808222-01
4.830	4.495112-03	4.638981-03	5.775714-03	5.793664-01
4.835	4.470435-03	4.613377-03	5.742652-03	5.779128-01
4.840	4.445896-03	4.587916-03	5.709784-03	5.764613-01
4.845	4.421494-03	4.562598-03	5.677110-03	5.750121-01
4.850	4.397228-03	4.537422-03	5.644629-03	5.735651-01
4.855	4.373097-03	4.512388-03	5.612338-03	5.721203-01
4.860	4.349101-03	4.487495-03	5.580238-03	5.706778-01
4.865	4.325239-03	4.462741-03	5.548326-03	5.692374-01
4.870	4.301510-03	4.438127-03	5.516602-03	5.677993-01
4.875	4.277913-03	4.413651-03	5.485065-03	5.663634-01
4.880	4.254448-03	4.389312-03	5.453713-03	5.649298-01
4.885	4.231114-03	4.365109-03	5.422546-03	5.634984-01
4.890	4.207910-03	4.341043-03	5.391561-03	5.620692-01
4.895	4.184835-03	4.317112-03	5.360759-03	5.606423-01
4.900	4.161889-03	4.293315-03	5.330137-03	5.592176-01
4.905	4.139070-03	4.269651-03	5.299696-03	5.577952-01
4.910	4.116379-03	4.246121-03	5.269432-03	5.563751-01
4.915	4.093814-03	4.222722-03	5.239347-03	5.549572-01
4.920	4.071375-03	4.199455-03	5.209438-03	5.535416-01
4.925	4.049061-03	4.176318-03	5.179705-03	5.521282-01
4.930	4.026871-03	4.153311-03	5.150146-03	5.507172-01
4.935	4.004805-03	4.130432-03	5.120760-03	5.493084-01
4.940	3.982862-03	4.107683-03	5.091547-03	5.479019-01
4.945	3.961040-03	4.085060-03	5.062505-03	5.464977-01
4.950	3.939341-03	4.062565-03	5.033634-03	5.450957-01
4.955	3.917762-03	4.040195-03	5.004931-03	5.436961-01
4.960	3.896303-03	4.017951-03	4.976397-03	5.422988-01
4.965	3.874963-03	3.995831-03	4.948030-03	5.409037-01
4.970	3.853743-03	3.973836-03	4.919828-03	5.395110-01
4.975	3.832640-03	3.951963-03	4.891792-03	5.381206-01
4.980	3.811655-03	3.930213-03	4.863921-03	5.367325-01
4.985	3.790787-03	3.908585-03	4.836212-03	5.353467-01
4.990	3.770034-03	3.887078-03	4.808665-03	5.339632-01
4.995	3.749397-03	3.865691-03	4.781280-03	5.325821-01
5.000	3.728875-03	3.844424-03	4.754055-03	5.312032-01

X	K1/3(X)	K2/3(X)	K5/3(X)	G
5.010	3.688172-03	3.802247-03	4.700081-03	5.284525-01
5.020	3.647921-03	3.760540-03	4.646736-03	5.257112-01
5.030	3.608115-03	3.719299-03	4.594013-03	5.229791-01
5.040	3.568751-03	3.678517-03	4.541903-03	5.202565-01
5.050	3.529823-03	3.638190-03	4.490401-03	5.175432-01
5.060	3.491325-03	3.598313-03	4.439497-03	5.148394-01
5.070	3.453255-03	3.558880-03	4.389186-03	5.121449-01
5.080	3.415606-03	3.519887-03	4.339460-03	5.094599-01
5.090	3.378373-03	3.481328-03	4.290312-03	5.067844-01
5.100	3.341552-03	3.443199-03	4.241735-03	5.041183-01
5.110	3.305139-03	3.405494-03	4.193722-03	5.014618-01
5.120	3.269129-03	3.368208-03	4.146266-03	4.988147-01
5.130	3.233517-03	3.331338-03	4.099362-03	4.961772-01
5.140	3.198299-03	3.294878-03	4.053001-03	4.935492-01
5.150	3.163470-03	3.258824-03	4.007178-03	4.909308-01
5.160	3.129026-03	3.223170-03	3.961886-03	4.883219-01
5.170	3.094962-03	3.187913-03	3.917119-03	4.857227-01
5.180	3.061275-03	3.153048-03	3.872870-03	4.831329-01
5.190	3.027960-03	3.118570-03	3.829134-03	4.805528-01
5.200	2.995013-03	3.084475-03	3.785904-03	4.779823-01
5.210	2.962430-03	3.050759-03	3.743174-03	4.754215-01
5.220	2.930206-03	3.017418-03	3.700938-03	4.728702-01
5.230	2.898337-03	2.984447-03	3.659190-03	4.703286-01
5.240	2.866821-03	2.951841-03	3.617925-03	4.677966-01
5.250	2.835652-03	2.919598-03	3.577137-03	4.652743-01
5.260	2.804827-03	2.887712-03	3.536819-03	4.627616-01
5.270	2.774342-03	2.856180-03	3.496968-03	4.602586-01
5.280	2.744192-03	2.824998-03	3.457575-03	4.577652-01
5.290	2.714375-03	2.794161-03	3.418638-03	4.552815-01
5.300	2.684887-03	2.763666-03	3.380149-03	4.528074-01
5.310	2.655724-03	2.733509-03	3.342103-03	4.503431-01
5.320	2.626882-03	2.703687-03	3.304497-03	4.478884-01
5.330	2.598357-03	2.674194-03	3.267324-03	4.454433-01
5.340	2.570147-03	2.645029-03	3.230578-03	4.430080-01
5.350	2.542246-03	2.616186-03	3.194255-03	4.405823-01
5.360	2.514654-03	2.587662-03	3.158351-03	4.381664-01
5.370	2.487364-03	2.559454-03	3.122859-03	4.357601-01
5.380	2.460375-03	2.531559-03	3.087775-03	4.333634-01
5.390	2.433683-03	2.503972-03	3.053095-03	4.309765-01
5.400	2.407285-03	2.476690-03	3.018813-03	4.285992-01

X	K1/3(X)	K2/3(X)	K5/3(X)	G
5.410	2.381177-03	2.449710-03	2.984925-03	4.262316-01
5.420	2.355355-03	2.423028-03	2.951426-03	4.238737-01
5.430	2.329818-03	2.396641-03	2.918311-03	4.215254-01
5.440	2.304561-03	2.370545-03	2.885577-03	4.191868-01
5.450	2.279582-03	2.344738-03	2.853218-03	4.168578-01
5.460	2.254877-03	2.319216-03	2.821230-03	4.145385-01
5.470	2.230443-03	2.293976-03	2.789608-03	4.122289-01
5.480	2.206278-03	2.269015-03	2.758349-03	4.099289-01
5.490	2.182378-03	2.244329-03	2.727448-03	4.076386-01
5.500	2.158740-03	2.219915-03	2.696901-03	4.053578-01
5.510	2.135362-03	2.195771-03	2.666704-03	4.030867-01
5.520	2.112240-03	2.171894-03	2.636852-03	4.008252-01
5.530	2.089372-03	2.148280-03	2.607342-03	3.985733-01
5.540	2.066755-03	2.124926-03	2.578169-03	3.963310-01
5.550	2.044386-03	2.101829-03	2.549329-03	3.940983-01
5.560	2.022261-03	2.078988-03	2.520819-03	3.918752-01
5.570	2.000380-03	2.056398-03	2.492635-03	3.896616-01
5.580	1.978738-03	2.034056-03	2.464773-03	3.874576-01
5.590	1.957334-03	2.011962-03	2.437229-03	3.852632-01
5.600	1.936164-03	1.990110-03	2.409999-03	3.830782-01
5.610	1.915226-03	1.968499-03	2.383080-03	3.809029-01
5.620	1.894517-03	1.947126-03	2.356469-03	3.787370-01
5.630	1.874035-03	1.925988-03	2.330160-03	3.765806-01
5.640	1.853778-03	1.905083-03	2.304152-03	3.744338-01
5.650	1.833742-03	1.884408-03	2.278439-03	3.722964-01
5.660	1.813925-03	1.863960-03	2.253020-03	3.701685-01
5.670	1.794325-03	1.843738-03	2.227890-03	3.680500-01
5.680	1.774940-03	1.823737-03	2.203047-03	3.659410-01
5.690	1.755766-03	1.803957-03	2.178486-03	3.638414-01
5.700	1.736802-03	1.784394-03	2.154204-03	3.617512-01
5.710	1.718046-03	1.765046-03	2.130199-03	3.596704-01
5.720	1.699495-03	1.745911-03	2.106467-03	3.575990-01
5.730	1.681146-03	1.726986-03	2.083005-03	3.555370-01
5.740	1.662998-03	1.708269-03	2.059809-03	3.534843-01
5.750	1.645049-03	1.689757-03	2.036876-03	3.514410-01
5.760	1.627295-03	1.671449-03	2.014205-03	3.494069-01
5.770	1.609736-03	1.653341-03	1.991790-03	3.473822-01
5.780	1.592368-03	1.635433-03	1.969630-03	3.453668-01
5.790	1.575190-03	1.617720-03	1.947722-03	3.433606-01
5.800	1.558199-03	1.600203-03	1.926062-03	3.413637-01

X	K1/3(X)	K2/3(X)	K5/3(X)	G
5.810	1.541394-03	1.582877-03	1.904647-03	3.393760-01
5.820	1.524772-03	1.565742-03	1.883476-03	3.373975-01
5.830	1.508332-03	1.548794-03	1.862544-03	3.354282-01
5.840	1.492071-03	1.532032-03	1.841850-03	3.334681-01
5.850	1.475987-03	1.515454-03	1.821390-03	3.315172-01
5.860	1.460079-03	1.499058-03	1.801161-03	3.295754-01
5.870	1.444344-03	1.482841-03	1.781162-03	3.276427-01
5.880	1.428781-03	1.466802-03	1.761389-03	3.257191-01
5.890	1.413388-03	1.450939-03	1.741840-03	3.238047-01
5.900	1.398162-03	1.435249-03	1.722512-03	3.218992-01
5.910	1.383102-03	1.419731-03	1.703402-03	3.200028-01
5.920	1.368207-03	1.404383-03	1.684509-03	3.181155-01
5.930	1.353473-03	1.389203-03	1.665829-03	3.162371-01
5.940	1.338900-03	1.374190-03	1.647360-03	3.143677-01
5.950	1.324486-03	1.359340-03	1.629100-03	3.125073-01
5.960	1.310229-03	1.344653-03	1.611046-03	3.106558-01
5.970	1.296127-03	1.330127-03	1.593196-03	3.088132-01
5.980	1.282179-03	1.315759-03	1.575547-03	3.069796-01
5.990	1.268382-03	1.301549-03	1.558098-03	3.051548-01
6.000	1.254735-03	1.287494-03	1.540845-03	3.033389-01
6.010	1.241237-03	1.273593-03	1.523787-03	3.015317-01
6.020	1.227886-03	1.259843-03	1.506921-03	2.997334-01
6.030	1.214680-03	1.246244-03	1.490245-03	2.979439-01
6.040	1.201618-03	1.232793-03	1.473757-03	2.961631-01
6.050	1.188697-03	1.219490-03	1.457455-03	2.943911-01
6.060	1.175918-03	1.206331-03	1.441337-03	2.926278-01
6.070	1.163277-03	1.193317-03	1.425400-03	2.908731-01
6.080	1.150773-03	1.180444-03	1.409642-03	2.891272-01
6.090	1.138406-03	1.167712-03	1.394062-03	2.873898-01
6.100	1.126172-03	1.155119-03	1.378657-03	2.856611-01
6.110	1.114072-03	1.142663-03	1.363425-03	2.839410-01
6.120	1.102103-03	1.130343-03	1.348365-03	2.822295-01
6.130	1.090264-03	1.118158-03	1.333474-03	2.805265-01
6.140	1.078553-03	1.106105-03	1.318750-03	2.788320-01
6.150	1.066970-03	1.094184-03	1.304192-03	2.771461-01
6.160	1.055513-03	1.082393-03	1.289797-03	2.754686-01
6.170	1.044180-03	1.070731-03	1.275564-03	2.737995-01
6.180	1.032969-03	1.059195-03	1.261490-03	2.721389-01
6.190	1.021881-03	1.047786-03	1.247575-03	2.704867-01
6.200	1.010913-03	1.036500-03	1.233816-03	2.688428-01

X	K1/3(X)	K2/3(X)	K5/3(X)	G
6.210	1.000064-03	1.025338-03	1.220211-03	2.672073-01
6.220	9.893319-04	1.014297-03	1.206759-03	2.655801-01
6.230	9.787167-04	1.003377-03	1.193457-03	2.639612-01
6.240	9.682166-04	9.925751-04	1.180305-03	2.623506-01
6.250	9.578304-04	9.818911-04	1.167300-03	2.607483-01
6.260	9.475567-04	9.713234-04	1.154441-03	2.591541-01
6.270	9.373944-04	9.608707-04	1.141726-03	2.575681-01
6.280	9.273422-04	9.505317-04	1.129154-03	2.559903-01
6.290	9.173989-04	9.403053-04	1.116722-03	2.544207-01
6.300	9.075634-04	9.301901-04	1.104429-03	2.528591-01
6.310	8.978343-04	9.201849-04	1.092274-03	2.513057-01
6.320	8.882107-04	9.102886-04	1.080255-03	2.497603-01
6.330	8.786913-04	9.004999-04	1.068370-03	2.482229-01
6.340	8.692749-04	8.908176-04	1.056618-03	2.466935-01
6.350	8.599604-04	8.812405-04	1.044998-03	2.451721-01
6.360	8.507469-04	8.717676-04	1.033507-03	2.436587-01
6.370	8.416330-04	8.623977-04	1.022145-03	2.421532-01
6.380	8.326177-04	8.531295-04	1.010910-03	2.406556-01
6.390	8.237000-04	8.439620-04	9.998005-04	2.391659-01
6.400	8.148788-04	8.348941-04	9.888149-04	2.376840-01
6.410	8.061529-04	8.259247-04	9.779521-04	2.362099-01
6.420	7.975215-04	8.170527-04	9.672104-04	2.347436-01
6.430	7.889834-04	8.082770-04	9.565887-04	2.332851-01
6.440	7.805376-04	7.995966-04	9.460854-04	2.318343-01
6.450	7.721831-04	7.910104-04	9.356994-04	2.303912-01
6.460	7.639189-04	7.825175-04	9.254292-04	2.289558-01
6.470	7.557440-04	7.741166-04	9.152734-04	2.275281-01
6.480	7.476575-04	7.658069-04	9.052309-04	2.261080-01
6.490	7.396584-04	7.575874-04	8.953003-04	2.246955-01
6.500	7.317457-04	7.494571-04	8.854803-04	2.232905-01
6.510	7.239185-04	7.414148-04	8.757698-04	2.218931-01
6.520	7.161758-04	7.334598-04	8.661675-04	2.205032-01
6.530	7.085167-04	7.255911-04	8.566720-04	2.191208-01
6.540	7.009403-04	7.178076-04	8.472822-04	2.177458-01
6.550	6.934457-04	7.101085-04	8.379969-04	2.163783-01
6.560	6.860320-04	7.024929-04	8.288150-04	2.150182-01
6.570	6.786984-04	6.949598-04	8.197352-04	2.136654-01
6.580	6.714439-04	6.875083-04	8.107565-04	2.123200-01
6.590	6.642676-04	6.801375-04	8.018775-04	2.109819-01
6.600	6.571688-04	6.728465-04	7.930973-04	2.096511-01

X	K1/3(X)	K2/3(X)	K5/3(X)	G
6.610	6.501466-04	6.656345-04	7.844147-04	2.083276-01
6.620	6.432001-04	6.585006-04	7.758286-04	2.070113-01
6.630	6.363286-04	6.514439-04	7.673379-04	2.057022-01
6.640	6.295312-04	6.444637-04	7.589415-04	2.044003-01
6.650	6.228070-04	6.375590-04	7.506383-04	2.031055-01
6.660	6.161553-04	6.307289-04	7.424273-04	2.018178-01
6.670	6.095753-04	6.239728-04	7.343075-04	2.005373-01
6.680	6.030663-04	6.172898-04	7.262778-04	1.992638-01
6.690	5.966274-04	6.106791-04	7.183372-04	1.979973-01
6.700	5.902580-04	6.041399-04	7.104847-04	1.967379-01
6.710	5.839571-04	5.976715-04	7.027194-04	1.954854-01
6.720	5.777241-04	5.912729-04	6.950400-04	1.942399-01
6.730	5.715582-04	5.849435-04	6.874459-04	1.930013-01
6.740	5.654588-04	5.786826-04	6.799359-04	1.917696-01
6.750	5.594250-04	5.724893-04	6.725092-04	1.905447-01
6.760	5.534563-04	5.663630-04	6.651648-04	1.893267-01
6.770	5.475517-04	5.603029-04	6.579018-04	1.881155-01
6.780	5.417108-04	5.543083-04	6.507192-04	1.869111-01
6.790	5.359327-04	5.483784-04	6.436161-04	1.857135-01
6.800	5.302168-04	5.425125-04	6.365917-04	1.845225-01
6.810	5.245624-04	5.367100-04	6.296450-04	1.833383-01
6.820	5.189688-04	5.309702-04	6.227753-04	1.821607-01
6.830	5.134355-04	5.252924-04	6.159815-04	1.809898-01
6.840	5.079616-04	5.196758-04	6.092629-04	1.798255-01
6.850	5.025466-04	5.141199-04	6.026186-04	1.786678-01
6.860	4.971899-04	5.086239-04	5.960478-04	1.775166-01
6.870	4.918908-04	5.031873-04	5.895496-04	1.763719-01
6.880	4.866486-04	4.978093-04	5.831232-04	1.752338-01
6.890	4.814628-04	4.924894-04	5.767679-04	1.741021-01
6.900	4.763328-04	4.872268-04	5.704828-04	1.729769-01
6.910	4.712578-04	4.820210-04	5.642671-04	1.718581-01
6.920	4.662375-04	4.768714-04	5.581201-04	1.707457-01
6.930	4.612711-04	4.717772-04	5.520410-04	1.696396-01
6.940	4.563580-04	4.667380-04	5.460290-04	1.685399-01
6.950	4.514977-04	4.617532-04	5.400834-04	1.674465-01
6.960	4.466897-04	4.568220-04	5.342034-04	1.663593-01
6.970	4.419332-04	4.519440-04	5.283882-04	1.652784-01
6.980	4.372279-04	4.471186-04	5.226373-04	1.642037-01
6.990	4.325731-04	4.423452-04	5.169498-04	1.631353-01
7.000	4.279682-04	4.376232-04	5.113250-04	1.620729-01

X	K1/3(X)	K2/3(X)	K5/3(X)	G
7.010	4.234128-04	4.329521-04	5.057622-04	1.610167-01
7.020	4.189064-04	4.283313-04	5.002607-04	1.599667-01
7.030	4.144482-04	4.237602-04	4.948199-04	1.589227-01
7.040	4.100379-04	4.192384-04	4.894391-04	1.578848-01
7.050	4.056750-04	4.147653-04	4.841175-04	1.568528-01
7.060	4.013588-04	4.103403-04	4.788546-04	1.558269-01
7.070	3.970890-04	4.059630-04	4.736496-04	1.548070-01
7.080	3.928650-04	4.016328-04	4.685020-04	1.537930-01
7.090	3.886863-04	3.973491-04	4.634110-04	1.527849-01
7.100	3.845523-04	3.931116-04	4.583761-04	1.517828-01
7.110	3.804628-04	3.889197-04	4.533966-04	1.507865-01
7.120	3.764171-04	3.847728-04	4.484718-04	1.497960-01
7.130	3.724147-04	3.806706-04	4.436013-04	1.488113-01
7.140	3.684553-04	3.766125-04	4.387844-04	1.478324-01
7.150	3.645383-04	3.725981-04	4.340204-04	1.468593-01
7.160	3.606633-04	3.686268-04	4.293088-04	1.458919-01
7.170	3.568298-04	3.646982-04	4.246490-04	1.449302-01
7.180	3.530374-04	3.608118-04	4.200405-04	1.439741-01
7.190	3.492856-04	3.569673-04	4.154825-04	1.430238-01
7.200	3.455740-04	3.531640-04	4.109747-04	1.420790-01
7.210	3.419022-04	3.494016-04	4.065164-04	1.411398-01
7.220	3.382697-04	3.456797-04	4.021071-04	1.402062-01
7.230	3.346761-04	3.419977-04	3.977462-04	1.392782-01
7.240	3.311210-04	3.383553-04	3.934332-04	1.383556-01
7.250	3.276040-04	3.347520-04	3.891675-04	1.374386-01
7.260	3.241246-04	3.311874-04	3.849487-04	1.365270-01
7.270	3.206825-04	3.276612-04	3.807762-04	1.356208-01
7.280	3.172772-04	3.241727-04	3.766494-04	1.347201-01
7.290	3.139083-04	3.207217-04	3.725679-04	1.338247-01
7.300	3.105755-04	3.173078-04	3.685313-04	1.329347-01
7.310	3.072784-04	3.139305-04	3.645388-04	1.320500-01
7.320	3.040166-04	3.105895-04	3.605902-04	1.311706-01
7.330	3.007896-04	3.072843-04	3.566849-04	1.302965-01
7.340	2.975972-04	3.040147-04	3.528224-04	1.294277-01
7.350	2.944389-04	3.007800-04	3.490021-04	1.285641-01
7.360	2.913144-04	2.975801-04	3.452238-04	1.277056-01
7.370	2.882233-04	2.944145-04	3.414869-04	1.268524-01
7.380	2.851653-04	2.912829-04	3.377909-04	1.260043-01
7.390	2.821399-04	2.881848-04	3.341353-04	1.251613-01
7.400	2.791469-04	2.851200-04	3.305199-04	1.243235-01

X	K1/3(X)	K2/3(X)	K5/3(X)	G
7.410	2.761859-04	2.820880-04	3.269440-04	1.234907-01
7.420	2.732566-04	2.790886-04	3.234072-04	1.226629-01
7.430	2.703585-04	2.761213-04	3.199092-04	1.218402-01
7.440	2.674915-04	2.731858-04	3.164494-04	1.210224-01
7.450	2.646550-04	2.702818-04	3.130276-04	1.202097-01
7.460	2.618489-04	2.674089-04	3.096431-04	1.194019-01
7.470	2.590727-04	2.645667-04	3.062957-04	1.185990-01
7.480	2.563262-04	2.617551-04	3.029848-04	1.178010-01
7.490	2.536091-04	2.589735-04	2.997102-04	1.170079-01
7.500	2.509209-04	2.562218-04	2.964714-04	1.162196-01
7.510	2.482615-04	2.534995-04	2.932680-04	1.154361-01
7.520	2.456305-04	2.508064-04	2.900996-04	1.146575-01
7.530	2.430275-04	2.481421-04	2.869659-04	1.138836-01
7.540	2.404523-04	2.455063-04	2.838663-04	1.131145-01
7.550	2.379047-04	2.428988-04	2.808007-04	1.123501-01
7.560	2.353842-04	2.403192-04	2.777685-04	1.115904-01
7.570	2.328906-04	2.377672-04	2.747694-04	1.108353-01
7.580	2.304237-04	2.352425-04	2.718031-04	1.100849-01
7.590	2.279830-04	2.327448-04	2.688692-04	1.093392-01
7.600	2.255684-04	2.302738-04	2.659673-04	1.085980-01
7.610	2.231796-04	2.278293-04	2.630971-04	1.078615-01
7.620	2.208162-04	2.254110-04	2.602582-04	1.071294-01
7.630	2.184781-04	2.230185-04	2.574503-04	1.064020-01
7.640	2.161649-04	2.206516-04	2.546730-04	1.056790-01
7.650	2.138763-04	2.183100-04	2.519260-04	1.049605-01
7.660	2.116122-04	2.159935-04	2.492089-04	1.042465-01
7.670	2.093722-04	2.137017-04	2.465215-04	1.035369-01
7.680	2.071561-04	2.114345-04	2.438634-04	1.028317-01
7.690	2.049636-04	2.091914-04	2.412343-04	1.021309-01
7.700	2.027945-04	2.069724-04	2.386339-04	1.014345-01
7.710	2.006485-04	2.047771-04	2.360617-04	1.007424-01
7.720	1.985254-04	2.026052-04	2.335176-04	1.000547-01
7.730	1.964249-04	2.004566-04	2.310012-04	9.937121-02
7.740	1.943468-04	1.983309-04	2.285122-04	9.869203-02
7.750	1.922908-04	1.962279-04	2.260504-04	9.801711-02
7.760	1.902567-04	1.941474-04	2.236153-04	9.734641-02
7.770	1.882443-04	1.920891-04	2.212068-04	9.667992-02
7.780	1.862533-04	1.900528-04	2.188245-04	9.601761-02
7.790	1.842836-04	1.880382-04	2.164681-04	9.535947-02
7.800	1.823348-04	1.860452-04	2.141373-04	9.470547-02

X	K1/3(X)	K2/3(X)	K5/3(X)	G
7.810	1.804068-04	1.840734-04	2.118320-04	9.405558-02
7.820	1.784993-04	1.821227-04	2.095517-04	9.340979-02
7.830	1.766121-04	1.801929-04	2.072962-04	9.276807-02
7.840	1.747450-04	1.782836-04	2.050653-04	9.213040-02
7.850	1.728977-04	1.763947-04	2.028586-04	9.149676-02
7.860	1.710702-04	1.745259-04	2.006759-04	9.086713-02
7.870	1.692620-04	1.726771-04	1.985169-04	9.024148-02
7.880	1.674732-04	1.708481-04	1.963814-04	8.961980-02
7.890	1.657033-04	1.690385-04	1.942692-04	8.900205-02
7.900	1.639523-04	1.672483-04	1.921798-04	8.838823-02
7.910	1.622199-04	1.654771-04	1.901132-04	8.777831-02
7.920	1.605060-04	1.637249-04	1.880691-04	8.717226-02
7.930	1.588103-04	1.619913-04	1.860471-04	8.657006-02
7.940	1.571326-04	1.602762-04	1.840471-04	8.597171-02
7.950	1.554727-04	1.585795-04	1.820688-04	8.537716-02
7.960	1.538306-04	1.569008-04	1.801121-04	8.478641-02
7.970	1.522058-04	1.552400-04	1.781765-04	8.419943-02
7.980	1.505984-04	1.535969-04	1.762620-04	8.361620-02
7.990	1.490080-04	1.519713-04	1.743682-04	8.303670-02
8.000	1.474346-04	1.503630-04	1.724950-04	8.246091-02
8.010	1.458778-04	1.487719-04	1.706422-04	8.188880-02
8.020	1.443376-04	1.471978-04	1.688094-04	8.132036-02
8.030	1.428138-04	1.456404-04	1.669965-04	8.075557-02
8.040	1.413062-04	1.440996-04	1.652033-04	8.019440-02
8.050	1.398146-04	1.425753-04	1.634296-04	7.963684-02
8.060	1.383389-04	1.410671-04	1.616750-04	7.908287-02
8.070	1.368788-04	1.395750-04	1.599395-04	7.853246-02
8.080	1.354342-04	1.380989-04	1.582228-04	7.798560-02
8.090	1.340050-04	1.366384-04	1.565247-04	7.744226-02
8.100	1.325910-04	1.351935-04	1.548450-04	7.690243-02
8.110	1.311920-04	1.337640-04	1.531836-04	7.636608-02
8.120	1.298078-04	1.323497-04	1.515401-04	7.583320-02
8.130	1.284383-04	1.309505-04	1.499144-04	7.530376-02
8.140	1.270834-04	1.295661-04	1.483064-04	7.477776-02
8.150	1.257429-04	1.281965-04	1.467157-04	7.425515-02
8.160	1.244166-04	1.268415-04	1.451423-04	7.373594-02
8.170	1.231044-04	1.255009-04	1.435859-04	7.322010-02
8.180	1.218061-04	1.241745-04	1.420464-04	7.270760-02
8.190	1.205215-04	1.228623-04	1.405235-04	7.219843-02
8.200	1.192507-04	1.215640-04	1.390171-04	7.169258-02

X	K1/3(X)	K2/3(X)	K5/3(X)	G
8.210	1.179933-04	1.202796-04	1.375271-04	7.119001-02
8.220	1.167492-04	1.190088-04	1.360531-04	7.069072-02
8.230	1.155183-04	1.177515-04	1.345951-04	7.019469-02
8.240	1.143006-04	1.165076-04	1.331529-04	6.970189-02
8.250	1.130957-04	1.152769-04	1.317263-04	6.921231-02
8.260	1.119036-04	1.140593-04	1.303151-04	6.872592-02
8.270	1.107241-04	1.128547-04	1.289191-04	6.824271-02
8.280	1.095572-04	1.116629-04	1.275383-04	6.776267-02
8.290	1.084026-04	1.104837-04	1.261724-04	6.728576-02
8.300	1.072603-04	1.093171-04	1.248213-04	6.681198-02
8.310	1.061301-04	1.081628-04	1.234847-04	6.634131-02
8.320	1.050118-04	1.070209-04	1.221626-04	6.587373-02
8.330	1.039055-04	1.058910-04	1.208548-04	6.540921-02
8.340	1.028108-04	1.047732-04	1.195611-04	6.494775-02
8.350	1.017278-04	1.036673-04	1.182814-04	6.448932-02
8.360	1.006562-04	1.025731-04	1.170155-04	6.403391-02
8.370	9.959601-05	1.014905-04	1.157633-04	6.358150-02
8.380	9.854704-05	1.004195-04	1.145247-04	6.313207-02
8.390	9.750919-05	9.935977-05	1.132994-04	6.268560-02
8.400	9.648233-05	9.831133-05	1.120873-04	6.224208-02
8.410	9.546635-05	9.727404-05	1.108883-04	6.180149-02
8.420	9.446114-05	9.624775-05	1.097022-04	6.136381-02
8.430	9.346657-05	9.523236-05	1.085290-04	6.092903-02
8.440	9.248252-05	9.422775-05	1.073684-04	6.049712-02
8.450	9.150892-05	9.323381-05	1.062203-04	6.006807-02
8.460	9.054562-05	9.225042-05	1.050847-04	5.964187-02
8.470	8.959252-05	9.127747-05	1.039612-04	5.921849-02
8.480	8.864952-05	9.031484-05	1.028499-04	5.879793-02
8.490	8.771650-05	8.936244-05	1.017506-04	5.838015-02
8.500	8.679336-05	8.842014-05	1.006632-04	5.796516-02
8.510	8.587999-05	8.748784-05	9.958742-05	5.755292-02
8.520	8.497629-05	8.656543-05	9.852328-05	5.714342-02
8.530	8.408216-05	8.565281-05	9.747062-05	5.673666-02
8.540	8.319749-05	8.474987-05	9.642930-05	5.633260-02
8.550	8.232218-05	8.385651-05	9.539921-05	5.593124-02
8.560	8.145614-05	8.297262-05	9.438021-05	5.553255-02
8.570	8.059925-05	8.209810-05	9.337218-05	5.513653-02
8.580	7.975144-05	8.123287-05	9.237502-05	5.474316-02
8.590	7.891259-05	8.037681-05	9.138861-05	5.435241-02
8.600	7.808262-05	7.952982-05	9.041282-05	5.396428-02

X	K1/3(X)	K2/3(X)	K5/3(X)	G
8.610	7.726144-05	7.869182-05	8.944754-05	5.357875-02
8.620	7.644893-05	7.786270-05	8.849265-05	5.319580-02
8.630	7.564503-05	7.704238-05	8.754805-05	5.281542-02
8.640	7.484962-05	7.623074-05	8.661362-05	5.243759-02
8.650	7.406263-05	7.542771-05	8.568924-05	5.206229-02
8.660	7.328396-05	7.463319-05	8.477482-05	5.168952-02
8.670	7.251352-05	7.384710-05	8.387023-05	5.131925-02
8.680	7.175123-05	7.306933-05	8.297538-05	5.095148-02
8.690	7.099699-05	7.229979-05	8.209016-05	5.058618-02
8.700	7.025074-05	7.153842-05	8.121446-05	5.022333-02
8.710	6.951236-05	7.078511-05	8.034819-05	4.986294-02
8.720	6.878180-05	7.003979-05	7.949123-05	4.950497-02
8.730	6.805896-05	6.930236-05	7.864350-05	4.914943-02
8.740	6.734375-05	6.857274-05	7.780487-05	4.879628-02
8.750	6.663611-05	6.785084-05	7.697527-05	4.844551-02
8.760	6.593594-05	6.713660-05	7.615458-05	4.809712-02
8.770	6.524317-05	6.642991-05	7.534273-05	4.775109-02
8.780	6.455772-05	6.573071-05	7.453959-05	4.740739-02
8.790	6.387952-05	6.503891-05	7.374509-05	4.706603-02
8.800	6.320847-05	6.435444-05	7.295913-05	4.672698-02
8.810	6.254452-05	6.367722-05	7.218161-05	4.639022-02
8.820	6.188757-05	6.300715-05	7.141244-05	4.605576-02
8.830	6.123756-05	6.234418-05	7.065155-05	4.572356-02
8.840	6.059443-05	6.168823-05	6.989883-05	4.539362-02
8.850	5.995808-05	6.103923-05	6.915418-05	4.506592-02
8.860	5.932845-05	6.039709-05	6.841755-05	4.474046-02
8.870	5.870547-05	5.976174-05	6.768882-05	4.441721-02
8.880	5.808907-05	5.913312-05	6.696791-05	4.409615-02
8.890	5.747918-05	5.851115-05	6.625474-05	4.377729-02
8.900	5.687572-05	5.789576-05	6.554924-05	4.346060-02
8.910	5.627864-05	5.728688-05	6.485130-05	4.314608-02
8.920	5.568786-05	5.668444-05	6.416085-05	4.283370-02
8.930	5.510331-05	5.608837-05	6.347782-05	4.252345-02
8.940	5.452492-05	5.549860-05	6.280211-05	4.221532-02
8.950	5.395265-05	5.491507-05	6.213365-05	4.190931-02
8.960	5.338641-05	5.433771-05	6.147237-05	4.160538-02
8.970	5.282615-05	5.376646-05	6.081818-05	4.130354-02
8.980	5.227180-05	5.320125-05	6.017101-05	4.100377-02
8.990	5.172330-05	5.264201-05	5.953078-05	4.070605-02
9.000	5.118059-05	5.208869-05	5.889742-05	4.041037-02

X	K1/3(X)	K2/3(X)	K5/3(X)	G
9.010	5.064360-05	5.154121-05	5.827085-05	4.011672-02
9.020	5.011227-05	5.099953-05	5.765099-05	3.982509-02
9.030	4.958655-05	5.046356-05	5.703778-05	3.953546-02
9.040	4.906637-05	4.993326-05	5.643115-05	3.924782-02
9.050	4.855168-05	4.940857-05	5.583102-05	3.896217-02
9.060	4.804242-05	4.888942-05	5.523732-05	3.867847-02
9.070	4.753852-05	4.837575-05	5.464997-05	3.839673-02
9.080	4.703994-05	4.786751-05	5.406893-05	3.811694-02
9.090	4.654661-05	4.736464-05	5.349411-05	3.783907-02
9.100	4.605849-05	4.686708-05	5.292545-05	3.756312-02
9.110	4.557551-05	4.637478-05	5.236288-05	3.728907-02
9.120	4.509762-05	4.588768-05	5.180634-05	3.701692-02
9.130	4.462477-05	4.540572-05	5.125576-05	3.674665-02
9.140	4.415691-05	4.492886-05	5.071107-05	3.647824-02
9.150	4.369397-05	4.445703-05	5.017222-05	3.621169-02
9.160	4.323591-05	4.399018-05	4.963914-05	3.594699-02
9.170	4.278269-05	4.352826-05	4.911176-05	3.568412-02
9.180	4.233423-05	4.307122-05	4.859003-05	3.542308-02
9.190	4.189050-05	4.261900-05	4.807388-05	3.516384-02
9.200	4.145144-05	4.217155-05	4.756325-05	3.490640-02
9.210	4.101701-05	4.172883-05	4.705809-05	3.465074-02
9.220	4.058716-05	4.129079-05	4.655834-05	3.439687-02
9.230	4.016183-05	4.085736-05	4.606394-05	3.414476-02
9.240	3.974099-05	4.042851-05	4.557482-05	3.389440-02
9.250	3.932458-05	4.000419-05	4.509094-05	3.364578-02
9.260	3.891255-05	3.958434-05	4.461223-05	3.339889-02
9.270	3.850486-05	3.916893-05	4.413864-05	3.315372-02
9.280	3.810146-05	3.875789-05	4.367012-05	3.291026-02
9.290	3.770231-05	3.835119-05	4.320661-05	3.266849-02
9.300	3.730737-05	3.794879-05	4.274805-05	3.242841-02
9.310	3.691658-05	3.755063-05	4.229439-05	3.219001-02
9.320	3.652990-05	3.715666-05	4.184558-05	3.195327-02
9.330	3.614730-05	3.676685-05	4.140158-05	3.171818-02
9.340	3.576872-05	3.638116-05	4.096231-05	3.148474-02
9.350	3.539413-05	3.599953-05	4.052775-05	3.125293-02
9.360	3.502348-05	3.562192-05	4.009782-05	3.102274-02
9.370	3.465674-05	3.524830-05	3.967249-05	3.079417-02
9.380	3.429385-05	3.487862-05	3.925171-05	3.056719-02
9.390	3.393478-05	3.451283-05	3.883542-05	3.034181-02
9.400	3.357949-05	3.415090-05	3.842357-05	3.011800-02

X	K1/3(X)	K2/3(X)	K5/3(X)	G
9.410	3.322793-05	3.379279-05	3.801613-05	2.989576-02
9.420	3.288008-05	3.343845-05	3.761304-05	2.967509-02
9.430	3.253588-05	3.308785-05	3.721425-05	2.945596-02
9.440	3.219530-05	3.274093-05	3.681972-05	2.923837-02
9.450	3.185831-05	3.239768-05	3.642940-05	2.902232-02
9.460	3.152486-05	3.205804-05	3.604325-05	2.880778-02
9.470	3.119492-05	3.172199-05	3.566123-05	2.859475-02
9.480	3.086845-05	3.138947-05	3.528328-05	2.838322-02
9.490	3.054541-05	3.106046-05	3.490936-05	2.817318-02
9.500	3.022577-05	3.073491-05	3.453944-05	2.796462-02
9.510	2.990949-05	3.041279-05	3.417346-05	2.775753-02
9.520	2.959654-05	3.009407-05	3.381138-05	2.755190-02
9.530	2.928687-05	2.977870-05	3.345318-05	2.734772-02
9.540	2.898046-05	2.946666-05	3.309879-05	2.714499-02
9.550	2.867728-05	2.915790-05	3.274818-05	2.694368-02
9.560	2.837728-05	2.885239-05	3.240131-05	2.674380-02
9.570	2.808043-05	2.855010-05	3.205814-05	2.654533-02
9.580	2.778670-05	2.825099-05	3.171863-05	2.634827-02
9.590	2.749606-05	2.795503-05	3.138274-05	2.615260-02
9.600	2.720847-05	2.766219-05	3.105044-05	2.595831-02
9.610	2.692391-05	2.737243-05	3.072167-05	2.576541-02
9.620	2.664234-05	2.708573-05	3.039642-05	2.557386-02
9.630	2.636372-05	2.680204-05	3.007462-05	2.538368-02
9.640	2.608804-05	2.652133-05	2.975626-05	2.519485-02
9.650	2.581524-05	2.624358-05	2.944130-05	2.500736-02
9.660	2.554532-05	2.596876-05	2.912968-05	2.482119-02
9.670	2.527823-05	2.569682-05	2.882139-05	2.463635-02
9.680	2.501395-05	2.542775-05	2.851639-05	2.445283-02
9.690	2.475244-05	2.516151-05	2.821463-05	2.427061-02
9.700	2.449368-05	2.489807-05	2.791608-05	2.408968-02
9.710	2.423763-05	2.463740-05	2.762072-05	2.391005-02
9.720	2.398428-05	2.437948-05	2.732851-05	2.373169-02
9.730	2.373358-05	2.412426-05	2.703940-05	2.355461-02
9.740	2.348552-05	2.387174-05	2.675338-05	2.337878-02
9.750	2.324006-05	2.362187-05	2.647040-05	2.320421-02
9.760	2.299718-05	2.337462-05	2.619043-05	2.303089-02
9.770	2.275686-05	2.312998-05	2.591345-05	2.285880-02
9.780	2.251905-05	2.288791-05	2.563941-05	2.268794-02
9.790	2.228374-05	2.264839-05	2.536829-05	2.251831-02
9.800	2.205090-05	2.241138-05	2.510006-05	2.234988-02

X	K1/3(X)	K2/3(X)	K5/3(X)	G
9.810	2.182050-05	2.217687-05	2.483468-05	2.218266-02
9.820	2.159252-05	2.194482-05	2.457212-05	2.201663-02
9.830	2.136694-05	2.171521-05	2.431236-05	2.185180-02
9.840	2.114372-05	2.148802-05	2.405537-05	2.168814-02
9.850	2.092284-05	2.126321-05	2.380111-05	2.152566-02
9.860	2.070428-05	2.104077-05	2.354955-05	2.136434-02
9.870	2.048802-05	2.082067-05	2.330067-05	2.120418-02
9.880	2.027402-05	2.060288-05	2.305444-05	2.104516-02
9.890	2.006227-05	2.038737-05	2.281082-05	2.088729-02
9.900	1.985275-05	2.017414-05	2.256980-05	2.073055-02
9.910	1.964542-05	1.996314-05	2.233134-05	2.057494-02
9.920	1.944026-05	1.975436-05	2.209541-05	2.042044-02
9.930	1.923726-05	1.954778-05	2.186200-05	2.026706-02
9.940	1.903638-05	1.934336-05	2.163106-05	2.011478-02
9.950	1.883761-05	1.914109-05	2.140258-05	1.996359-02
9.960	1.864093-05	1.894095-05	2.117653-05	1.981350-02
9.970	1.844631-05	1.874291-05	2.095288-05	1.966448-02
9.980	1.825373-05	1.854695-05	2.073161-05	1.951654-02
9.990	1.806317-05	1.835305-05	2.051269-05	1.936966-02
10.000	1.787461-05	1.816119-05	2.029609-05	1.922385-02

END 99052 MLSEC

Optical Properties of the Cd_3As_2 - Cd_3P_2 Semiconductor Alloy System*

M. Zivitz and J. R. Stevenson

School of Physics, Georgia Institute of Technology, Atlanta, Georgia 30332

ABSTRACT

The near-normal-incidence, room-temperature reflectance spectra of the Cd_3As_2 - Cd_3P_2 semiconductor alloy system have been measured for photon energies $0.083 < E < 21$ eV. Synchrotron radiation has been used to extend the measurements to 30 eV for Cd_3As_2 . These spectra are similar to those of III-V compounds. Comparison of the primary, reflectance data with the results of others and with the band-structure calculations has been made. The reflectance has been analyzed via the Kramers-Kronig relations. We report curves for n , k , K_1 , K_2 , and n_{EFF} for all the alloys studied. Strong structure in the fundamental absorption scales approximately linearly with alloy composition. Structure at 11 eV is associated with Cd d-band excitation.

I. INTRODUCTION

Considerable attention has been given to the II-V compounds of Zn_3As_2 , Zn_3P_2 , Cd_3As_2 , and Cd_3P_2 as a result of their interesting transport properties: for example, Cd_3As_2 is a degenerate n-type semiconductor with an exceptionally large mobility, low effective mass, and a small band gap, whereas Zn_3As_2 is a p-type semiconductor with very low mobility, a comparatively large effective mass, and a large band gap¹⁻¹⁶. The practical interest in these binary semiconductors has been extended to the alloy systems $\text{Zn}_3\text{As}_2 - \text{Cd}_3\text{As}_2$ ^{17,18}, $\text{Cd}_3\text{As}_2 - \text{Cd}_3\text{P}_2$ ¹⁹⁻²², and $\text{Cd}_3\text{As}_2 - \text{Zn}_3\text{P}_2$ ²³. Since Cd_3As_2 is an end member of each of these alloy systems, it has undergone much investigation. As found in the above references, some controversy has centered on the nature of the fundamental absorption edge in Cd_3As_2 .

Numerous investigations of the band structure of groups IV, III-V, and II-VI binary compounds (and their alloys) have been conducted by means of the analysis of their reflectance spectra. The interpretation of the results is facilitated whenever tentative band-structure calculations have been available²⁴. Band-structure calculations^{25,26} have recently been performed for several II-V compounds. As little research has been performed on these alloys beyond the fundamental-absorption edge²⁷⁻³⁰, the interpretation of our results has been aided by comparison with the above band-structure calculations and with some of the work on III-V semiconductors.

We have measured the near-normal-incidence reflectance spectra of these II-V alloys over a very large range (.03 eV to 50 eV) of photon energy. The high-energy limit of our measurements was extended by use of ultraviolet radiation from the electron storage ring at the University of Wisconsin Physical Sciences Laboratory (31). A Kramers-Kronig analysis was used to generate the optical constants, and we have compared results with the limited (spectrally speaking) results of others^{8,10,27,29}. An assignment of a number of interband-transitions has been made, and these transitions have been located as a function of alloy composition. Qualitative agreement has been obtained with the available band-structure calculations. .

A brief discussion of the chemical considerations and the current band-structure calculations is presented in Sec. II. The experimental techniques are presented in Sec. III. and the primary results are given in Sec. IV. Included in this latter section is a discussion of the reflectance structure above 0.7 eV. Section V presents the optical constants and our interpretation of the transitions which underlie the fundamental absorption edge.

II. THEORETICAL CONSIDERATIONS

The $II_{\frac{1}{3}}^B V_{\frac{2}{3}}^A$ compounds $Cd_{\frac{1}{3}}As_{\frac{2}{3}}$ and $Cd_{\frac{1}{3}}P_{\frac{2}{3}}$ belong to the tetragonal crystal system. The space group for $Cd_{\frac{1}{3}}As_{\frac{2}{3}}$ is $I 4_1 cd$ ^{32,33} and that for $Cd_{\frac{1}{3}}P_{\frac{2}{3}}$ is $P 4_2/n mc$ ^{5,34}. The unit cell for $Cd_{\frac{1}{3}}As_{\frac{2}{3}}$ is composed of 32 formula units, and the unit cell for $Cd_{\frac{1}{3}}P_{\frac{2}{3}}$ is composed of 8 formula units. On the basis of Masumoto's x-ray work² and a discussion of the polymorphic transformation³² in the related $Cd_{\frac{1}{3}}As_{\frac{2}{3}} - Zn_{\frac{1}{3}}As_{\frac{2}{3}}$ alloy system, we believe the $Cd_{\frac{1}{3}}P_{\frac{2}{3}}$ unit cell is related to the $Cd_{\frac{1}{3}}As_{\frac{2}{3}}$ unit cell as depicted in Figure 1.

In either of these alloy systems, the relative disposition of vacancies which occur in the ideal crystal structures differentiates the unit cells of the arsenides from those of the phosphides. In Cd_3As_2 the large As ions are cubic close-packed, and three-fourths of the tetrahedral interstices are occupied by Cd ions. Each As ion is surrounded by Cd ions at six of the eight corners of a cube. If one envisages a lattice of arrows connecting adjacent pairs of these vacant sites, then the repeat distance along the c-axis of the pattern of arrows differs for the arsenides and phosphides.

Although Cd_3As_2 and Cd_3P_2 possess slightly different crystal structures, the more important features of their electronic structures seem related to their similar chemical composition. The Cd and Zn atoms have an outer filled "s" shell, an empty "p" shell, and a filled "d" shell about 9 eV below the filled "s" shell. The As and P atoms have a filled "s" shell and three electrons in their outer "p" shell. No other electrons lie at energies accessible to our measurements. Figure 2 illustrates the ionization energies³⁵, referred to vacuum, of the neutral atomic components of the alloys investigated. The 4d level at 17.6 eV for Cd has been obtained from the multiplicity-weighted average of the $^2\text{D}_{3/2}$ and $^2\text{D}_{5/2}$ terms given by Harrison³⁶. A first approximation to the separation of the "d" band and valence band in the solid is given by the difference between the "d" shell in the group-IIIB atom and "p" shell of the group-V atom.

The above approximation ignores the energy shift caused by a transfer of charge in the more ionic crystals. In the event of such a shift, one should more appropriately use the first ionization energies of the stripped atoms³⁷. Suchet³⁸ has formulated an empirical, electronegativity theory from which the homopolar ϵ_1 and heteropolar ϵ_2 contributions to the

fundamental energy gap, $\epsilon_g = \epsilon_1 + \epsilon_2$, have been computed for a large number of semiconducting, binary compounds. We define the fraction f_i of ionic character as $f_i = \epsilon_2/\epsilon_g$. For Cd_3As_2 , f_i is found to be on the order of 1.0 while a value of 0.3 is found for Cd_3P_2 .

Lin-Chung^{25,26} has performed pseudopotential calculations for the energy-band structures of Cd_3As_2 , Zn_3As_2 , Cd_3P_2 , and Zn_3P_2 . The crystal structure has been simplified by filling all the vacancies. For example in Cd_3As_2 the vacancies are filled with Cd ions. This hypothetical unit cell then transforms into 16 fluorite unit cells with As^{3-} replacing the Ca^{2+} and the Cd^{2+} replacing F^- in the calcium-fluoride structure. The Brillouin zone for this fluorite structure is much larger than that for either Cd_3As_2 or Cd_3P_2 and is identical to that of the fcc structure. The high symmetry points (39) of this fluorite structure are also symmetry points of the real Brillouin zone. Figure 3 demonstrates these two Brillouin zones. The Brillouin zone for the fcc structure is 16 times larger than that for Cd_3As_2 and 8 times larger than that for Cd_3P_2 (this follows since the real unit cells of Cd_3As_2 and Cd_3P_2 have a direct volume ratio of two-to-one).

There is a strong similarity between the overall energy-band structures of Cd_3As_2 and Cd_3P_2 , and both resemble those of the III-V compounds (InAs, GaSb, etc.). Figure 4 gives the energy-band structures for Cd_3As_2 and Cd_3P_2 as calculated by Lin-Chung. The lowest valence-band is an anion s-like level, the second valence band is a Cd s-like level; and the third and fourth are s-like about Cd and p-like about the anion. The valence band maximum for Cd_3P_2 is at Γ ; that for Cd_3As_2 , slightly ($\sim 12\%$) off center of the Brillouin zone. The bottom of the conduction band at Γ has an s-like representation Γ_1 . The predicted energy gap for Cd_3As_2 is ~ 0.2 eV or smaller.

III. MEASUREMENTS

The energy range 0.005 to 30 eV required the use of four optical systems. The description of these systems has been reported in detail⁴⁰. The region $0.005 < E < 1.9$ eV (1.5 to 0.65 μ) was investigated by using a Perkin-Elmer Corp. "Optical Reflectance Attachment" and a Perkin-Elmer model 99 monochromator with a NaCl prism. Both a globar and tungsten-halogen lamp were used as sources, and a Reeder Corp. thermocouple was used with a synchronous-rectification detection scheme. The reflectance measurements were taken at room temperature and atmospheric pressure.

From 1.9 to 7.3 eV (6500 to 1700 Å) the sample environment was more carefully controlled than in other spectral regions by use of an ultrahigh-vacuum (10^{-8} Torr) reflectometer of conventional design and an ion pump. A McPherson 0.3-m, scanning monochromator with provisions for evacuation and easy interchange of gratings (1500 Å and 5000 Å-blaze angles) served to span this range. A lithium-fluoride-window flange was used to support the pressure differential between the reflectometer and monochromator. Both a tungsten-halogen lamp and a glow discharge in several Torr of hydrogen provided continuum sources in this range. A 13-stage PM tube and light pipe (phosphor coated above 3 eV) served as the base for simple dc detection.

The region from 7.3 to 21 eV (1700 to 600 Å) was investigated by means of a General Electric GEI-44854, 1-m, normal-incidence monochromator, similar to that designed by Johnson⁴¹. This monochromator was highly modified and provided with an 800-Å blazed grating. The sample chamber used by Hinson⁴² was slightly improved. A 13-stage PM tube was used with a sodium-salicylate-coated light pipe and synchronous-rectification detection schemes. Below 13 eV, a glow-discharge lamp was operated in a dc mode to provide the many-

lined hydrogen spectrum. A tuning-fork chopper interrupted the emergent beam from the monochromator and provided a reference signal. Above 13 eV, the glow-discharge lamp was operated in a repetitive, condensed discharge mode to provide the H α continuum. The ac line to a McPherson 720 spark supply was interrupted to generate a 50-Hz fundamental in the radiation which reached the PM tube.

Synchrotron radiation from the 240-MeV electron storage ring at the University of Wisconsin's Physical Sciences Laboratory provided an intense continuum which extended the high-energy of our data to 30 eV. A simple reflectometer, employing a channel-electron multiplier in a current-integrated mode, was attached to the exit-slit housing of a 1-m, normal-incidence monochromator. Repeated scans were employed for the "sample-in" and "sample-out" configurations. The count rates were normalized to the electron-beam currents.

A total of eight samples were obtained from the Naval Research Laboratory (N.R.L.) of Washington, D. C. All the members $\text{Cd}_3(\text{As}_x\text{P}_{1-x})_2$, where $0 \leq x \leq 1$, were prepared by a modified Bridgman method⁴³. Our observations, as well as those of Wagner et al.²⁰, were that the $\text{Cd}_3(\text{As}_{0.25}\text{P}_{0.75})_2$ and the $\text{Cd}_3(\text{As}_{0.12}\text{P}_{0.88})_2$ crystals are not mechanically strong. Radoff and Bishop²² have reported that for $x = 0.25$ the Bridgman-grown ingots show cracks associated with a solid-solid phase transition¹⁹. Table 1 summarizes the appearance of this set of samples.

Mechanical polishing and etching techniques were developed along lines suggested by the group at N.R.L.⁴⁴. Polishing began with a mixture of 1- μ Alumina powder (Union Carbide) and tap water, and was continued until no scratches were visible except those left by the powder. This was followed by polishing with a suspension of 1/4- μ diamond compound (Buchler AB Metadi) in a lapping oil (Buchler AB Antomet). Final polishing was performed with a mixture of 0.05 (500 Å)-Alumina powder and distilled water. Only limited success was

obtained with an etch consisting of a solution of HNO_3 in Methanol (5 to 0.03% by vol.). Little effort was expended toward orientation of the crystallographic axes. Although etched, the crystalline regions of several of the samples were sizeable.

As discussed above, several monochromators (gratings, prism), light sources, and sample chambers were used to span the energy range 0.033 to 30 eV. Table II gives an overview of the component spaces that linked to form the entire region of interest. In the following presentation, samples will be denoted by the integer indices defined in Table I. These indices are numbered one through eight and increase somewhat in proportion to the concentration of the arsenic constituent of these alloys. The index "1" denotes P_2 . The index "8" denotes Ca_3As_2 .

IV. RESULTS AND TRENDS ABOVE 0.7 eV

The results of the near-normal-incidence reflectance measurements are presented in Figure 5. For several typical results, the nearly transparent or plasmon region is also shown in Figure 6. The results of the extreme-UV measurements are presented in Figure 7. Included in this latter figure are the results of measurements on the related compound Zn_3As_2 ²⁵. We note that the structure in the reflectance curves of the mid-members of this alloy system is as well defined as that for the end-members.

We redraw the primary data of Figure 5, as shown in Figure 8. These curves are zero-shifted in relation to the percentage of the anion concentration ("x" values of Table I). We defer treatment of the sharp structure below 0.7 eV and begin with a discussion of the structure in the range of 2 eV. Figure 8 suggests a linear scaling of the position of this peak versus

the alloy composition. In accordance with the work of Sobolev et al. on Cd_3As_2 , we label this peak E_1 . The more refined data of Sobolev has shown this peak to be split by ~ 0.2 eV (see Figure 9). The center of gravity of the peak for Cd_3As_2 agrees well with Min-Chung's band structure (B.S.) calculation. The corresponding peak for Cd_3P_2 agrees poorly with the respective B.S. calculation. See Table III for a comparison of these observed peaks with the B.S. calculations. The probable assignments are made by analogy to the zinc-blende III-V compounds (e.g., GaAs).

The doublet character of this peak in Cd_3As_2 is presumably due to the spin-orbit splitting of the upper valence band (Λ_3) along the Λ direction. This upper valence band is p-like about the As atom. A good estimate of the spin-orbit splitting⁴⁵⁻⁴⁷ of the upper valence band at the Γ point can be obtained from the spin-orbit splitting of the states of "p" character of the isolated anion atom (e.g., the terms $^2P_{1/2}$ and $^2P_{3/2}$ of As III). In going from the isolated anion atom to the solid, the splitting is enhanced by the factor 29/11. Using Moore's tabulation³⁷ of atomic terms, we thereby obtain 0.1 and 0.35 eV for the spin-orbit splitting at Γ for Cd_3P_2 and Cd_3As_2 respectively.

In analogy to the III-V compounds, the splitting observed in the reflectance structure is along the Λ direction. Along this direction the upper valence band is, presumably, further spin-orbit split. The degree of the latter splitting is 2/3 of the splitting at the Γ point.

We therefore expect the observed splitting of the reflectance peak in the range of 2 eV to be 0.067 and 0.35 for Cd_3P_2 and Cd_3As_2 , respectively. This estimate of 0.35 eV is in qualitative agreement with the 0.2-eV splitting observed by Sobolev. The resolution of our instrumentation in this region has prevented our observation of this splitting in Cd_3As_2 . However, our estimated splitting of 0.067 eV for Cd_3P_2 would surely be obscured by lifetime broadening at room

temperature. It is clear that the contribution to the "joint density of states" is large along a range of the line from Γ to L, since the bands Λ_1 and Λ_3 are nearly parallel in both Cd_3P_2 and Cd_3As_2 near the L point.

The peak in the range of 4 eV is labeled $E_{3,4}$, since it corresponds to an average of the locations of the peaks E_3 and E_4 found by Sobolev in Cd_3As_2 (see Figure 9). In both end-members of this alloy system we assume that the peak E_3 corresponds to the transition $X'_5 \rightarrow X_3$ and that E_4 corresponds to $\Lambda_3 \rightarrow \Lambda_1$. In Cd_3P_2 , the nearby transition $\Gamma_{15} \rightarrow \Gamma_{25}$ appears to be as likely an assignment as $\Lambda_3 \rightarrow \Lambda_1$ for peak E_4 . The peak E_2 is not resolved in our data. We assume that peak $E_{3,4}$ scales with the composition as shown in Figure 8. If the peak $E_{3,4}$ indeed scales as illustrated, then our results are in qualitative agreement with the B.S. calculations (see Table 3).

The structure of this peak $E_{3,4}$ represents a departure from the corresponding structure in the III-V compounds. In GaAs the similar peak, which is located around 5 eV, is associated with the transition $X_5 \rightarrow X_1$. A slightly higher-energy (~ 0.5 eV) satellite is identified with $X_5 \rightarrow X_3$ and a lower-energy (~ 0.5 eV) energy shoulder is identified with $\Gamma_{15} \rightarrow \Gamma_{15}$ transitions. [The above representations belong to GaAs⁴⁸]. In contrast to this distribution of oscillator strengths in GaAs, we associate vanishingly small oscillator strength in the II-V alloys with the $X'_5 \rightarrow X_1$ transition. The B.S. calculations predict $X'_5 \rightarrow X_1$ to be at 3.4 eV and 2.7 eV in Cd_3P_2 and Cd_3As_2 , respectively. The assignments $\Lambda_3 \rightarrow \Lambda_1$ for a contribution to the peak $E_{3,4}$ are nearly zone centered, and thus correspond to $\Gamma_{15} \rightarrow \Gamma_{15}$ in GaAs. However, in the $\text{Cd}_3\text{As}_2 - \text{Cd}_3\text{P}_2$ system, the transition $\Lambda_3 \rightarrow \Lambda_1$ lies above $X'_5 \rightarrow X_3$ (at least in Cd_3As_2), and in GaAs the transition $\Gamma_{15} \rightarrow \Gamma_{15}$ lies below $X_5 \rightarrow X_1$.

The decrease in reflectance between peak $E_{g,h}$ and the rise at 11 eV is similar to that found in III-V compounds and corresponds to the near exhaustion of the f-sum rule for interband transitions⁴⁹. This overall decrease in reflectance typically signals the onset of the plasmon region. Below, we shall find a broad peak in the characteristic-energy-loss function in the range of 9.5 eV for all members of this alloy system.

Figure 6 shows that all samples exhibit a sharp increase in the reflectance at ~ 11 eV. Since the bonding in these alloys appears to have a large ionic character, it is reasonable to assume that the Cd 4d atomic levels generate a narrow band below the valence bands (in a tight-binding picture, charge transfer will lower these levels in the solid). This consideration of the relative position of the "d" band in these alloys and the fact that this onset at 11 eV is independent of alloy composition lead us to the conjecture that this threshold corresponds to the onset of "real" "d" band-to-conduction-band transitions. The data obtained for Cd_3As_2 and Zn_3As_2 at the electron storage ring provide evidence that this structure at 11 eV is not due to an instrumental error (see Figure 7).

In the ionic II-VI compounds CdS, CdSe, and CdTe Freeour⁵⁰ has identified a doublet at ~ 13.5 eV with the spin-orbit-split transition from the Cd 4d level. In contrast, rudimentary measurements⁵¹ on elemental Cd have revealed no semblance of structure in this spectral region.

Since we have thus far chosen to interpret the reflectance structure directly and since there exists no values of the optical constants beyond the fundamental edge, we find it convenient to compare our reflectance values with the results of others at this stage of the exposition. A detailed account has been reported⁴⁰. We merely note here that the apparent structure beyond the point labeled "MIN" in Figure 6 is due to a systematic error.

Both Turner et al.³ and Haidemenakis et al.¹⁴ have reported infrared, plasma-edge, reflectance measurements for Cd_3As_2 . These measurements overlap our low-energy reflectance spectra and provide a check on our absolute values. We obtain better agreement with Reference (3) and the percentage difference of the present results with respect to those of Turner et al. is +8% at 0.25 eV. Since both References (3) and (14) located the IR plasma edge at ~ 0.05 eV, we shall subsequently define the optical dielectric constant to be that dielectric constant between the fundamental-absorption edge and the Reststrahlen bands or the IR plasma edge. We find that this definition is compatible with the optical properties of Cd_3As_2 , since the photon-energy interval between the plasma edge and the fundamental edge (~ 0.6 eV) is so large.

At higher, photon energy we compare our reflectance values for the end member Cd_3As_2 with those of Sobolev et al.²⁹ in Figure 9. The curves labeled "B" and "C" are equally zero-shifted as indicated to prevent overlap. The measurements of Sobolev have been performed on single, unoriented crystals. His 293°K data is discontinuous not only in absolute magnitude, but also in shape. (Our data suffered background problems in the encircled region of this figure). At 1.6 eV our data has an absolute error of +12% with respect to the data of Sobolev. In view of our error analysis⁴⁰, we believe the data of Sobolev is not well disposed to an absolute scale.

When the data of Figure 9 are inspected more closely, it is seen that our structure is poorly defined relative to that of Sobolev. We can only assume that this lack of definition is due to the poor crystalline quality or that the damaged layer incurred during the mechanical polishing has not been removed by the etchant. Between 5 and 12 eV, Sobolev also obtained a series of peaks labeled $E_5 - E_9$.

Sobolev et al.³⁷ has also performed rudimentary reflectance measurements on Cd_3P_2 . Figure 10 displays the present results for Cd_3P_2 and those of Sobolev, whose curve is given in arbitrary units. Their peak at ~ 4 eV is reasonable in view of our results. Note the strong similarity of this peak in our results for all members of this alloy system in Figure 5. The fact that Sobolev has used a polycrystalline sample of Cd_3P_2 leads us to believe that the departure of our results from those (on single crystals) of Sobolev in Figure 9 is attributable to a polycrystalline surface of our prepared samples. The remaining portion of their data on Cd_3P_2 does not seem reasonable.

V. OPTICAL CONSTANTS

Since the present results are representative of a polycrystalline surface, we have used the simple expressions

$$n = (1 - |\tilde{r}|^2) / (1 - 2|\tilde{r}| \cos \theta + |\tilde{r}|^2) \quad (1)$$

$$k = 2|\tilde{r}| \sin \theta / (1 - 2|\tilde{r}| \cos \theta + |\tilde{r}|^2) \quad (2)$$

for the real and imaginary components of the complex index of refraction

$$\tilde{N} = (n + ik). \quad (3)$$

The reflectivity is defined via

$$\tilde{r} = |\tilde{r}| e^{i\theta}, \quad 0 \leq \theta < \pi \quad (4)$$

so that the phase shift θ is that of the magnetic field^{40,52}. We have integrated the Kramers-Kronig integral

$$\theta(E) = (-1/2\pi) P \int_0^\infty \left[\frac{d \ln R(E')}{dE'} \right] \ln \left| \frac{E' + E}{E' - E} \right| dE' \quad (5)$$

by choosing the upper-energy limit of the integral, so that the phase shift vanishes below the fundamental band gap.

Our assumed form for the reflectance ($R = |\tilde{r}|^2$) above 21 eV is not completely arbitrary. If indeed the absorption above 11 eV is due to the Cd 4d levels, then the reflectance curve of Figure 7 for $\text{Cd}_{1/3}\text{As}_2$ provides an "assumed" form for all members of this alloy system. That portion of the reflectance data below the adjusted upper limit has been numerically integrated by means of a computer program kindly furnished by Shay⁵³. The gap energies at which the phase shifts vanish are the room-temperature gaps reported by Wagner et al.²⁰.

We present the results of the phase-shift analysis in the form of curves for the dual quantities "n" and "k". These curves are given in Figure 11. The zero shifting for either family of curves is in the successive amount of one unit.

At 0.4 eV, we obtain the value of $n = 4.04$ for $\text{Cd}_{1/3}\text{As}_2$. In this same region, Haidemenakis et al.⁸ obtained the estimate $n = 4.3$ ($n_\infty = k_\infty^{1/2}$). Zdanowicz¹⁰ found $n = 5$ and $k = 0.04$ ($k = \alpha/2\omega$) at 0.413 eV (3μ). These latter values of "n" and "k" yield a normal-incidence reflectance of $0.44[\tilde{r} = (\tilde{N}-1)/(\tilde{N}+1)]$, which is even 10% greater than our value. Recall that our reflectance was greater than that of both References (3) and (8). Of greater significance is the fact that both these other results lead to an energy dependence of "n" (and "R") opposite ours in this low-energy region. The cause of the disagreement is not apparent.

Zdanowicz has found a sharp peak in "n" at ~ 0.6 eV. This peak has been associated^{10,25} with the fundamental-absorption edge in $\text{Cd}_{1/3}\text{As}_2$. The underlying transition is thought to be zone centered in the real crystal structure ($\Gamma_{15} \rightarrow \Gamma_1$). Our $\text{Cd}_{1/3}\text{As}_2$ data exhibit only a weak shoulder in "n" at ~ 0.6 eV.

Now use is made of the relations

$$\kappa_1 = n^2 - k^2 \quad (6)$$

and

$$\kappa_2 = 2nk$$

which yield the real and imaginary components of the complex dielectric constant (relative permittivity)

$$\tilde{\kappa} = \kappa_1 + i\kappa_2 \quad (8)$$

The families of these quantities are given in Figure 12. As usual, the structure in the κ_2 curve is seen to follow that in the reflectance.

We now turn our attention to the structure below 0.7 eV. The structure in this particular region is sufficiently well defined as to be amenable to a description in terms of the joint density of states.

Several characteristic shapes in κ_2 resemble four basic forms ($M_0 \rightarrow M_4$) of the joint density of states in the range of allowed transitions at critical points which are also symmetry points²⁴. This structure in κ_1 and κ_2 , along with the reflectance "R" is illustrated in both Figures 13 and 14.

With the exception of Cd_3As_2 , we have marked two discontinuities in the slopes of the κ_2 curves. The solid arrow locates what appears to be an M_0 critical point; the dotted arrow, an M_1 critical point. In the case of Cd_3As_2 , the arrow appears to locate an M_0 critical point; however, we have encountered large relative error in this spectral region.

We have been aided in the determination of the location of the M_0 critical points by the room-temperature gaps of Wagner et al.²⁰. The underlying trans-

ition is $\Gamma_{15} \rightarrow \Gamma_1$, according to Lin-Chung's B.S. calculations. Figure 15 gives a plot of the location of this M_0 critical point as a function of alloy composition. Note the agreement with the transmission edges found by Reference (20).

These critical-point identifications have been made in the following way. The sharp rise in the κ_2 curves at the point labeled by the solid arrow is characteristic of an M_0 critical point⁵⁴. Were this the only nearby contribution to the joint density of states, one would further expect κ_1 (and "R", since "k" is small here) to peak at the same location. We observe that in all cases, except for Cd_3As_2 , the κ_1 curve peaks above the location of the M_0 critical point. An explanation of this relative shift in structure is readily obtained if the change in slope of the κ_2 curves (located by the dotted lines) is due to an M_1 critical point. An M_1 critical point gives rise to peaking of the κ_1 curve slightly below the location of the M_1 critical point⁵⁵. Thus, we find that the interpretation of two nearby critical points, M_0 and M_1 , contributing to a peaking of κ_1 (and "R") between the location of these critical points is consistent with the dielectric constants.

The location of the M_1 critical point is in qualitative agreement with Lin-Chung's B.S. calculations. The "X" point and the Γ point of the hypothetical structures are equivalent in the real crystal structure: the "X" point becomes a Γ point. We, therefore, envisage the direct transitions in the real structure giving rise to the M_1 critical point to be $\Gamma_{15} \rightarrow X_1$ in these alloys. We are unable to identify the exact type of critical point in Cd_3As_2 , but we assume the same transition is involved. Lin-Chung has placed this transition $\Gamma_{15} \rightarrow X_1$ at 1.2 eV in Cd_3As_2 , and believes that it corresponds to the direct gap ϵ_g found by Adamowicz¹⁰ at ~ 0.6 eV. In Cd_3P_2 , she has placed the transition $\Gamma_{15} \rightarrow X_1$ at 1.875 eV. We find this transition at ~ 0.63 eV in Cd_3P_2 , and there-

There have the same qualitative agreement with the M.S. calculations as did Klemm for Cd_3As_2 . Figure 15 also displays the composition dependence of this H_1 critical point and includes the low-temperature gaps given by Radoff and Misher²².

Error estimates for the dielectric constants have been discussed elsewhere⁴⁰. We report here that the optical dielectric constants have probable errors of $\pm 18\%$. In view of the above comparisons of our primary data with that of others, the optical constants at higher energy are only qualitatively correct.

The expression ("partial" sum rule)

$$n_{\text{EFF}} = [2m/N(\text{he})^2] \int_0^E E' \kappa_2(E') dE' \quad (9)$$

yields an effective number of free electrons contributing to the optical properties over a finite range $0 < E' < E$. "N" is the atomic density of the solid. The successive values of n_{EFF} are displayed in Figure 16. Since there are exactly 3.2 valence electrons per atom, we are somewhat surprised to find that these curves nearly saturate (before the rise at 12 eV) at a value of ~ 2.2 . In particular, since the Cd d-band transitions are expected to overlap nearly the tail of the fundamental absorption spectra in these alloys, we should look for an enhancement of n_{EFF} over the valence-electron contribution of 3.2. We attribute this disagreement to absolute reflectance values which are low above ~ 6 eV. Sample No. 2 appears to represent a favorable counter example to the failure of n_{EFF} to reach a higher level; however, the absolute reflectance data of this sample has been found to be inconsistent with our Kramers-Kronig extrapolation scheme.

The f-sum rule for interband transitions which involve the valence bands is nearly exhausted in the range of 9 eV. This remark is complemented by these curves of n_{imp} . It is also usually the case that these valence electrons, in conjunction with d-band contributions are able to participate in bulk plasmons. Figure 17 in fact shows a broad peak in the characteristic-energy-loss function $\text{Im}(1/K)$. If the absolute values of our primary data indeed drop too fast in this photon-energy range, then these peaks provide a lower estimate of ~ 9.5 eV for the plasmon energy. For comparison, the free-electron plasmon energy, due to the valence electrons only, is 13.13 eV for Cd_3As_2 . This latter number is given for crude comparison only. The d-bands not only enhance the effective number of electrons available to contribute to a plasmon, but also provide a measure of shielding of the Coulomb interactions. Furthermore, the dependence of the plasmon energy on the volume of the unit cells is weak ($E_p \sim V^{-\frac{1}{3}}$). Since the unit-cell volume change from Cd_3As_2 to Cd_3P_2 is small, we do not list the free-electron plasmon energies for the other alloys.

A partial summary of our results is presented in the form of a plot of the structure in K_2 or "R" versus the alloy composition. We present these findings in Figure 18. The upper two curves have been obtained from the peaks in the reflectance data; the lower two curves, from the structure in K_2 .

VI. ACKNOWLEDGMENTS

We wish to acknowledge the assistance of H. W. Ellis and S. P. Zehner in making the extreme-UV measurements and of those for operating the electron storage ring. Helpful discussions and comments from T. C. Collins, F. C. Brown, G. W. Hubloff and B. Sonntag are gratefully acknowledged. The efforts of E. M. Swiggard of NRL in growing the crystals and the discussions with E. D. Palik and P. J. Liu-Chung have been most valuable.

Research sponsored by the Air Force Office of Scientific Research, Air Force Systems Command, USAF, under Grant No. AFOSR-70-1892. The synchrotron Radiation Facility at the University of Wisconsin is supported under Air Force Contract No. F44620-70-0009.

1. T. S. Moss, Proc. Phys. Soc. (London) B63, 167 (1950).
2. W. J. Turner, A. S. Fischler, and W. E. Reese, Phys. Rev. 121, 759 (1961).
3. W. J. Turner, A. S. Fischler, and W. E. Reese, J. Appl. Phys. Suppl. 32, 2241 (1961).
4. G. Haacke and G. A. Castellion, J. Appl. Phys. 35, 2484 (1964).
5. W. Zdanowicz and A. Wojakowski, Phys. Stat. Sol. 8, 569 (1965).
6. Y. A. Ugai and T. A. Zyubina, Izvest. Akad. Nauk SSSR, Neorgan. Mater 1 866 (1965). [Sov. Phys. - Inorg. Mater. 1, 790 (1965)].
7. D. P. Spitzer, G. A. Castellion, and G. Haacke, J. Appl. Phys. 37, 3795 (1966). Appendix.
8. E. D. Haidemenakis, M. Dalkanski, E. D. Pakik, and J. Tavernier, J. Phys. Soc. Japan Suppl. 21, 189 (1966).
9. H. Sexter, Phys. Stat. Sol. 21, 225 (1967).
10. L. Zdanowicz, Phys. Stat. Sol. 20, 473 (1967).
11. D. Armitage and H. J. Goldsmid, Phys. Letters 28A, 149 (1968).
12. F. A. P. Blom and J. T. Schrama, Phys. Letters 30A, 245 (1969).
13. I. Rosenman, J. Phys. Chem. Solids 30, 1385 (1969).
14. S. G. Bishop, W. J. Moore, and E. M. Swiggard, Proc. Third Int. Conf. on Photoconductivity, Stanford University, 1969, edited by F. M. Pell (Pergamon Press, Oxford, 1971), p. 205.
15. S. G. Bishop, W. J. Moore, E. M. Swiggard, Appl. Phys. Letters 16, 459 (1970).

16. M. W. Heller, J. Balchukin, and P. L. Radoff, Phys. Letters 36A, 363 (1971).
17. R. J. Wagner, E. D. Palik, and E. M. Swiggard, Phys. Letters 30A, 175 (1969).
18. L. M. Rogers, R. M. Jenkins, and A. J. Crocker, J. Phys. D: Appl. Phys., 7 793 (1971). Appendices.
19. K. Marumoto and S. Isomura, Energy Convers. 10, 129 (1970).
20. R. J. Wagner, E. D. Palik, and E. M. Swiggard, J. Phys. Chem. Solids Suppl. 1, 471 (1971).
21. S. G. Bishop and P. L. Radoff, Solid State Communications 9, 133 (1971).
22. P. L. Radoff and S. G. Bishop, Phys. Rev. B 5, 442 (1972).
23. W. Zdanowicz, F. Krolicki, P. Pleniewicz, Acta Phys. Polon. A 41, 27 (1972).
24. J. C. Phillips, Solid State Physics 18, 55-164 (1966).
25. P. J. Lin-Chung, Phys. Rev. 188, 1272 (1969).
26. P. J. Lin-Chung, Phys. Stat. Sol. 47, 33 (1971).
27. V. V. Sobolev, N. N. Syrbu, and S. D. Shutov, Chemical Bonds in Semiconductors and Thermodynamics, edited by N. N. Sirota (Consultants Bureau, New York, 1968), p. 165.
28. M. Zivitz, R. J. Bartlett, and J. R. Stevenson, Bull. Am. Phys. Soc. 15, 1343 (1970).
29. V. V. Sobolev, N. N. Syrbu, T. A. Zyubina, and Y. A. Ugai, Fiz. Tekh. Poluprov. 5, 327 (1971). [Sov. Phys.-Semicond. 5, 279 (1971)].
30. J. R. Stevenson, M. Zivitz, H. Ellis, R. J. Bartlett, Third Int. Conf. on Vacuum Ultraviolet Radiation Physics, Tokyo, Japan, 30 Aug. - 2 Sept. 1971.
31. E. M. Rowe, R. A. Otte, C. H. Pruett, and J. D. Steben, Trans. IEEE Nucl. Sci. NP-16, 159 (1969).
32. W. Zdanowicz, K. Lachowicz, and W. Trzebiatowski, Bull. Acad. Polon. Sci., Sér. sci. Tech. 12, 169 (1964).
33. G. A. Steigman and J. Goodyear, Acta Cryst. B24, 1062 (1968).

Table I

Index of Samples and Qualitative Comment on
Crystalline Quality of Samples

Sample	End Member	(N.R.L.) Ingot Number	$\text{Cd}_3(\text{As}_x\text{P}_{1-x})_2$	Comment
1	✓	----	$x=0.00$	cracked
2	----	8-151-3E	$x=0.12$	good
3	----	8-149-8B	$x=0.25$	badly cracked
4	----	8-111-7	$x=0.50$	good
5	----	8-111-8	$x=0.50$	very good
6	----	8-59-13B	$x=0.75$	cracked
7	----	8-59-13C	$x=0.75$	good
8	✓	----	$x=1.00$	badly cracked

Table II. Summary of Experimental Instrumentation and Conditions.

Scan No.	Light Source	Monochromator	Dispersing Element	Wavelength Span	Resolution $\sim \Delta\lambda$	Chamber Pressure [Torr]	Mode of Acquisition
0	Synchrotron	1-m Normal Incidence	800-Å Blaze Grating	400-1200 Å	5 Å	$\sim 1 \times 10^{-7}$	Repeated Scans
1	Glow Discharge H ₂ I	1-m Normal Incidence	800-Å Blaze Grating	584 Å	4 Å	$\sim .6 \times 10^{-1}$	Point by Point
2	Condensed Discharge He ₂	1-m Normal Incidence	800-Å Blaze Grating	650-950 Å	5 Å	$\sim .2 \times 10^{-1}$	Point by Point
3	Glow Discharge H ₂	1-m Normal Incidence	800-Å Blaze Grating	950-1700 Å	10 Å	$\sim .6 \times 10^{-1}$	Point by Point
4	Glow Discharge H ₂	.3-m Czerny-Turner	1500-Å Blaze Grating	1700-3050 Å	5 Å	$\sim 1 \times 10^{-8}$	Repeated Scans
5	Glow Discharge H ₂	.3-m Czerny-Turner	5000-Å Blaze Grating	3050-3600 Å	5 Å	$\sim 1 \times 10^{-8}$	Repeated Scans
6	Tungsten Halogen Lamp	.3-m Czerny-Turner	5000-Å Blaze Grating	3600-6500 Å	5 Å	$\sim 1 \times 10^{-8}$	Repeated Scans
7	Tungsten Halogen Lamp	Littrow Mounting	NaCl Prism	0.65-1.4 μ	20 \rightarrow 160 Å	Atm.	Point by Point
8	Globar	Littrow Mounting	NaCl Prism	1.4-15 μ	.016 \rightarrow .9 μ	Atm.	Point by Point

Table III. Probable Assignments, between 0.7 and 6 eV, of Interband Transitions.

Ref. No. 29	Peaks	$\text{Cd}_{1-x}\text{As}_x$ 295°K 77°K	B.S. Calculation	Probable Location
	E_1	1.7 1.74	} 1.7 {	$\Lambda_3 \rightarrow \Lambda_1$
	E_1'	1.88 1.90		$\Lambda_3 \rightarrow \Lambda_1$
	E_2	2.86 2.86	2.7	$\Sigma_4 \rightarrow \Sigma_1$
	E_3	3.33 3.26	2.8	$X_5' \rightarrow X_3$
	E_4	3.7 3.7	3.9	$\Lambda_3 \rightarrow \Lambda_1$
	E_5	5.15 ...	{ 4.7	$\Lambda_3 \rightarrow \Lambda_3$
			{ 5.2	$X_4' \rightarrow X_1$
Present Results	Peaks	$\text{Cd}_{1-x}\text{As}_x$ 297°K	B.S. Calculation	Probable Location
	E_1	1.7	1.7	$\Lambda_3 \rightarrow \Lambda_1$
	$E_{3,4}$	3.6	{ 2.8	$X_5' \rightarrow X_3$
			{ 3.9	$\Lambda_3 \rightarrow \Lambda_1$
Present Results	Peaks	$\text{Cd}_{1-x}\text{P}_x$ 297°K	B.S. Calculation	Probable Location
	E_1	1.9	2.4	$\Lambda_3 \rightarrow \Lambda_1$
	$E_{3,4}$	4.0	{ 3.9	$X_5' \rightarrow X_3$
			{ 5.1	$\Lambda_3 \rightarrow \Lambda_1$

REF 33

($a = 12.67 \text{ \AA}$)
($c = 25.48 \text{ \AA}$)

REF 34

($a' = 8.74 \text{ \AA}$)
($c' = 12.28 \text{ \AA}$)

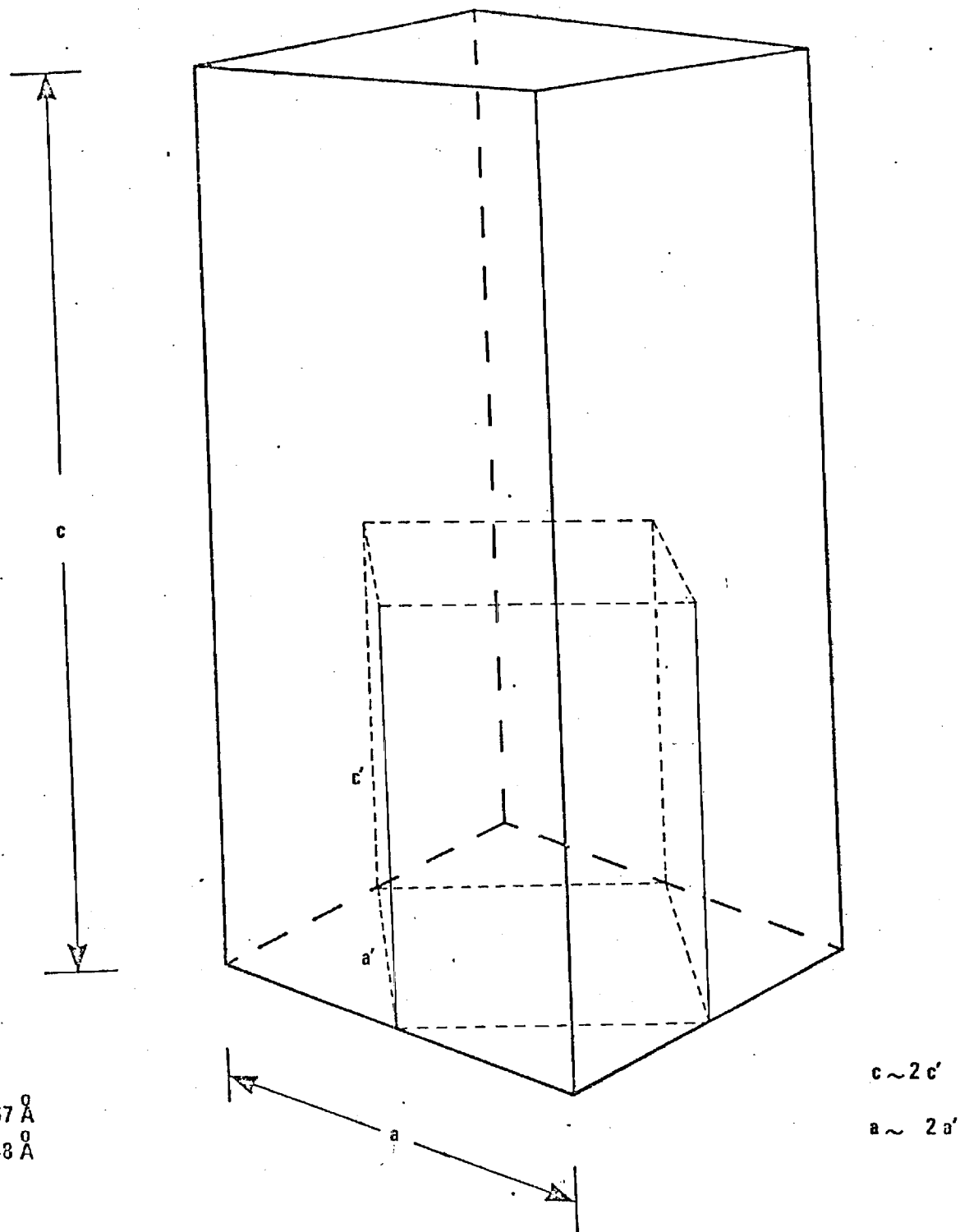


Figure 1. Relative Sizes and Orientations
of the Cd_3As_2 and Cd_3P_2 Unit Cells

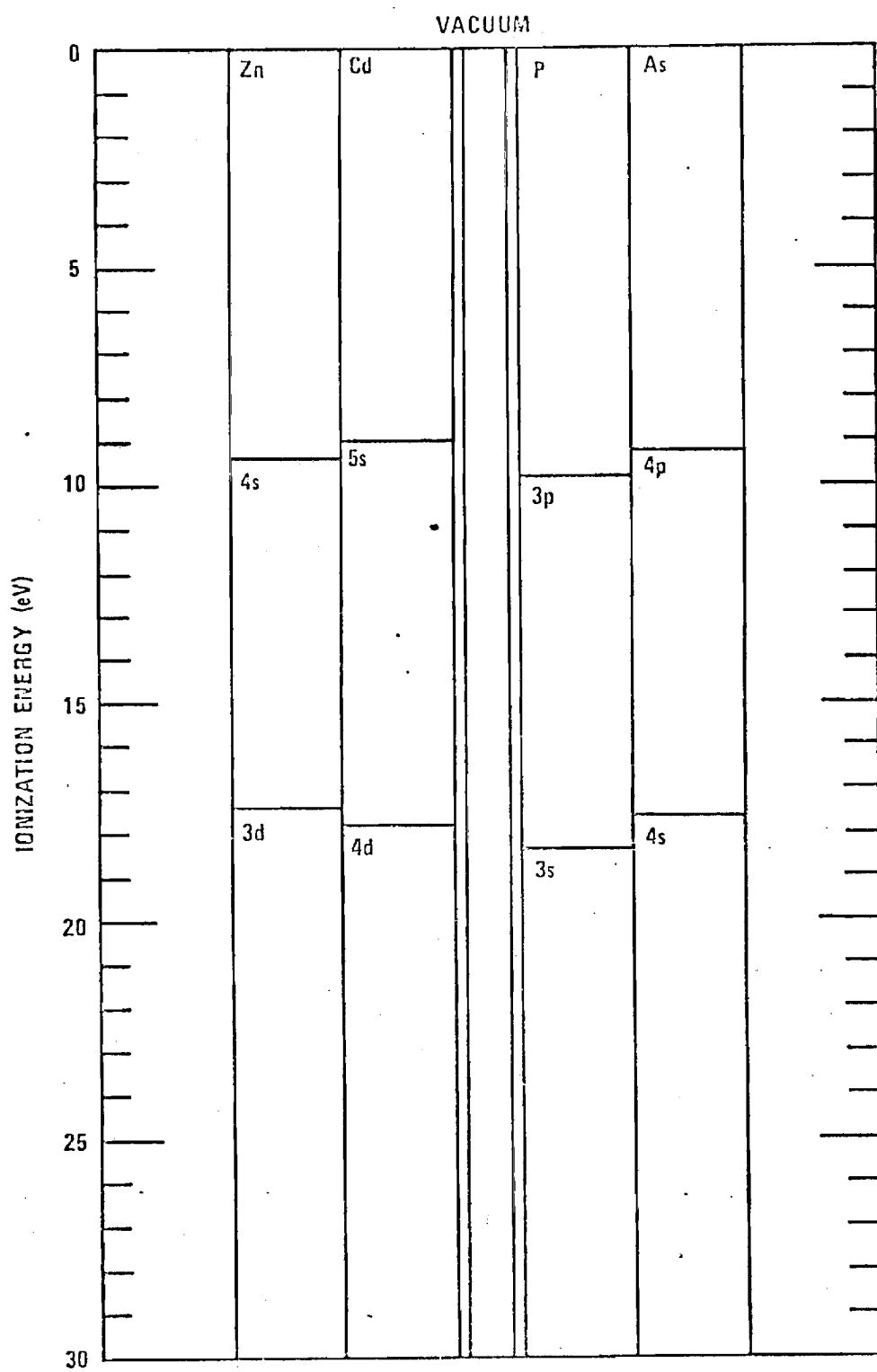


Figure 2. Ionization Energies for the Atomic Components of the II-V Alloys Investigated

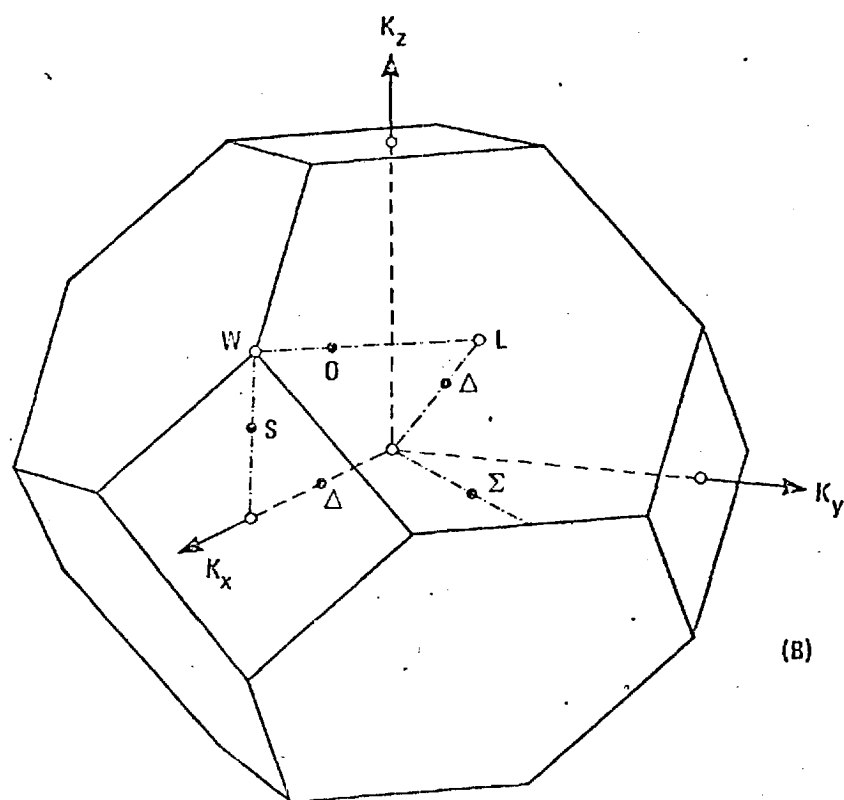
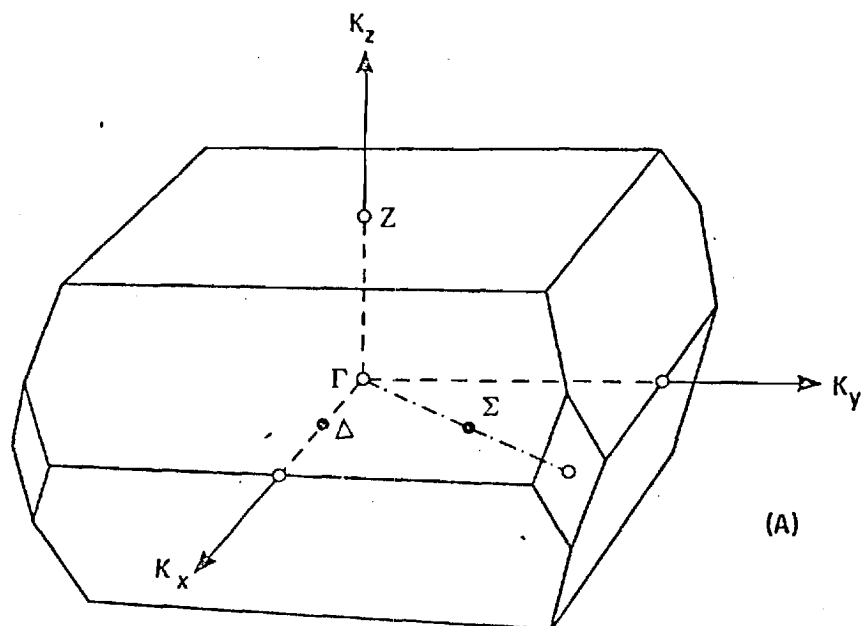


Figure 3. The First Brillouin Zone of (A) Body-Centered Tetragonal Structure, and (B) Fluorite Structure.

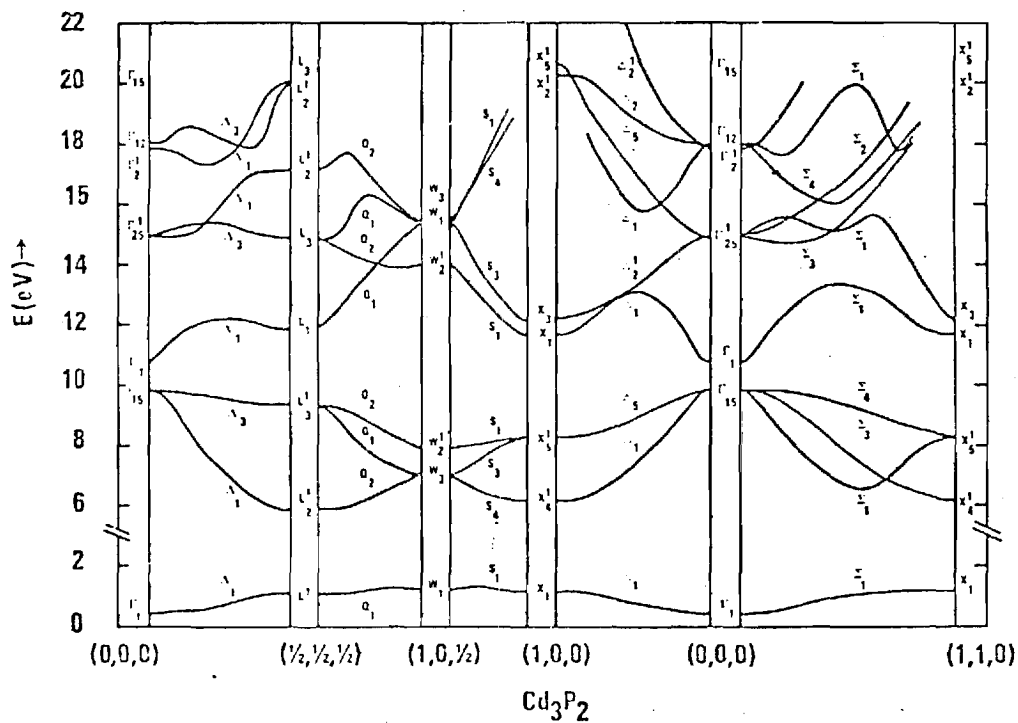


FIGURE 4. ENERGY BAND STRUCTURES FOR Cd_3As_2 AND Cd_3P_2 COMPOUNDS AS CALCULATED IN THE HYPOTHETICAL STRUCTURE.

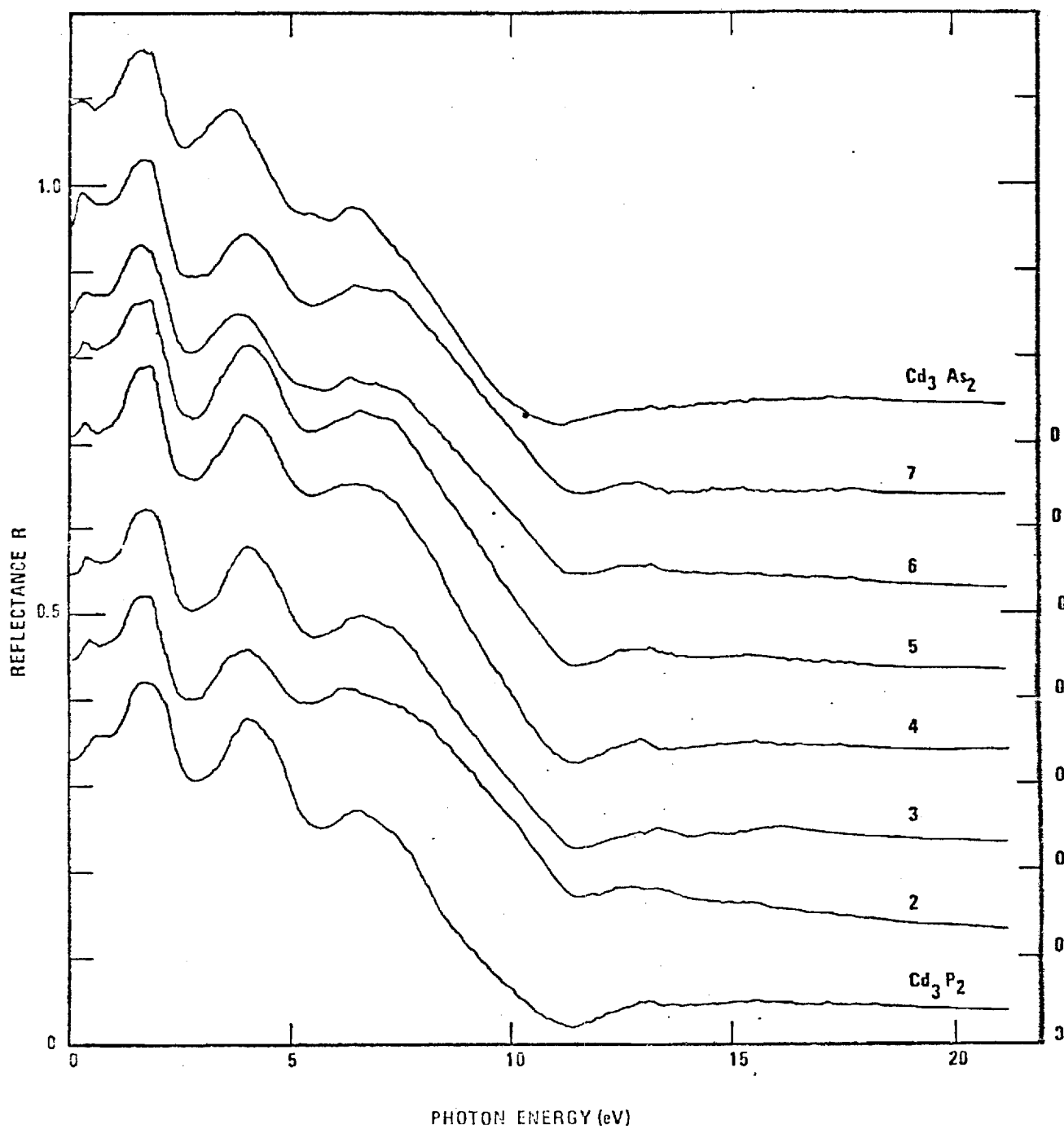


Figure 5. The Reflectance Spectra of the $\text{Cd}_3\text{As}_2 - \text{Cd}_3\text{P}_2$ Alloy System at 297° K
(The curves are zero shifted as indicated to prevent overlap)

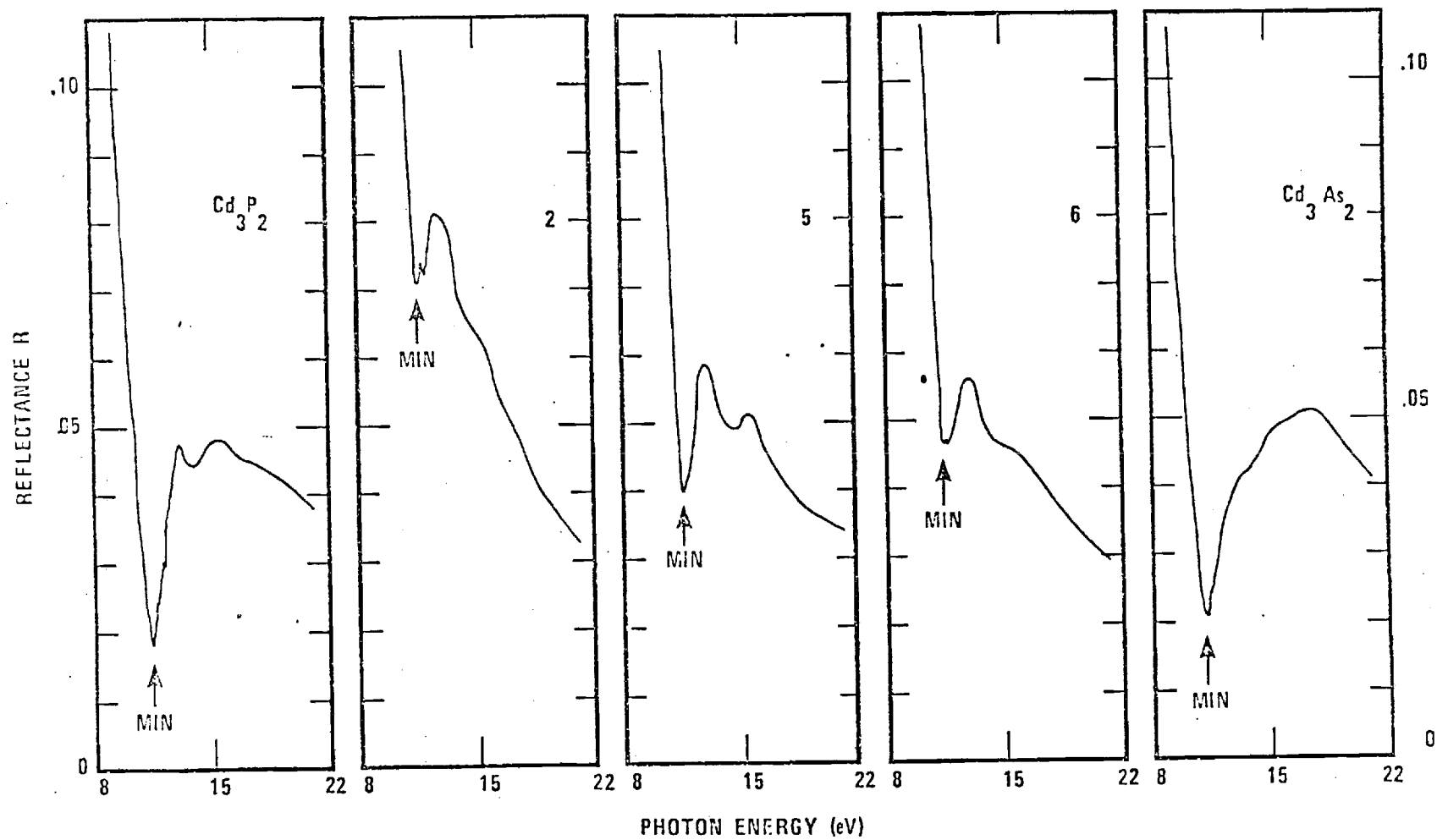


Figure 6. The Reflectance Spectra of the $\text{Cd}_3\text{As}_2\text{-Cd}_3\text{P}_2$ Alloy System in the Plasmon Region.

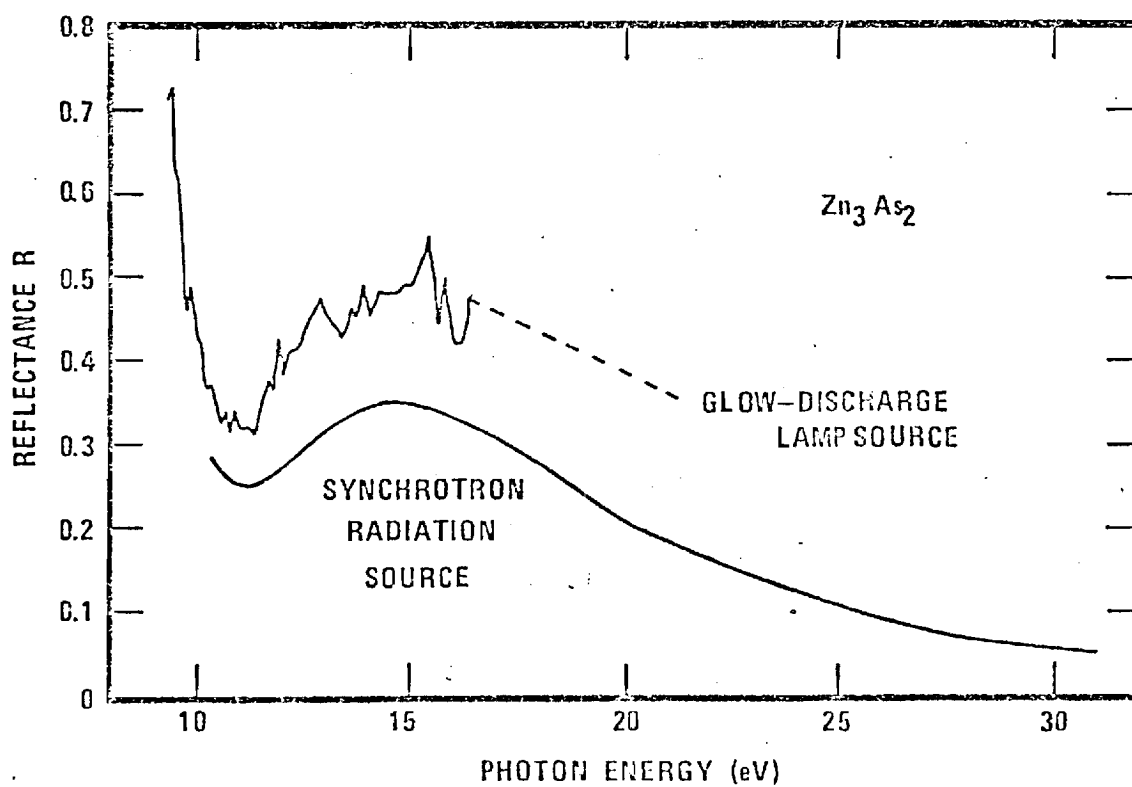
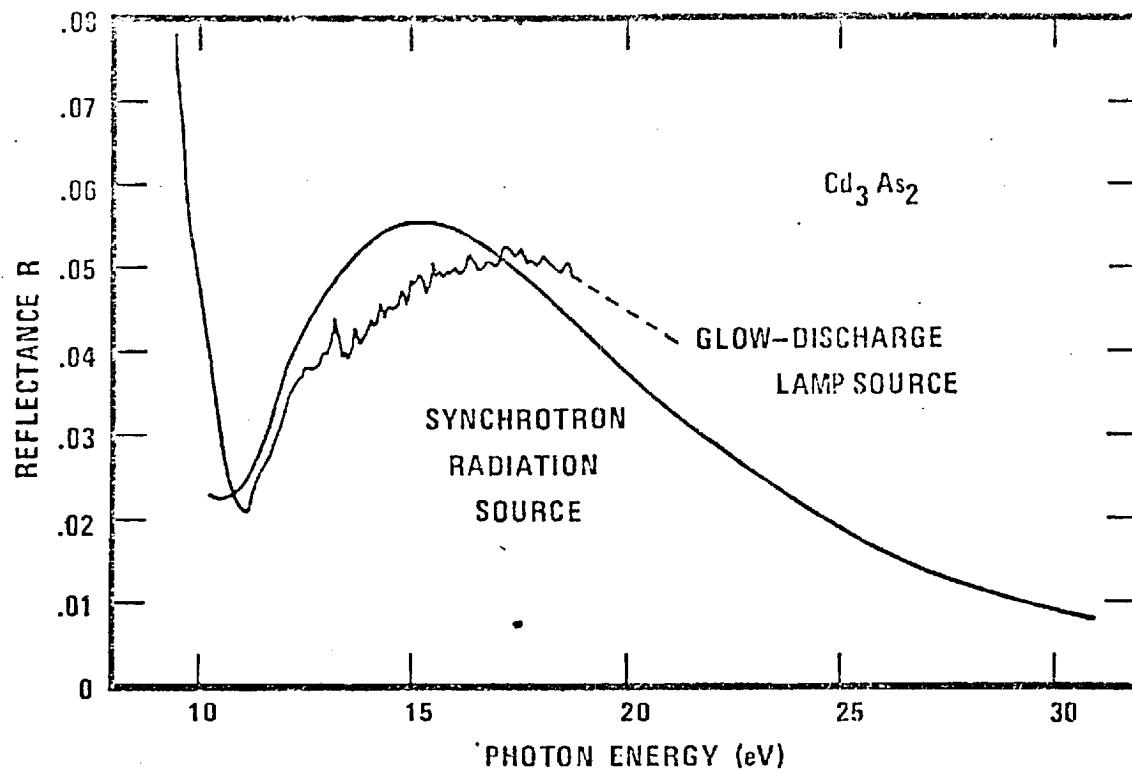


Figure 7. The Reflectance Spectra of Cd_3As_2 and Zn_3As_2

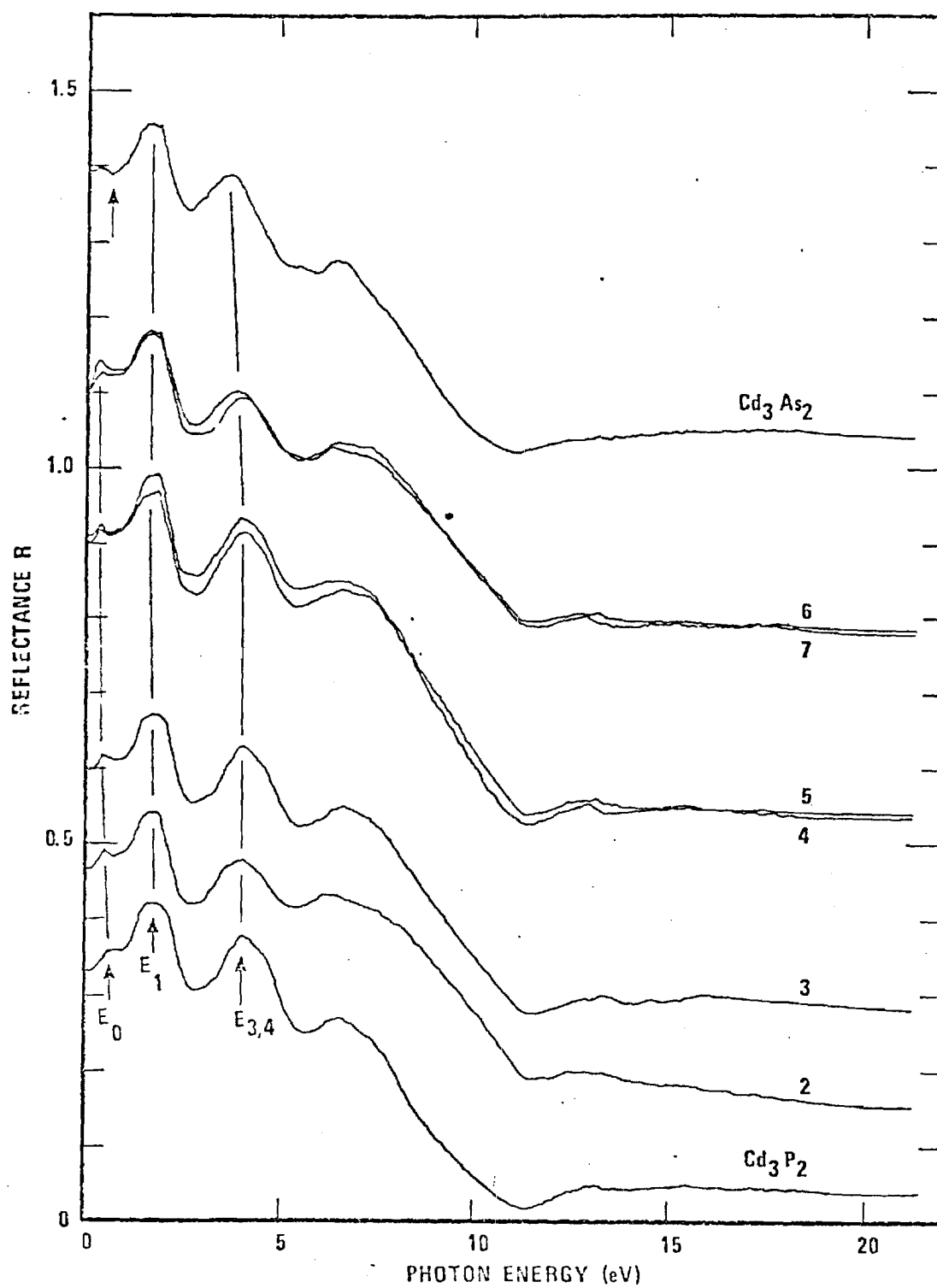


Figure 8. The Reflectance Spectra of the $\text{Cd}_3\text{As}_2 - \text{Cd}_3\text{P}_2$ Alloy System at 297°K
 (The curves are zero shifted as explained in the text)

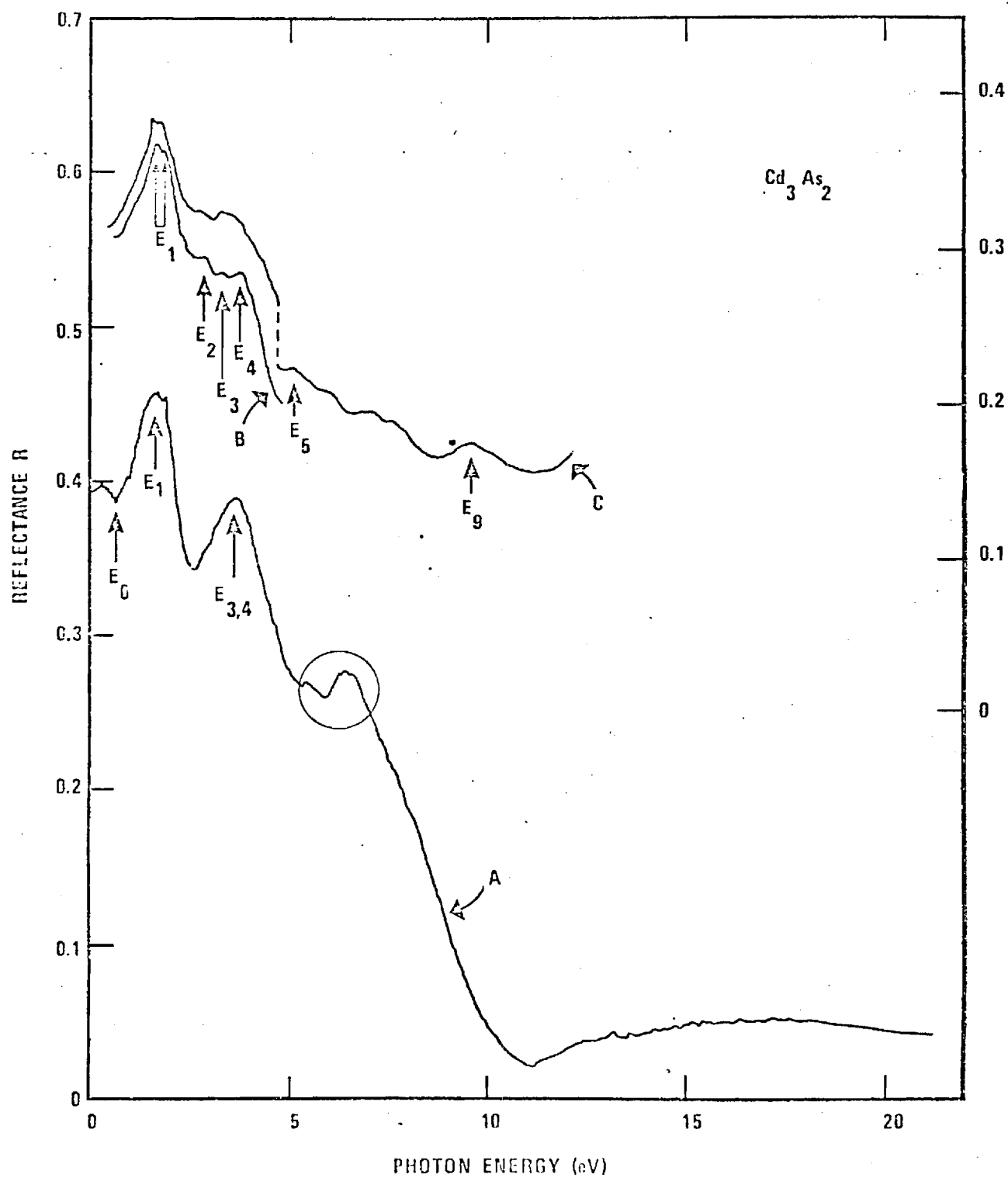


Figure 9. Relation of (A) the Present Results to (B) the 77°K Data and to (C) the 293°K Data of Reference (29) (the upper curves are zero shifted)

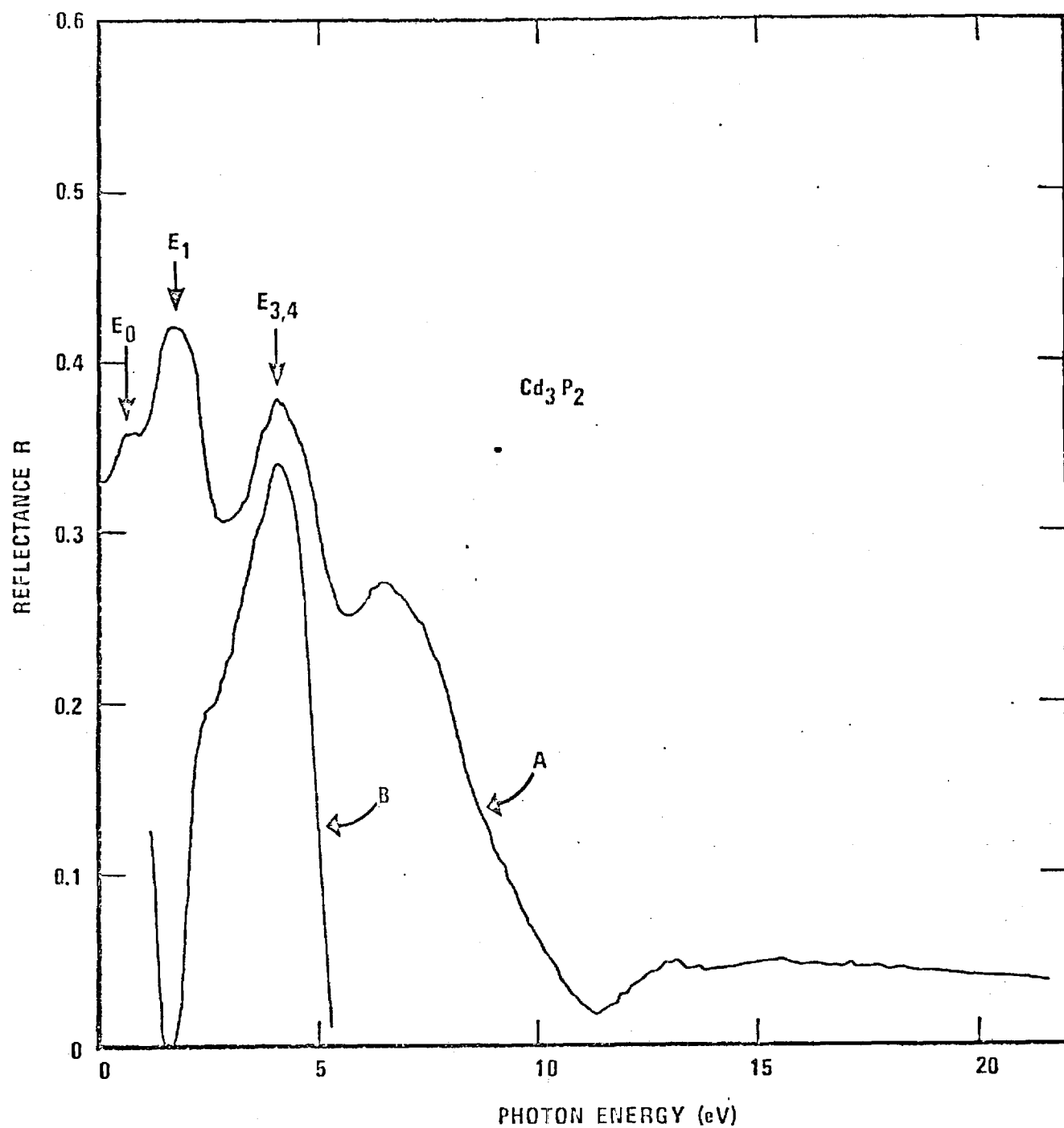


Figure 10. Relation of (A) the Present Results to (B) the 293°K Data of Reference (27) (The lower curve is given in arbitrary units)

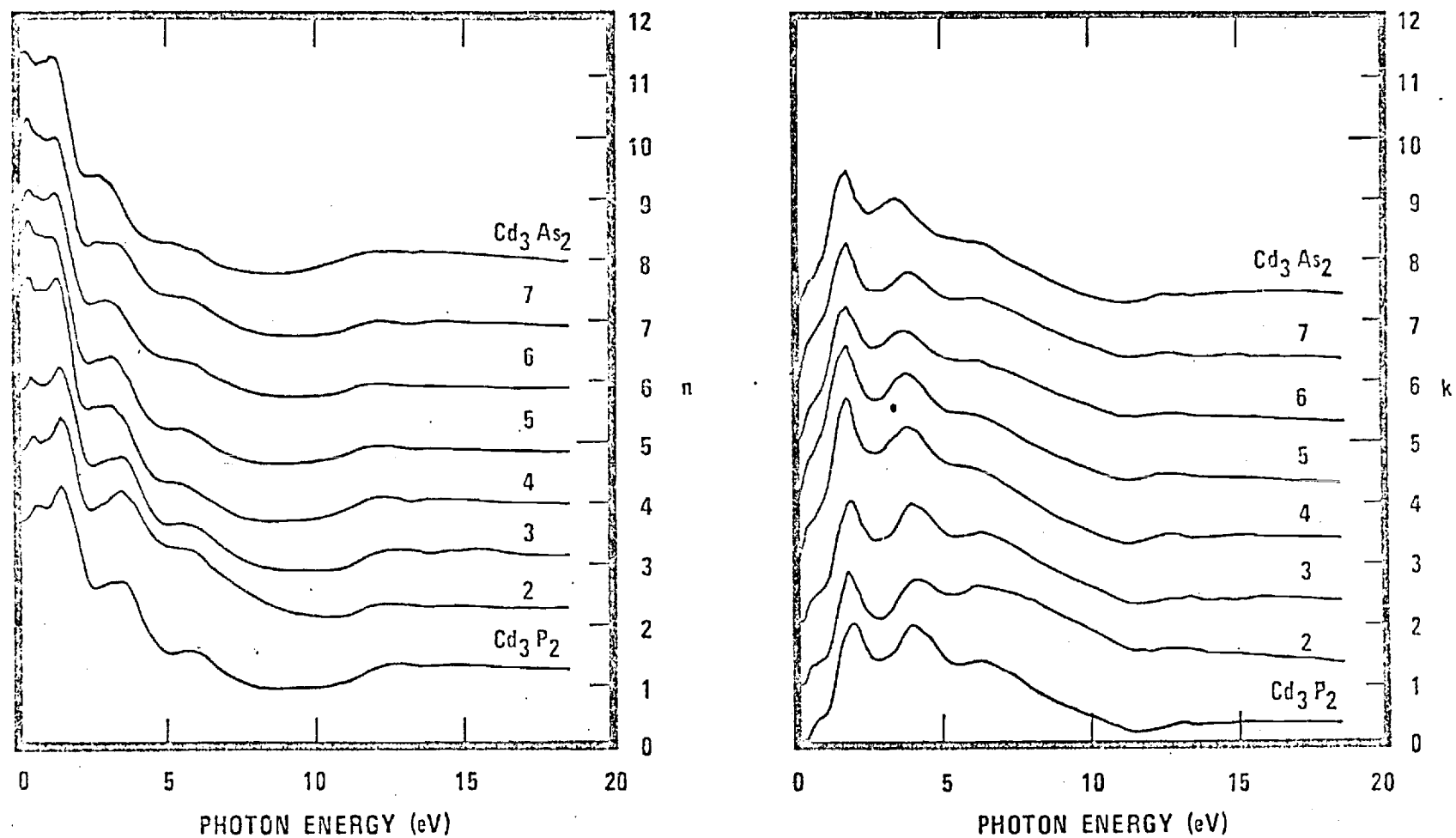


Figure 11. The Optical Constants " n " and " k " for the $\text{Cd}_3\text{As}_2 - \text{Cd}_3\text{P}_2$ Alloy System (The curves are successively zero shifted in the amount of one unit)

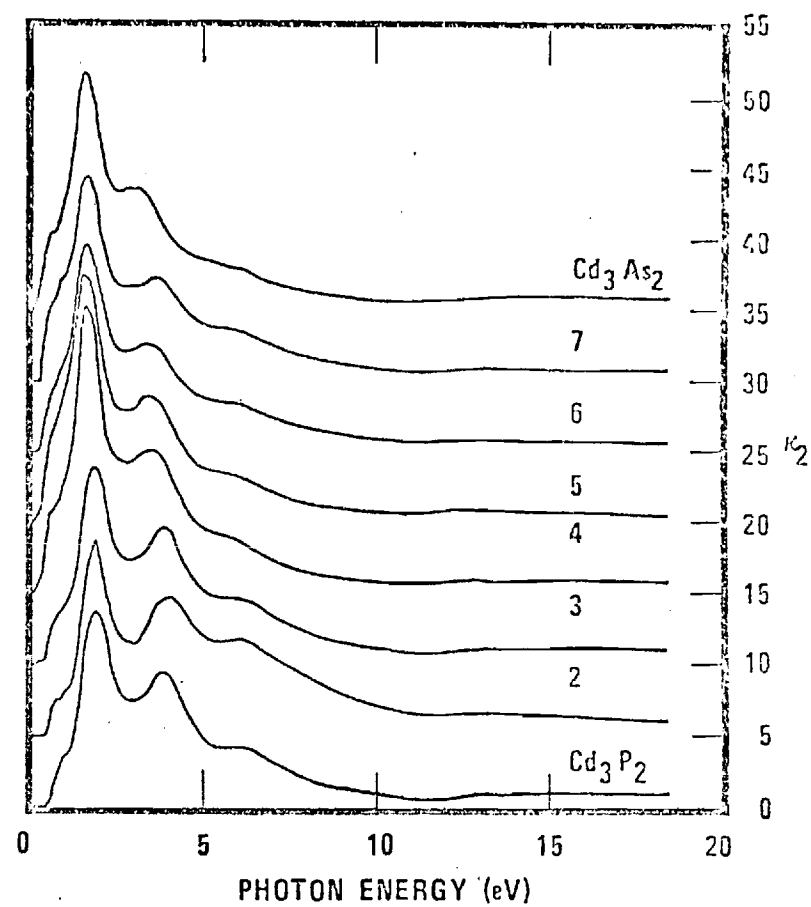
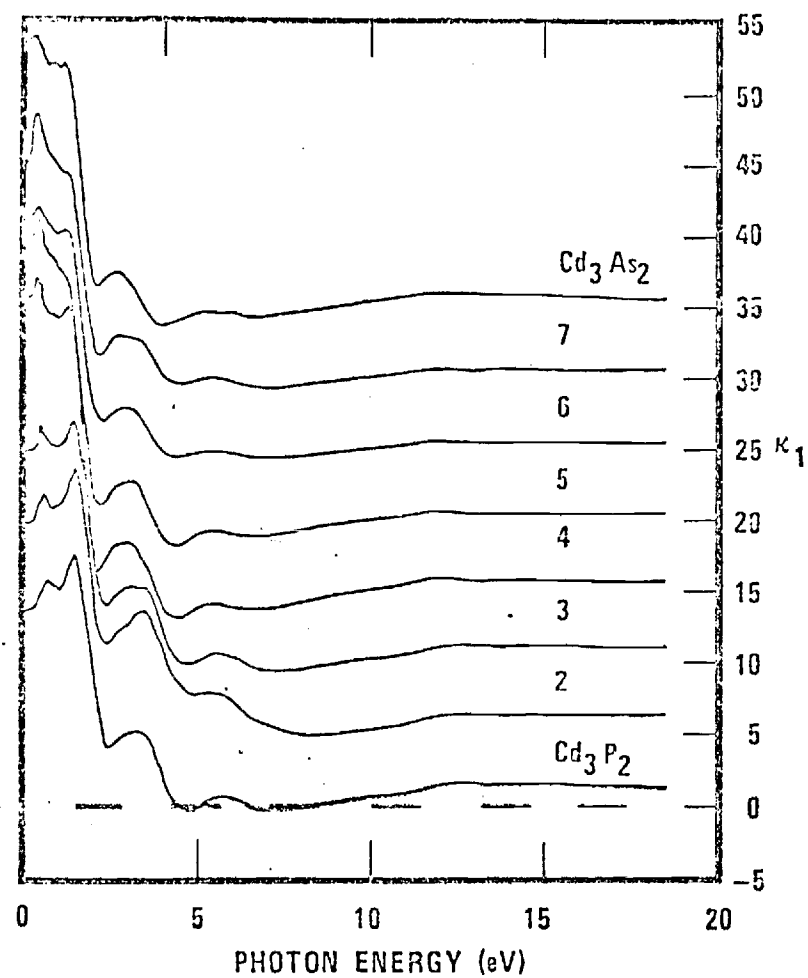


Figure 12. The Dielectric Constants κ_1 and κ_2 for the $\text{Cd}_3\text{As}_2 - \text{Cd}_3\text{P}_2$ Alloy System (The curves are successively zero shifted in the amount of five units)

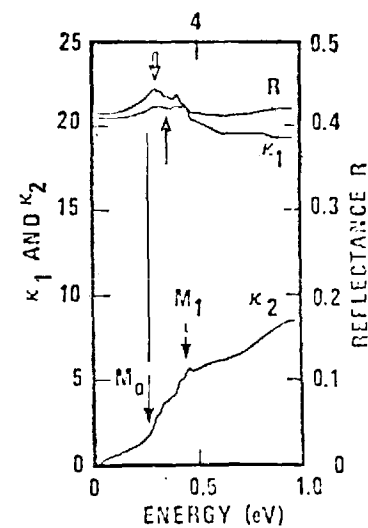
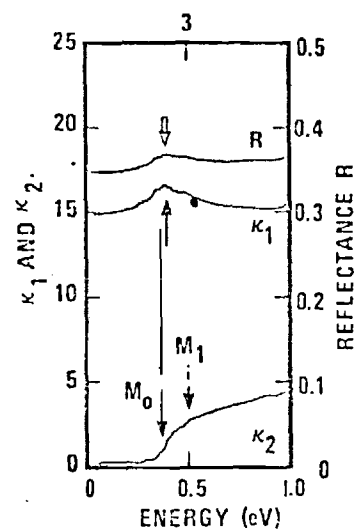
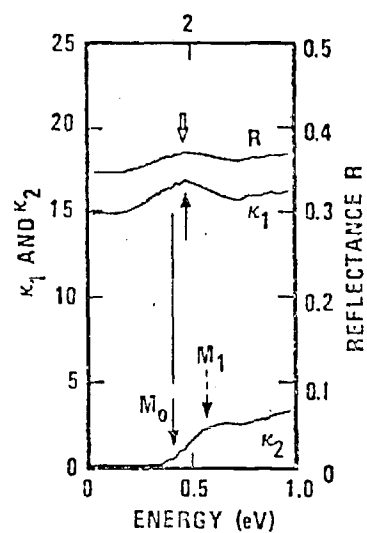
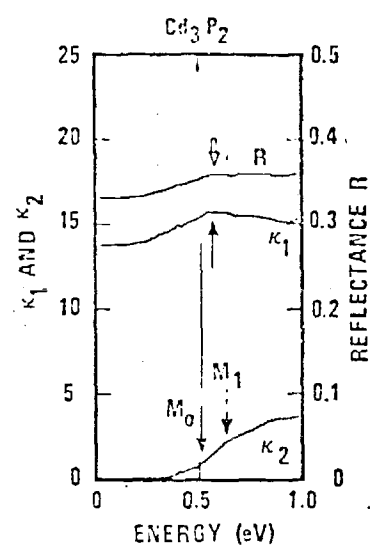


Figure 13. Dielectric Constants for Samples One through Four

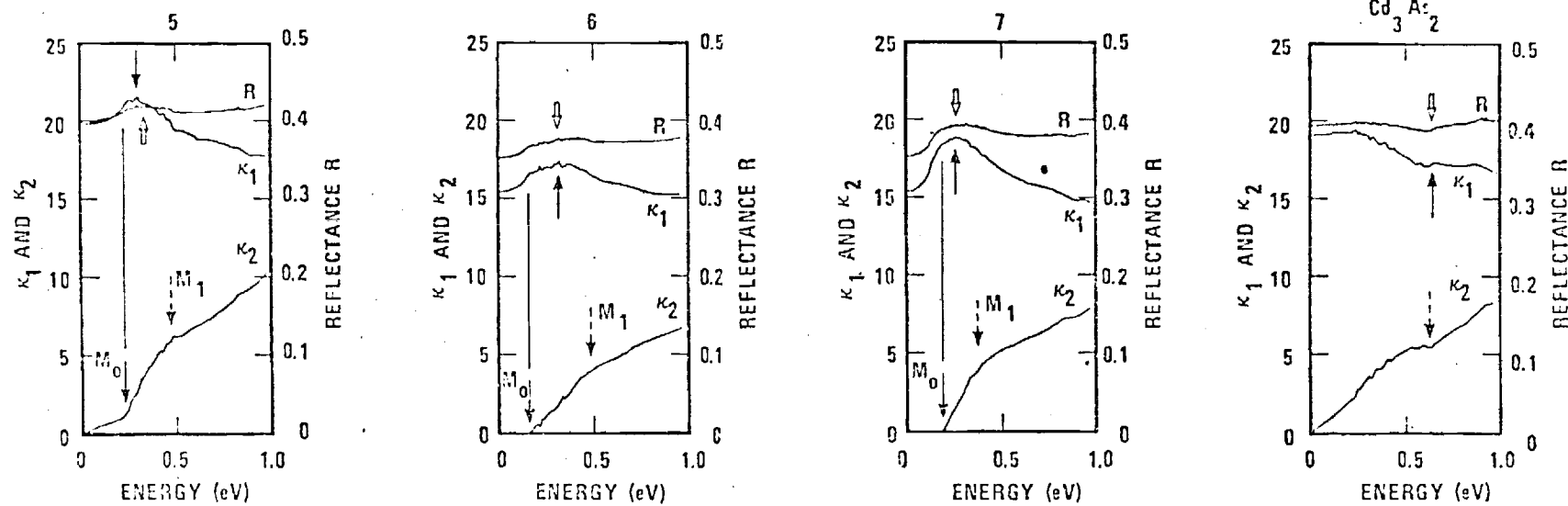


Figure 14. Dielectric Constants for Samples Five through Eight

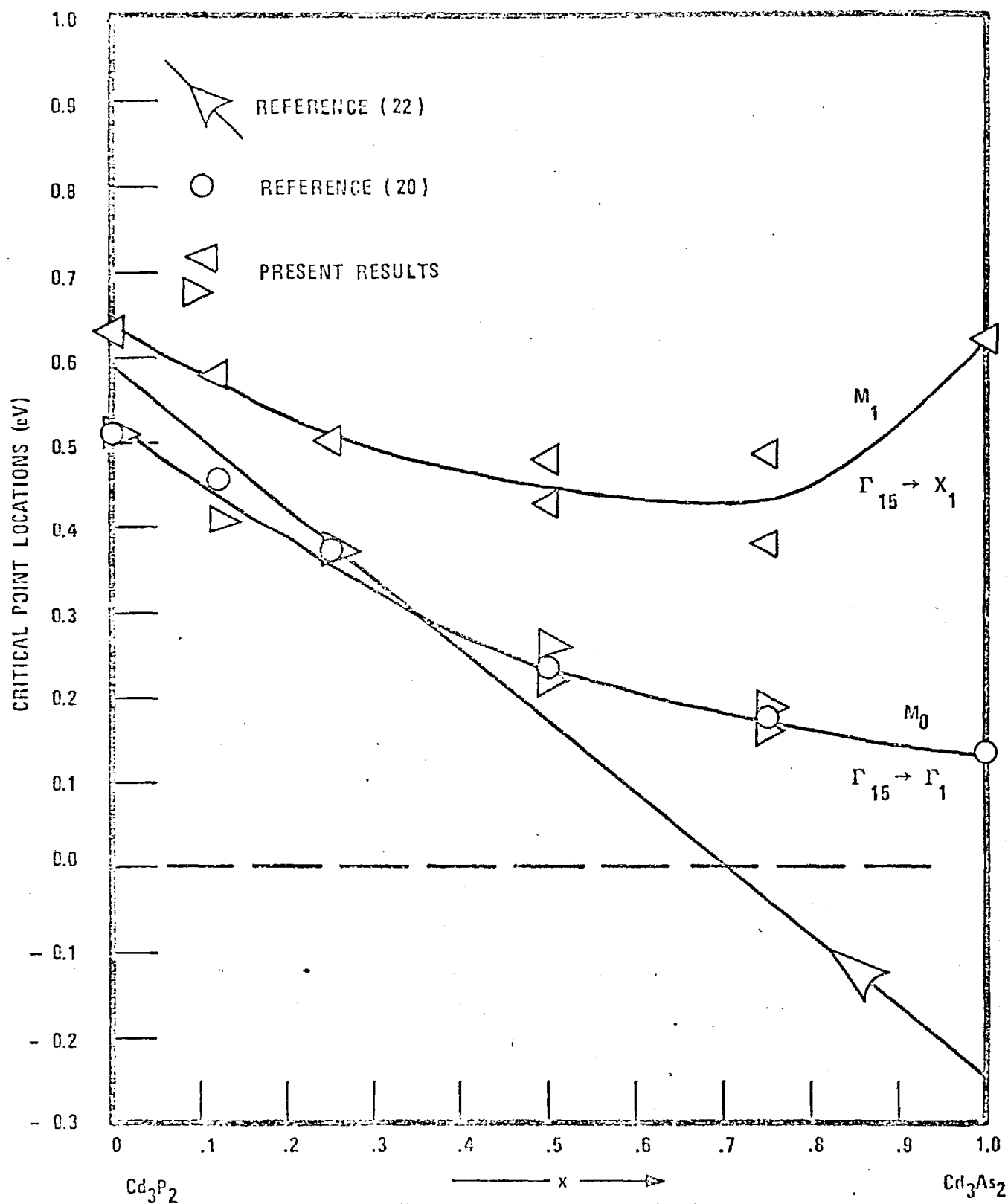


Figure 15. Location of the Band-Edge Critical Points as Determined by the Structure in κ_2

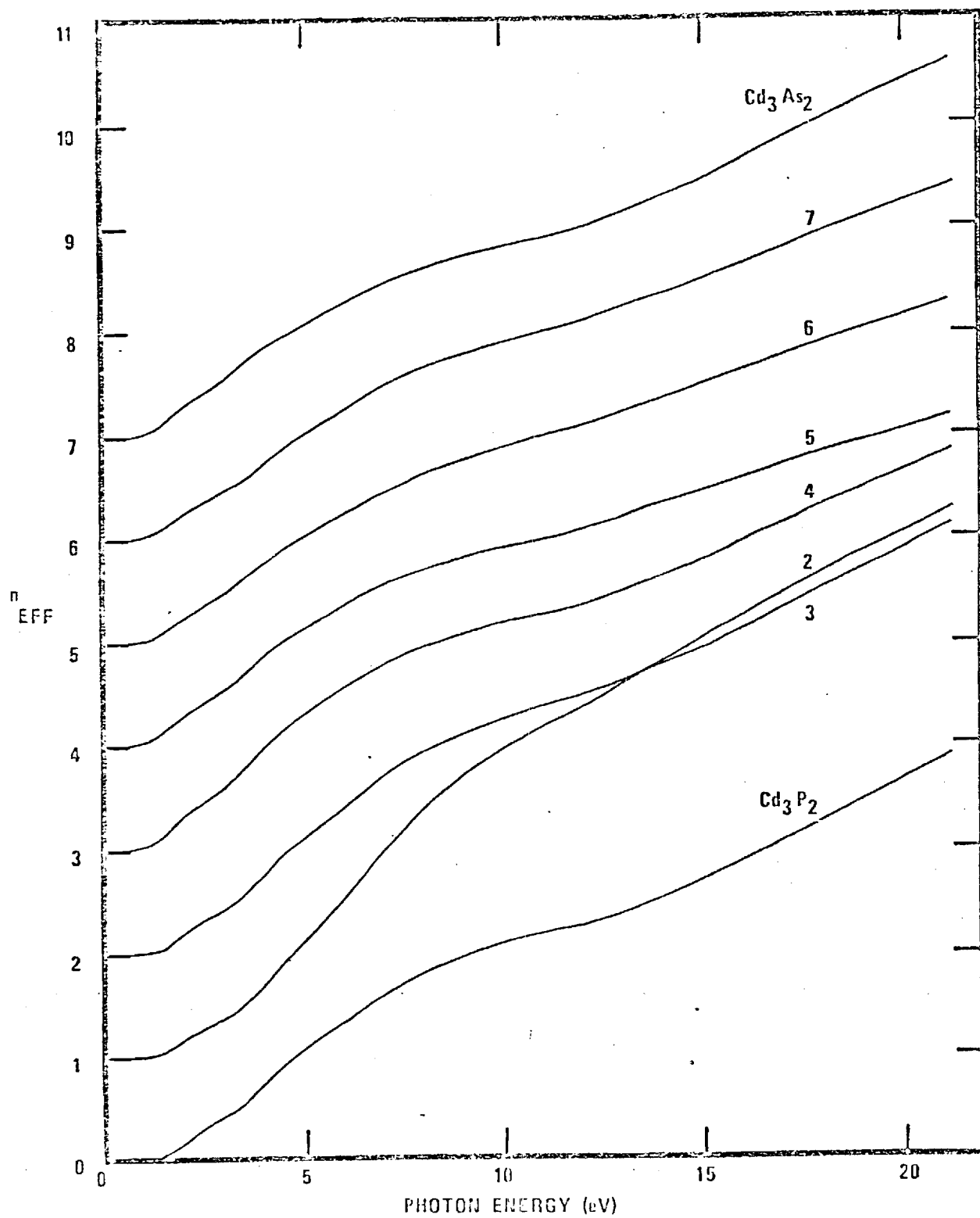


Figure 16. Successive Contributions to n_{EFF}
 (The curves are repeatedly zero
 shifted in the amount of one unit)

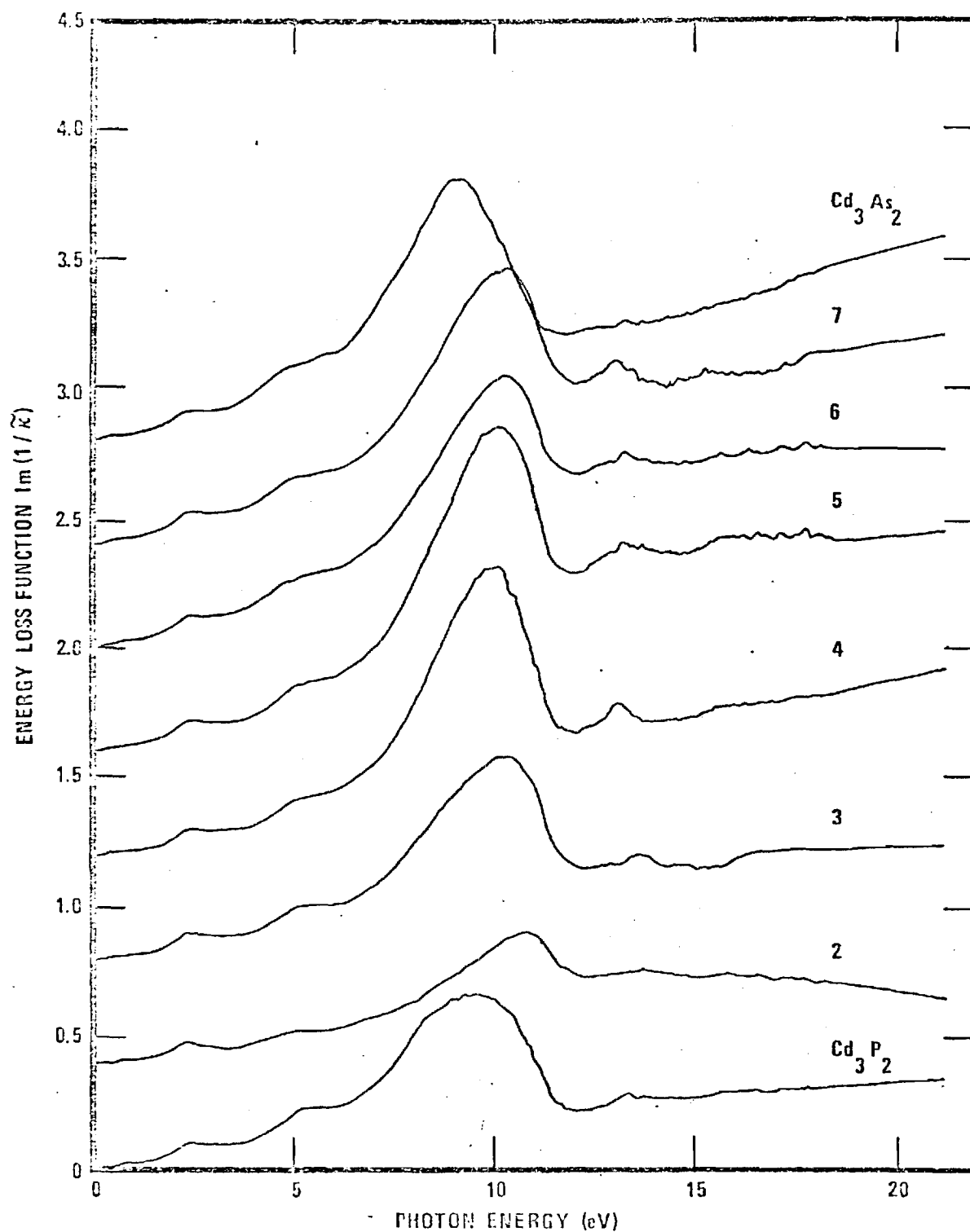


Figure 17. Characteristic Energy Loss Function as Derived from the Dielectric Constants (The curves are successively zero shifted in the amount of 0.4 units)

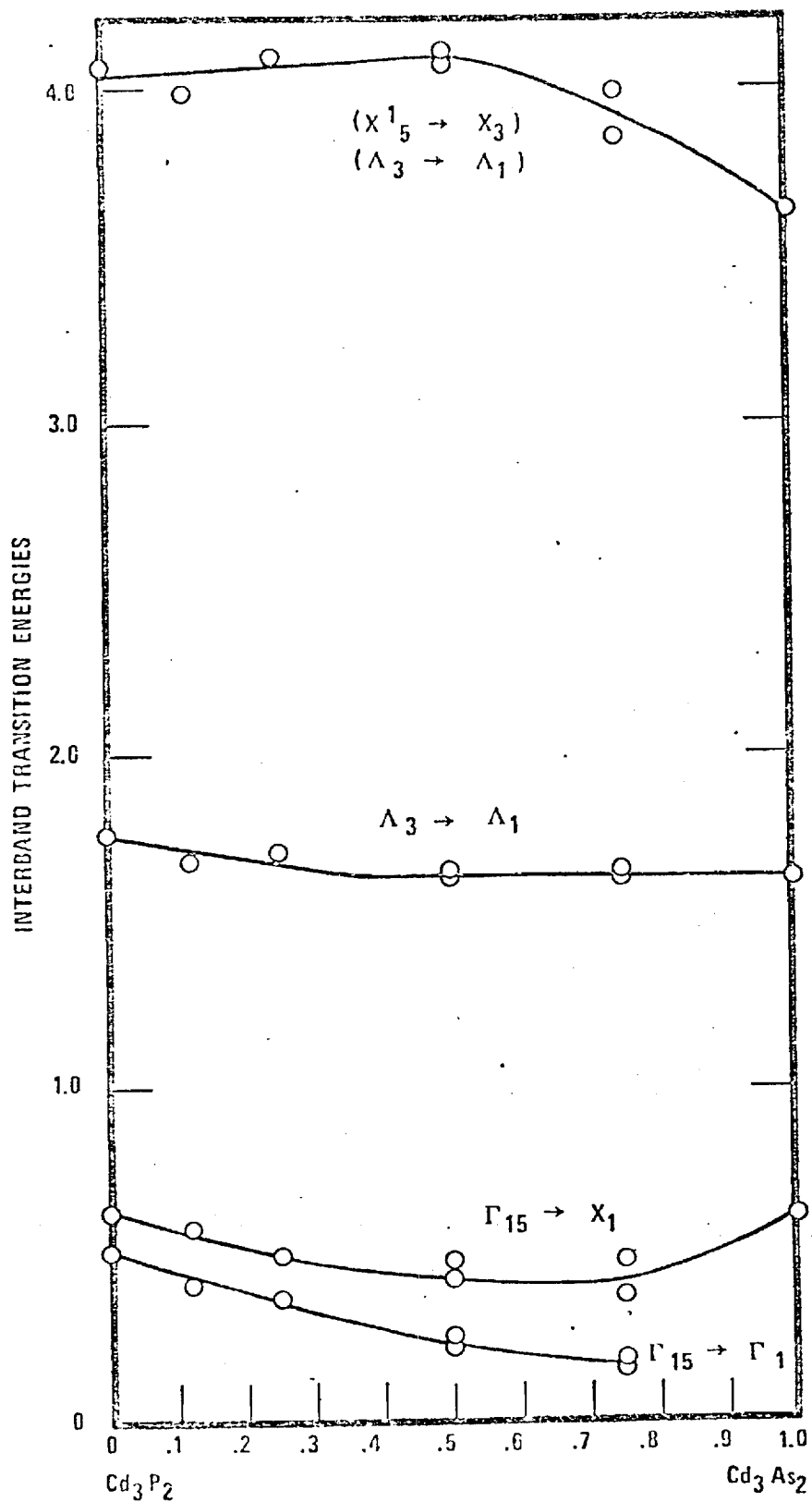


Figure 18. Probable Assignments of Direct Transitions in the $\text{Cd}_3\text{As}_2 - \text{Cd}_3\text{P}_2$ Alloy System

Appendix A
Interim Scientific Report -
James R. Stevenson
Grant No. AFOSR 70-1892
January 23, 1974

Technical Report

School of Physics

Georgia Institute of Technology

Atlanta, Georgia 30332

by

M. Zivitz and J. R. Stevenson

Research sponsored by the U.S. Air Force
Office of Scientific Research

Optical Properties of the Cd_3As_2 - Cd_3P_2 Alloy System

November 1973

Technical Report

School of Physics

Georgia Institute of Technology

Atlanta, Georgia 30332

by

M. Zivitz and J. R. Stevenson

Research sponsored by the U.S. Air Force
Office of Scientific Research

Optical Properties of the Cd_3As_2 - Cd_3P_2 Alloy System

November 1973

PREFACE

The text of this Report is identical to that of a thesis, entitled, "The Optical Properties of the Cd_3As_2 - Cd_3P_2 Alloy System", submitted by Maury Zivitz to the faculty of the Georgia Institute of Technology, in partial fulfillment of the requirements for the degree of Doctor of Philosophy. The thesis, having been accepted, and all other requirements having been satisfied, Mr. Zivitz has been awarded a Certificate of Approval, and he will be formally awarded this degree at the next Commencement of the Georgia Institute of Technology in December, 1973.

In view of the bulk of this thesis and the attendant costs of its reproduction, the present report will not be given routine distribution following the procedures of the Air Force Office of Scientific Research. It is issued as a Technical Report of the School of Physics, Georgia Institute of Technology, and will be made available to interested parties on request for as long as the supply lasts.

TABLE OF CONTENTS

ACKNOWLEDGMENTS.	Page ii
LIST OF TABLES	v
LIST OF ILLUSTRATIONS.	vi
SUMMARY.	ix
Chapter	
I. INTRODUCTION.	1
The Interest	
Crystal Structure	
Crystalline Quality	
Principal Band-Edge Structure	
Fundamental-Absorption Edge	
Optical Properties Beyond the Fundamental Edge	
II. THEORY OF OPTICAL PROPERTIES.	27
Wave-Vector-Dependent Dielectric Constant	
Alternative Definition of Dielectric Constant	
Significance of Wave-Vector Dependence of Dielectric Constant	
Kinematics of Energy and Crystal Momentum Conservation	
Intraband Transitions	
Interband Transitions	
Relation of Transition Rates to κ_2 and Line Shapes	
Normal-Incidence Reflectance and the Optical Constants	
III. APPARATUS	67
Optical Systems	
Instrumentation	
IV. EXPERIMENTAL PROCEDURE.	116
Sample Preparation	
Alignment of Sample	
Reflectance Measurements	
Determination of Backgrounds	

TABLE OF CONTENTS (Concluded)

Chapter	Page
V. RESULTS AND DISCUSSION.	123
Primary Data	
Interpretation of Reflectance Structure	
Errors in the Reflectance Values	
Optical Constants and Further Interpretation	
Errors in the Optical Constants	
Summary	
Recommendations for Further Research	
APPENDICES	166
A. THEORETICAL CONSIDERATIONS.	167
The Classical Oscillator Model for Dielectric Constants	
The Classical Polarizability	
Dielectric Energy-Loss Formulation	
Merit of the Transition Rate as Given by the Golden Rule	
B. EXACT GEOMETRY OF THE GRATING DRIVE	188
C. ZERO-VOLTAGE SWITCHING.	192
BIBLIOGRAPHY	199
VITA	205

LIST OF TABLES

Tables	Page
1. Crystal Structure of $\text{II}_3^{\text{B}}\text{-V}_2^{\text{A}}$ Compounds	5
2. Calibration of Wavelength Drum with a Quadratic Fit	86
3. Index of Samples and Qualitative Comment on Crystalline Quality of Samples.	117
4. Summary of Experimental Instrumentation and Conditions.	121
5. Probable Assignments, between 0.7 and 6 eV, of Interband Transitions	130

LIST OF ILLUSTRATIONS

Figure		Page
1.	Relation of (A) the Fluorite Structure to (B) the Cd_3As_2 Structure and to (C) the Cd_3P_2 Structure	6
2.	Relative Sizes and Orientations of the Cd_3As_2 and Cd_3P_2 Unit Cells.	8
3.	Phase Diagram for $\text{Cd}_3(\text{As}_x\text{P}_{1-x})_2$ Solid Solutions	11
4.	The First Brillouin Zone of (A) Body-centered Tetragonal Structure, and (B) Fluorite Structure.	22
5.	Energy-Band Structures for Cd_3As_2 and Cd_3P_2 Compounds as Calculated in the Hypothetical Structure	23
6.	Ionization Energies for the Atomic Components of the II-V Alloys Investigated.	25
7.	Sample-in and Sample-out Configurations	68
8.	Spectral Resolution of a Single-Pass Monochromator with Slits of 100 Microns and Sodium Chloride Prism	70
9.	High-Vacuum Reflectometer	72
10.	Sample-in and Sample-out Configurations	74
11.	Detailed View of Sample Holder and Pedestal for Ultrahigh-Vacuum System	75
12.	Bellows Assembly.	79
13.	Monochromator and Rowland Circle.	81
14.	Concave Grating and Fixed Slits	83
15.	Vacuum Ultraviolet Reflectometer.	88
16.	Northwest Port of Storage Ring.	90
17.	Object Slug Profile in Orbit Plane.	92

LIST OF ILLUSTRATIONS (Continued)

Figure		Page
18.	Off-axis Ellipsoidal and Plane Mirrors.	94
19.	Chopper Circuit (13 Hz)	98
20.	Block Diagram of Infrared Span.	100
21.	Modifications of Unijunction Transistor Oscillator Circuit.	101
22.	Block Diagram of Visible Span	104
23.	Schematic Diagram of Lamp Ignition.	106
24.	Schematic Diagram of Motor Control Circuit.	107
25.	Block Diagram of VUV Span	108
26.	Parameters as Adjusted for the 720 Supply	110
27.	Schematic Diagram of Analog Shaft-Angle Encoder	112
28.	Block Diagram of Extreme UV Span.	113
29.	Electron Beam Current Monitor	115
30.	The Reflectance Spectra of the $\text{Cd}_3\text{As}_2\text{-Cd}_3\text{P}_2$ Alloy System at 297°K	124
31.	The Reflectance Spectra of the $\text{Cd}_3\text{As}_2\text{-Cd}_3\text{P}_2$ Alloy System in the Plasmon Region.	126
32.	The Reflectance Spectra of Cd_3As_2 and of Zn_3As_2	127
33.	The Reflectance Spectra of the $\text{Cd}_3\text{As}_2\text{-Cd}_3\text{P}_2$ Alloy System at 297°K	128
34.	A Display of the Relative Error in the Reflectance Measurements.	135
35.	Relation of (C) the Infrared Results to the Plasma-Edge-Reflectance Measurements of (A) Reference (28) and of (B) Reference (34).	139

LIST OF ILLUSTRATIONS (Concluded)

Figure	Page
36. Relation of (A) the Present Results to (B) the 77°K Data and to (C) the 293°K Data of Reference (40).	142
37. Relation of (A) the Present Results to (B) the 293°K Data of Reference (38).	144
38. The Optical Constants "n" and "k" for the Cd ₃ As ₂ -Cd ₃ P ₂ Alloy System	147
39. The Dielectric Constants κ_1 and κ_2 for the Cd ₃ As ₂ -Cd ₃ P ₂ Alloy System	149
40. Dielectric Constants for Samples One through Four	151
41. Dielectric Constants for Samples Five through Eight	152
42. Location of the Band-Edge Critical Points as Determined by the Structure in κ_2	154
43. Successive Contributions to the Optical Dielectric Constant $\kappa_1(0)$	156
44. Consistency of the Optical Dielectric Constants	157
45. Successive Contributions to n_{EFF}	160
46. Characteristic Energy Loss Function as Derived from the Dielectric Constants	161
47. Probable Assignments of Direct Transitions in the Cd ₃ As ₂ -Cd ₃ P ₂ Alloy System	164
48. Schematic of the Grating Drive.	189
49. Block Diagram of the 30-Hz Chopper Circuitry.	193
50. Isolation Transformer and Power Supplies.	194
51. Line Sense, Schmidt Trigger, and Monostable Multivibrator	195
52. Bistable Multivibrator, Relay Driver, and Relay	196
53. Waveforms Related to 30-Hz ac Line.	198

SUMMARY

The near-normal-incidence, room-temperature reflectance spectra of the Cd_3As_2 - Cd_3P_2 semiconductor alloy system have been measured over the photon-energy range 0.14 to 21.2 eV. Use of synchrotron radiation from the Electron Storage Ring of the University of Wisconsin allowed the extension of this high-energy limit to 30 eV in the case of Cd_3As_2 . Comparison of our primary, reflectance data with the limited (spectrally speaking) results of others as well as with the available band-structure calculations has been made. We have adopted this procedure, since there exist no values of the optical constants above the infrared region.

The optical constants have been generated from 0.14 to 21.2 eV by a Kramers-Kronig analysis of our primary data. As a result of the generation of the optical constants, we have been able to interpret more fully the contributions to the fundamental-absorption edges. The interpretation of the optical properties of these semiconductors in the range of the fundamental absorption is based on the primordial entity "the joint density of states."

We summarize the trends of our primary data and the results of our analysis as follows. The reflectance spectra are qualitatively similar to those of III-V compounds, and the strong structure in these spectra scales approximately linearly with composition. Good agreement is obtained with the previously reported, fundamental band gaps. However, our data indicate the presence of a nearby transition which also underlies this

fundamental edge. The optical dielectric constants range from 14 to 18 for Cd_3P_2 to Cd_3As_2 , respectively. Furthermore, transitions near the "L" point below 2 eV contribute strongly to the optical dielectric constant, as in the III-V compounds. We find contributions, which we attribute to the cadmium d-bands, to the reflectance at 11 eV. Finally, the plasmon energy lies at least as high as 9.5 eV in these alloys.

CHAPTER I

INTRODUCTION

The Interest

Special attention has been given to the II-V compounds of Zn_3As_2 , Zn_3P_2 , Cd_3As_2 , and Cd_3P_2 as a result of their interesting transport properties: for example, Cd_3As_2 is a degenerate n-type semiconductor with an exceptionally large mobility, low effective mass, and a small band gap, whereas Zn_3As_2 is a p-type semiconductor with very low mobility, a comparatively large effective mass, and a large band gap. The practical interest in these binary semiconductors has been extended to the alloy systems Zn_3As_2 - Cd_3As_2 , Cd_3As_2 - Cd_3P_2 , and Cd_3As_2 - Zn_3P_2 .

A fundamental understanding of the energy-band structures of these alloys will eventually lead to more complete explanations of these properties. Of course, there is also intrinsic interest in the scaling of these same properties as a function of alloy composition. Numerous investigations of the band structure of groups IV, III-V, and II-VI binary compounds (and their alloys) have been performed by means of the analysis of their reflectance spectra. The interpretation of the results is greatly facilitated, if tentative band-structure calculations have also been performed. Band-structure calculations have recently been performed for several of these compounds, and we have undertaken an investigation of the reflectance spectra of the Cd_3As_2 - Cd_3P_2 semiconductor alloy system.

We have measured the near-normal-incidence reflectance spectra of these alloys over a very large range of photon energy. The high-energy limit of our measurements has been extended by use of ultraviolet radiation from the electron storage ring of the University of Wisconsin. We have unfolded the optical constants and compared our results with the limited (spectrally speaking) results of others. A number of probable, interband-transition assignments have been made, and these transitions have been located as a function of alloy composition. We have obtained qualitative agreement with the available band-structure calculations.

The concepts, techniques, and results which have been summarized above are discussed at length in the following chapters of this dissertation. Presented in the remainder of this chapter are several sections which provide structural and historical background material. The division of these topics is somewhat arbitrary. The following chapter treats a number of theoretical considerations, in particular, the "joint density of states." Some of the material in this theoretical chapter is indeed tutorial in nature; not all of the concepts introduced will be used in the interpretation of the results. In Chapter III, we cover in some detail the four experimental systems that have been employed.

This apparatus chapter is followed with a brief description of our procedures, and the final chapter is concerned with the data obtained from these alloys and their interpretation.

Crystal Structure

Of the II-V compounds, four are known which have both the formula $\text{II}_3^{\text{B}}\text{-V}_2^{\text{A}}$ and belong to the tetragonal crystal system: Cd_3As_2 , Zn_3As_2 ,

Cd_3P_2 , and Zn_3P_2 . Naake and Belcher (1) first reported that the Zn_3As_2 - Cd_3As_2 alloys formed solid solutions. Solid solutions of the Cd_3As_2 - Cd_3P_2 system were first reported by Masumoto and Isomura (2). More recently, Zdanowicz et al. reported solid solutions of Cd_3As_2 - Zn_3P_2 (3). The unit cells of the compounds have "grown" with the passage of time.

In 1928, Natta and Passerini (4) reported cubic cells for Zn_3As_2 and Cd_3As_2 . Seven years later, Stackelberg and Paulus (5) determined that all four compounds had the same tetragonal space group $\text{P4}_2/\text{nmc}$ ($\text{D}_{4\text{h}}^{15}$). In 1956, Cole et al. (6) reported a body centered cell with probable space group $\text{I4}_1/\text{acd}$ ($\text{D}_{4\text{h}}^{20}$) for Zn_3As_2 . In 1963 the crystal structure of Cd_3As_2 was also found to have the space group $\text{I4}_1/\text{acd}$ ($\text{D}_{4\text{h}}^{20}$) by Zdanowicz et al. (7). These more recent determinations of cell size (or lattice parameters) for Cd_3As_2 and Zn_3As_2 have been such that the unit cell is now $4 \times 2 \times 2$ times larger than that reported by Natta and Passerini and $2 \times \sqrt{2} \times \sqrt{2}$ times larger than that reported by Stackelberg and Paulus. The parameters for Cd_3P_2 of Stackelberg and Paulus have been confirmed (8); those for Zn_3As_2 of Cole et al. have been confirmed (7). Those for Cd_3As_2 of Zdanowicz et al. have been confirmed by Steigmann and Goodyear (9); however, they reported the space group $\text{I4}_1/\text{cd}$ ($\text{C}_{4\text{v}}^{12}$). Table 1 summarizes this discussion; "Z" is the number of formula units per unit cell.

The ideal (ignores details of lattice distortions) crystal structures of all four compounds are intimately related (5,7,9). Consider, for example, the structure of Cd_3As_2 . The large As ions are cubic close-packed, and three-fourths of the tetrahedral interstices are occupied by Cd ions. Each As ion is thereby surrounded by Cd ions at six of the eight

Table 1. Crystal Structure of $\text{II}_3^{\text{B}}\text{-V}_2^{\text{A}}$ Compounds
(The number of Formula Units is "Z")

Compound	Reference	Space Group	Lattice Parameters	c/a	Z
Cd_3As_2	(4)	?	$a = 6.29 \text{ \AA}$	1	2
	(5)	$\text{P4}_2/\text{n mc}$	$a = 8.94 \text{ \AA}$ $c = 12.65 \text{ \AA}$	1.41	8
	(7)	$\text{I4}_1/\text{a cd}$	$a = 12.654 \text{ \AA}$ $c = 25.458 \text{ \AA}$	2.012	32
	(2)	---	$a = 12.67 \text{ \AA}$ $c = \text{---}$	---	32
	(9)	$\text{I4}_1/\text{cd}$	$a = 12.67 \text{ \AA}$ $c = 25.48 \text{ \AA}$	2.011	32
Zn_3As_2	(4)	?	$a = 5.81 \text{ \AA}$	1	2
	(5)	$\text{P4}_2/\text{n mc}$	$a = 8.31 \text{ \AA}$ $c = 11.76 \text{ \AA}$	1.418	8
	(6)	$\text{I4}_1/\text{a cd}$	$a = 11.78 \text{ \AA}$ $c = 23.65 \text{ \AA}$	2.007	32
	(7)	$\text{I4}_1/\text{a cd}$	$a = 11.783 \text{ \AA}$ $c = 23.652 \text{ \AA}$	2.007	32
Cd_3P_2	(5)	$\text{P4}_2/\text{n mc}$	$a = 8.74 \text{ \AA}$ $c = 12.28 \text{ \AA}$	1.404	8
	(8)	---	$a = 8.76 \text{ \AA}$ $c = 12.27 \text{ \AA}$	1.401	8
Zn_3P_2	(5)	$\text{P4}_2/\text{n mc}$	$a = 8.09 \text{ \AA}$ $c = 11.45 \text{ \AA}$	1.418	8

corners of a cube, the two vacant sites being at diagonally opposite corners of a cube face. With the possible exception of the unit cells reported by Natta and Passerini, this description of the structure of Cd_3As_2 is identical to that for the other three compounds. What differentiates the unit cells of the arsenides from those of the phosphides is the relative disposition of the vacancies; this is the same reason for the "growth" of the arsenides' cells since the time they were determined by Stackelberg and Paulus. These remarks are clarified when the relationship of these cells to the fluorite cell is exploited (9). For concreteness, consider filling all the vacancies in Cd_3As_2 with Cd ions. This hypothetical unit cell then transforms into 16 fluorite unit cells with As^{3-} replacing the Ca^{2+} and the Cd^{2+} replacing F^- in the calcium-fluoride structure. Figure 1 gives this fluorite structure in part (A), the relation of the Cd_3As_2 structure to the fluorite structure in part (B), and the relation of the Cd_3P_2 structure to the fluorite structure in part (C).

It is worth repeating here that part (C) also gives the relation of Stackelberg and Paulus' Cd_3As_2 structure to the fluorite structure. Part (A) is constructed with the choice of the origin at an As ion, and the 16 fluorite unit cells stacked two by two are viewed along the "c" parameter. As ions are represented by "X" at ΔZ equals $C/16$ below each plane, and Cd ions are represented by circles on each plane. Part (B) is drawn to indicate the relative disposition of the Cd vacancies; this is done with the tail and head of each arrow situated at the lower and upper vacant sites, respectively. The arrows lie along the body diagonal of the fluorite cells. In part (C) it is seen that the repeat configuration of

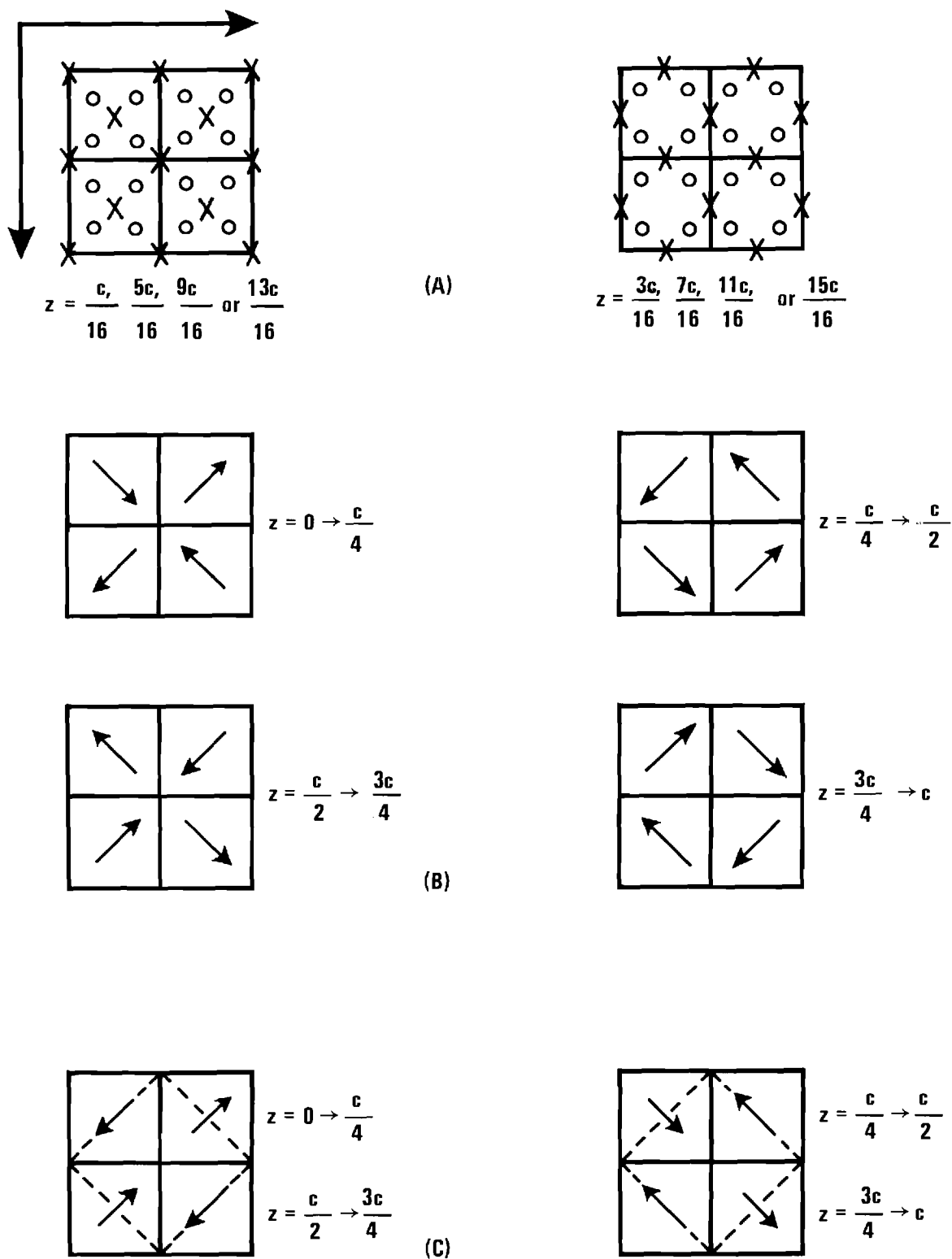


Figure 1. Relation of (A) the Fluorite Structure to (B) the Cd_3As_2 Structure and to (C) the Cd_3P_2 Structure.

the arrows occurs in half the distance of that in part (B). Hence, there is a reduction in the "c" parameter by a factor of two. In part (C), the broken line indicates the base of the Cd_3P_2 unit cell. Figure 2 shows the relative sizes of the unit cells for Cd_3As_2 and Cd_3P_2 . For convenience in the discussion below we shall define parameters for a multiplied unit cell for Cd_3P_2 . From part (C) of Figure 1 we have both

$$c = 2c' \quad (1)$$

and

$$a = \sqrt{2} a' \quad (2)$$

as parameters for a multiplied unit cell. Using Table 1, we find that

$$c = 25.54 \text{ \AA}, \quad (3)$$

$$a = 12.39 \text{ \AA}, \quad (4)$$

and

$$c/a = 2.061. \quad (5)$$

These defined parameters for Cd_3P_2 are close to those for Cd_3As_2 (see Table 1).

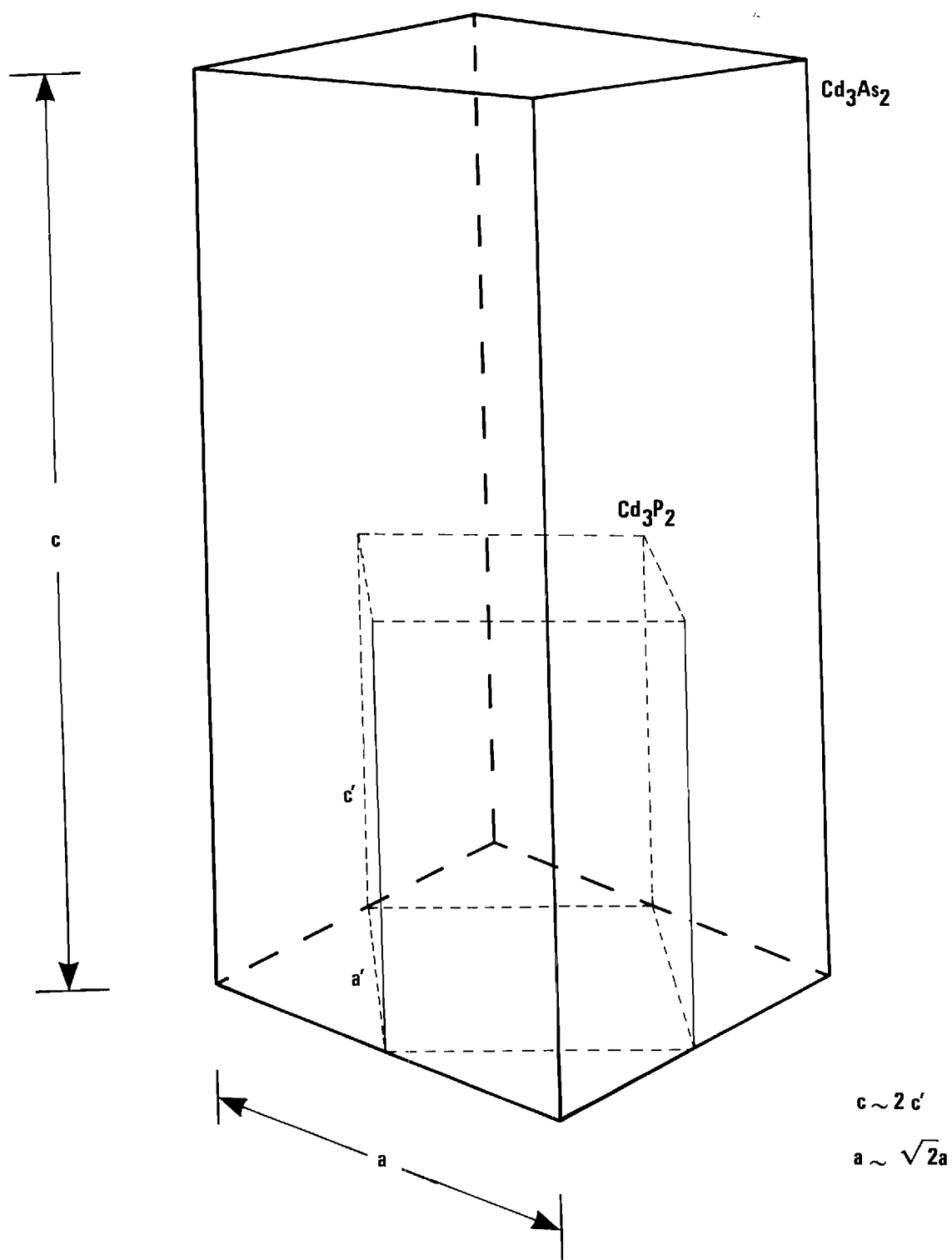


Figure 2. Relative Sizes and Orientations of the Cd_3As_2 and Cd_3P_2 Unit Cells.

Masumoto and Isomura (2) demonstrated the linear dependence (Vegard's Law) of the "a" parameter on the composition of the alloy system; they thereby concluded that the $\text{Cd}_3(\text{As}_x\text{P}_{1-x})_2$ alloy system consists of a continuous series of solid solutions. The index "x" runs from 0 to 1 and relates to the molecular percentage of the anion constituents. Their Bridgman-grown crystals failed to produce a single "phase" compound for Cd_3P_2 ; that is, there were precipitates of Cd or P at opposite ends of their ingots. They made use of the x-ray work of others (5,8) for the "a" parameter of Cd_3P_2 (see Table 1). A multiplied Cd_3P_2 cell, (the same as the one in the above discussion), was used in their work. It is found from their work that the "a" parameter for any member may be written

$$a(x) = (.30 x + 12.37) \text{ \AA}. \quad (6)$$

If it be assumed that the "c" parameter also varies linearly with composition, then by reference (9) of Table 1 for the "c" parameter of Cd_3As_2 and Equation (3) for that of Cd_3P_2 it follows that we may write

$$c(x) = (.92 x + 24.56) \text{ \AA}. \quad (7)$$

From Equations (6) and (7) we have the volume, a^2c , of the unit cell in the form

$$V(x) = (3758 + 323 x + 9.0 x^2) \text{ \AA}^3, \quad (8)$$

where the cubic term is outside the known accuracy of the lattice parameters.

Figure 3 is a schematic version of Masumoto and Isomura's phase diagram (2). They tentatively considered the solid-phase transformation to be a kind of polymorphic transformation (7) as in the Cd_3As_2 - Zn_3As_2 alloys: for example, another choice of a multiplied cell for Cd_3P_2 is obtained by a vertical stacking of two of the primed cells in Figure 2. The melting temperature of $(739 \pm 2)^\circ\text{C}$ for Cd_3P_2 was also obtained from reference (8). For Cd_3As_2 , Zemczuzny (10) has published a melting temperature of 721°C and a solid-solid phase transition at 578°C ; associated with this dimorphic transformation is a large increase of specific volume. Zemczuzny investigated the melting-point curve of the Cd-As system. Stackelberg and Paulus (5) reported a melting temperature of 720°C for Cd_3As_2 .

Crystalline Quality

The Bridgman-grown samples of Masumoto and Isomura (2) had grain sizes of about 1-5 mm. Haecke and Castellion (11) obviated the difficulties of the Bridgman method and prepared both single and polycrystalline samples of Cd_3P_2 . Zdanowicz and Wojakowaki (8) also obtained single and polycrystalline samples of Cd_3P_2 using a sublimation technique.

More recently Wagner et al. (12) prepared Cd_3As_2 by the direct reaction of the elements and used a sublimation technique to prepare Cd_3P_2 ; a modified Bridgman method was used to prepare the members of the alloy system. They found the $\text{Cd}_3(\text{As}_{0.25}\text{P}_{0.75})_2$ and $\text{Cd}_3(\text{As}_{0.12}\text{P}_{0.88})_2$ samples not to be physically sound; a Bridgman-grown Cd_3P_2 sample was also of poor quality. Radoff and Bishop (13), also from the Naval Research

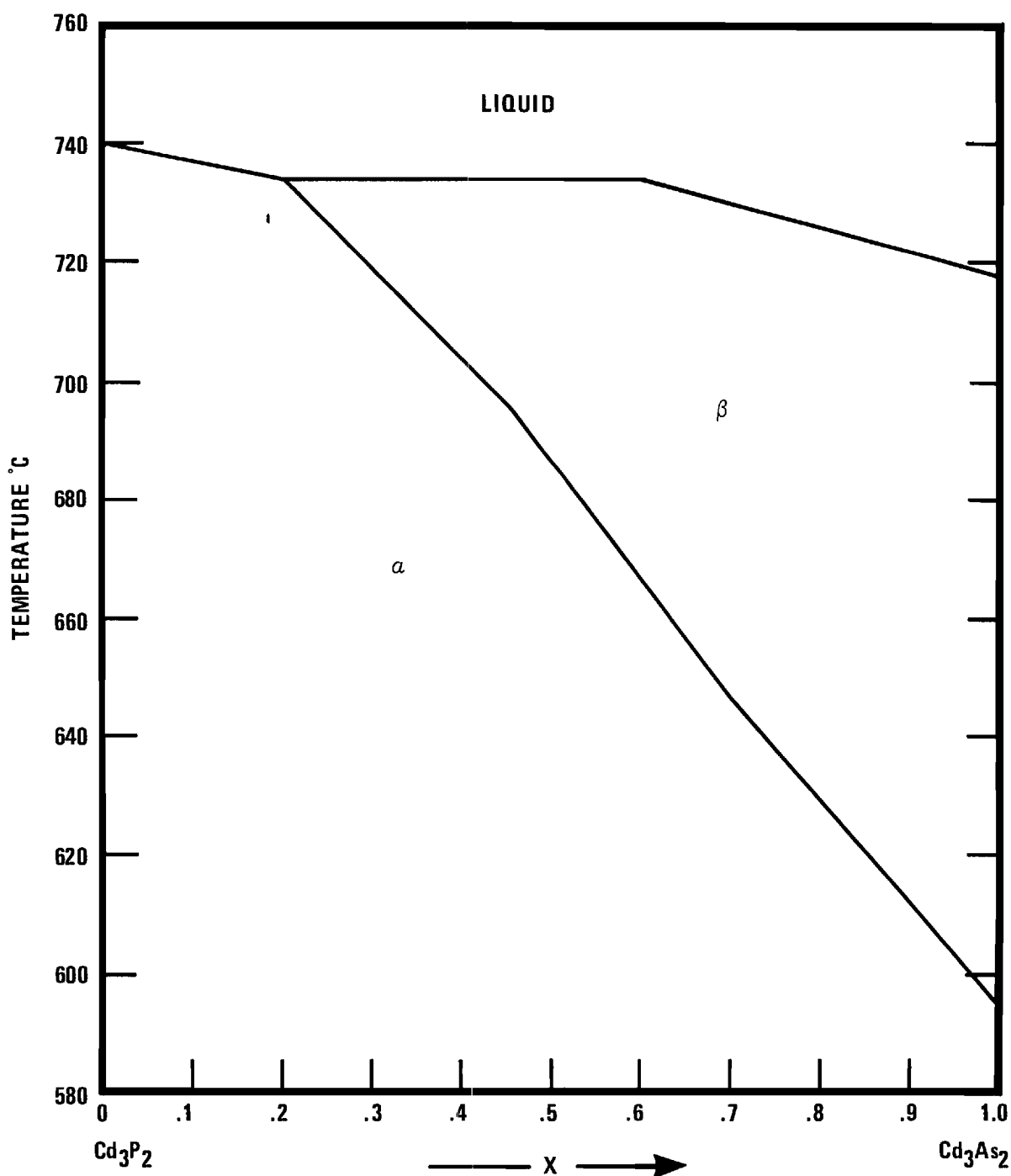


Figure 3. Phase Diagram for $\text{Cd}_3(\text{As}_{1-x}\text{P}_x)_2$ Solid Solutions.

Laboratory of Washington, D. C., reported that for "x" greater than or equal to 0.25 Bridgman-grown ingots showed cracks attributed to the phase transition shown in Figure 3; they reported similar problems with Bridgman-grown Cd_3As_2 .

Principal Band-Edge Structure

From the number of formula units ($Z = 32$) per unit cell and the compound formula $\text{Cd}_3(\text{As}_x\text{P}_{1-x})_2$ it follows that there are exactly 3.2 electrons per ion which contribute to the valence bands. This corresponds to the enormous number of 512 valence electrons per unit cell. Although a detailed investigation (5) of the bond lengths in Cd_3As_2 has been performed, the bonding (ionic versus covalent) is not yet clear. It can be safely assumed that there is a sizeable ionic content. All the zinc blend III-V semiconductors whose constituents come from the same row of the periodic table have higher melting points than the corresponding column IV valence semiconductor; this is commonly attributed to the departure from pure valence bonding (14). However, the energy of formation of vacancies in these zinc blend semiconductors is quite small.

When a compound semiconductor is composed of constituents less symmetrically disposed about column IV, it can become quite polar as in the case of PbS (galena), PbSe, and PbTe (14,15). The polar semiconductor $\text{Pb}_{1+\delta}$ can exist in a single "phase" (that is, lacking precipitates) with δ being a fraction up to about 10^{-3} . Each excess Pb atom acts as a donor impurity whose ionization level is very close to the conduction band. The mechanism for this "impurity" level is the formation of an S ion vacancy which has an effective positive charge with respect to the perfect crystal. The excess Pb atom is thought to enter the lattice in a normal

site as Pb^{2+} , and the two electrons are freed to occupy the As vacancy. (In alkali halides, the binding energy of the single electron within the vacancy is of the order of 1 eV, and these charged vacancies are known as F-centers). The binding energy (first ionization potential of an electron trapped at a divalent ion vacancy) is so small that it is released into the conduction band except for very low temperatures. More generally, a cation vacancy can also be formed from an excess of the anion; however, whether or not acceptors readily contribute holes to the valence band will depend again on the ionization potential of the holes trapped at the cation vacancy.

Suchet (16) has formulated an empirical electronegativity theory from which the homopolar ϵ_1 and heteropolar ϵ_2 contributions to the fundamental energy gap ϵ_g ($\epsilon_g = \epsilon_1 + \epsilon_2$) have been computed for a large number of semiconducting, binary compounds. The fraction of ionic character f_i ($f_i \equiv \epsilon_2/\epsilon_g$) for Cd_3As_2 was computed to be on the order of 1.0; for Cd_3P_2 , on the order of 0.8.

Haacke and Castellion (11) performed annealing experiments on Cd_3P_2 , the results of which support the assumption that the high electron concentration of undoped samples is due to phosphorous vacancies. (One must distinguish sharply between the impurity vacancies, just discussed, which follow a law of "mass-action" and the one-fourth unfilled interstices in the perfect crystal.)

To date, no one has reported a p-type member of this alloy system. With one noteworthy exception, all work on as-grown alloys (2,12,13,17) has been done on degenerate (reduced Fermi level η as large as 5) samples.

Conduction-band electronic densities run from 5×10^{17} for Cd_3P_2 to $5 \times 10^{18} \text{ cm}^{-3}$ for Cd_3As_2 . Ugai and Zyubina (18), using repeated zone recrystallization, obtained as-grown samples of Cd_3As_2 with an electron concentration of the order of $5 \times 10^{16} \text{ cm}^{-3}$.

The temperature dependence of an array of properties (Hall coefficient, resistivity, mobility, thermoelectric power) were measured along with the thermal conductivity by Masumoto and Isomura (2) for the alloy system. Below room temperature, down to 77°K , the negative Hall coefficients were quite independent of temperature, and the temperature coefficient of the resistivity was always positive. The Hall mobilities obeyed the $CT^{-\alpha}$ law; below 90°C the value of α spanned the range 0.71 to 1.16. These results represent a degenerate (19) electronic conduction. The Hall mobility was largest, $9400 \text{ cm}^2 \text{ V}^{-1} \text{ sec}^{-1}$, for Cd_3As_2 . Estimates for the effective-mass ratio were found to center about the value 0.09. [In the English language, Haacke and Castellion (11), Spitzer et al. (20), and Rogers et al. (21) relate various transport coefficients to the scattering factor "s" and the reduced Fermi level η for degenerate semiconductors. These latter sources enable one to obtain similar estimates for the effective mass and to partition the thermal conductivity into electronic and lattice contributions.] Turner et al. (22), who measured a number of properties of Cd_3As_2 , reported that even at 4°K the Hall coefficient remained flat and the resistivity never reached a minimum.

In these thermal measurements, the thermoelectric power is the primordial coefficient as it enables an estimate of the Fermi level; therefore, it deserves mention that the thermoelectric power (Seebeck coefficient) of a thermocouple can be written as

$$\alpha_{12} = \alpha_2 - \alpha_1, \quad (9)$$

where α_1 is the absolute power of the semiconductor and α_2 is that of a metal. Usually α_1 is an order of magnitude (23) greater than α_2 so that, to within the usual limits of accuracy, we have the approximation

$$\alpha_{21} \approx \alpha_1. \quad (10)$$

The fundamental energy gaps of this alloy system have been the subject of extensive investigation by the Naval Research Laboratory of Washington, D. C. Interband magnetoabsorption (IMO) experiments were conducted by Wagner et al. (24,12) in an effort to obtain the energy gaps unaffected by the large conduction-band electronic density (Burstein-Moss shift). They obtained gaps which spanned the range 0.57 for Cd_3P_2 to about 0.1 eV for $\text{Cd}_3(\text{As}_{0.25}\text{P}_{0.75})_2$. Interband magnetoabsorption was not observed for Cd_3As_2 . Between "x" values of 0.0 and 0.75 [$\text{Cd}_3(\text{As}_x\text{P}_{1-x})_2$] the low-temperature (30°K) IMO gaps varied quite linearly, whereas their room-temperature optical gaps bowed upward for "x" greater than 0.50. (A large Burstein-Moss shift is expected, given the combination of small gap and large electron-to-hole effective mass ratio, even for intrinsic semiconductors.)

In the course of their investigation, a Kane model was proposed for the conduction band, which was basically of the form

$$\frac{\hbar^2 K^2}{2m_n^*} \approx \epsilon_c + \delta \epsilon_c^2 \quad (11)$$

for the choice of the zero of energy at the bottom of the conduction band [we denote the electronic wave vector by "K"]. This nonparabolic model has been used for "negative" gap system, and the gaps were given as a function of composition by

$$\epsilon_g(x) = (0.588 - 0.834 x) \text{ eV.} \quad (16)$$

They also tabulated the bottom-of-the-band effective-mass ratios (m_n^*/m). That for Cd_3P_2 was found to be 0.047 and for Cd_3As_2 , 0.014. It should be noted that these II-V semiconductors have another property in common with the III-V zinc blend semiconductors: the gap is smaller for the heavier of the two anions.

Naturally, most investigations to date have centered on the end-members, Cd_3P_2 and Cd_3As_2 , of this system. Armitage and Goldsmid (26), who first reported the large departure from parabolicity of the conduction band for Cd_3As_2 , obtained a vanishing value for m_n^* ; he thereby implied the existence of a zero energy gap at 80°K and that $\epsilon_c(K)$ was exactly linear. Next, Blom and Schrama (27) reported a value of (m_n^*/m) equal to 0.012 and a band gap of 0.15 eV at 300°K. More recently, Rogers et al. (21) reported the value of 0.10 for this effective-mass ratio and a value of zero for the band gap (corrected for the Burstein-Moss shift) at 300°K. All three of these reports of nonparabolicity were in essential agreement, in so far as $\epsilon_c(K)$ was approximately a straight line for Cd_3As_2 and the band gap was quite small.

Earlier, Haidemenakis et al. (28) observed the infrared plasma

reflection edge, performed free-carrier magneto-plasma experiments, and observed IMO in Cd_3As_2 . They reported effective-mass ratios of 0.041, 0.042, and 0.045 for temperatures of 4°K , 77°K , and 300°K respectively. The IMO measurements gave directly the reduced-mass ratio of 0.031 for the valence and conduction bands; this gave a valence-band mass ratio of 0.12.

In 1967, Sexter (29) proposed two conduction bands for Cd_3As_2 separated by 0.15 eV with effective masses of 0.06 and 0.12 m . In 1968, Rosenman (30) by measurement of the oscillatory magnetoresistance (Shubnikov de Hass oscillations, SdH) established that the constant-energy surfaces for the principal band edge departed very little (anisotropy axis ratio was 1.18) from sphericity and was zone centered. Also from the observation of Shubnikov de Hass oscillations, Heller et al. (31) found that for Cd_3P_2 the constant-energy surfaces of the principal band edge departed immeasurably from sphericity and was zone centered. They reported an effective mass of 0.06 m for n_e equal to $1.2 \times 10^{18} \text{ cm}^{-3}$ and 0.05 m for n_e equal to $2.2 \times 10^{17} \text{ cm}^{-3}$.

Fundamental-Absorption Edge

Although much effort has been expended in the investigation of the principal band-edge structure of Cd_3P_2 and particularly that of Cd_3As_2 , there remains little agreement as to the assignment of optical transitions in Cd_3As_2 .

The first report (1950) of an optical gap and a thermal gap was that of Moss (32) in a study of the photoconductivity of Cd_3As_2 . The photoconductive edge lay just below 0.6 eV. He obtained the thermal gap from resistance measurements, the results of which were plotted as log

(resistance) against reciprocal temperature. With the assumption that intrinsic conductivity had been reached at high temperature (180 to 390°K), the value of the gap was obtained from the elementary relation

$$R = R_0 \exp (\mathcal{E}_g / 2kT), \quad (17)$$

where \mathcal{E}_g was found to be 0.14 eV. (This value for the gap is an extrapolated value, to $T = 0^\circ\text{K}$; the temperature dependence of the gap has been lumped into R_0 .)

Such thermal measurements are full of pitfalls (14), particularly in semiconductors with polar binding and with such great degeneracy (33). Thermal measurements continued to be reported which agreed nicely with the work of Möss, except for the thermal work of Ugai and Zyubina (18). Then Turner et al. (34) reported optical absorption edges in Cd_3As_2 as a function of temperature. When their results (300°K optical gap of 0.13 eV) were extrapolated to zero degrees Kelvin, one obtained a gap of 0.184 eV. Zdanowicz (33) investigated the fundamental optical edge of Cd_3As_2 films, whose electrical properties were comparable with those of bulk material. She endeavored to explain the discrepancy of the gap of Turner et al. and those of the thermal measurements of others. The hitherto reported thermal gaps, in the range of 0.14 eV determined in the manner of Equation (17), were dispelled as shortcomings of the technique. One was left with the following picture: the optical absorption edge (at 300°K) at about 0.6 eV was due to direct transitions ($\Delta K = 0$ in Brillouin zone) and the lower energy edge at say, 0.13 eV, was attributed to indirect

transitions. These conclusions were based on the spectral dependence of the absorption coefficient, α . This view of Zdanowicz has been affirmed by Rogers et al. (20) who proposed, along with Armitage and Goldsmid (26), that the lower energy gap was largely due to a Burstein-Moss shift.

Bishop et al. (35) investigated the photoconductivity and photoluminescence in Cd_3P_2 and established the intrinsic optical gap of 0.60 eV; they, thereby, confirmed the earlier estimate of Haacke and Castellion (11). These measurements were followed with a report of optically pumped, coherent, laser oscillation in Cd_3P_2 (36) and measurement of the temperature dependence of photoluminescence in this alloy system by Bishop and Radoff (17). In this latter report it was proposed that the fundamental edge for Cd_3P_2 was underlain by a direct transition, and the absence of photoluminescence in Cd_3As_2 appeared consistent with the result of Lin-Chung's energy-band calculations for Cd_3As_2 (37) that the lowest energy gap was indirect. In a subsequent publication, however, Radoff and Bishop (13), affirmed the 4-band, Kane model proposed by Wagner et al. (12). In this model, the relatively small absorption coefficient (α) observed just above 0.13 eV by Zdanowicz (33) was attributed to a forbidden direct transition. (The four bands include the mirror-like "s" and "p" bands discussed above, and all four bands are zone centered.)

Optical Properties Beyond The Fundamental Edge

In 1968 Sobolev et al. (38) studied the reflectance spectra of a large number of compounds belonging to groups II-V, V-VI, and III-VI. Crude reflectance measurements were performed on polycrystalline samples of Cd_3P_2 and Cd_3As_2 . For Cd_3P_2 , a well defined peak was found at 4.0 eV, and there was a suggestion of weak structure between 2.5 and 3.1 eV. For

Cd_3As_2 , peaks were found at 3.65 eV and 1.7 eV. Direct interband transitions were assumed to be responsible for these peaks. The structure of the reflectance strongly resembled that of substances belonging to groups IV and III-V.

In 1970 Zivitz et al. (39) reported the results of preliminary measurements on the reflectance of Cd_3As_2 polycrystalline samples. The span of photon energy was 4 to 20 eV. In 1971 Sobolev et al. (40) obtained reflectance measurements on single, unoriented crystals of Cd_3As_2 . From 1 to 5 eV, measurements were taken at 293°K and 77°K; from 5 to 12 eV, at 293°K. A total of nine peaks appeared in their reflectance curves, and they were interpreted on the basis of direct transitions. On the basis of Lin-Chung's (37) energy-band calculation, probable assignments were made for these transitions. As mentioned above, their earlier work (38) located a peak at 1.7 eV. In this more recent study of a single crystalline sample, a doublet peak was found where $E_1 = 1.7$ eV and $E'_1 = 1.88$ eV. The splitting was attributed to the spin-orbit splitting of the upper valence band along the Λ direction (this band is p-like about the arsenic atoms). Generally excellent agreement was obtained with Lin-Chung's calculated band structure.

Also in 1971 Stevenson et al. (41) generated the optical constants for Cd_3As_2 and calculated the effective number of free electrons per atom contributing to the optical properties in the photon-energy range 0 to $\hbar\omega_0$ (42). This quantity n_{EFF} was shown to saturate in the range of 3.2, before the d-bands began to contribute to the optical properties above, say 12 eV.

In addition to the energy-band calculation for Cd_3As_2 , Lin-Chung (43) has performed a very similar calculation for Cd_3P_2 . Pseudopotential calculations were performed for these two crystals in a hypothetical fluorite structure (see the section Crystal Structure). The Brillouin zone for this fluorite structure was much larger than that for either Cd_3As_2 or Cd_3P_2 and was identical to that of the fcc structure. The high symmetry points (44) of this fluorite structure were also symmetry points of the real Brillouin zones. Figure 4 demonstrates these two Brillouin zones. The Brillouin zone for the fcc structure was sixteen times larger than that for Cd_3As_2 and four times larger than that for Cd_3P_2 (this follows since the real unit cells of Cd_3As_2 and Cd_3P_2 have a direct volume ratio of four-to-one).

There was a strong similarity between the overall energy-band structures of Cd_3As_2 and Cd_3P_2 , and they were found to resemble those of the III-V compounds (InAs, GaSb, etc.). Figure 5 gives the energy-band structures for Cd_3As_2 and Cd_3P_2 as calculated by Lin-Chung. The lowest valence band was an anion s-like level, the second valence band was a Cd s-like level, and the third and fourth were s-like about Cd and p-like about the anion. The valence-band maximum for Cd_3P_2 was at Γ ; that for Cd_3As_2 , slightly (~ 12 percent) off center of the Brillouin zone. The bottom of the conduction band at Γ had an s-like representation Γ_1 . A number of prescriptions were given for relating the band structure in this hypothetical fluorite structure to the band structure in the real crystals. Her predicted band-edge structure for Cd_3As_2 gave an energy gap of about 0.2 eV or smaller. She briefly discussed the alternative views as to

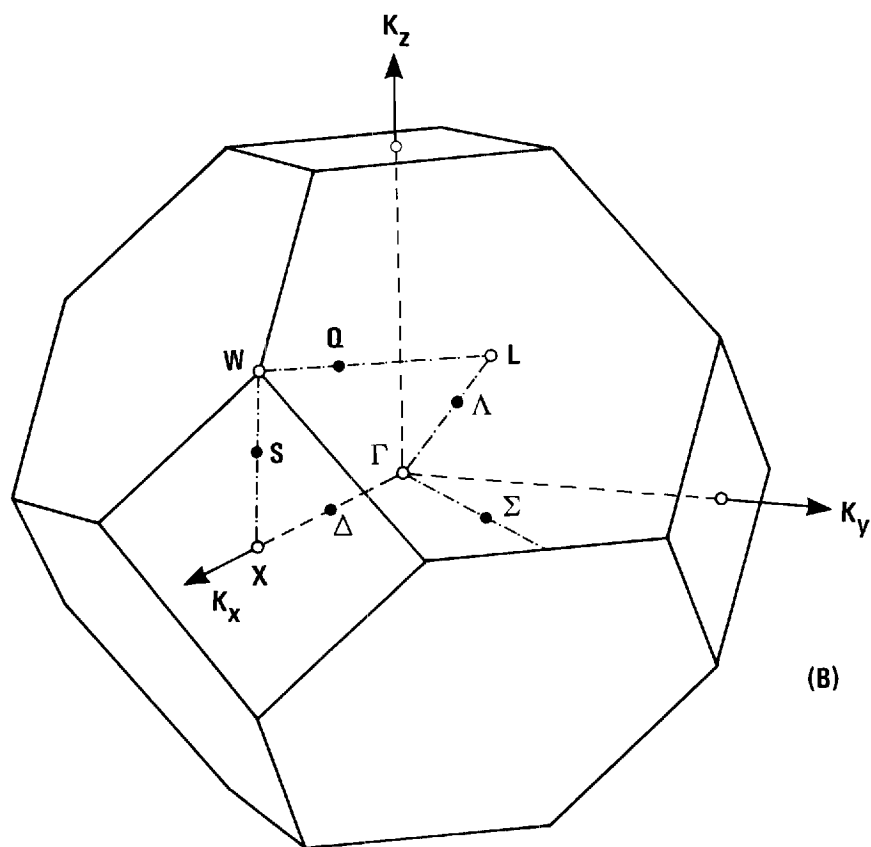
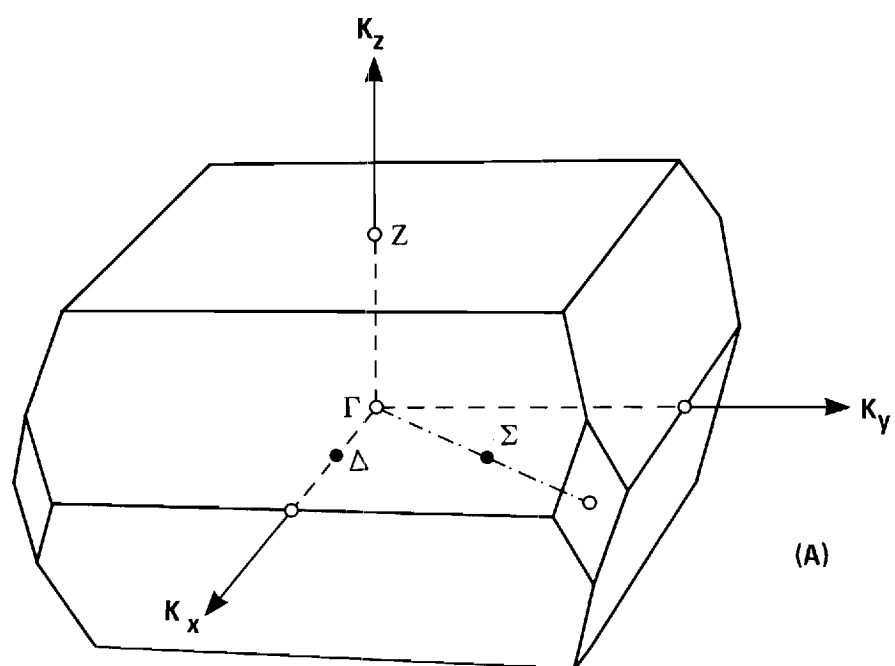


Figure 4. The First Brillouin Zone of (A) Body-centered Tetragonal Structure, and (B) Fluorite Structure.

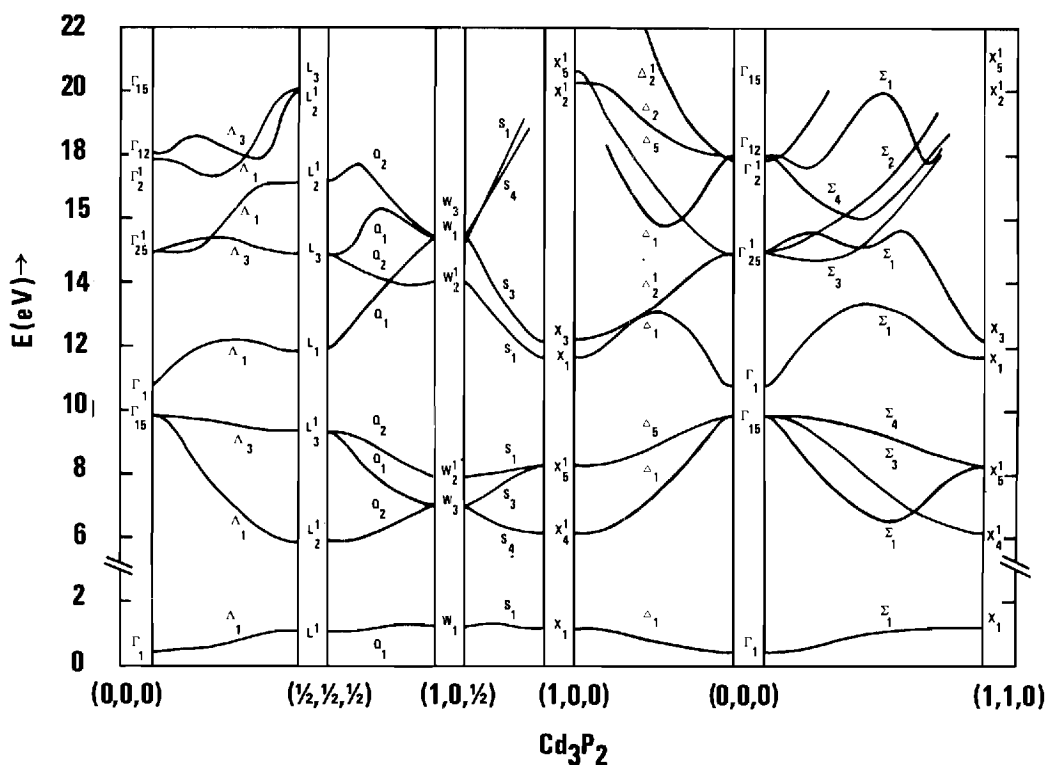
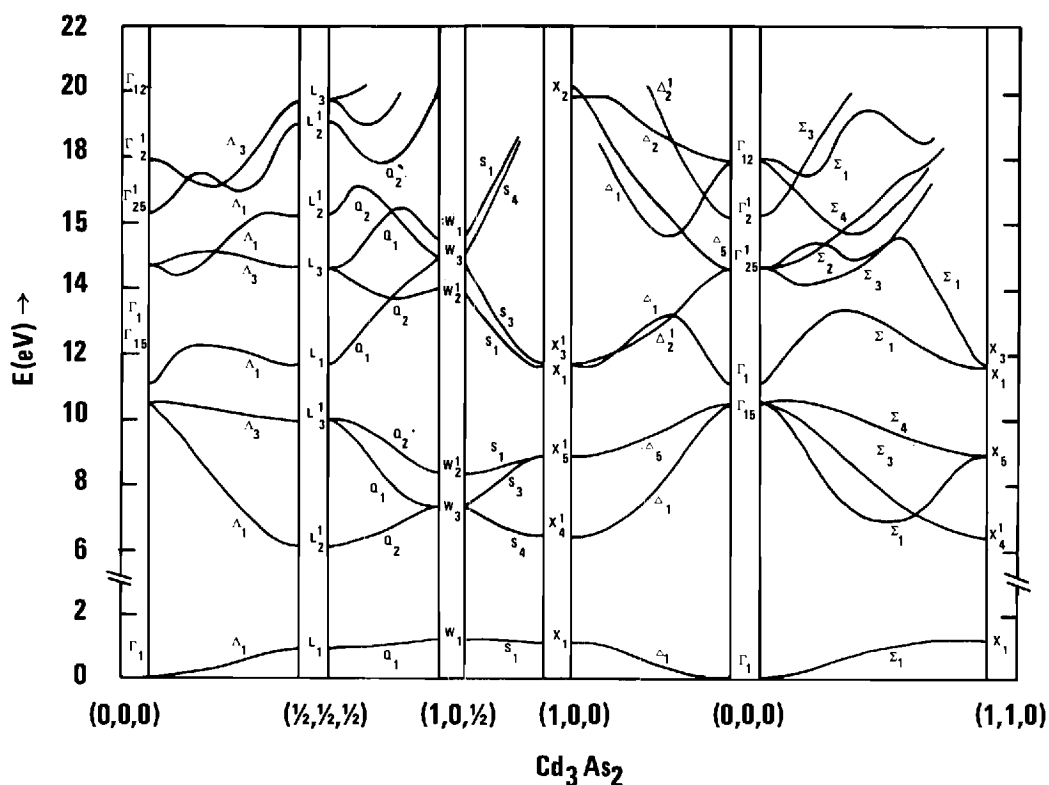


Figure 5. Energy-Band Structures for Cd_3As_2 and Cd_3P_2 Compounds as Calculated in the Hypothetical Structure.

whether or not this gap gave rise to direct or indirect transitions. In these publications (37,43) a few of the calculated interband-energy differences were tabulated for ready comparison with experiment.

Although Cd_3As_2 and Cd_3P_2 possessed slightly different crystal structures, the more important features of the electronic structure were presumably related to their similar chemical composition. The group-IIIB atoms both had an outer filled "s" shell, an empty "p" shell, and a filled "d" shell about 9 eV below the filled "s" shell. The group-V atoms had a filled "s" shell and three electrons in their outer "p" shell. No other electrons lie at energies accessible to our measurements. Figure 6 depicts the ionization energies (45), referred to vacuum, of the neutral atomic components of the alloys investigated. The 4d level at 17.6 eV for cadmium was obtained from the multiplicity-weighted average of the $^2\text{D}_{3/2}$ and $^2\text{D}_{5/2}$ terms given by Harrison (46).

A first approximation to the separation of the "d" band and valence band in the solid is given by the difference between the "d" shell in the group-IIIB atom and "p" shell of the group-V atom. This approximation ignores the large energy shift caused by a transfer of charge in the more ionic crystals; in the event of such a shift, one should more appropriately use the first ionization energies of the stripped atoms (47).

It was clear that the bonding of these compounds involved hybridization of the "s" and "p" orbitals of both atoms (the third and fourth bands were s-like about Cd and p-like about the anion). This hybridization limited the ability to use the language of atomiclike orbitals. However, since the bottom of the conduction band at Γ_1 had an s-like representation,

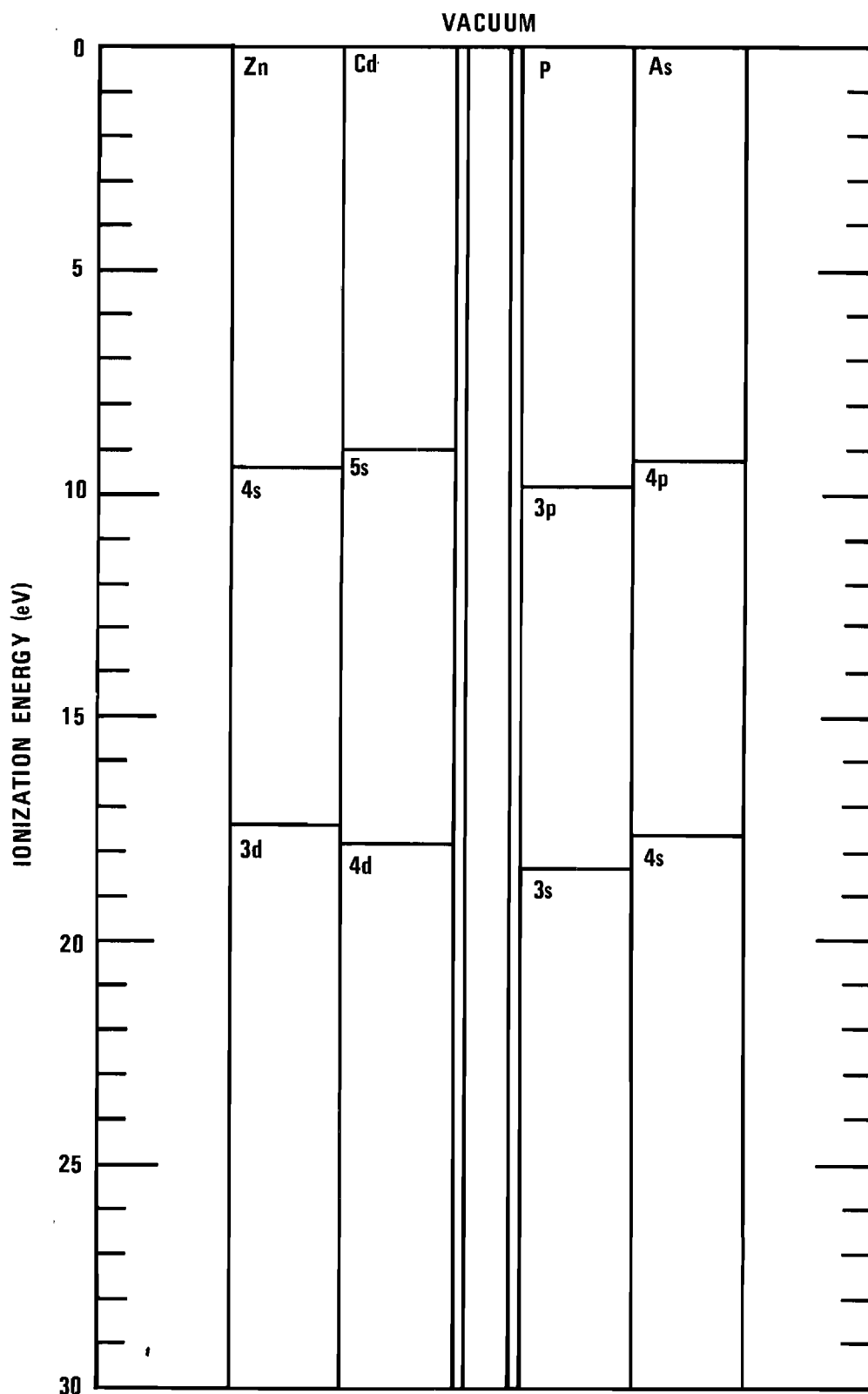


Figure 6. Ionization Energies for the Atomic Components of the II-V Alloys Investigated.

it appeared that one could crudely associate the first vertical valence-band to conduction-band transition with a measure of reverse charge transfer from, say, the "p" shell of the anion to the "s" shell of the "partially ionized" IIB atom.

Given the demonstrated interest in the end-members of this alloy system and the availability of samples from the Semiconductors Branch of the U. S. Naval Research Laboratory in Washington, D. C., an effort was made to extend the knowledge of the optical properties of this alloy system beyond the fundamental edge.

CHAPTER II

THEORY OF OPTICAL PROPERTIES

This dielectric formulation of the optical properties of a crystalline solid is essentially a linear formulation which is valid for weak fields of wavelength large compared to that of a crystallographic unit cell.

Within this formulation we shall use a one-electron picture, ignore effective-field corrections, the interaction with the lattice (phonons), and the first excitation of the crystal, the exciton. Finally, the anisotropy of these crystals will be ignored (symmetry arguments provide the logical extension of the results). The notation of Stern (48), as well as several of his topics, is closely followed herein.

The "joint density of states" is treated in some detail by means of geometrical arguments. Since it is often stated that a one-electron treatment is equivalent to Hartree calculations (in certain approximations), this equivalence is shown to hold exactly.

Wave-vector-dependent Dielectric Constant

The framework for the dielectric formulation is given by Maxwell's equations:

$$\nabla \cdot \bar{B} = 0 \quad (18)$$

$$\nabla \cdot \bar{D} = \rho \quad (19)$$

$$\nabla \times \bar{E} = -\partial \bar{B} / \partial t \quad (20)$$

$$\nabla \times \bar{H} = \bar{J} + \partial \bar{D} / \partial t \quad (21)$$

where ρ is the external (free, excess)-charge density; and \bar{J} includes both the conduction-current and the external-current densities. When use is made of the derived field quantities

$$\bar{D} = \epsilon_0 \bar{E} + \bar{P} \quad (22)$$

and

$$\bar{H} = \mu_0^{-1} \bar{B} - \bar{M}, \quad (23)$$

and of the dimensional (49) relation

$$\epsilon_0 = (\mu_0 c^2)^{-1} \quad (24)$$

we find that Equations (18-21) may be rewritten as follows:

$$\nabla \cdot \bar{B} = 0 \quad (25)$$

$$\epsilon_0 \nabla \cdot \bar{E} = \rho - \nabla \cdot \bar{P} \quad (26)$$

$$\nabla \times \bar{E} + \partial \bar{B} / \partial t = 0 \quad (27)$$

$$\nabla \times \bar{B} - c^{-2} \partial \bar{E} / \partial t = \mu_0 (\bar{J} + \partial \bar{P} / \partial t + \nabla \times \bar{M}). \quad (28)$$

It is simplest to allow for phase shifts (say, inertial effects) between the polarization and the electric field, by representing the fields as the real parts of complex quantities. For example, we may write

$$\bar{E} = \text{Re } \widetilde{E} \quad (29)$$

$$= \text{Re } [\widetilde{E}_0 \exp(i \widetilde{k} \cdot \bar{r} - i\omega t)]$$

$$= \text{Re } [\widetilde{E}_0 \exp(i \bar{k}_1 \cdot \bar{r} - i\omega t)] \exp(-\bar{k}_2 \cdot \bar{r})$$

Generally, we find that

$$\widetilde{k} = \bar{k}_1 + i\bar{k}_2 \quad (30)$$

where \bar{k}_1 is normal to the planes of constant phase and \bar{k}_2 is normal to the planes of constant amplitude. We may now handle phase shifts by writing, for example,

$$\widetilde{D} = \widetilde{\epsilon} \widetilde{E} \quad (31)$$

where \widetilde{D} , \widetilde{E} , and $\widetilde{\epsilon}$ may all be complex.

The conduction current \bar{J}_{cond} which contributes to Equation (21) may be written

$$\bar{J}_{\text{cond}} = \sigma \bar{E} \quad (32)$$

(This assumed "local response" will be re-examined below) and the displacement in phase with the field is given by

$$\bar{D} = \epsilon \bar{E}. \quad (33)$$

For fields with time variation given by Equation (29), we can artificially combine the conduction and displacement currents in the form

$$\begin{aligned} \bar{J}_{\text{cond}} + \partial \bar{D} / \partial t &= \sigma \bar{E} + \epsilon \partial \bar{E} / \partial t = \text{Re} [(\sigma - i\omega\epsilon) \tilde{E}] \\ &= \text{Re} \{ -i\omega [\epsilon + i(\sigma/\omega)] \tilde{E} \}. \end{aligned} \quad (34)$$

From Equations (34) we have two alternatives for compressing the algebra. A complex dielectric constant (relative permittivity) $\tilde{\kappa}$ may be employed in the form

$$\tilde{\kappa}(\omega) = \tilde{\epsilon}(\omega) / \epsilon_0 \quad (35)$$

together with

$$\tilde{\epsilon}(\omega) = \epsilon(\omega) + i[\sigma(\omega)/\omega] \quad (36)$$

$$= \epsilon_1 + i\epsilon_2.$$

Or a complex conductivity

$$\tilde{\sigma}(\omega) = \sigma(\omega) - i\omega\epsilon(\omega) \quad (37)$$

may be used. By analogy, the constitutive relation for the magnetic fields may be written

$$\tilde{\mathbf{B}} = \tilde{\mu} \tilde{\mathbf{H}}. \quad (38)$$

For the complex permeability (relative permeability) we have the expressions

$$\tilde{\kappa}_m(\omega) = \tilde{\mu}/\mu_0 \quad (39)$$

and

$$\tilde{\mu} = \mu_1 + i\mu_2$$

More formal expressions for the fields due to external sources $\rho(\bar{\mathbf{r}}, t)$ and $\bar{\mathbf{J}}_{\text{ext}}(\bar{\mathbf{r}}, t)$ may be obtained with the use of Fourier analysis. The introduction of a scalar potential φ and vector potential $\bar{\mathbf{A}}$ leads to the Fourier-transformed equations

$$\tilde{\mathbf{B}}(\bar{\mathbf{k}}, \omega) = i\bar{\mathbf{k}} \times \tilde{\mathbf{A}}(\bar{\mathbf{k}}, \omega) \quad (40)$$

and

$$\widetilde{E}(\bar{k}, \omega) = -i\bar{k}\widetilde{\varphi}(\bar{k}, \omega) + i\omega\widetilde{A}(\bar{k}, \omega) \quad (41)$$

At this point it is convenient to generalize the complex dielectric constant and permeability of Equations (31) and (38) and allow them to depend on the wave vector \bar{k} as well as on the angular frequency ω as follows:

$$\widetilde{D}(\bar{k}, \omega) = \widetilde{\epsilon}(\bar{k}, \omega)\widetilde{E}(\bar{k}, \omega) \quad (42)$$

$$\widetilde{H}(\bar{k}, \omega) = \widetilde{B}(\bar{k}, \omega)/\widetilde{\mu}(\bar{k}, \omega) \quad (43)$$

where the conductivity is included in $\widetilde{\epsilon}(\bar{k}, \omega)$, as above. (This dependence is not only suggested by the symmetry of these equations, but will be shown to be explicitly required by quantum mechanics for intraband absorption.) Equations (19) and (21) become

$$\bar{k} \cdot \bar{k}\widetilde{\varphi} - \omega\bar{k} \cdot \widetilde{A} = \widetilde{\rho}/\widetilde{\epsilon} \quad (44)$$

$$[\bar{k} \cdot \bar{k} - \omega^2\widetilde{\mu}\widetilde{\epsilon}]\widetilde{A} + [\omega\widetilde{\mu}\widetilde{\epsilon}\widetilde{\varphi} - \bar{k} \cdot \widetilde{A}]\bar{k} = \widetilde{\mu}\widetilde{J}_{\text{ext}}, \quad (45)$$

wherein quantities with a tilde are functions of k and ω . The Lorentz condition may be used to reduce Equations (44) and (45) to the symmetrical forms

$$[\bar{k} \cdot \bar{k} - \omega^2\widetilde{\mu}\widetilde{\epsilon}]\widetilde{\varphi} = \widetilde{\rho}/\widetilde{\epsilon} \quad (46)$$

$$[\bar{k} \cdot \bar{k} - \omega^2\widetilde{\mu}\widetilde{\epsilon}]\widetilde{A} = \widetilde{\mu}\widetilde{J}_{\text{ext}}. \quad (47)$$

Alternatively, Equations (44) and (45) may be simplified by a partition of \tilde{A} and \tilde{J}_{ext} respectively, into longitudinal and transverse components as follows:

$$\tilde{A}(\bar{k}, \omega) = \tilde{A}_L(\bar{k}, \omega) + \tilde{A}_T(\bar{k}, \omega) \quad (48)$$

$$\bar{k} \times \tilde{A}_L = \bar{k} \cdot \tilde{A}_T = 0. \quad (49)$$

Making use of this partition scheme and charge conservation [contained in Equations (20) and (21)],

$$\bar{k} \cdot \tilde{J}_{\text{ext}}(\bar{k}, \omega) = \omega \tilde{\rho}(\bar{k}, \omega), \quad (50)$$

we readily obtain

$$\bar{k} \cdot \bar{k} \tilde{\phi} - \omega \bar{k} \cdot \tilde{A}_L = \tilde{\rho} / \tilde{\epsilon} \quad (51)$$

and

$$[\bar{k} \cdot \bar{k} - \omega^2 \tilde{\mu} \tilde{\epsilon}] \tilde{A}_T = \tilde{\mu} \tilde{J}_T \quad (52)$$

as alternatives to Equations (46) and (47). The arbitrariness in Equation (51) may be reduced by either the choice of a gauge in which the scalar potential $\tilde{\phi}$ vanishes so that we have

$$\tilde{A}_L(\bar{k}, \omega) = - \bar{k} \tilde{\phi}(\bar{k}, \omega) / [\omega \bar{k} \cdot \bar{k} \tilde{\epsilon}(\bar{k}, \omega)] \quad (53)$$

or that gauge (Coulomb) in which the component \tilde{A}_L vanishes so that we have

$$\tilde{\varphi}(\bar{k}, \omega) = \tilde{\rho}(\bar{k}, \omega) / [\bar{k} \cdot \tilde{\epsilon}(\bar{k}, \omega)]. \quad (54)$$

We now consider the propagation of waves in the absence of external charges or currents. Equation (52) shows that a transverse wave can exist if there is a dispersion relation of the form

$$\bar{k} \cdot \bar{k} = \tilde{\mu}(\bar{k}, \omega) \epsilon(\bar{k}, \omega) \omega^2 \quad (55)$$

A less formal, single, plane-wave treatment yields this same relation. Furthermore, the plane-wave treatment allows \bar{k} and ω to be complex (the Fourier analysis restricts \bar{k} and ω to real values). Equations (53) and (54) yield as the condition for the existence of a longitudinal wave in the absence of sources

$$\kappa(\bar{k}, \omega) = 0. \quad (56)$$

This condition is found to hold approximately for real solids and is optically associated with the threshold for transparency in the ultraviolet region and a similar threshold for transparency in the infrared region when there exists a Reststrahlen band. We see here that an external source $\rho(\bar{k}, \omega)$ will produce a large, longitudinal response in the solid. Furthermore, Equation (53) or (54) leads to a vanishing magnetic field by the use of Equation (40). So these longitudinal waves consists of purely electric fields and are called plasma oscillations.

Alternative Definition of Dielectric Constant

Theoretical investigations of the electronic properties of the free-electron gas often introduce an alternative definition of the dielectric constant for transverse fields. This alternative arises in an effort to relate the magnetization to the more fundamental magnetic-field quantity \tilde{B} . Many equations are simplified by the introduction of the reciprocal relative permeability

$$\tilde{\kappa}(\bar{k}, \omega) = [\kappa_m(\bar{k}, \omega)]^{-1}. \quad (57)$$

In particular, we can write the magnetization as

$$\tilde{M}(\bar{k}, \omega) = [1 - \tilde{\kappa}(\bar{k}, \omega)] \tilde{B}(\bar{k}, \omega) / \mu_0. \quad (58)$$

Now the $\nabla \times M$ term which appears in Equation (28) may be considered to be another current term in the fashion that the displacement current was lumped into the conduction current in Equation (34). First we rewrite Equation (28) in the form

$$\begin{aligned} \mu_0^{-1} \nabla \times \bar{B} &= \bar{J}_{\text{ext}} + \sigma \bar{E} + \partial \bar{D} / \partial t + \nabla \times \bar{M} \\ &= \bar{J}_{\text{ext}} + \bar{J}_{\text{ind}} \end{aligned} \quad (59)$$

Now if no external change is present and if we choose the gauge in which the scalar potential vanishes, we may write \bar{J}_{ind} in the following forms

$$\tilde{\mathbf{J}}_{\text{ind}} = [i\omega(\sigma - i\omega\epsilon) + \bar{\mathbf{k}} \cdot \bar{\mathbf{k}} (1 - \tilde{\mathcal{K}}) \mu_0^{-1}] \tilde{\mathbf{A}}(\bar{\mathbf{k}}, \omega) \quad (60)$$

$$= [i\omega \tilde{\sigma}^{\text{tr}}(\bar{\mathbf{k}}, \omega)] \tilde{\mathbf{A}}(\bar{\mathbf{k}}, \omega)$$

$$= \omega^2 \epsilon_0 \tilde{\kappa}^{\text{tr}}(\bar{\mathbf{k}}, \omega) \tilde{\mathbf{A}}(\bar{\mathbf{k}}, \omega)$$

Since the magnetic effects have been lumped into $\tilde{\sigma}^{\text{tr}}$ or $\tilde{\kappa}^{\text{tr}}$, we have the degenerate constitutive relation

$$\tilde{\mathbf{H}}(\bar{\mathbf{k}}, \omega) = \mu_0^{-1} \tilde{\mathbf{B}}(\bar{\mathbf{k}}, \omega). \quad (61)$$

Significance of Wave-Vector Dependence of Dielectric Constant

Consider a freely propagating wave of fixed frequency ω . Equation (55), which we may rewrite by the use of Equation (24) as

$$\bar{\mathbf{k}} \cdot \bar{\mathbf{k}} = (\omega^2/c^2) \tilde{\kappa}(\bar{\mathbf{k}}, \omega) \tilde{\kappa}_m(\bar{\mathbf{k}}, \omega) \quad (62)$$

is an implicit equation which must, in principle, be solved for $\bar{\mathbf{k}}$. The resulting value of $\bar{\mathbf{k}}$ is then substituted into κ and κ_m . The behavior of the wave is then completely specified within a solid of infinite extension. Let us now consider a mechanism responsible for this wave-vector dependence. Equation (32), which is the constitutive relation for the conduction-current density, is not well-founded, even classically. The nature of the invalidity of this constitutive relation is not directly related to relaxation effects. When we consider the free-carrier contribution of

say a single group of electrons [see Equation (215) of Appendix A] to $\tilde{\kappa}(\omega)$, and identify Γ' with the reciprocal of a mean free time, we see that for ω much less than Γ' $\tilde{\kappa}(\omega)$ is totally complex. If we now compare this $\tilde{\kappa}(\omega)$ with Equation (36), it is seen that $\tilde{\sigma}(\omega)$ is totally real; that is, we consider frequencies (10^9 Hertz) for which relaxation effects are negligible.

This constitutive relation is based on the implicit assumption (50) that the spacial variation of the electric field is long compared to an electronic mean free path. When the field varies rapidly (spacially) within a mean free path, the current density will no longer be the result of a "local" field. (The word "local" as used here, bears no relation to the Lorentz local or effective field.) Between randomizing collisions, the electron will experience a varying field strength; the acquired drift velocity will be related to the field strength at all points along its path. Retardation effects appear and we have a nonlocal response. The wave-vector-dependent dielectric constant, introduced above, affords the means for handling this nonlocal response.

In fact, for strong wave-vector dependence of the dielectric constant, there arise serious difficulties in handling boundaries between solids. Since the current at a point will depend on the field at other points, the effects of a boundary will be felt at considerable depths. This gives rise to the anomalous skin effect in metals. The conventional boundary-condition treatment fails. It is well known that the conventional boundary-condition treatment leads to algebraic relationships between the reflectance (specular) and a complex index of refraction (see below); however, in view of the above, a proper utilization of this algebra requires weak wave-vector dependence of the dielectric constant.

It is a comfort to the experimentalist to know that, even for the case of very strong wave-vector dependence of the dielectric constant, a phenomenological quantity exists which is descriptive of the surface of a solid. This quantity is the surface impedance (51) for normal incidence \tilde{Z} , and is given by

$$\tilde{\mathbf{E}} = \tilde{Z}(\tilde{\mathbf{H}} \times \hat{\mathbf{n}}). \quad (63)$$

Now, $\tilde{\mathbf{E}}$ and $\tilde{\mathbf{H}}$ are evaluated at the surface of the solid and $\hat{\mathbf{n}}$ is a unit vector in the propagation direction, which we choose to be the positive "z," and if we choose to polarize the electric field in the "x" direction, we find that the surface impedance is given by

$$\tilde{Z} = \tilde{E}_x / \tilde{H}_y. \quad (64)$$

The reflectance may be expressed in terms of \tilde{Z} . If we assume a uniform time dependence given by $\exp(-i\omega t)$ and that the wave is incident from the vacuum, then we can express the magnetic field for negative "z" as the sum of an incident and a reflected wave in the form

$$\tilde{H}_y(z) = \tilde{H}_i \exp(ikz) + \tilde{H}_r \exp(-ikz) \quad (65)$$

where the propagation vector is given by

$$k = |k| = \omega / c. \quad (66)$$

Without the loss of generality, we may express Equation (19), within the vacuum, in the form

$$\tilde{\mathbf{k}} \times \tilde{\mathbf{E}} = \mu_0 \tilde{\mathbf{H}}. \quad (67)$$

This Equation (67) combined with Equation (65) leads to the expression

$$\tilde{\mathbf{E}}_x(z) = Z_0 [\tilde{\mathbf{H}}_i \exp(ikz) - \tilde{\mathbf{H}}_r \exp(-ikz)], \quad (68)$$

where Z_0 , defined by the equation

$$Z_0 = \mu_0 c, \quad (69)$$

is called the impedance of the vacuum or of free space. We now define the amplitude reflection coefficient by the expression

$$\tilde{r} = \tilde{\mathbf{H}}_r / \tilde{\mathbf{H}}_i. \quad (70)$$

This definition obviates the difficulties in "bookkeeping" which arise if one chooses to define the reflection coefficient in terms of the electric field. (The literature is full of inconsistencies which arise from this latter choice; very often authors carelessly drop or add a factor of 180° . This subject will be mentioned below.)

We now solve Equations (64), (65), and (68) for \tilde{r} in terms of \tilde{Z} and find the expression

$$\tilde{r} = (z_o - \tilde{z}) / (z_o + \tilde{z}). \quad (71)$$

The reflectance may be written

$$R = |\tilde{r}|^2 \quad (72)$$

$$= |z_o - z|^2 / |z_o + z|^2.$$

Equation (71) shows that we have obtained, independently of the details of the wave-vector dependence of the dielectric constant, the algebra of transmission lines. We will now briefly consider the quantum mechanical introduction of this wave-vector dependence and then see in what fashion we can legitimately relate the surface impedance to the dielectric or optical constants.

Kinematics of Energy and Crystal Momentum Conservation

With the aid of quantum mechanics, we now consider interactions of electromagnetic radiation with our solid. A one-electron picture is used and this electron moves in an average potential $V_o(x)$. The total energy of this electron in the presence of an electromagnetic field is given simply by

$$H = V_o - e\tilde{\phi} + mv^2/2 \quad (73)$$

and the canonical momenta (52) are given by

$$p_i = mv_i - eA_i. \quad (74)$$

We find, by substituting Equation (74) into (73), the expression

$$H = V_0 - e\tilde{\varphi} + (\bar{p} + e\bar{A})^2/2m \quad (75)$$

for the Hamiltonian. We choose that gauge in which the scalar potential φ vanishes and consider a single plane wave with vector potential given by

$$\begin{aligned} \bar{A} &= \text{Re} [\tilde{A}_0 \exp(i\bar{k} \cdot \bar{r} - i\omega t)] \\ &= \text{Re} \tilde{A}. \end{aligned} \quad (76)$$

From this Equation (76) and the operation relation

$$\bar{p} = -i\hbar \nabla \quad (77)$$

we find the symmetrized expressions

$$\begin{aligned} \tilde{A} \cdot \bar{p} + \bar{p} \cdot \tilde{A} &= 2\tilde{A} \cdot (\bar{p} + \hbar\bar{k}/2) \\ &= 2\tilde{A} \cdot \bar{p}^+ \end{aligned} \quad (78)$$

The additional term $\hbar\bar{k}/2$ need only be included for longitudinal fields.

The first-order interaction term ($H = H_0 + H_I$) is given by

$$H_I = \tilde{Q} \exp(-i\omega t) + \tilde{Q}^* \exp(i\omega t) \quad (79)$$

and

$$\tilde{Q} = (e/2m)\tilde{A}_0 \exp(i\vec{k}\cdot\vec{r})\cdot\vec{p}^+ . \quad (80)$$

One term in Equation (79) induces upward transitions; the other, downward transitions at the same rate (53).

In the visible and near ultraviolet regions (54) of the spectrum, we may write the one-electron wavefunctions as $|\vec{K}j\rangle$ where the wave vector \vec{K} labels the irreducible representation of the translation group (44) according to which the one-electron state transforms. The three dimensional domain of \vec{K} is the Brillouin zone. The energy of an eigenstate is not a single-valued function of this wave vector; so we represent the energy by the quasicontinuous function $\mathcal{E}_j(\vec{K})$. The index "j" allows us to define a single-valued function; the lowest lying state of wave vector \vec{K} is said to be in the "first band."

It is assumed that the potential of the solid has the full translational symmetry of the lattice; the degree to which the following analysis is valid for an alloy, in which the translational symmetry will not be perfect, can be judged by comparison of the experimental results for the mid-members of the alloy system with those for the end-members (55). It is found that when the "impurity" belongs to the same column of the periodic table as the host element it replaces, the consequences of the destruction of the translational symmetry are mild (56).

For the moment, we consider the first term of Equation (79). If

the electron was initially in the state $|\bar{K}j\rangle$, then the transition rate for the absorption of a photon (53) which takes the electron to the state $|\bar{K}'m\rangle$ is shown by the golden rule number 2 in the form

$$r_o = (2\pi/\hbar) |\langle \bar{K}'m | \tilde{Q} | \bar{K}j \rangle|^2 \rho(\epsilon) \quad (81)$$

where $\rho(\epsilon)$ may be considered to be a density (as yet unspecified) of states per unit energy in K -space that relates to a lack of perfect monochromaticity of the incident radiation. The kinematics of energy and crystal momentum ($\hbar\bar{K}$) conservation will dictate the precise interpretation of this term. The energy difference between the upper and lower states is given by

$$\hbar\omega = \epsilon_m(\bar{K}') - \epsilon_j(\bar{K}). \quad (82)$$

When we consider the second term of Equation (79), we find an expression identical to Equation (81); however, this latter transition corresponds to the emission of a photon or a sign change in Equation (82). The net transition rate from state $|\bar{K}j\rangle$ to state $|\bar{K}'m\rangle$ will depend on their relative occupancies as given by the Fermi-Dirac distribution function

$$f[\epsilon_j(\bar{K})] = (\exp\{[\epsilon_j(\bar{K}) - \epsilon_F]/kT\} + 1)^{-1} \quad (83)$$

where ϵ_F is the Fermi level. This net rate is given by the expressions

$$r_{ind} = r_o [f[\epsilon_m(\bar{K}')] \{1 - f[\epsilon_j(\bar{K})]\} - f[\epsilon_j(\bar{K})] \{1 - f[\epsilon_m(\bar{K}')]\}] \quad (84)$$

$$= r_o \{ f[\varepsilon_m(\bar{K}')] - f[\varepsilon_j(\bar{K})] \}$$

$$= r_o \{ F.D. \}$$

The abbreviation F. D. is introduced for convenience. Substitution of Equation (80) into (81) and then Equation (81) into (84) yields the results

$$r_{ind} = [\pi e^2 |\tilde{A}_o|^2 / (2m^2 h)] |M|^2 \rho(\varepsilon) \{F.D.\} \quad (85)$$

and

$$M = (\bar{K}'_m | \exp(i\bar{k} \cdot \bar{r}) \hat{a}_o \cdot \bar{p}^+ | \bar{K}_j) \quad (86)$$

where we have introduced a unit polarization vector \hat{a}_o .

This matrix element given by Equation (86) contains the selection rule based on the conservation of crystal momentum. To see this rule, we introduce the Bloch function as follows:

$$|u_{\bar{K}_j}\rangle = \exp(-i\bar{K} \cdot \bar{r}) |\bar{K}_j\rangle \quad (87)$$

and

$$|\bar{K}_j\rangle = \exp(i\bar{K} \cdot \bar{r}) |u_{\bar{K}_j}\rangle. \quad (88)$$

These Bloch functions have the full translational symmetry of the lattice. By substitution of Equation (88) into Equation (86) we obtain

$$M = (\psi_{\bar{K},m} | \hat{a}_0 \exp[i(\bar{k} - \bar{K}') \cdot \bar{r}] \cdot \bar{p}^+ \exp(i\bar{K} \cdot \bar{r}) | \psi_{\bar{K},j}). \quad (89)$$

We now operate with \bar{p}^+ and obtain

$$M = (\psi_{\bar{K},m} | \exp[i(\bar{K} + \bar{k} - \bar{K}') \cdot \bar{r}] \hat{a}_0 \cdot \hbar(\bar{K} + 1/2 \bar{k} - i\nabla) | \psi_{\bar{K},j}). \quad (90)$$

It is well known that the term $\exp[i(\bar{K} + \bar{k} - \bar{K}') \cdot \bar{r}]$ contributes extremely rapid oscillations to such an integral over macroscopic dimensions, so the integral (Matrix Element) vanishes unless we have the selection rule

$$\bar{K}' = \bar{K} + \bar{k} \quad (91)$$

for the conservation of crystal momentum ($\hbar\bar{K}$).

We now restrict our attention to transverse waves and consider two possibilities for the states $|\bar{K},j\rangle$ and $|\bar{K}',m\rangle$: the first, in which we have

$$\bar{K}' = \bar{K} + \bar{k} \quad (92)$$

and

$$m = j; \quad (93)$$

the second, in which we have

$$\bar{K}' \approx \bar{K} \quad (94)$$

and

$$m \neq j. \quad (95)$$

Intraband Transitions

This first possibility corresponds to no change in the band index and is an "intraband" transition. (Although this free-carrier contribution to the dielectric constant is not of much consequence in the analysis of the absorption mechanisms of semiconductors beyond the fundamental edge, it is considered here for the reason that the wave vector \bar{k} enters the transition rate explicitly.) We again consider the vector potential of Equation (76) to be propagating in the z-direction and polarized in the x-direction. From Equations (90, (91), and the orthogonality of the Bloch functions we have for the matrix element M the expression

$$M = (u_{(\bar{K} + \bar{k})j} | -i\hbar \partial / \partial x | u_{\bar{K}j}). \quad (96)$$

We rewrite the conservation Equations (91) and (82) in the forms

$$\bar{K}' = \bar{K} + \bar{k} \quad (97)$$

and

$$\bar{K}'^2 = \bar{K}^2 + 2m^* \omega / \hbar, \quad (98)$$

where for convenience we consider spherical constant-energy surfaces with

parabolic dependence on the wave vector \bar{K} . Squaring Equation (97) and subtracting Equation (98) gives

$$K_z = (m^*\omega/\hbar k) - k/2 \quad (99)$$

where we have used the fact that "k" lies in the z-direction. Quite generally, the density of electronic states in \bar{K} -space is given by

$$W(\bar{K}) = 2V/(2\pi)^3 \quad (100)$$

where the volume of the crystalline solid is V. We now seek that number of states in \bar{K} -space that relates to the lack of perfect monochromaticity of the incident radiation [see Equation (81)]. This number of states may be written

$$\rho(\mathcal{E})d\mathcal{E} = W(\bar{K})d^3K \quad (101)$$

where the volume element d^3K is that domain of \bar{K} -space in which this "blurring" occurs.

From Equation (99) we see that changing ω by $\hbar^{-1}d\mathcal{E}$ changes K_z by $(m^*/\hbar^2 k)d\mathcal{E}$. So Equation (101) becomes

$$\rho(\mathcal{E}) = [m^*/(4\pi\hbar^2 k)]dK_x dK_y \quad (102)$$

where we have used Equation (100) and divided by $d\mathcal{E}$ and by the volume V. Substitution of Equations (96) and (102) into (85) yields for the transi-

tion rate for intraband absorption

$$r_{\text{ind}} = [\pi e^2 |\tilde{A}_0|^2 / (2m^2 \hbar)] (u_{(\bar{K} + \bar{k})j} | - i\hbar \partial / \partial x | u_{\bar{K}j})^2 \quad (103)$$

$$\times [m^* / (4\pi^3 \hbar^2 k)] dK_x dK_y \{F.D.\}$$

where it is seen that there is explicit dependence on the wave vector \bar{k} . (We will see below that this leads to a dependence of the dielectric constant on \bar{k} .) We note in ending this discussion of intraband transitions that, experimentally, the initial state of the electron $|\bar{K}j\rangle$ is not known so that we must perform an integration of Equation (103) over the Brillouin zone.

Interband Transitions

The second possibility corresponds to approximately no change in the electron wave vector \bar{K} and is a direct or vertical "interband" transition. The approximation, as given by Equation (94), consists of the neglect of the photon wave vector \bar{k} in Equation (91). For photons of energy less than say 10 eV this wave vector is indeed small compared to those of the electronic states, whose wave-vector domain is the Brillouin zone. (We recall that radiation must reach the x-ray region, about 1 keV, before Bragg diffraction occurs. This approximation is analogous to the dipole approximation in the perturbation theory of isolated atoms.) The classical analogue of this transition (absorption mechanism) is given by the motion of a damped, harmonically bound electron in the presence of the electromagnetic field (see Appendix A). As in the case of interband transitions, we must again find that number of states in \bar{K} -space that relates to the

lack of perfect monochromaticity of the incident radiation [see Equation (81)].

In order to find that number of states, we first rewrite Equation (82) in the form

$$\hbar\omega = \epsilon_m(\bar{\mathbf{K}}) - \epsilon_j(\bar{\mathbf{K}}). \quad (104)$$

In sharp contrast to the procedure used above for interband transitions, we see that a change of the angular frequency of the incident radiation by an amount $d\omega$ cannot be related to a "blurring" of the wave vector of only one of the two electronic states. This inability to relate the "blurring" to only one of the two states involved is due to the symmetry of Equations (94) and (104). We proceed as follows, with the justification that the results are in exact agreement with those of Hartree calculations in which small relaxation terms are ignored.

First, we substitute Equation (100) in (101) and obtain

$$\rho(\epsilon)d\epsilon = [2V/(2\pi)^3]d^3K \quad (105)$$

We now see that changing ω by $\hbar^{-1}d\epsilon$ introduces a change in the wave vector $\bar{\mathbf{K}}$ of amount $d\bar{\mathbf{K}}$; this follows from the differentiation of Equation (104) in the form

$$d\epsilon = \nabla_{\bar{\mathbf{K}}}[\epsilon_m(\bar{\mathbf{K}}) - \epsilon_j(\bar{\mathbf{K}})] \cdot d\bar{\mathbf{K}}. \quad (106)$$

We now rewrite Equation (106) in the form

$$d\mathcal{E} = |\nabla_{\bar{\mathbf{K}}}[\mathcal{E}_m(\bar{\mathbf{K}}) - \mathcal{E}_j(\bar{\mathbf{K}})]| dK_{\perp}. \quad (107)$$

This change dK_{\perp} may be considered to be the normal to a surface element $dS_{\bar{\mathbf{K}}}$, in $\bar{\mathbf{K}}$ -space, on which Equation (104) holds true; that is, on which energy is conserved. By substituting Equation (107) in (105) and by replacing $d^3\mathbf{K}$ with $dS_{\bar{\mathbf{K}}}dK_{\perp}$, we therefore obtain

$$\rho(\mathcal{E}) = [2/(2\pi)^3] dS_{\bar{\mathbf{K}}} / |\nabla_{\bar{\mathbf{K}}}[\mathcal{E}_m(\bar{\mathbf{K}}) - \mathcal{E}_j(\bar{\mathbf{K}})]| \quad (108)$$

where we have divided by $d\mathcal{E}$ and by the volume V .

For these interband transitions, Equation (90) becomes

$$M = (u_{\bar{\mathbf{K}}m} | \hat{\mathbf{a}}_o \cdot \bar{\mathbf{p}} | u_{\bar{\mathbf{K}}j}) \quad (109)$$

where it is assumed that the Bloch functions of differing indices are orthogonal. The substitution of Equations (108) and (109) into (85) yields the result

$$\begin{aligned} r_{\text{ind}} = & -[\pi e^2 |\tilde{\mathbf{A}}_o|^2 / (2m^2 \hbar)] (u_{\bar{\mathbf{K}}m} | \hat{\mathbf{a}}_o \cdot \bar{\mathbf{p}} | u_{\bar{\mathbf{K}}j})^2 \\ & \times [2/(2\pi)^3] dS_{\bar{\mathbf{K}}} / |\nabla_{\bar{\mathbf{K}}} [\mathcal{E}_m(\bar{\mathbf{K}}) - \mathcal{E}_j(\bar{\mathbf{K}})]|. \end{aligned} \quad (110)$$

The term $F \cdot D$ has been set equal to minus one; that is, we shall assume that the initial state j is occupied and the final state m is empty.

As mentioned above, experimentally the initial state $|\bar{\mathbf{K}}j\rangle$ of the electron is not known. Every pair of states within the Brillouin zone that

satisfies the kinematics of energy and crystal momentum conservation can contribute to the absorption process. It is claimed (54) that the matrix element "M" is a slowly varying function of wave vector \bar{K} and that we have to perform an integral of this result over the Brillouin zone. We obtain for the observed induced transition rate the expression

$$r_{\text{obs}} = - [\pi e^2 |\tilde{A}_0|^2 / (2m^2 \hbar)] (u_{\bar{K}m} | \hat{a}_0 \cdot \vec{p} | u_{\bar{K}j})^2 J_{mj} \quad (111)$$

where we have introduced the "joint density of states" J_{mj} in the usual form

$$J_{mj} = [2/(2\pi)^3] \int dS_{\bar{K}} / |\nabla_{\bar{K}} [\epsilon_m(\bar{K}) - \epsilon_j(\bar{K})]|. \quad (112)$$

The small volume element $dS_{\bar{K}} dK_{\perp}$ has become a thin shell in which energy is conserved. We shall further discuss Equation (111) below.

Relation of Transition Rates to κ_2 and Line Shapes

In the following, we restrict the fields to single plane waves, we agree to time-average field quantities over one period, and we continue to use that gauge in which the scalar potential vanishes. Maxwell's equations in the absence of sources may be written for a plane wave

$$\tilde{\mu} \vec{k} \cdot \vec{H} = 0, \quad (113)$$

$$\tilde{\epsilon} \vec{k} \cdot \vec{E} = 0, \quad (114)$$

$$\tilde{\mathbf{k}} \times \tilde{\mathbf{E}} = \omega \tilde{\mu} \tilde{\mathbf{H}}, \quad (115)$$

and

$$\tilde{\mathbf{k}} \times \tilde{\mathbf{H}} = -\omega \tilde{\epsilon} \tilde{\mathbf{E}}. \quad (116)$$

As previously mentioned [see Equation (55)], for plane waves we may write

$$\tilde{\mathbf{k}} \cdot \tilde{\mathbf{k}} = \tilde{\mu}(\tilde{\mathbf{k}}, \omega) \tilde{\epsilon}(\tilde{\mathbf{k}}, \omega) \omega^2. \quad (117)$$

We now introduce the index of refraction "n" and the extinction coefficient "k" by the expressions

$$\tilde{\mathbf{k}} \cdot \tilde{\mathbf{k}} = \tilde{\mu} \tilde{\epsilon} \omega^2 = \tilde{\kappa} \tilde{\kappa}_m \omega^2 / c^2 = (n + ik)^2 \omega^2 / c^2 \quad (118)$$

$$= |\bar{\mathbf{k}}_1|^2 - |\bar{\mathbf{k}}_2|^2 + 2i\bar{\mathbf{k}}_1 \cdot \bar{\mathbf{k}}_2$$

For the case of $\bar{\mathbf{k}}_1$ and $\bar{\mathbf{k}}_2$ parallel (homogeneous plane wave), we find

$$|\bar{\mathbf{k}}_1| = n\omega/c \quad (119)$$

and

$$|\bar{\mathbf{k}}_2| = k\omega/c. \quad (120)$$

We also find for the time-averaged energy flow (Poynting vector)

$$\langle S \rangle = 1/2 \operatorname{Re}(\tilde{\mathbf{E}} \times \tilde{\mathbf{H}}^*) \quad (121)$$

$$= (nc \epsilon_0 / 2\kappa_m) (\tilde{\mathbf{E}}_0^* \cdot \tilde{\mathbf{E}}_0) \hat{\mathbf{k}}_1 \exp(-2\bar{\mathbf{k}}_2 \cdot \bar{\mathbf{r}})$$

where $\hat{\mathbf{k}}_1$ is a unit vector in the direction of $\bar{\mathbf{k}}_1$ and $\bar{\mathbf{k}}_2$; use has been made of Equation (29). From Equation (121) we have the following expressions for the absorption coefficient:

$$\alpha = 2|\bar{\mathbf{k}}_2| \quad (122)$$

or

$$\alpha = 2k\omega/c. \quad (123)$$

We earlier identified $\omega\epsilon_2$ with the conductivity in Equation (36). Stern (48) states that $1/2 \omega\epsilon_2 \tilde{\mathbf{E}} \cdot \tilde{\mathbf{E}}^*$ gives the time-averaged power dissipation per unit volume due to Joule heating and that $1/2 \omega\tilde{\mu}_2 \tilde{\mathbf{H}} \cdot \tilde{\mathbf{H}}^*$ gives the magnetic-power dissipation. The power dissipation arises from the phase shift between the polarization (magnetization) and the electric (magnetic) field, since it is the imaginary part of $\tilde{\epsilon}$ ($\tilde{\mu}$) which appears. (Much discussion centers about this interpretation, because the electromagnetic energy density is not given by $1/2 \operatorname{Re}(\tilde{\mathbf{E}} \cdot \tilde{\mathbf{D}} + \tilde{\mathbf{H}} \cdot \tilde{\mathbf{B}})$ in a dispersive medium.) We henceforth restrict ourselves to the case where κ_m is unity (this is valid at optical frequencies).

We now identify the power dissipation per unit volume, $1/2 \omega\epsilon_2 \tilde{\mathbf{E}} \cdot \tilde{\mathbf{E}}^*$, with the quantum mechanical quantity $\hbar\omega_{\text{obs}}$; so we write

$$1/2 \omega \epsilon_2 \tilde{\mathbf{E}} \cdot \tilde{\mathbf{E}}^* = -\hbar \omega r_{\text{obs}}. \quad (124)$$

For our choice of gauge we also have the relation

$$1/2 \omega \epsilon_2 \tilde{\mathbf{E}} \cdot \tilde{\mathbf{E}}^* = 1/2 \omega^3 \epsilon_0 \kappa_2 \tilde{\mathbf{A}} \cdot \tilde{\mathbf{A}}^* \quad (125)$$

By combining Equations (111), (124), and (125) we obtain the desired expressions

$$\kappa_2 = [\pi e^2 / (m^2 \epsilon_0 \omega^2)] |M|^2 J_{mj}, \quad (126)$$

$$M = (u_{\bar{\mathbf{K}}m} | \hat{\mathbf{a}}_0 \cdot \bar{\mathbf{p}} | u_{\bar{\mathbf{K}}j}), \quad (127)$$

and

$$J_{mj} = [2/(2\pi)^3] \int d\bar{\mathbf{S}}_{\bar{\mathbf{K}}} / |\nabla_{\bar{\mathbf{K}}} [\epsilon_m(\bar{\mathbf{K}}) - \epsilon_j(\bar{\mathbf{K}})]|. \quad (128)$$

Equations (127) and (128) are merely repeated for convenience.

This expression for the contribution of interband transitions to the complex dielectric constant forms the basis for much of the analysis of the "one-electron" (54) spectra of crystalline solids. Appendix A contains a classical model for this absorption process, introduces the longitudinal dielectric constant, and shows that within certain approximations this expression for κ_2 agrees with the results of a self-consistent field method for calculating the complex dielectric constant. (Hereafter, we shall refer to the complex dielectric constant as, simply, the "dielectric

constant.")

It is seen from Equation (128) that, within the above approximations, a large contribution to κ_2 occurs at those frequencies for which $\nabla_{\bar{K}}[\epsilon_m(\bar{K}) - \epsilon_j(\bar{K})]$ vanishes at some point on the energy-conserving surface $[\hbar\omega = \epsilon_m(\bar{K}) - \epsilon_j(\bar{K})]$ in \bar{K} -space. Such "critical points" were first stressed by Van Hove; Phillips (54) further delineated the number of such points by symmetry arguments. Two types of points are distinguished: those which occur at symmetry points for which we have

$$\nabla_{\bar{K}}\epsilon_m(\bar{K}) = \nabla_{\bar{K}}\epsilon_j(\bar{K}) = 0 \quad (129)$$

and those which occur at general points for which we have

$$\nabla_{\bar{K}}\epsilon_m(\bar{K}) = \nabla_{\bar{K}}\epsilon_j(\bar{K}) \neq 0. \quad (130)$$

Cardona (57) states that such critical points can be localized in a small domain of \bar{K} -space or can range over large portions of the Brillouin zone over which filled and empty bands are parallel or nearly parallel.

The analytic behavior of the joint density of states J_{mj} near a critical point (and consequently the behavior of the κ_2) can be found by expanding $\epsilon_m(\bar{K}) - \epsilon_j(\bar{K})$ in a Taylor series about the critical point \bar{K}_0 as follows:

$$\epsilon_m(\bar{K}) - \epsilon_j(\bar{K}) = \epsilon_0(\bar{K}_0) + \sum_{i=1}^3 a_i (\bar{K}_i - \bar{K}_{0i})^2. \quad (131)$$

Depending on the relative signs of the a_i , four shapes (54,58) are found for J_{mj} . These four kinds of critical points are labeled M_0 to M_3 . The M_0 critical point, for which all a_i are positive, yields the familiar dependence on photon energy $(\hbar\omega - \epsilon_0)^{\frac{1}{2}}$; this dependence vanishes for $\hbar\omega$ less than ϵ_0 .

The behavior of J_{mj} is somewhat similar for each of the four kinds of critical points. The significant feature is that a critical point only produces an edge in J_{mj} and thus in κ_2 . To obtain a peak (due solely to interband transitions) there must be two critical points almost accidentally degenerate.

Several broadening mechanisms tend to complicate the assignment of these interband transitions. Within the fundamental absorption region, electron-phonon interactions (54) may be considered to replace the Hartree-energy difference $\epsilon_m(\bar{K}) - \epsilon_j(\bar{K})$ by

$$\epsilon_m(\bar{K}) + \delta\epsilon_m - \epsilon_j(\bar{K}) - \delta\epsilon_j - (i\hbar/\tau_{mj}) \quad (132)$$

where

$$1/\tau_{mj} = (1/\tau_m) + (1/\tau_j) \quad (133)$$

gives the lifetime broadening [see also Equation (241) of Appendix A]. These shifts $\delta\epsilon_j(\bar{K})$ as well as the lifetime broadening are temperature dependent. At room temperature, the lifetime broadening is of the order of 0.1 eV in semiconductors. In addition to this intrinsic broadening, the edges in κ_2 (or the primary reflectance data) are broadened extrin-

sically by mechanical polishing and by oxide layers.

The shift of the energy bands with hydrostatic pressure may be regarded as the limiting case of an interaction with long-wavelength phonons. The effect of hydrostatic pressure is qualitatively similar to that of temperature: there is a change of the lattice constants. Another qualitative similarity has been demonstrated, theoretically, between the shift of energy levels in Ge with hydrostatic pressure and the shift of the same energy levels in Ge-Si alloys. These shifts in the alloys are observed as a function of composition (chemical shifts).

The energy shifts with hydrostatic pressure occur because the interatomic distances decrease, whereas the core (to which the valence electron wave functions are orthogonal) can be regarded as incompressible (58). The result is a rearrangement of the valence wave functions relative to these unaltered core functions. For a given change in lattice constant, the energy shifts are greater in the alloys than those observed in either, elemental solid under hydrostatic pressure. This enhancement of the energy shifts in alloys follows from the admixture of other core functions.

Until now, we have considered the matrix element "M" which enters the Equation (126) for κ_2 to be a nonvanishing constant. According to Seitz (59) we may rewrite the Equation (127) for "M" in the form

$$\begin{aligned}
 M &= (u_{\bar{K}m} | \hat{a}_0 \cdot \bar{p} | u_{\bar{K}j}) \\
 &= (u_{\bar{K}m} | \hat{a}_0 \cdot \bar{r} | u_{\bar{K}j}) (mi/\hbar) [\epsilon_m(\bar{K}) - \epsilon_j(\bar{K})]
 \end{aligned}
 \tag{134}$$

where $\hat{a}_0 \cdot \bar{r}$ is the magnitude of the displacement \bar{r} in the direction of the

magnetic vector potential \tilde{A} . To obtain this important result, Fermi (60) outlined a simple derivation which made use of the fact that within the perturbation scheme p_n is simply $m\dot{x}_n$ [see Equation (74)]. When this fact is realized, we may use Dirac's analogue (61) for relating \dot{x}_n to the quantum theory; that is, \dot{x}_n is given by $(i/\hbar) (H_0 x_n - x_n H_0)$. Since the unperturbed Hamiltonian H_0 is diagonal, we immediately obtain Equation (134).

The symmetry properties of the wavefunctions readily allow us to determine whether or not "M" has zero or finite values at those critical points which occur at symmetry points of the Brillouin zone. It can be shown (62) that if one chooses the active point of view (fixed coordinate system, but "rotated" solid), then the action of a point-group operator R_i on a Bloch type wavefunction (the solid) is such that the matrix α^i which subsequently "rotates" the wave vector of the electronic state forms an irreducible representation of the operator R_i . We illustrate this result schematically by writing

$$R_i |\bar{K}j\rangle = |\bar{K}'j\rangle \quad (135)$$

and

$$\bar{K}' = \alpha^i [R_i] \bar{K} \quad (136)$$

for each rotation R_i of the point group (these are not quantum-mechanical operators). Consequently, the application of all the symmetry operations

of the group to the wavefunction $|\bar{K}j\rangle$ generates the "star" (55) of \bar{K} . Since these symmetry operations take the Hamiltonian into itself, these states are degenerate. (It follows that the bands have the full symmetry of the solid.) The dimensionality of an irreducible representation α^i gives the degeneracy, and the trace of an irreducible representation gives the character $\chi(R_i)$. There are a number of sets of irreducible representations of differing dimensionality.

For special choices of \bar{K} , there are subgroups of the full point group which take \bar{K} into itself rather than into a distinct wave vector; this subgroup is called the "group of \bar{K} ." Such a choice might be along a [100] direction in a cubic crystal. At special points in the Brillouin zone, the group of the wave vector may be larger than that on symmetry lines which thread it; these are called symmetry points. [Recall the mention of symmetry points at Equation (129).]

We have now defined the formalism which enables the determination of whether the dipole transition is allowed or forbidden. From Equation (134) and from the orthogonality of functions belonging to different irreducible representations, one obtains (58) the selection rule

$$C_p^q = \frac{1}{h} \sum_{i=1}^h \chi_q(R_i) \chi_{x,y,z}(R) \chi_p(R) \quad (137)$$

$$\begin{cases} = 0 & \text{forbidden} \\ \neq 0 & \text{allowed} \end{cases}$$

where $\chi_p(R)$, $\chi_q(R)$ are the characters of the pth or qth representation, respectively, of the rotation "R" (states j, m transform according to the

p,qth irreducible representations). The characters of the irreducible representation according to which the coordinates x,y,z transform are given by $\chi_{x,y,z}(R)$. The total number of rotations (elements) "R" in the group is "h".

Normal-Incidence Reflectance and the Optical Constants

As can be seen from Equation (103), the intraband contribution to κ_2 is strongly wave-vector dependent. In contrast to this strong dependence, we have seen that the vertical interband contribution to κ_2 has a wave-vector dependence that can be ignored (see also Appendix A). Since we envisage interband transitions to be responsible for the structure in κ_2 beyond the fundamental edge, we may safely (see above, the section Significance . . . Constant) employ the conventional boundary conditions in a derivation (48) of the amplitude reflection coefficients.

Before presenting any results of such a derivation, we shall first simplify several equations and introduce the Kramers-Kronig integral dispersion relations. We recall that we have set κ_m equal to unity, so we may combine Equations (24), (35), and (118) in the forms

$$\tilde{\kappa} = \kappa_1 + i\kappa_2 = (n + ik)^2 \quad (138)$$

or

$$\tilde{\kappa} = \tilde{N}^2 \quad (139)$$

where we have introduced the complex index of refraction \tilde{N} ($\tilde{N} = n + ik$).

Equating real and imaginary components in Equation (138) leads to the simple relations

$$\kappa_1 = n^2 - k^2 \quad (140)$$

and

$$\kappa_2 = 2nk. \quad (141)$$

Furthermore, we now cease to indicate any wave-vector dependence of the dielectric constant. We write for the linear response of the solid to an electric field at a fixed point

$$\tilde{P}(t) = \int_{-\infty}^{\infty} [\tilde{\epsilon}(\omega) - \epsilon_0] \tilde{E}(\omega) \exp(-i\omega t) d\omega. \quad (142)$$

The use of such Fourier integrals leads to the result

$$\tilde{\epsilon}(-\omega) = \tilde{\epsilon}^*(\omega). \quad (143)$$

For this choice $(-i\omega t)$ of time dependence, it can be shown (48) that $[\tilde{\epsilon}(\omega) - \epsilon_0]$ defines a function which is analytic for complex values of ω having a positive imaginary part. The organic behavior of analytic functions eventually leads to the dispersion relations for the dielectric constant as follows:

$$\kappa_1(\omega) - 1 = (2/\pi) P \int_0^{\infty} \omega' \kappa_2(\omega') (\omega'^2 - \omega^2)^{-1} d\omega' \quad (144)$$

$$\kappa_2(\omega) - (\sigma_0/\epsilon_0\omega) = (2\omega/\pi)P \int_0^\infty \kappa_1(\omega')(\omega^2 - \omega'^2)^{-1}d\omega'. \quad (145)$$

The dc conductivity term arises from the consideration of boundedness of $\tilde{\epsilon}(\omega)$ in conductors. The derivation contains three major assumptions: boundedness, linearity, and causality (retarded times). These Kramers-Kronig dispersion relations are valid for other physical quantities which express a linear relation between an input and a retarded output.

If we drop the dc conductivity term in Equation (145) and perform an integration by parts, Equations (144) and (145) become

$$\kappa_1(\omega) - 1 = (1/\pi) \int_0^\infty [d\kappa_2(\omega')/d\omega'] \ln(|\omega'^2 - \omega^2|^{-1})d\omega' \quad (146)$$

and

$$\kappa_2(\omega) = - (1/\pi) \int_0^\infty [d\kappa_1(\omega')/d\omega'] \ln[(\omega' + \omega)/|\omega' - \omega|]d\omega'. \quad (147)$$

These latter expressions will be used in discussing qualitatively the experimental results below. One of the more important uses of these dispersion relations between the real and imaginary parts of the dielectric constant is the derivation of sum rules. (See Appendix A for an example of an f-sum rule.)

Since the only satisfactory (convenient) way of determining the optical constants n, k over a large photon-energy range is through the measurement of the normal-incidence reflectance (this is especially true for noncubic solids), we shall not dwell on the general case of arbitrary angle of incidence α . We merely note that within the present formalism,

Snell's law of refraction becomes

$$|\bar{k}_1| \sin \alpha = |\bar{k}_1'| \sin \alpha' \quad (148)$$

$$|\bar{k}_2| \sin \phi = |\bar{k}_2'| \sin \phi \quad (149)$$

and the simple relations given by Equations (119) and (120) no longer hold for \bar{k}_1 not parallel to \bar{k}_2 . It follows that the phase velocity ($v' = \omega/|k_1'$) in the second medium is no longer a function only of the optical constants n', k' but depends also on the angle of incidence α .

If our single plane wave is normally incident within a vacuum on a solid, it can be shown that the amplitude reflection coefficient of Equation (71) becomes

$$\tilde{r} = (\tilde{N} - 1)/(\tilde{N} + 1). \quad (150)$$

We can use the prescription

$$Z_o/\tilde{Z} = \tilde{N} \quad (151)$$

to obtain Equation (150) from (71). From Equations (138), (139), and (150) we readily obtain

$$n = (1 - |\tilde{r}|^2)/(1 - 2|\tilde{r}| \cos \theta + |\tilde{r}|^2) \quad (152)$$

$$k = 2|\tilde{r}| \sin \theta / (1 - 2|\tilde{r}| \cos \theta + |\tilde{r}|^2) \quad (153)$$

where we have explicitly employed the phase shift θ of the magnetic field in the form

$$\tilde{r} = |\tilde{r}| e^{i\theta}. \quad (154)$$

We observe that a knowledge of \tilde{r} (amplitude and phase shift) yields directly the optical constants n, k from Equations (152) and (153). Experimentally, we can determine $|\tilde{r}|$ from a measurement of the reflectance, which is given by

$$R = |\tilde{r}|^2. \quad (155)$$

Formally (this is not a derivation) we can define a logarithmic function of the amplitude reflection coefficient as follows:

$$\ln \tilde{r} = \ln |\tilde{r}| + i\theta, \quad 0 \leq \theta < 180^\circ \quad (156)$$

The positive branch chosen for θ relates to the fact that k in Equation (153) must be positive. From the analyticity of this function, we obtain the result

$$\theta(\omega) = (2\omega/\pi)P \int_0^\infty \ln |\tilde{r}(\omega')| (\omega^2 - \omega'^2)^{-1} d\omega'. \quad (157)$$

Compare this Equation (157) with Equation (145).

In addition to the direct experimental determination of $|\tilde{r}|$, it is seen that a numerical integration of the same primary data allows a

determination of the associated phase shift θ . So Equations (155) and (157) then give the optical constant n, k in a direct manner. The components of the dielectric constant κ_1, κ_2 are finally obtained from Equations (140 and (141).

In conclusion, we note that Equation (157) is dimensionless; that is, we may use any convenient unit for the angular frequency ω (photon energy). Whereas the literature is replete with inconsistent usage of these dispersion relations, several equivalent forms of Equation (157) are given here. (The inconsistencies arise, usually, from the failure to employ a consistent time dependence $\pm i\omega t$ and from the burden of book-keeping which arises if one defines the normal-incidence reflection coefficient in terms of the electric field; in this latter case, one must carry along an additional phase shift of 180° .) The consistent forms are given as follows:

$$\theta(\omega) = (\omega/\pi) P \int_0^\infty \frac{\ell n R(\omega')}{\omega^2 - \omega'^2} d\omega' \quad (158)$$

$$\theta(\omega) = (\omega/\pi) \int_0^\infty \frac{[\ell n R(\omega') - \ell n R(\omega)]}{\omega^2 - \omega'^2} d\omega' \quad (159)$$

$$\theta(\omega) = (-1/2 \pi) P \int_0^\infty \left[\frac{d \ell n R(\omega')}{d\omega'} \right] \ell n \left| \frac{\omega' + \omega}{\omega' - \omega} \right| d\omega' \quad (160)$$

$$\theta(\omega) = (1/2 \pi) P \int_0^\infty \ell n R(\omega') \frac{d}{d\omega'} \left(\ell n \left| \frac{\omega' + \omega}{\omega' - \omega} \right| \right) d\omega' \quad (161)$$

An unambiguous handling of the phase shift is only obtained when an author states the following:

- (1) time dependence of the field ($\bar{+} i\omega t$)
- (2) sign of the phase shift ($e^{\pm i\theta}$)
- (3) whether the amplitude reflection coefficient is that of the electric field \widetilde{E} or the magnetic field \widetilde{H} .

CHAPTER III

APPARATUS

Optical Systems

Infrared

The energy range from .083 to 1.9 eV (15 to 0.65 μ) was investigated by the implementation of a Perkin-Elmer Corporation "Optical Reflectance Attachment" and a Perkin-Elmer model 99 monochromator. Relatively minor alterations were made on both pieces of equipment in order to be compatible with sample dimensions (8-mm discs) and the instrumentation, which is to be described below.

The "sample-in" and "sample-out" configurations are illustrated in Figure 7. The two spherical mirrors, "B" and "C", were used slightly off axis (10°) and thereby produced astigmatic images. The mirror labeled "A" selected either a globar source or a Sylvania 6.6A/T2 $\frac{1}{2}$ /CL tungsten-halogen lamp; for either position, masks were constructed and placed as close as possible to the source in order to reduce the size of the images at "R", an aluminum coated reference mirror, or "S", the sample. The images at "R" and "S" were the circles of least confusion; that produced by "C" at the entrance slits of the monochromator was a horizontal focus. A 180° rotation of the pair of mirrors labeled "D" produced the change of configurations; reproducibility of positioning was effected by magnetic stops. The angle of incidence was 6° .

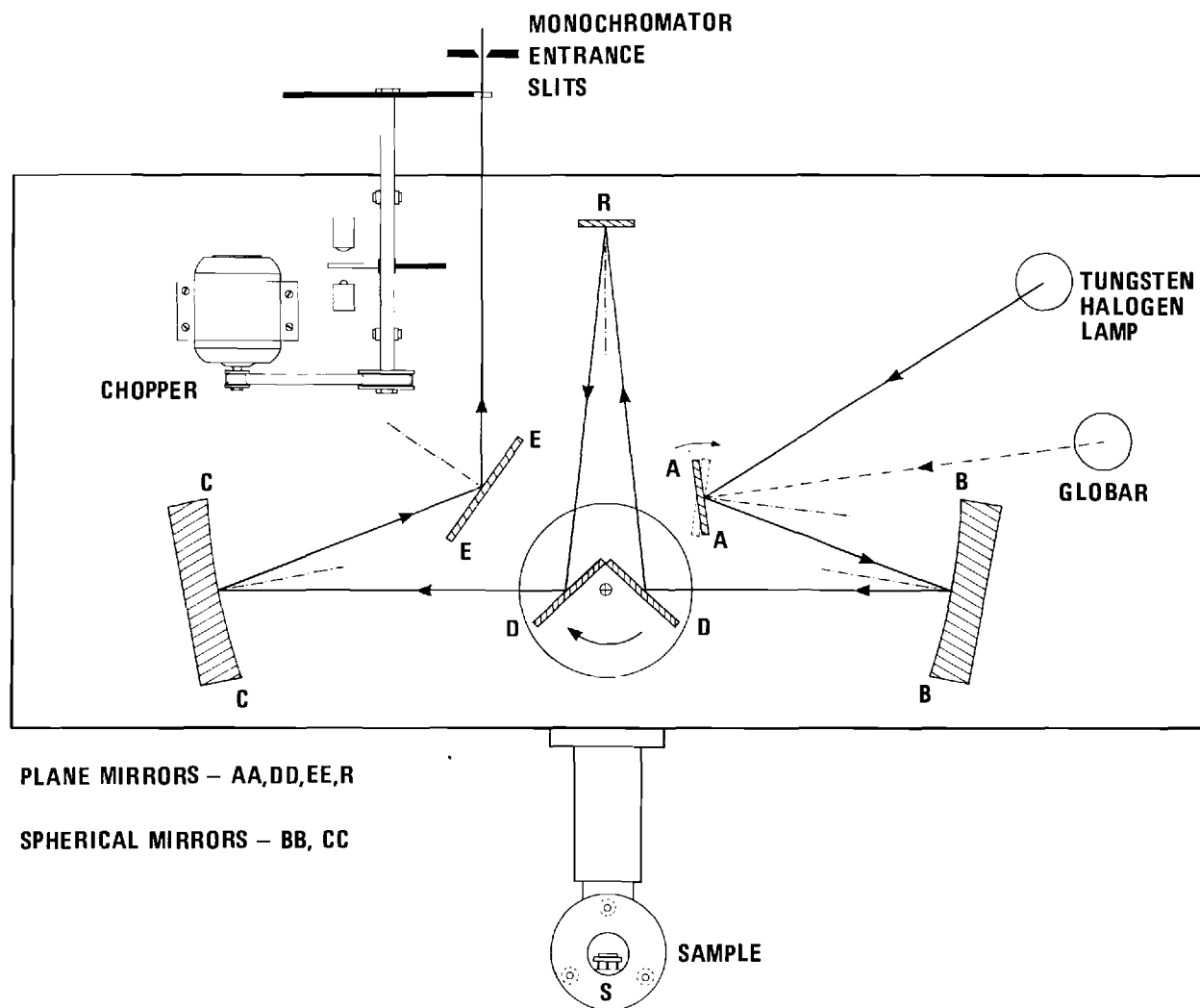


Figure 7. Sample-in and Sample-out Configurations.

A sodium-chloride prism was used to span the above range. The drum reading of the monochromator was calibrated using Friedel-Mckinney points (63) where convenient and, at the shorter wavelengths, use was made of the spectral lines produced by an AH-4 mercury lamp (64). From the smooth curve which passed through the limited number of calibration points, a larger number of points was tabulated for future use in Lagrange's Interpolation Formula (65).

As the monochromator (Littrow mounting) was a double-pass instrument, the undesired first-pass radiation appeared at the exit slit along with the second-pass and was of longer wavelength. Whereas the first pass suffered an inversion and the second pass did not, masking of corresponding halves of the entrance and exit slits reduced the first-pass radiation to the background level (66). The first-pass peak of the globar curve had been twice the magnitude of the second-pass peak prior to the masking. For ready comparison with the other spectral regions, Figure 8 displays the spectral resolution of a single-pass monochromator. This curve was generated from a similar one reported by Palik and Stevenson (67) and served as a basis for estimating the resolution of the double-pass instrument. For slits greater than $100\ \mu$, diffraction effects were ignorable, and the resolution for slits greater than $100\ \mu$ increased merely in the ratio of slit widths.

The potassium-bromide-windowed thermocouple supplied with the monochromator only reached 75 percent of its dc response at a chopping frequency of 13 Hz; it had a nominal responsivity of $4\ \mu\text{V}/\mu\text{W}$.

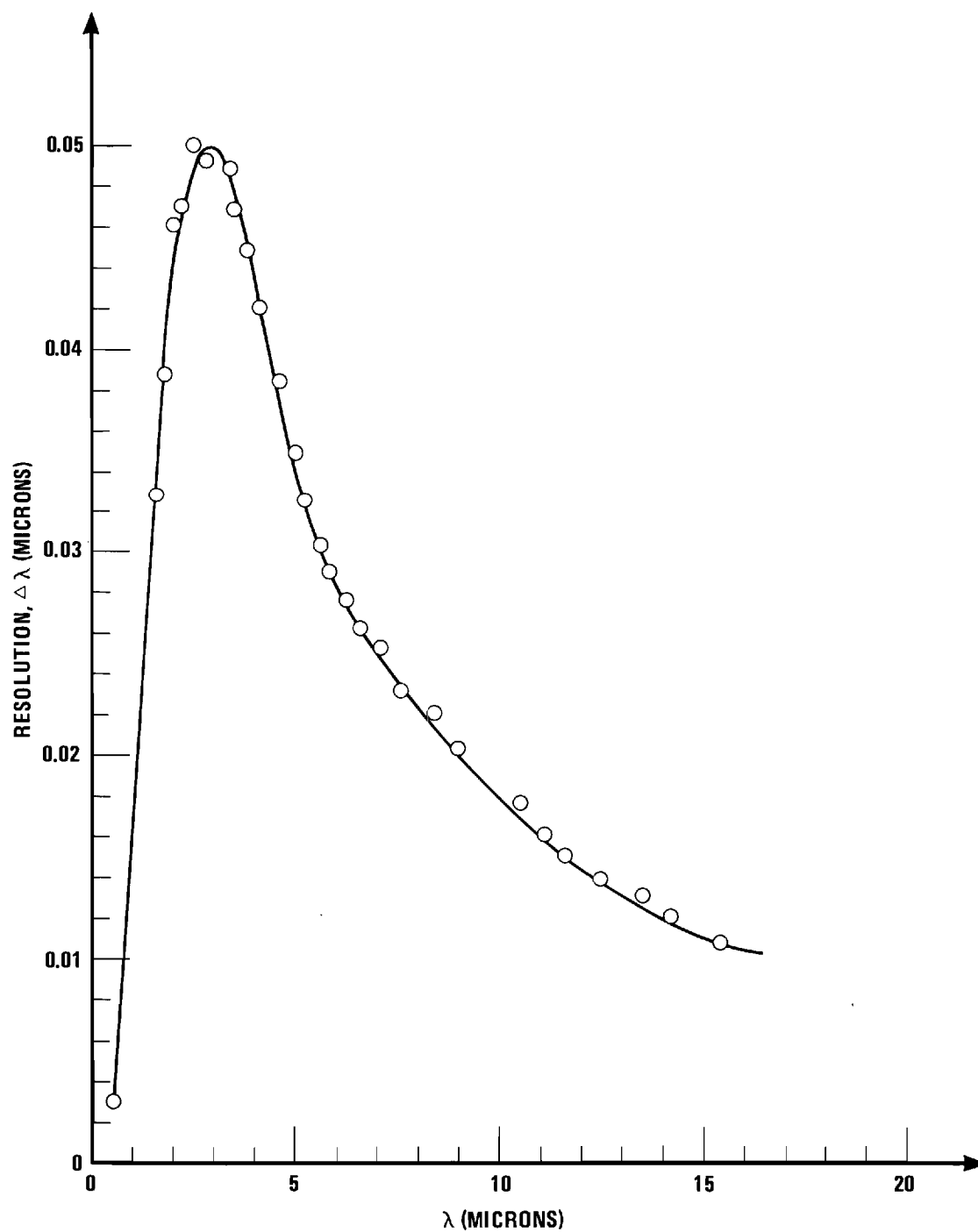


Figure 8. Spectral Resolution of a Single-Pass Monochromator with Slits of 100 Microns and Sodium Chloride Prism.

Visible and Near Ultraviolet

From 1.9 to 7.3 eV (6500 to 1700 Å) the sample environment was more carefully controlled than in the other spectral regions by the use of an ultrahigh-vacuum reflectometer of conventional design and an ion pump. A 0.3-m scanning monochromator with provisions for evacuation and easy interchange of gratings served to span this range. To support the pressure differential between the reflectometer and monochromator, a lithium-fluoride-windowed flange was used (lithium fluoride has a UV cutoff of $.105\ \mu$ and an IR cutoff of $9.0\ \mu$). Neither unit, reflectometer-with-pump or monochromator, could mechanically support the other; to that end, a two-level table was constructed along with an elegant bellows assembly of original design.

Figure 9 shows the reflectometer. A 1/6-inch walled, 4-inch inner-diameter, 10-inch long, seamed pipe (stainless-steel alloy number 304) with 6- and 8-inch "Lo-Torr" flanges attached at opposite ends of the pipe and six 2 3/4-inch ports attached (heliarc welded) radially to the pipe formed the vacuum chamber for the reflectometer. Hughes Aircraft Company provided the chamber as a modification of a large nipple. It was found that the only reliable way to locate the axis of the chamber was to make use of counter-bores that were provided in either of the larger flanges. Unfortunately, the run-out over the 10-inch length of the pipe was on the order of 1/16 inch. This necessitated re-boring of one of the flanges.

The construction followed that of Smith (68); that is, the reflectometer was of single-beam design with manual manipulation required for the change of configurations. For the sample-out condition, the monochromatic radiation was incident on a phosphor-coated (above 3 eV) light pipe which

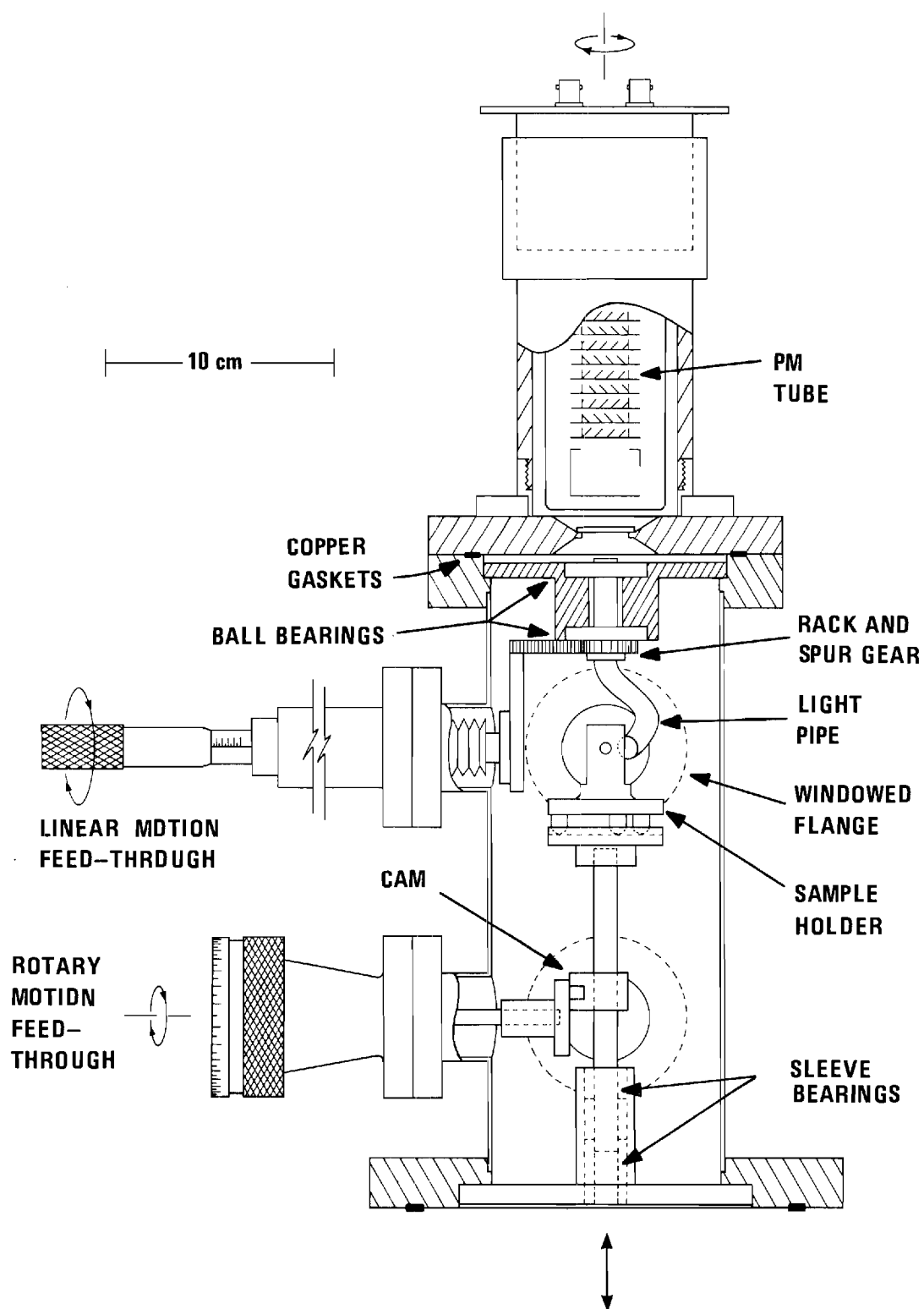


Figure 9. High-Vacuum Reflectometer (The light pipe is nearly facing the reader).

channeled the fluorescent radiation to a photomultiplier tube. For the sample-in condition, the sample was interposed between the exit beam from the monochromator and the light pipe, which then had to be rotated to accept the reflected beam. The angle of incidence was fixed at 15° .

As shown in Figure 10, the sample was inserted into the beam by raising and lowering the sample holder via the action of a cam consisting of a pin attached to a wheel: the pin traveled in a slotted bar attached to the vertical shaft. Two small brass rings served as bearing surfaces for the vertical shaft. The cam was actuated by an Ultek model 282-6050 rotary-motion feedthrough. Figure 11 shows the details of the sample holder; also illustrated in this figure is the pedestal for the ultra-high-vacuum system. Three spring-and-screw combinations allowed for tilt adjustment and lateral positioning; a piece of stainless-steel shim acted as a spring, to force the sample upward against a V-groove. It was convenient for all optical systems to employ a common sample mount. The tongs allowed easy handling of the sample holder.

A stainless-steel rack and pinion, supplied by PIC Design Corporation; along with a pair of stainless-steel bearings, supplied by New Departure Hyatt Bearings; and an Ultek model 282-6100 push-pull feedthrough (modified with a micrometer spindle) formed the system which effected the rotation of the light pipe. The angle of incidence on the sample was 15° , so that the reflected beam deviated 150° from the sample-out path. The light pipe was a solid Pyrex rod bent as shown in Figure 9. The straight segment of this rod was coincident with the axis of the chamber and the sample face. Its outer surface was coated with aluminum, and a sodium-

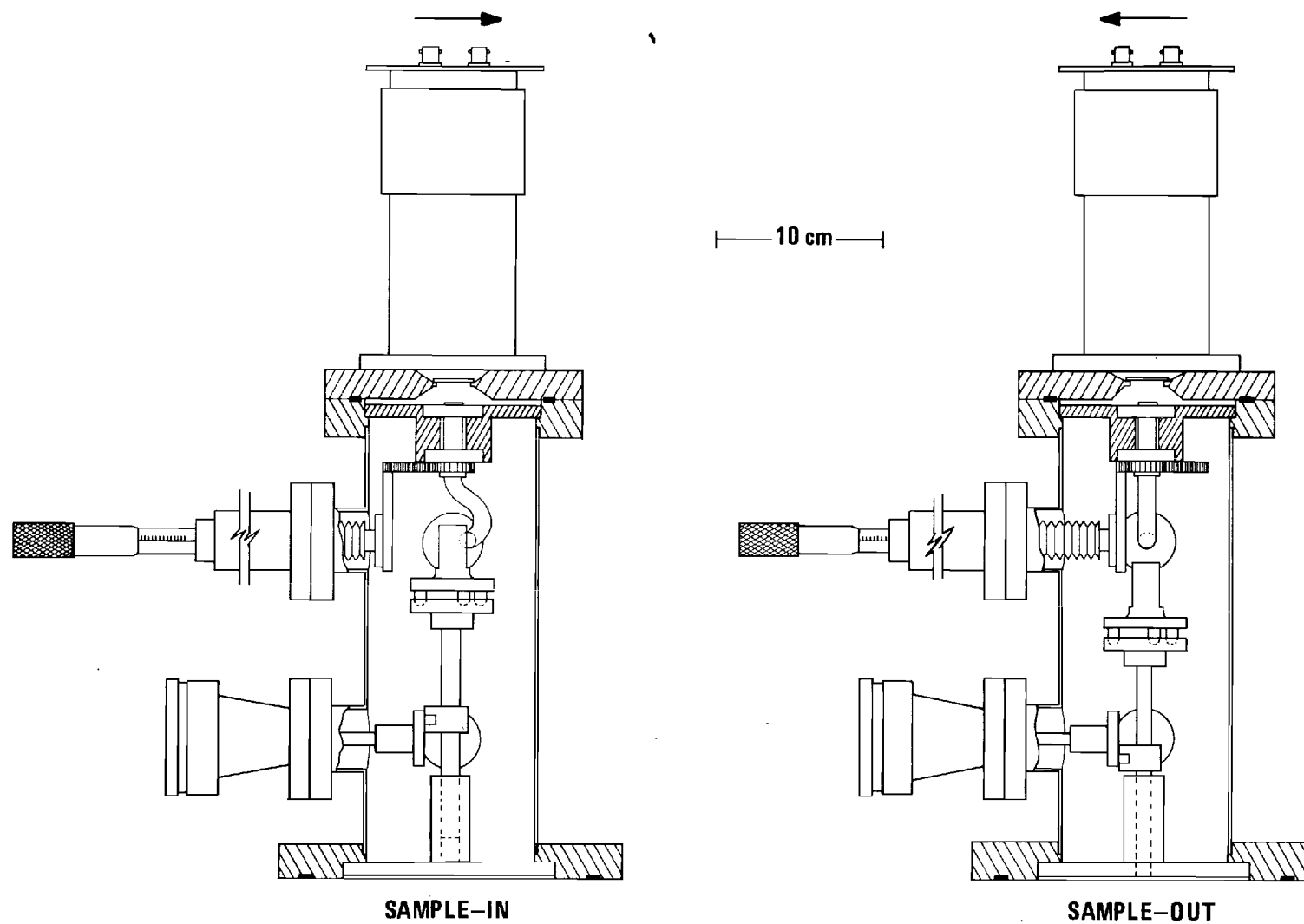


Figure 10. Sample-in and Sample-out Configurations.

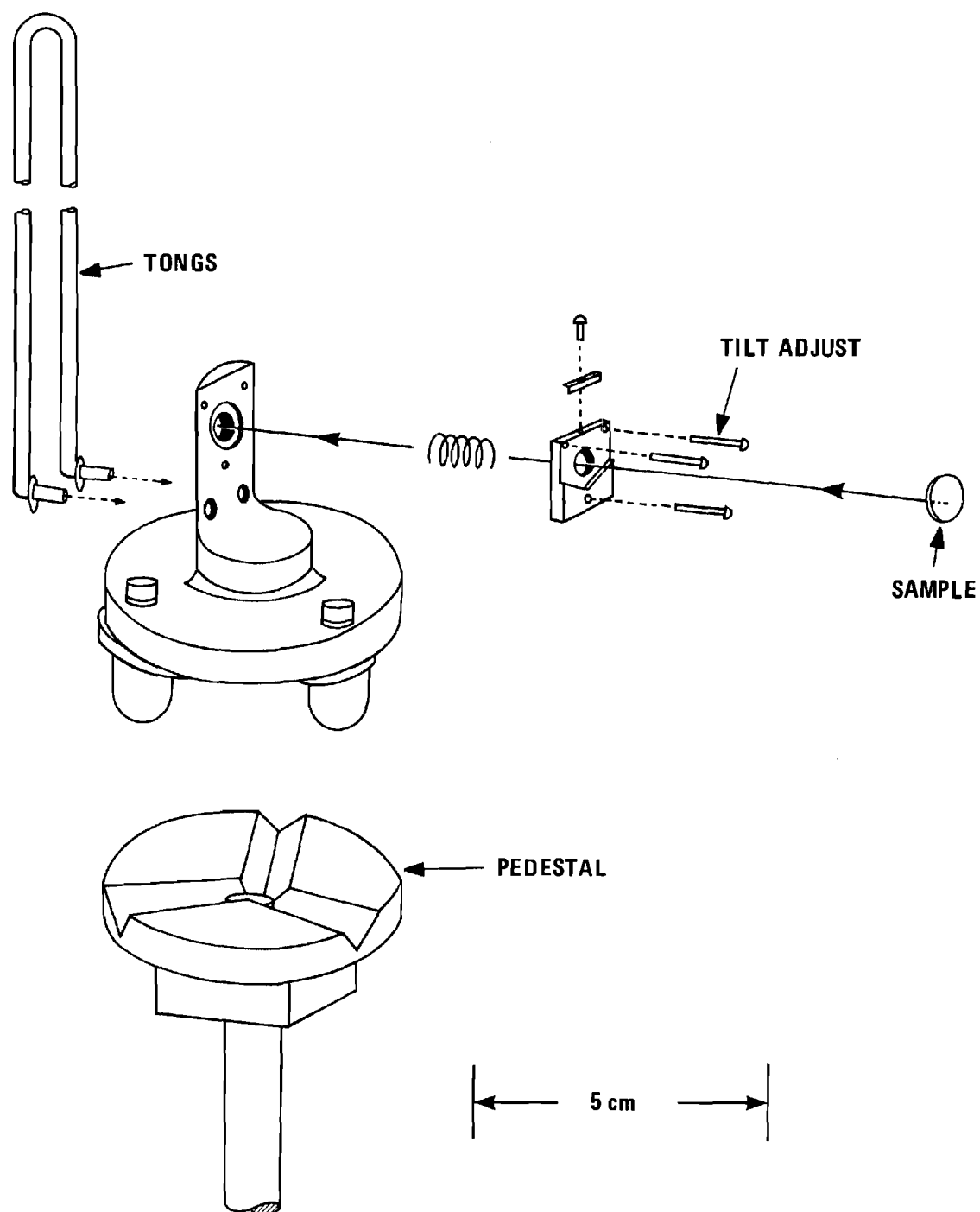


Figure 11. Detailed View of Sample Holder and Pedestal for Ultrahigh-Vacuum System.

salicylate phosphor coated the entrance end of the rod (69). Phosphor densities were at least 1 mg/cm^2 as suggested by Samson (70). A teflon bushing supported the rod between the inner races of the two bearings. The exit end of the rod faced a 6-inch Pyrex-windowed flange which was supplied by Hughes Aircraft Company (Hughes). On the other side of this window a 2-inch, end-on, photomultiplier tube, an EMI 9514S, was seated. This 13-stage tube had a nominal gain of 10^8 . Although there was no mechanical linkage between the rotary motion of the light pipe and a 150° rotation which could be executed with the photomultiplier tube, efforts were made to have them track at the extremity of their rotations. This was done to minimize systematic errors (71) (a few percent of the absolute value of the reflectance) due to areal inhomogeneity of the photocathode.

A sorption pump, Hughes model SP-9, was used to take the sample chamber from atmosphere to approximately 10^{-2} Torr (10μ); at this threshold (just below the glow-discharge range) the ion pump's pumping speed would begin its ascent ("come on") and then peak (after the throughput was considerably reduced) at its rated pumping speed in the range of 7×10^{-7} Torr. The 60-Lps ion pump, Hughes model VP-60, was provided with a glow-discharge screen.

The control unit, Hughes model VPC-60, allowed monitoring of the current supplied to the pump. Although the sample chamber contained ordinary red brass and teflon (teflon has a vapor pressure of 10^{-6} Torr), it reached a pressure of approximately 3×10^{-9} Torr overnight. Pressure was monitored by reading the current drawn by the ion pump: current flow is directly proportional to pressure in ion pumps. As a check against the nominal calibration curve (provided by Hughes) of current versus pressure,

an ionization gauge, Hughes model IG-7169, along with a gauge control unit, Hughes model IGC-TGC, was employed. By using this ionization gauge as a standard for comparison, we found the nominal calibration curve yielded a pressure which was too low by a factor of two.

A McPherson Instrument Corporation (McPherson) model 218, 0.3-m, scanning monochromator equipped with two, 1200-line/mm, plane diffraction gratings serviced this region. Since it formed a fast ($f/5.3$) system, this instrument used aspheric collimating and focusing mirrors to reduce aberrations; moreover, these mirrors were only slightly off axis as a result of the entrance and exit beams having been crossed (a modified Czerny-Turner mounting). This latter feature afforded compactness of design and large angular separation (44°) between the entrance- and exit-slit housings. Approximately one inch from the exit slits, a 1/6-inch, Fused-Quartz plate (1600-Å cutoff), General Electric type 101, was positioned; it was supported by a rod which passed through the monochromator cover by means of an O-ring seal and could be accurately positioned in the beam or removed from the beam path for "order" sorting.

The 1200-line/mm, replica gratings had plate factors (reciprocal linear dispersions) of 26.5 Å/mm and first-order resolutions of 0.6 Å . One had a first-order blaze angle for 1500 Å ; the other, for 5000 Å . By controlling the inclination--of each groove facet--to a grating's surface, the manufacturer can modulate the spectral distribution which results from the uncontrolled case (the arbitrarily shaped facet corresponds to the ordinary derivations wherein facet structure is ignored). The inclination (blaze angle) is so chosen that the reflectance relation, "the angle of incidence equals that of reflectance," is satisfied at the facet by the

ray incident on the grating and some particular diffracted ray. Once this relation is satisfied in first order, it will automatically be satisfied for all higher orders of the diffracted radiation. The net result is that there is an enhancement of the spectral distribution at the wavelength for which the reflectance relation is satisfied at the facet and a corresponding reduction elsewhere (72,73).

A two-stage mechanical pump, Welch model 1402, buffered by a Veeco VS-162 foreline trap, evacuated the monochromator when a capillary-discharge light source, McPherson model 630, was used in the windowless configuration. A hydrogen gas pressure of a few Torr was used to produce the intense molecular continuum; the "many-lined" hydrogen spectrum was effectively removed by the quartz filter. For wavelengths greater than 3600 Å, an unfocused tungsten-halogen lamp, Sylvania 250Q/CL, was used as a source.

Figure 12 gives an exploded view of the bellows assembly which was used. Also shown are the relative positions of the exit-slit housing of the monochromator and the entrance port of the ultrahigh-vacuum chamber. With the exception of the spacing studs, the piece which bolted to the monochromator was machined from a single brass rod. The 3/4-inch outer-diameter bellows, Cajon part number X-12-1, was shortened and then silver soldered to a brass flange which had an annular V-groove to mate with six studs. There were two advantages over commercial designs: (1) the flanges were 5 inches in outer diameter and thereby facilitated alignment checks and (2) tension and torsion on the bellows were absent as the bellows "floated" at one end. The usual trauma of coupling heavy vacuum equipment was reduced.

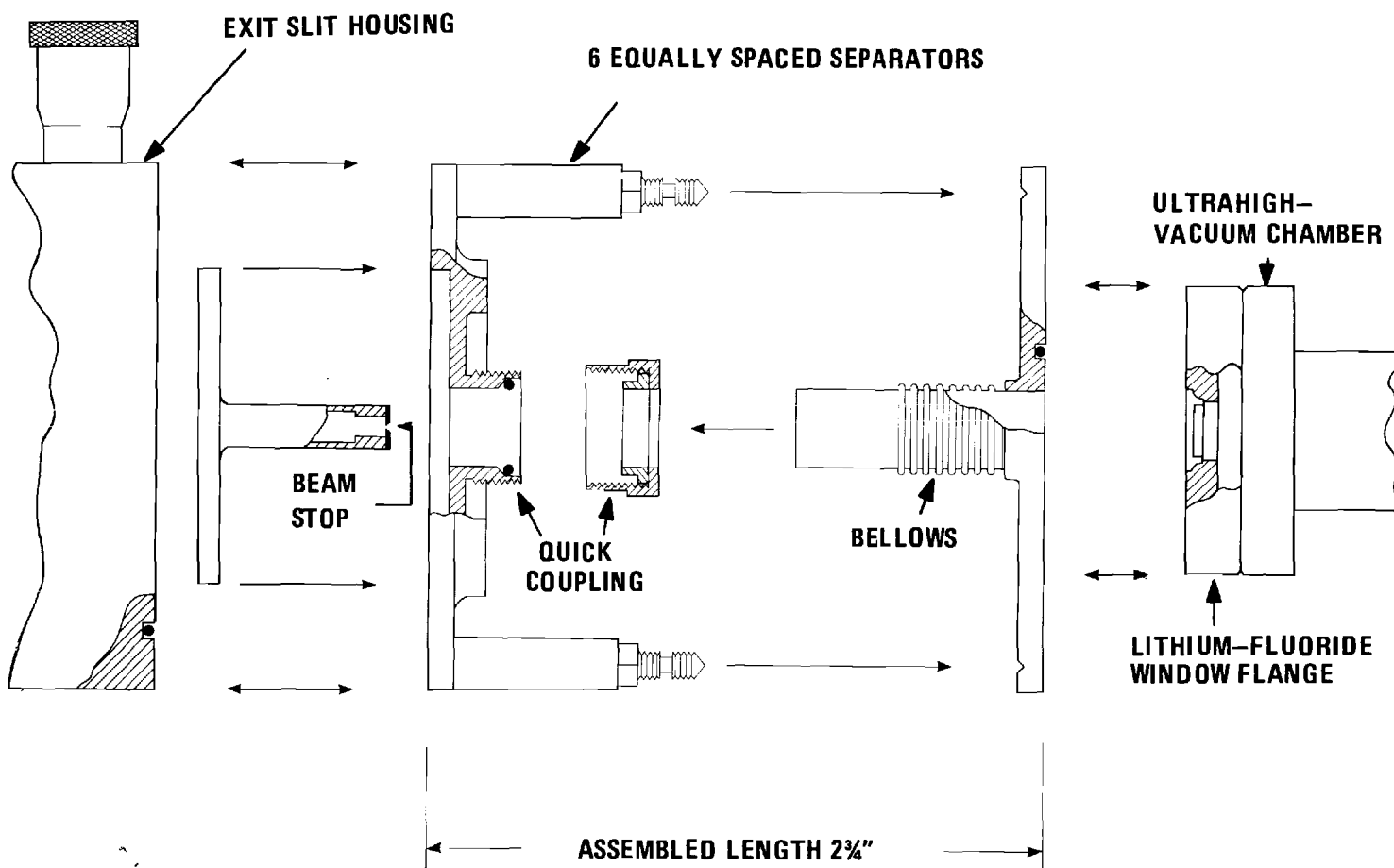


Figure 12. Bellows Assembly.

Vacuum Ultraviolet

The region from 7.3 to 21 eV (1700 to 600 Å) also required the use of an evacuated monochromator and reflectometer, due to the strong onset of atmospheric (oxygen below 2000 Å) absorption. As lithium fluoride, the only practical material for lenses or windows in the vacuum ultraviolet, has a transmission cutoff of 1050 Å, no windows were employed. Also the reflectance of mirror coatings is low at normal incidence and commercially available mirrors for use off axis (reflectance approaches 100 percent at grazing incidence) are limited in variety. A General Electric GEI-44854, 1-m, normal-incidence monochromator, similar to that designed by Johnson (74), was highly modified. The sample chamber used by Hinson (69) was but slightly improved.

The monochromator's design was such that a concave grating executed a simple rotation about its vertical tangent, which passed through a point approximately on the Rowland circle (lies in horizontal plane); the entrance-and exit-slit positions were fixed. The horizontal foci were precisely at the slit positions at the zero order, which was used for alignment. See Figure 13 for an overlay of the Rowland circle with the monochromator. The monochromator formed a slow (f/12) system.

The slit separation was 6 1/2 inches and their respective housings were constructed from 5-inch diameter, aluminum rods. A feeler gauge having been required for adjustment, the slit assemblies were of primitive design; however, small slits (less than 100 μ) were never used. The slit end plate was a 1/2-inch thick, 12-inch outer-diameter disc of aluminum. Aluminum baffles were installed to reduce the scattered light (espe-

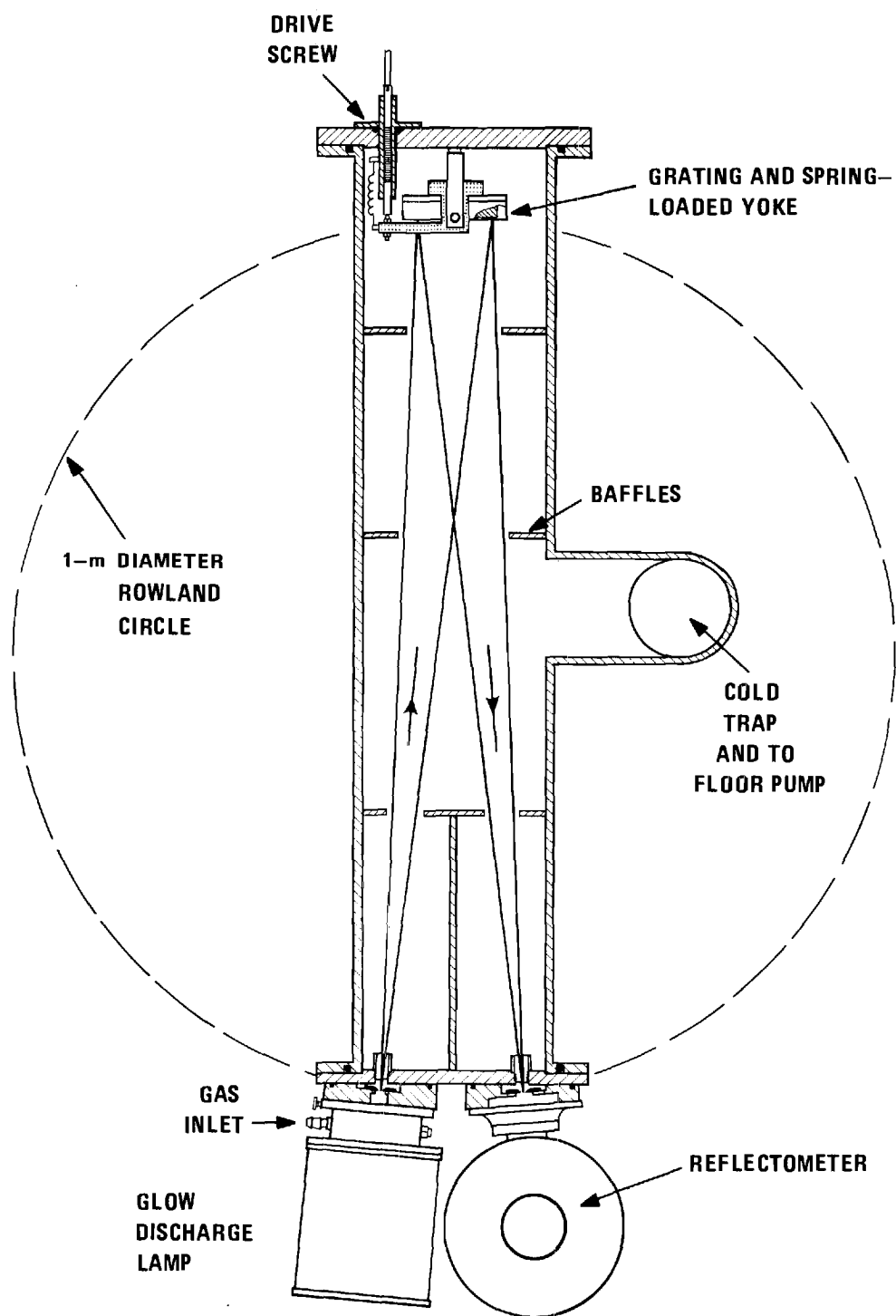


Figure 13. Monochromator and Rowland Circle.

cially, the central image's contribution). The aluminum surfaces were painted with a conductive black paint, Walsco Electronics C-R Tubecoat No. 199-02.

A platinum overcoated, replica grating, Baush and Lomb Catalog number 35-52-23-700, was chosen for this instrument. It was a 1200-line/mm, tripartite grating (the ruled area was 96 mm by 56 mm) of one-meter radius of curvature; the blaze angle was $2^{\circ}45'$ which gave a normal-incidence "blaze" wavelength of 800 Å. An aluminum grating holder, similar to the original, allowed for rotation of the grating about its normal and for tilt adjustment about its horizontal tangent. Focus was achieved by shimming the grating holder where it attached to the grating end plate.

Figure 14 illustrates the paths of the incident ray and the diffracted ray which reaches the exit slit. The concave-grating equation for the inside order (the spectrum lies between the grating normal and the exit slit, at the central image) is

$$n\lambda = d(\sin \alpha - \sin \beta) , \quad (162)$$

wherein α and β are defined to be positive as drawn. At the central image, α equals α_0 and β equals β_0 . It can be seen from the figure that a rotation of the grating by θ alters α and β as shown by

$$\alpha = \alpha_0 + \theta \quad (163)$$

and

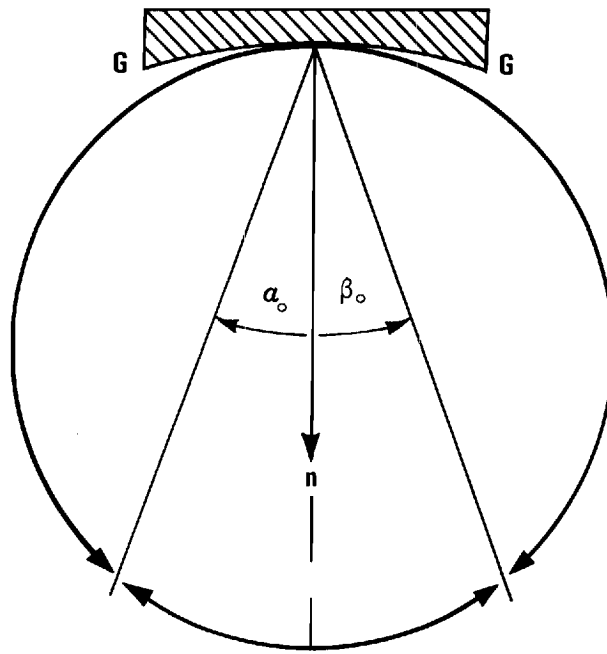
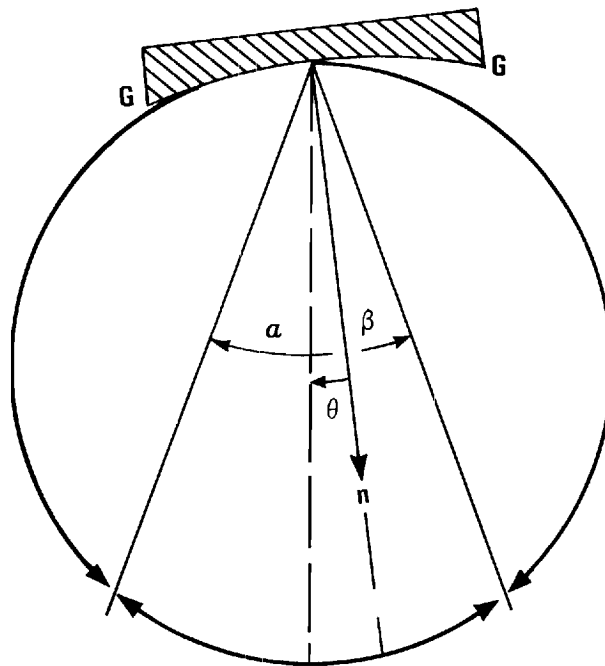
CENTRAL IMAGE, $\theta = 0$ INSIDE ORDER, $\theta > 0$

Figure 14. Concave Grating and Fixed Slits.

$$\beta = \beta_0 - \theta.$$

By substituting Equations (163) into Equation (162) and making use of the equality of α_0 to β_0 by design, one readily finds the result

$$n\lambda = d(2\cos \alpha_0)\sin \theta \quad (164)$$

The design was such that α_0 was about $4^\circ 30'$; so, to within the approximation that the grating remained on the Roland circle, we had

$$n\lambda = 2d'\sin \theta \quad (165)$$

as a working equation. The span used was 0 to 1700 Å in the first order; this corresponded to a grating rotation of θ of just under 6° . Having been pinned to a lengthwise slot in the grating-drive screw, a drum was calibrated in terms of wavelength; for small displacement of the screw, the drum reading DR was approximately proportional to $\sin \theta$. It was thus expected that the calibration would take the form

$$\lambda = \lambda_0 + mDR + n(DR)^2 + (\text{small higher order terms}). \quad (166)$$

This relationship was investigated by means of an analog shaft-angle encoder (to be described below) which fed one axis on a Hewlett Packard model 2D-2M X-Y recorder while the other axis monitored a voltage proportional to the current output of an EMI 9514S photomultiplier tube. The

possible error of the encoder was $\pm .2$ DR; this included reading errors attributed to the recorder and corresponded to an angular error of ± 0.72 . The full-width-at-half-maximum location of the spectral lines used gave rise to a similar error. The worst combination of possible errors yielded $\pm .5$ DR. With the slits set at 130μ , which corresponded to a theoretical bandpass greater than 1 \AA (plate factor or reciprocal linear dispersion of 8 \AA/mm), the calibration was executed. The results are summarized in Table 2. These four "lines" were least-squares fit to a quadratic form. Appendix B gives a detailed study of the actual geometry at the grating drive. The following calibration was employed:

$$\lambda[\text{\AA}] = - 1.08 \text{ \AA} + 1.9610(\text{DR}) + 0.000004281(\text{DR})^2. \quad (167)$$

The drum was motorized; and a 5-inch disc with four, equally-spaced, 1/8-inch holes was attached to the gear train. A tungsten lamp, photodiode combination formed the basis of a method for stepping the drum (this was convenient, as the drum and sample chamber were at opposite ends of a 1-m instrument). The lamp beam either passed through one of the 1/8-inch holes or was blocked by the disc. The latching circuit will be described below. One could step the drum either 2.5 DR ($\sim 5 \text{ \AA}$) or 5.0 DR ($\sim 10 \text{ \AA}$), without penalty of accumulated error.

The monochromator was evacuated by a 4-inch, Consolidated Vacuum Corporation type MCF 300-002, diffusion pump which was buffered by a water cooled baffle. This pump was backed by a two-stage, Welch model 1397, mechanical pump. This combination could provide a vacuum of approximately 3×10^{-6} Torr. Perhaps the free use of Apiezon "Q" wax (vapor pressure

Table 2. Calibration of Wavelength Drum with a Quadratic Fit

$$\lambda[\text{\AA}] = - 1.08 \text{\AA} + 1.9610(\text{DR}) + 0.000004281(\text{DR})^2$$

Spectral Line	Wavelength λ [\AA]	Drum Reading [DR]	Calculated Wavelength	$\Delta\lambda$ (error)
Central Image	0.000	0.64	0.179	- 0.18
HeI(r)	584.334	298.11	583.89	+ 0.44
HI(r)	1215.670	619.81	1215.99	- 0.32
HgI	2536.52	1290.4	2536.47	+ 0.05

of 10^{-5} Torr), in the sealing of the light baffles, limited this ultimate pressure. This performance could only be achieved when the McPherson model 630, discharge lamp was inoperative; that is, with no gas flow through the entrance slits. Both hydrogen and helium gases were used with dc current through the lamp; helium was also used with a repetitive, condensed discharge through the lamp to produce the Hopfield continuum.

The reflectometer description parallels that of the ultrahigh-vacuum reflectometer. For low strain on the exit-slit housing, aluminum was used in the construction of the 5-inch inner-diameter chamber; the "stop" assemblies were made of harder material. Figure 15 displays its salient features; it is shown in the sample-out configuration. An American Time Products L8CD optical chopper provided a chopping frequency of 400 Hz.

To obtain the sample-in configuration, one rotated the photomultiplier housing and light pipe (they moved as a unit) until the housing base was against a "stop". The sample pedestal was then raised until the push-pull driver reached a slotted "stop", so the sample was positioned at an angle of incidence of 20° . The photomultiplier housing was threaded for easy removal in subdued light, as the E.M.I. 9514S dark current required several hours to recover upon exposure to room lighting.

Extreme Ultraviolet

The energy range 21 to 30 eV (590 to 400 Å), and above, has but one source of radiation which is uniquely suited for optical measurements: synchrotron radiation from a beam of charged particles (75). The unique combination of features may be listed as follows:

1. intense continuum from, say, 50 Å to the infrared
2. ultrahigh-vacuum compatibility, affording windowless operation

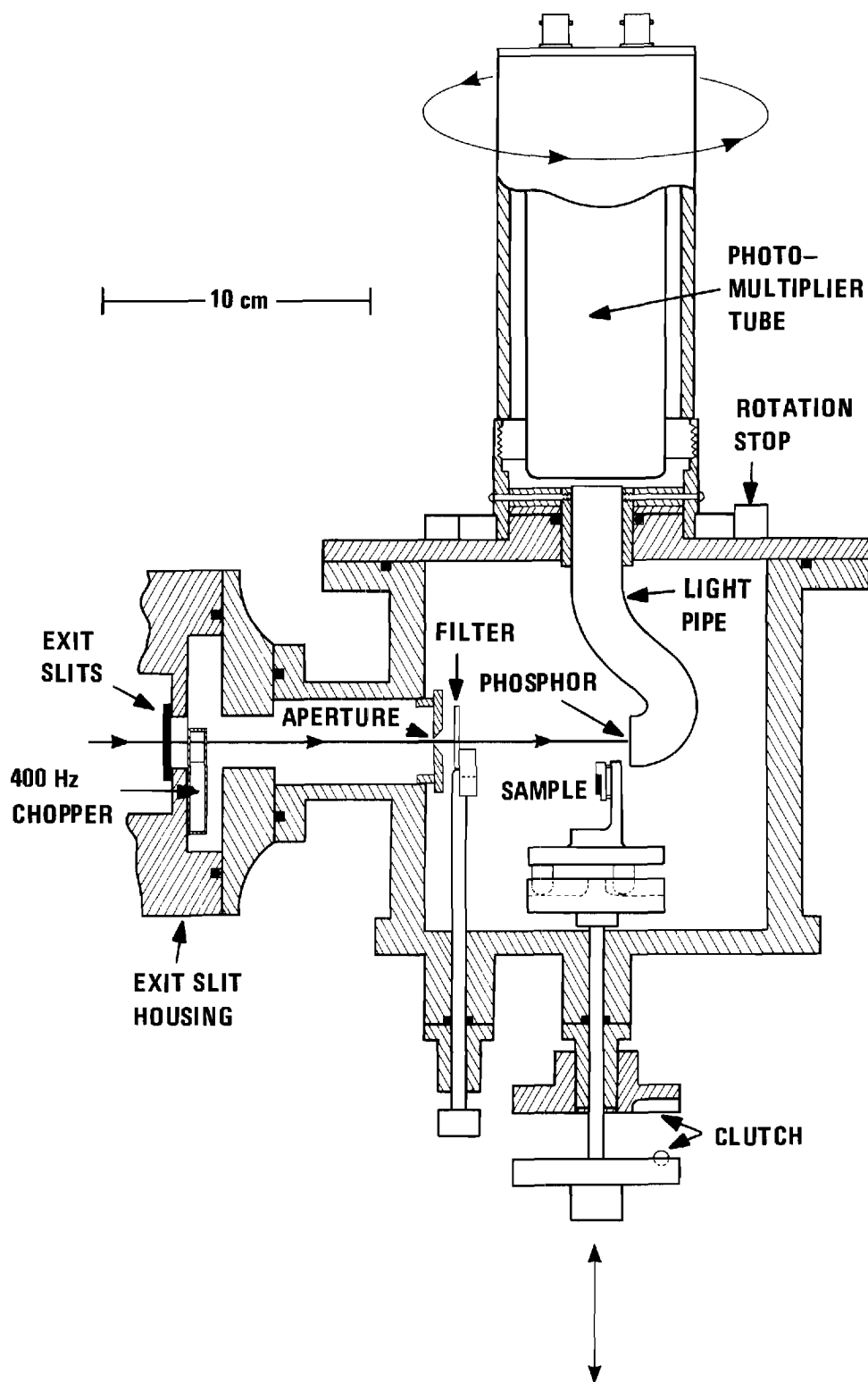


Figure 15. Vacuum Ultraviolet Reflectometer.

3. high degree of polarization, when viewed in the orbit plane, affording study of anisotropic crystals

4. known spectral distribution.

Use was made of the synchrotron radiation from the 240-MeV electron storage ring (76) at the University of Wisconsin Physical Sciences Laboratory. We obtained rudimentary results (39) with the emplacement of the ultrahigh-vacuum chamber at the position indicated by Figure 16, which is a diagram of the optical system as seen from above.

A centripetally accelerated, relativistic electron has a radiation pattern which is strongly peaked and approximately symmetrical about the instantaneous-velocity vector (77,78); so a continuous beam of electrons, constrained to orbit circularly, gives rise to a radiation pattern resembling a very flat doughnut. Near the wavelength peak of the spectral distribution for a single electron (the radiation is incoherent, so that the intensity is directly proportional to the number of electrons in the beam), the angular extent of the cone of radiation is indicated by the rms vertical angle

$$\langle \psi^2 \rangle^{1/2} \approx m_0 c^2 / E \quad (168)$$

where $m_0 c^2$ is the rest mass energy; "E", the energy of the monoenergetic electrons. This angle is 2 mrad for the 240-MeV electrons. Bending magnets, designated BM-n, supply magnetic fields normal to the orbit plane and thereby produce the centripetal acceleration along a bending radius of 0.635 m. To replenish the radiative energy loss during an orbit of

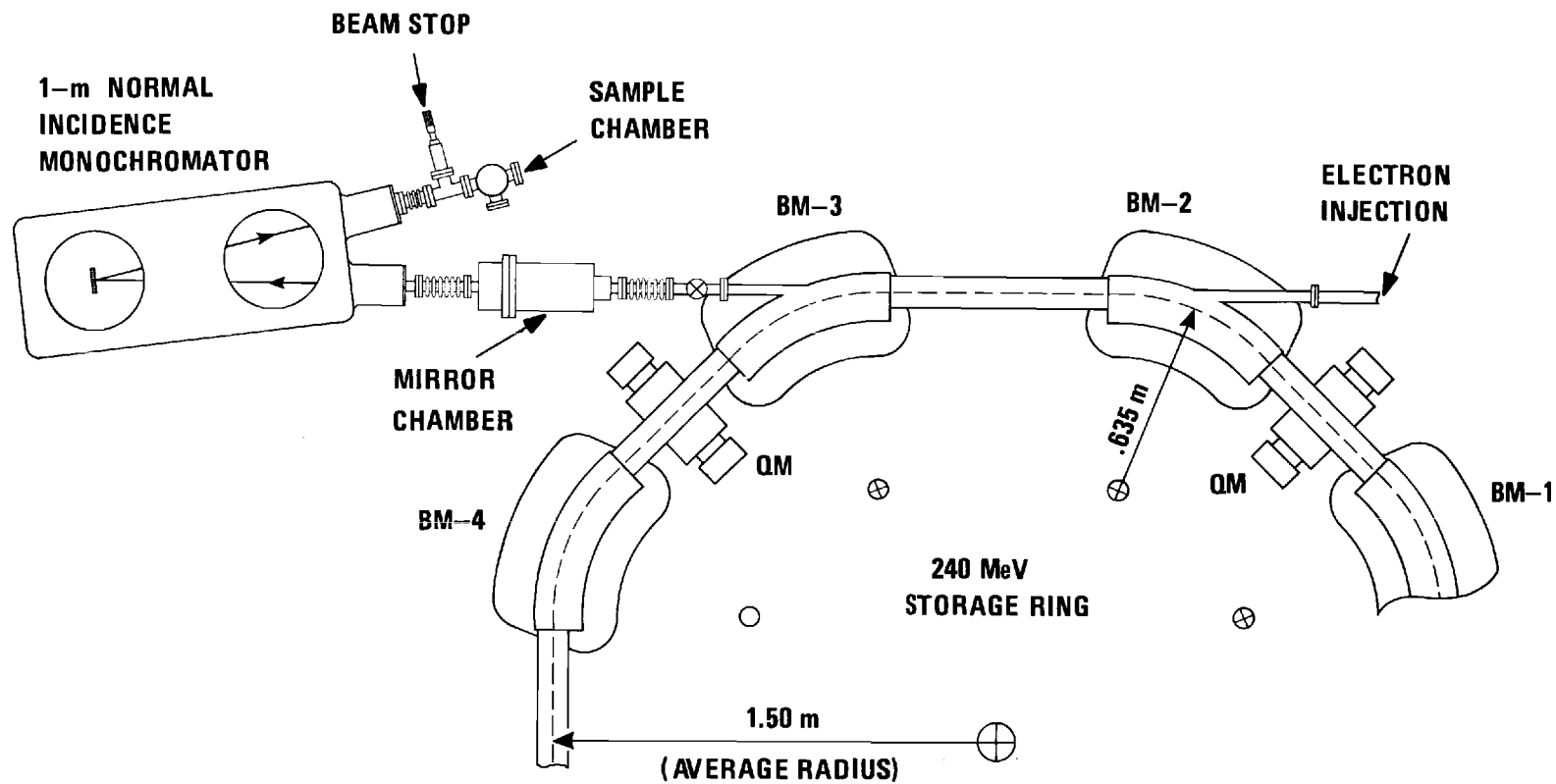


Figure 16. Northwest Port of Storage Ring.

the beam, an RF field within a cavity (not illustrated) surrounding one of the straight segments of the ring provides a linear acceleration once per revolution. This synchronous restoration of energy (repetition rate of 31.9 MHz) to the electron beam results in a bunched beam approximately 1/10 the total length of the orbit. The cross section of the electron beam is of the order .5 mm and the average stored current level is (1970) usually 1 mA (approx 2×10^9 electrons), with a "half-life" of 1 1/2 hours.

To accept the synchrotron radiation, the 1-m normal-incidence, McPherson model 225, monochromator's field of view (that of the exit slit) has to include a region of the electron beam within BM-2. Figure 17 depicts the viewable segment of the electron-beam channel; this segment is referred to here as the object slug. (The primordial consideration is the divergence in the horizontal plane as the Rowland mounting requires a horizontal focus in the entrance slits.) This object slug is obtained by geometrical construction: one extends the tangents from the electron-beam channel to the edges of the storage-ring port, recalling that the synchrotron radiation is directed along these tangents. This construction leads one to the definition of the acceptance angle α (79). For the port under consideration, α is 23 mrad.

As the monochromator is a 1-m, f/12 instrument with a grating similar (96 mm \times 56 mm) to that described in the "Vacuum Ultraviolet" section above, it has a nominal grating aperture given by

$$A = \frac{1 \text{ m}}{12} = 83 \text{ mm} . \quad (169)$$

This follows from the ordinary definition of f-number. One can obtain

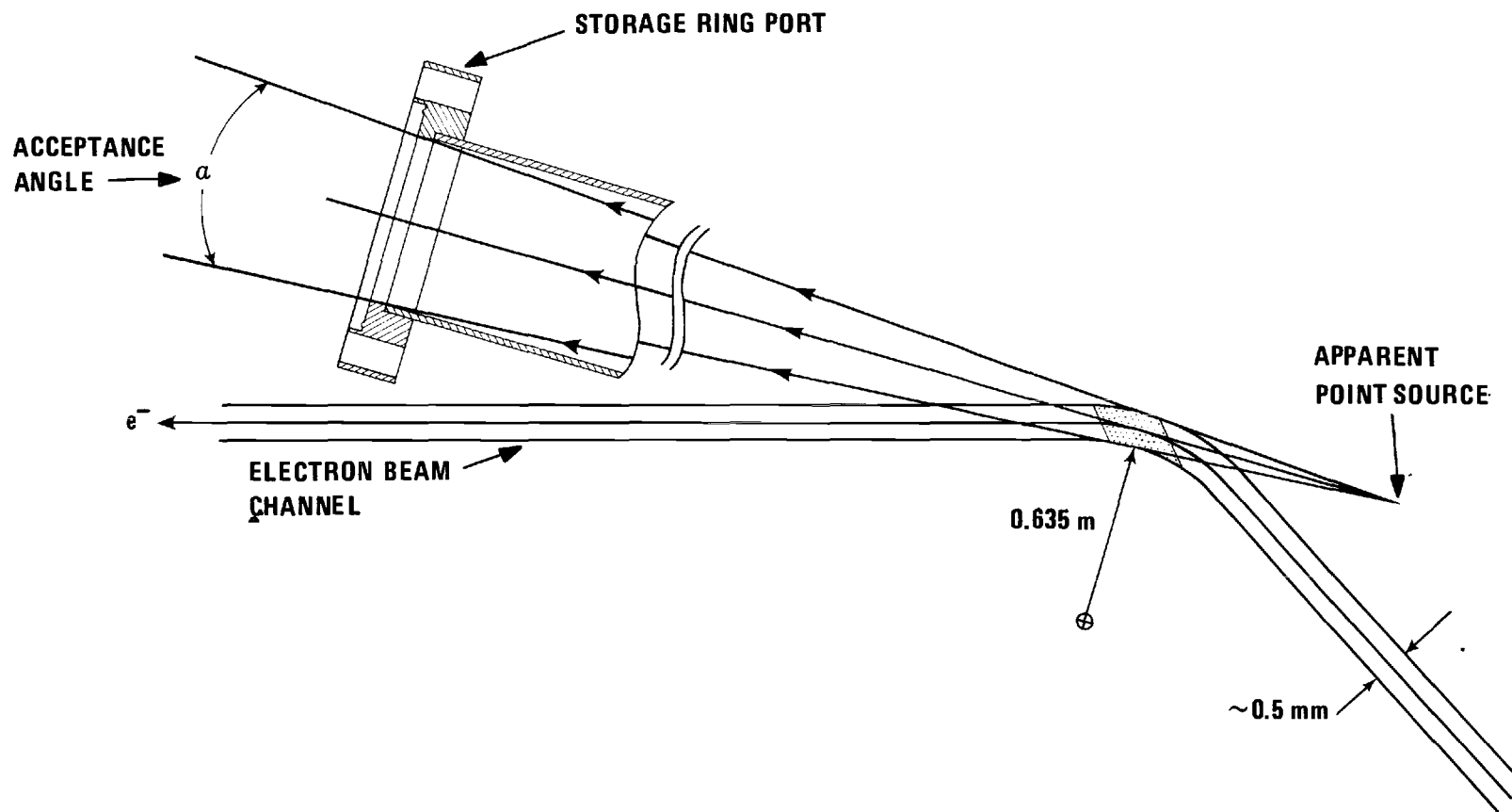


Figure 17. Object Slug Profile in Orbit Plane.

the same result from the grating dimensions directly, by computing the area of the ruled portion of the grating and finding the diameter of a circle which yields the same area. This diameter is given by

$$D = 2(96 \times \frac{56}{\pi})^{1/2} \text{ mm} = 83 \text{ mm} . \quad (170)$$

The above holds true, since the definition of f-number really involves a solid angle. (To ensure complete filling of the width of the grating, one should not use the f-number designation of the instrument; however, for this grating, the error is small.) The horizontal acceptance angle β of the grating is 96 mrad. To achieve the matching of β with α , the acceptance angle which relates to the length of the object slug, a mirror is required which focuses the object slug at the entrance slit position and which achieves a lateral magnification in the ratio given by

$$M = \frac{Y_i}{Y_o} = \frac{\tan \frac{\alpha}{2}}{\tan \frac{\beta}{2}} = \frac{\alpha}{\beta} = \frac{23}{96} \approx \frac{1}{4} . \quad (171)$$

It is also desirable to obtain a vertical focus at the entrance slits with this mirror in order to fill more completely the grating vertically, as radiation damage can occur (80). It should be noted that acceptance of all the radiation in the vertical plane is not directly compatible with the goal of those "users" who desire to exploit the high degree of polarization in the horizontal plane.

Figure 18 is a side view of the object slug, the mirrors housed by the mirror chamber, and the entrance slits to the monochromator. (Ignore

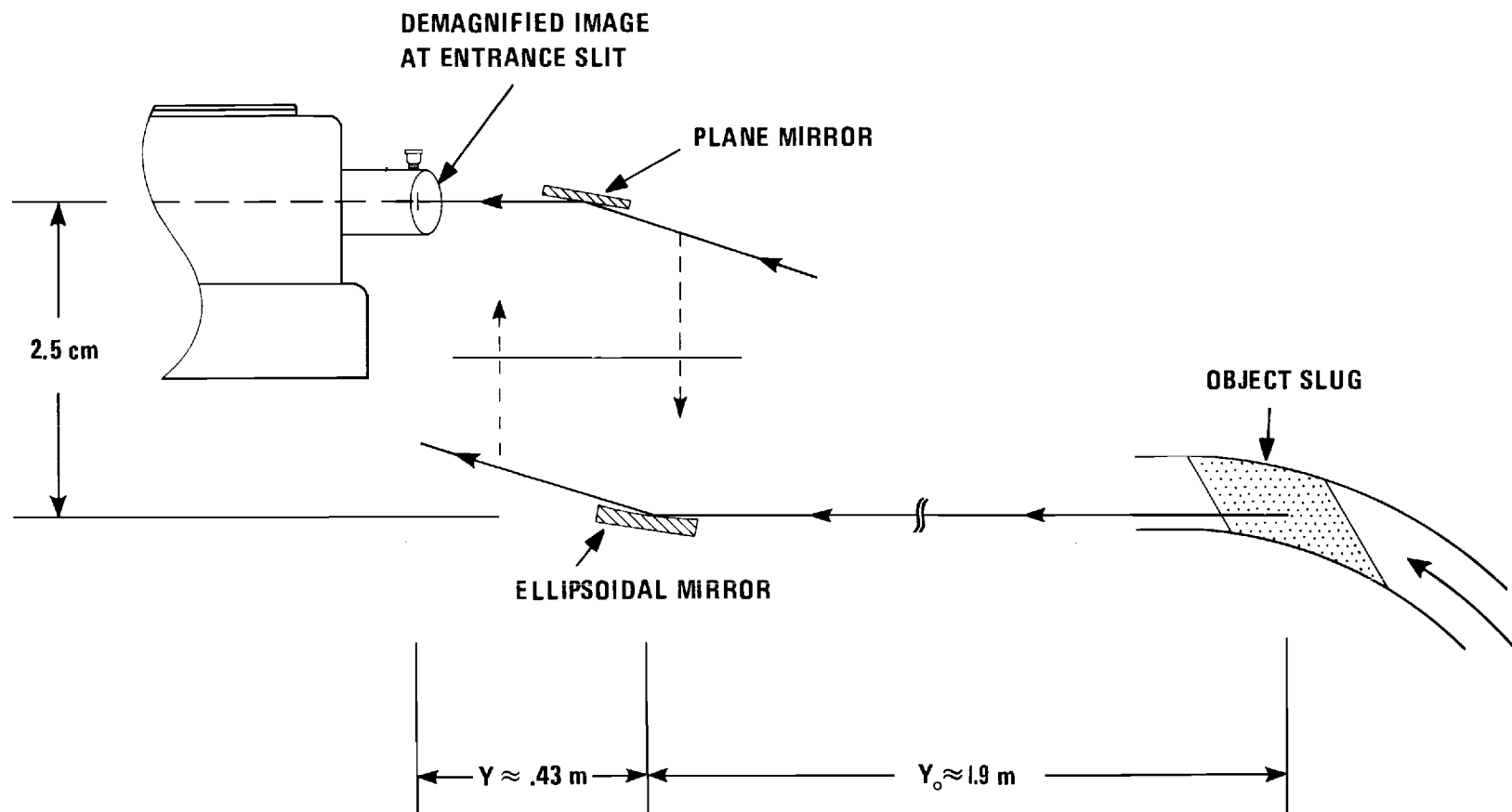


Figure 18. Off-axis Ellipsoidal and Plane Mirrors.

the plane mirror for the moment.) An off-axis section of an ellipsoid when positioned as shown is the mirror configuration which satisfies the above criteria. The mirror width or any additional length of vacuum pipe can further reduce the horizontal stop which delimits the acceptance angle α . The ellipsoid is the surface of revolution (actually a spheroid) of the ellipse whose foci define the object and image positions and whose complete specification is therefore given by the sum of the object and image distances from the mirror. As grazing-incidence optics are desired, the ellipsoid is very prolate.

In this mirror chamber, the angle of incidence is approximately 92° . At such an angle, there is no need to overcoat the mirror; and, aside from scattered light problems, two reflections in the vertical plane are at least as good as or better than one reflection in the horizontal plane (integration over the vertical angle yields radiation which is still more than 80 percent plane polarized (81,82,83). This second reflection is produced by a plane mirror which returns the central ray to the horizontal plane for ready acceptance by the monochromator. The image quality at the entrance slit is good, as the object slug is far from the mirror; that is, the depth of field is large. The image dimensions are on the order of $1/3$ mm. This discussion has been treated more generally (81,84).

Referring back to Figure 16, one sees the position occupied by the sample chamber. A modified push-pull feedthrough supported a small stop which reduced the field of view at the sample position; this was done with relative impunity as there was nearly always sufficient radiation to saturate (signal current becomes 10 percent of bias current) the solar-

blind Bendix channel electron multiplier (CEM), Model 4028. At the blaze wavelength of 800 Å, 20-μ exit slits provided count rates of $3 \times 10^4 \text{ sec}^{-1}$ in the sample-out configuration. This corresponded to approximately 5×10^{-7} amp if the CEM gain was indeed 10^8 . The reflectometer was crude. The CEM was rigidly affixed (with plexiglass) to a blank stainless-steel flange, with BNC feedthroughs, which capped the chamber, and the sample was supported by a stainless-steel spider assembly with no provision for the sample's insertion into or withdrawal from the beam other than direct handling when the system was vented to dry nitrogen. Depending on which configuration was to be run, the flange supporting the CEM was appropriately oriented by rotation through an angle (45°) determined by the bolt circle of the flange. The angle of incidence at the sample position was $22 \frac{1}{2}^\circ$. A conductive epoxy, Emerson & Cummings, Inc. Eccobond Solder 57C, was used to glue a 3/4-inch-square piece of stainless-steel shim stock, with a hole the diameter of the CEM funnel, to the funnel; this was an aid in mounting the CEM. The same epoxy was used with a small piece (say 2-mm square) of stainless-steel shim to cap the open anode end of the CEM. This is the same epoxy used in the CEM by The Bendix Corporation (85).

With an electron beam injected, the storage ring was maintained at a pressure of 2×10^{-9} Torr (76). The commercial monochromator was held at 2×10^{-8} Torr and the mirror chamber was held at 10^{-9} Torr. The mirror chamber served as part of a differential-pumping assembly: a low-conductance baffle could be placed at the entrance slits to the monochromator, as a focus in both planes was achieved there. Ion pumps of high speed (100 to 200 Lps) and titanium sublimator pumps produced the vacuum; roughing

was effected by the use of oil-less mechanical and cryosorption pumps. The above pressures were read from the logarithmic pressure scales of the associated ion-pump power supplies (recall, above, that the current supplied to an ion pump is directly proportional to the pressure within the pump). A low-conductance baffle was available for use at the exit-slit housing, to buffer the sample chamber from the heavy out-gassing of the slit housing. Rubloff (80) reported that sublimation pumping was found necessary to attain the low pressures required to start the ion pump. As we had no such pump (sublimator pump) the only manner in which we could limit the high throughput at our ion pump to a finite time interval was to remove the baffle. This severely affected the pressure maintained in our chamber during measurements: the pressure was in the low 10^{-7} Torr range.

Instrumentation

Infrared

It proved convenient to use a Perkin-Elmer chopping assembly external to the monochromator and mounted on the reflectometer about one inch from the entrance slits. The mechanical contacts on the assembly were not used for a reference-signal generator. Reference-signal contact noise was eliminated by the use of a light-emitting diode (LED) and photodiode pair: the LED beam was intercepted by a small, transparent disc (one half of which was painted black) which rode on the same shaft as the chopper wheel. See Figure 19.

The PAR HR-8, in the "Select-External" mode served as a synchronous rectifier (phase-sensitive detector): in this mode, it was insensitive to

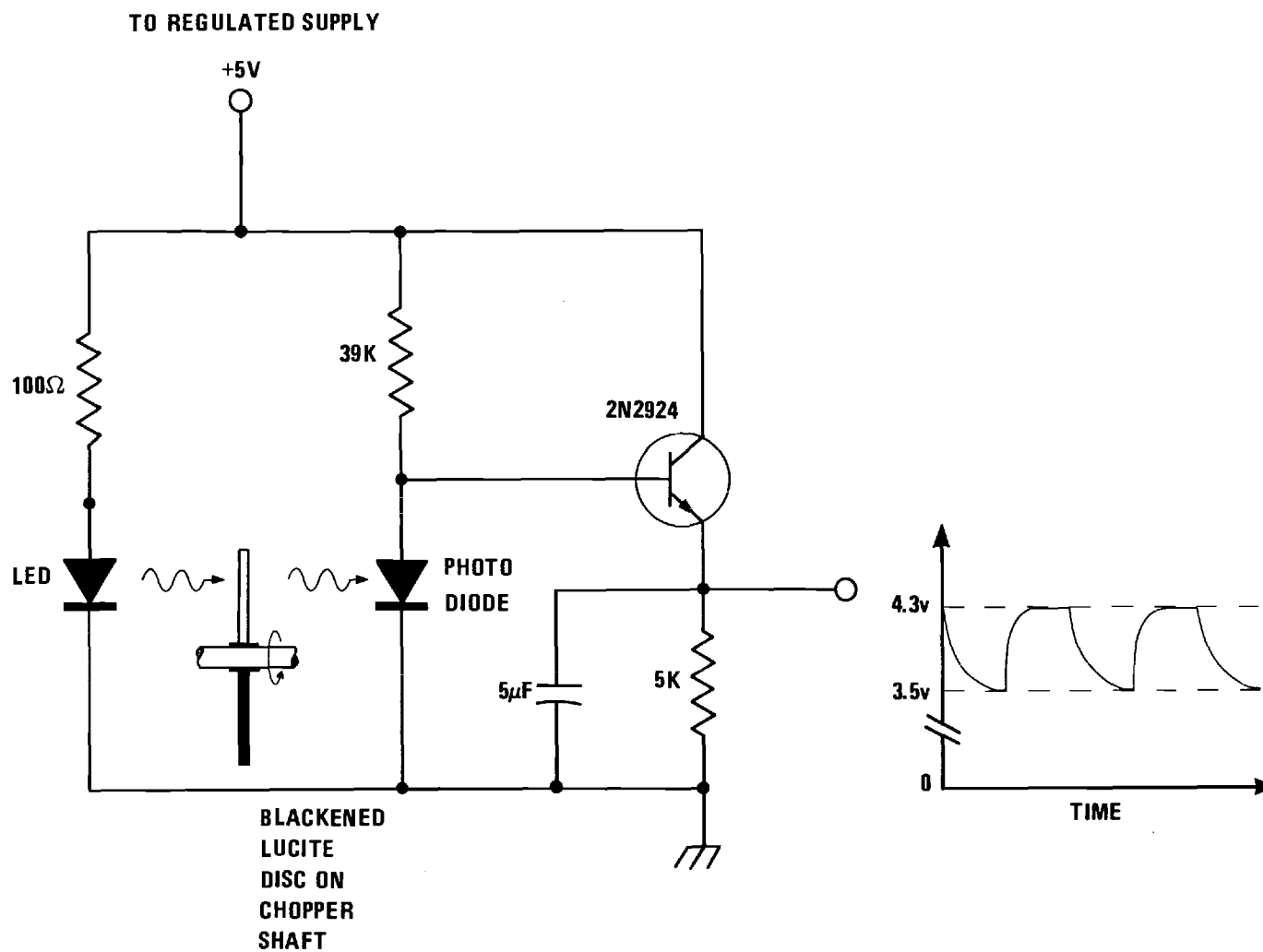


Figure 19. Chopper Circuit (13 Hz).

the exact shape of the reference signal. The 10-Meg, differential input, type "A" pre-amp was used in the PAR instrument. Between this pre-amp and the thermocouple was the Perkin-Elmer pre-amp, strapped to the bottom of the monochromator, and several stages of the Perkin-Elmer Model 107 Amplifier; these latter two units provided a voltage gain of 128 db so that the PAR pre-amp was receiving large signals (as large as 0.5 V).

Figure 20 shows the block diagram for the infrared span. The gated A-to-D converter was adapted from a United Systems Corporation Digitec DC voltmeter, model number 251A. This unit was comprised of a main frame with a Nixie Tube display and a voltmeter plug-in "module." The combined unit was accurate to within 0.01 percent (as specified by the manufacturer). The module had a continuous sampling rate which could not be gated: the module employed feedback of an error signal to compensate the clock frequency whenever the ramp generator produced a slope such that the calibration of clock pulses versus voltage tried to drift. However, the main-frame's update of the display was programmable to an extent. The heart of the update was a unijunction transistor; when it fired, the serial output of the module was encoded into the main frame for display. Readily available to the user was this serial output and, upon termination of each update, a system-ready pulse.

The modifications to the unijunction oscillator are shown in Figure 21; everything to the left of the points labeled "X" was added to the original circuitry. Assume the SCR was latched on (the unijunction's firing was thereby inhibited). The trailing edge of the update command turned off the SCR, with subsequent firing of the unijunction and the

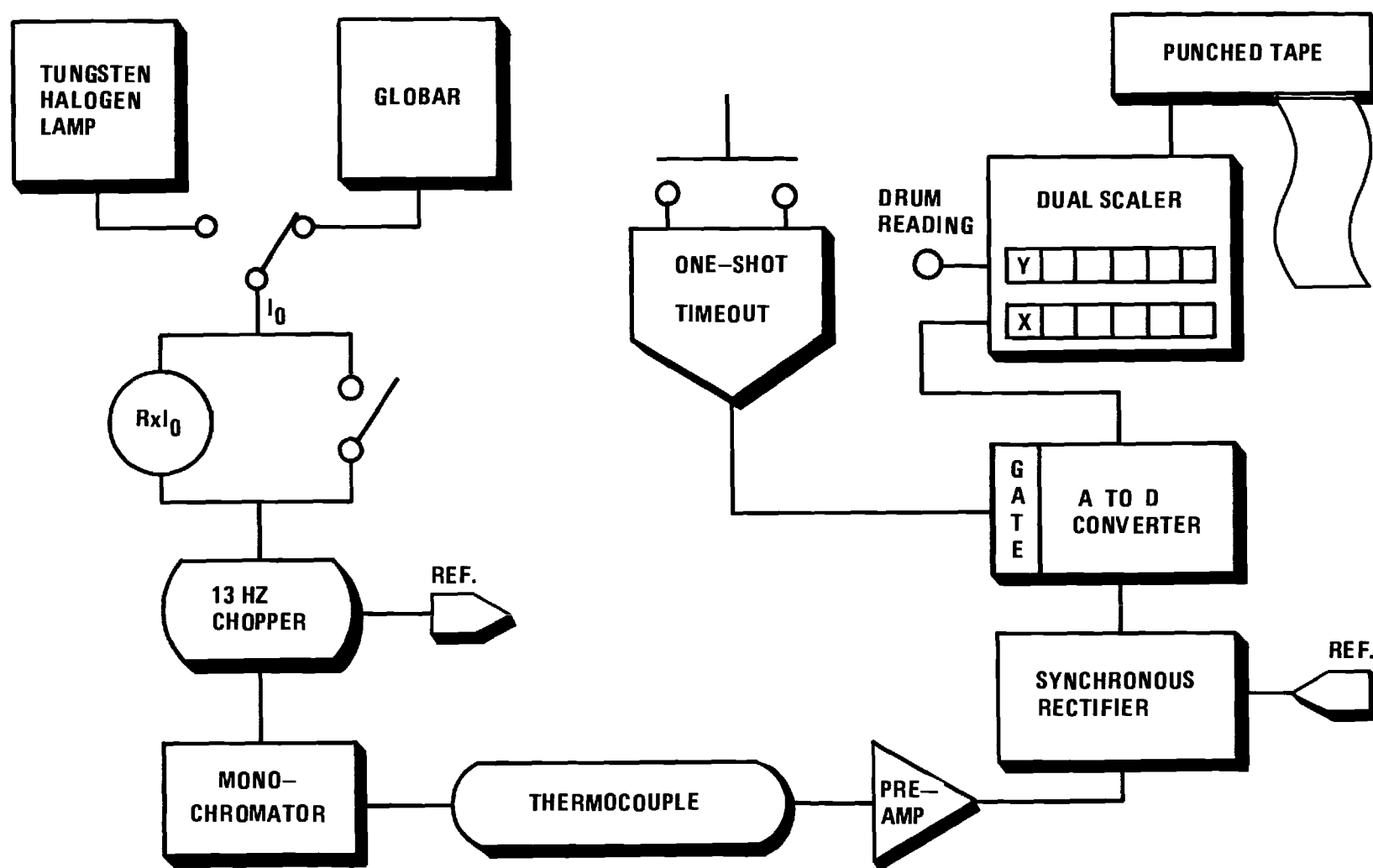


Figure 20. Block Diagram of Infrared Span.

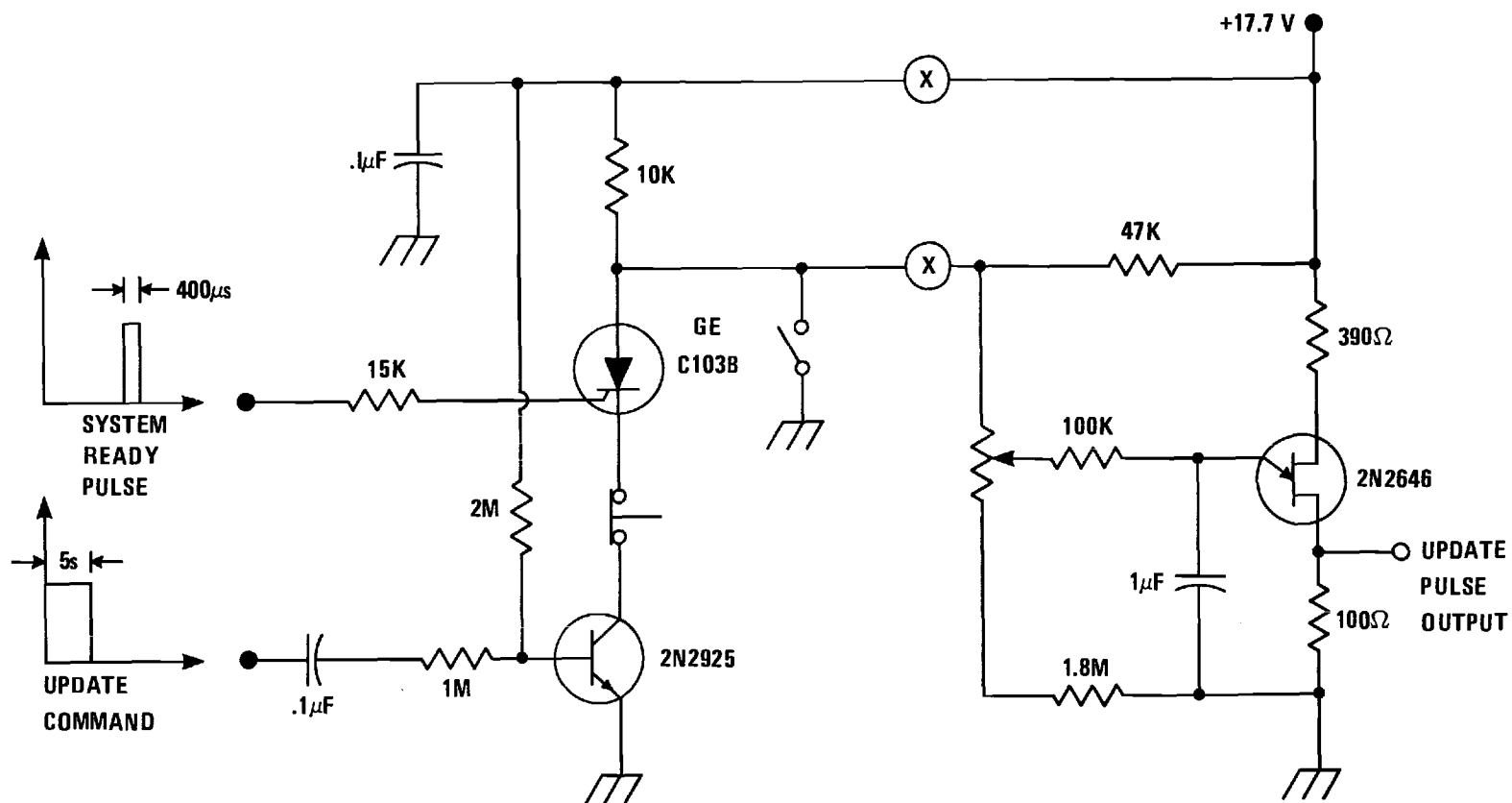


Figure 21. Modifications of Unijunction Transistor Oscillator Circuit.

release of the serial output, along with an update of the display. At the end of this update, a system ready pulse turned on the SCR before the uni-junction could effect another update.

The generator of the update command, illustrated in Figure 20 as the One-shot timeout, was an array of five timers. An array of five push buttons allowed the selection of the timeout compatible with the PAR low-pass filter; the update-command widths varied between 5 seconds and 2 1/2 minutes. Also shown in Figure 21 was a normally-closed push button whose depression effected an update without significant delay.

The printing loop was comprised of Ortec units. A model 715, dual scaler was slightly modified such that the highest decades of each scaler could be thumbwheel encoded (decimal to BCD) with a digit related to sample configuration or a digit related to the PAR scale respectively. This was possible as five digits were carried in the serial input, whereas the scalers were six- and seven-decade units. By combining these two thumbwheeled digits in a two dimensional array, we found it possible to extend the encoding to the PAR scales to a number greater than ten; this was necessary in the many-lined hydrogen region in the VUV (vacuum-ultraviolet) span. The output of the dual scaler was fed to a 222 (Modified Teletype ASP33) Page Printer by 432 Print-Out Control. The printing loop was initiated with the previously mentioned system ready pulse. The Teletype was equipped with a paper-tape punch. The scaler which received the serial output of the "module" was gated with a stretched version of the unijunction pulse.

Visible

Simple dc detection was employed throughout this range; a Keithley Instruments, model 414s picoammeter converted the photomultiplier current to a voltage for the A-to-D converter. Figure 22 illustrates the configuration that was used. The repeat cycle timer had a period of one minute; during which, ten microswitches were serially toggled at intervals of six seconds.

This battery of switches is illustrated in Figure 21 as a single-pole-single-throw switch (a momentary "shunt" unlatches the SCR in the same fashion as a momentary series "open"; that is, the current through the device is interrupted).

The monochromator, as well as the repeat cycle timer, was driven by synchronous motors; this allowed wavelength settings as good as $\pm 0.5 \text{ \AA}$. Initiation of a scan segment involved the monochromator's being started by a line-voltage relay controlled by the timer. The instrument labeled "repeat cycle timer" also generated a pulse which was counted by one of the scalers; this was an aid to the manipulation of the data, as it was related to the wavelength.

The tungsten-halogen lamp was powered by a passive current regulator which maintained a steady dc current to within ± 0.3 percent; the series-pass element was an Amperite Ballast Tube, model 22-4. The McPherson lamp was powered by a Kepco, Inc., model HB2050 voltage regulated supply. A ballast had to be employed to buffer this voltage regulated supply from the glow-discharge lamp, which also has a constant-voltage characteristic after it had fired: upon firing, the difference between the supply voltage and lamp voltage supported a current which was limited only by

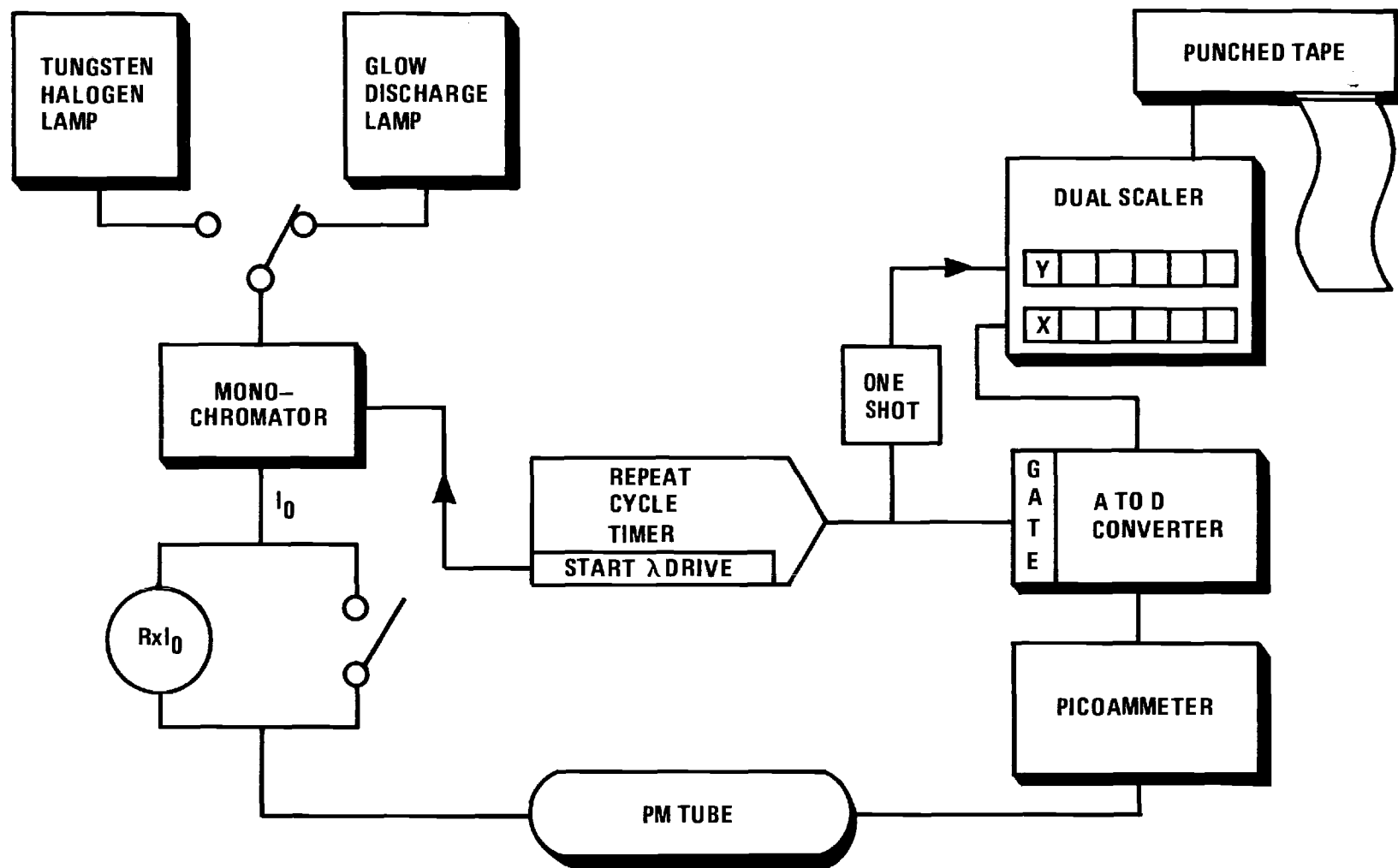


Figure 22. Block Diagram of Visible Span.

the low output impedance of the regulated supply. The supply with ballast is illustrated in Figure 23. Also shown is an ignition circuit which further reduced the transient in the regulated supply. The diode was reversed biased during the firing at the larger voltage, and this enabled the regulated supply to be preset. (This simple ignition circuit allows the use of a power supply with a much lower voltage rating than would otherwise be possible.)

The author found that the cosmetic condition of the aluminum cathode of this lamp strongly affected its performance, that is, its stability and ability to fire. Undoubtedly the cathode damage was caused by positive-ion bombardment. Every 200 hrs or so the cathode required resurfacing; this was easily done on a lathe, using mineral spirits and progressively finer-grit emery paper.

Vacuum Ultraviolet

The above mentioned schematic for the drum stepping mechanism is given in Figure 24. Only two integrated circuits were required. One was a quadruple two-input positive nand gate; the other, a dual D-type leading-edge-trigger flip-flop. Depression of the normally-open push button started the motor, which ran until one of the two configurations selected by the single-pole-single-throw switch interrupted the current to the motor relay. The configuration in which each pulse stopped the motor is labeled "E"; that in which every other pulse, "E.O.".

Figure 25 gives an overview of the instrumentation in this region. The 9514S PM tube and phosphor combination had a responsivity on the order of 4×10^{11} v/watt, when fed into a 100-K load resistor. This responsivity

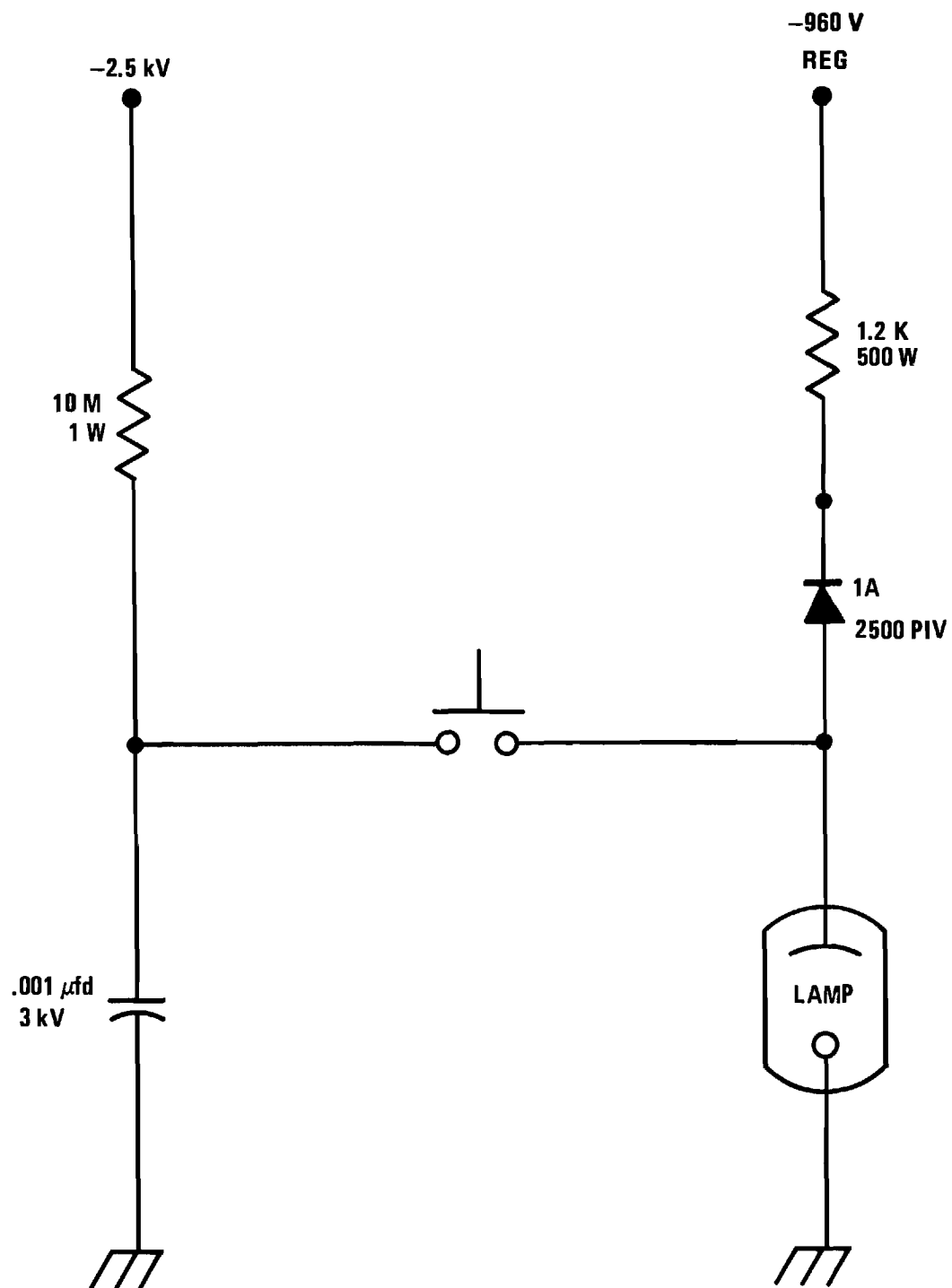


Figure 23. Schematic Diagram of Lamp Ignition.

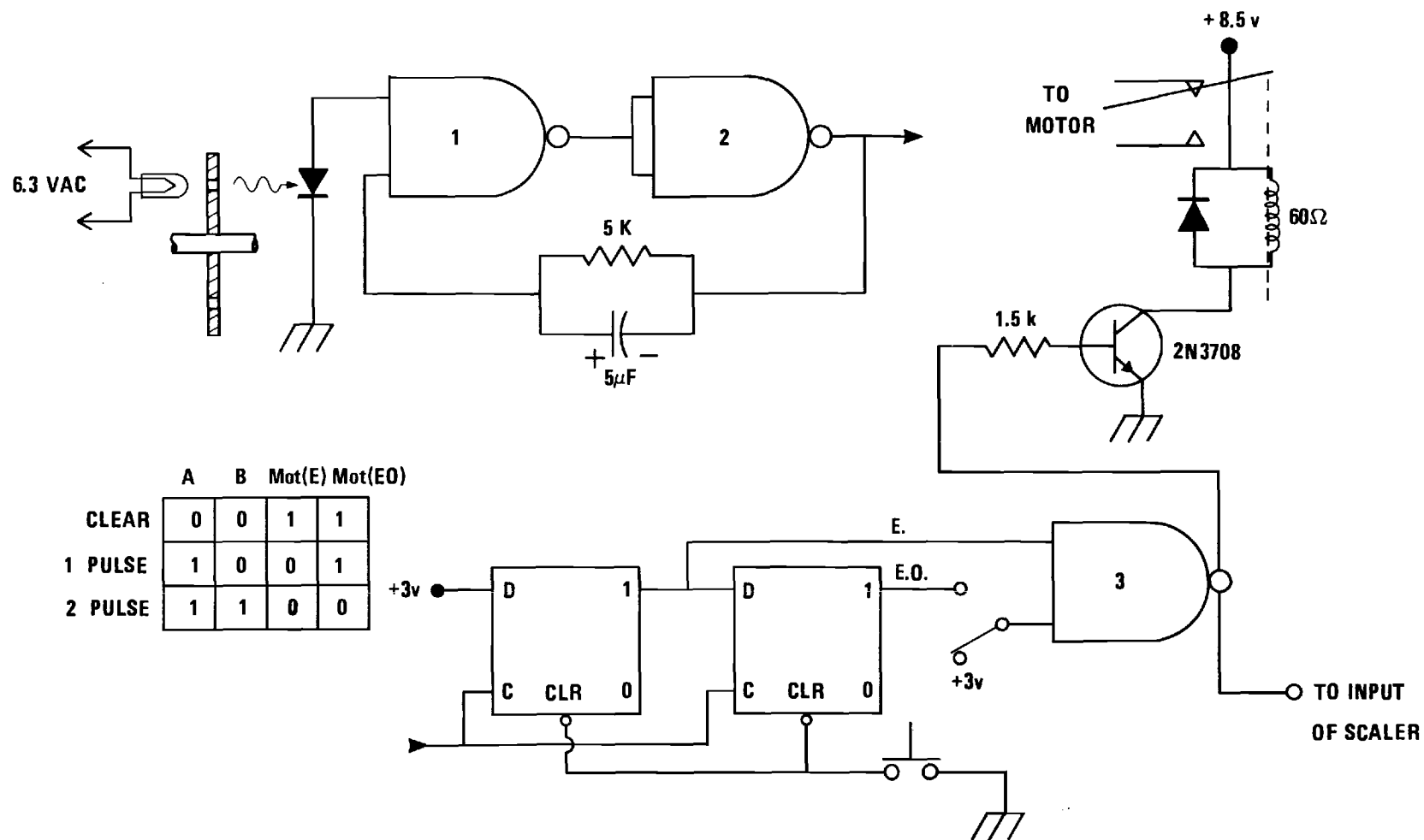


Figure 24. Schematic Diagram of Motor Control Circuit.

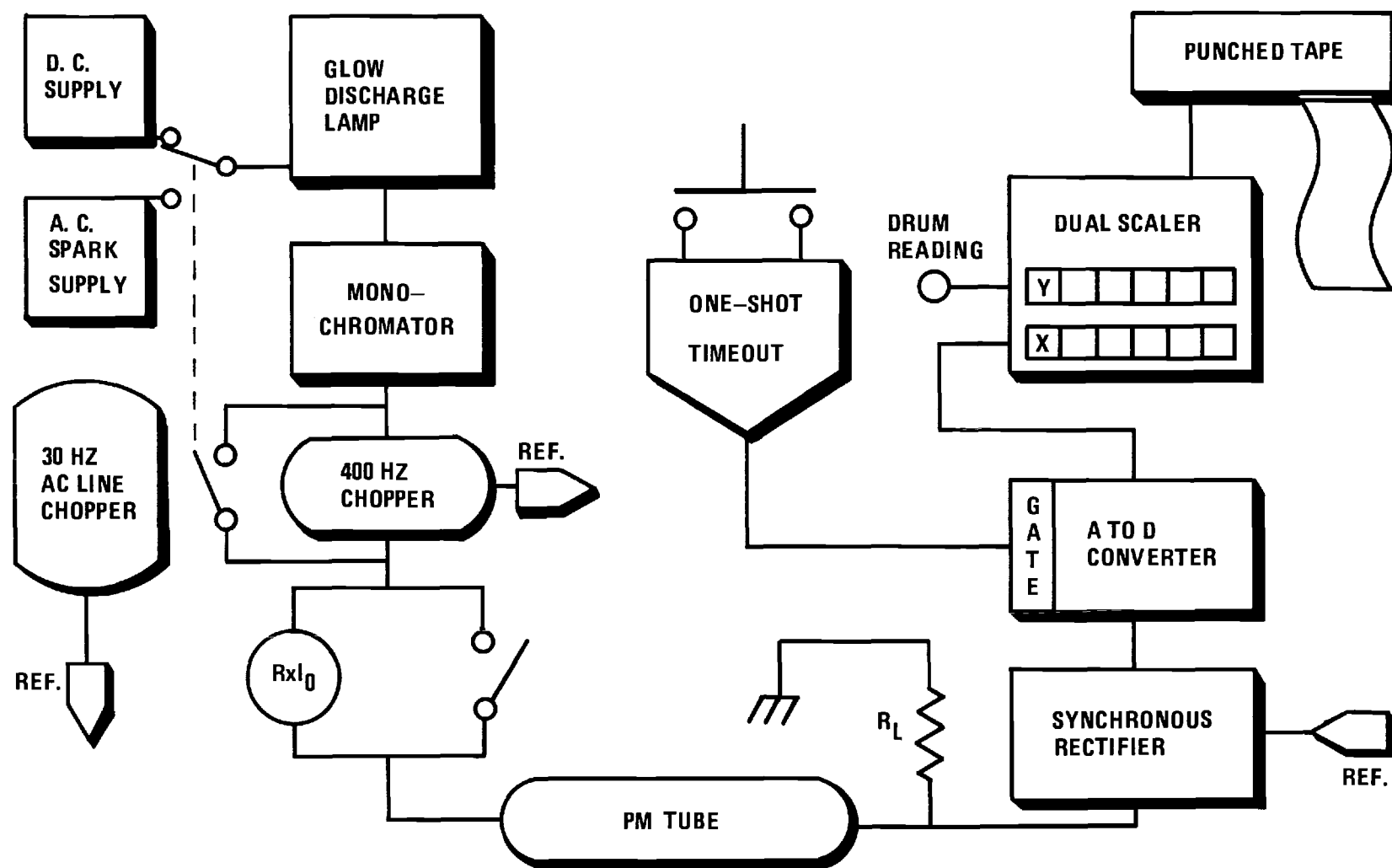


Figure 25. Block Diagram of VUV Span.

was wavelength independent below 3000 Å. Below 13 eV, the glow-discharge lamp was operated as in the visible region; however, the many-lined hydrogen spectrum was the desired spectrum here. Helium, at an arc pressure of a few Torr, was used to produce the helium resonance line at 21.2 eV; again the lamp was used in a dc mode with the 400-Hz chopper and PAR detector. Between 13 and 19 eV, a mildly condensed discharge through an arc pressure of 60 Torr of tank helium produced a weak Hopfield continuum (86). The combination of low specular reflectance and a weak source necessitated the use of a correlation technique for signal detection. Jordan's technique (87) of interrupting the ac line to the McPherson model 720 Dual Mode AC Power Supply was exploited, since the pulse repetition rate at the PM tube was far too low for use in conjunction with the 400-Hz mechanical chopper. Appendix C gives an account of how the ac line was interrupted in this experiment; there is no suggestion of the same in Jordan's discussion.

Figure 26 shows the elements of this power supply as adjusted for this spectral region. (For the discussion here, ignore the interruption of the ac line.) The spark-gap breakdown voltage was 3.0 kV which was much higher than the firing potential of the glow-discharge lamp, so the firing rate of the lamp was controlled by the condition of the gap. This spark gap was irradiated with a mercury lamp and continuously swept with an adjustable jet of air in an effort to obtain stable operation: that is, a constant repetition rate and equal energy fed to the lamp per firing. Adjustment of the repetition rate was affected by changing the variac setting, since an increase of the transformer secondary voltage increased

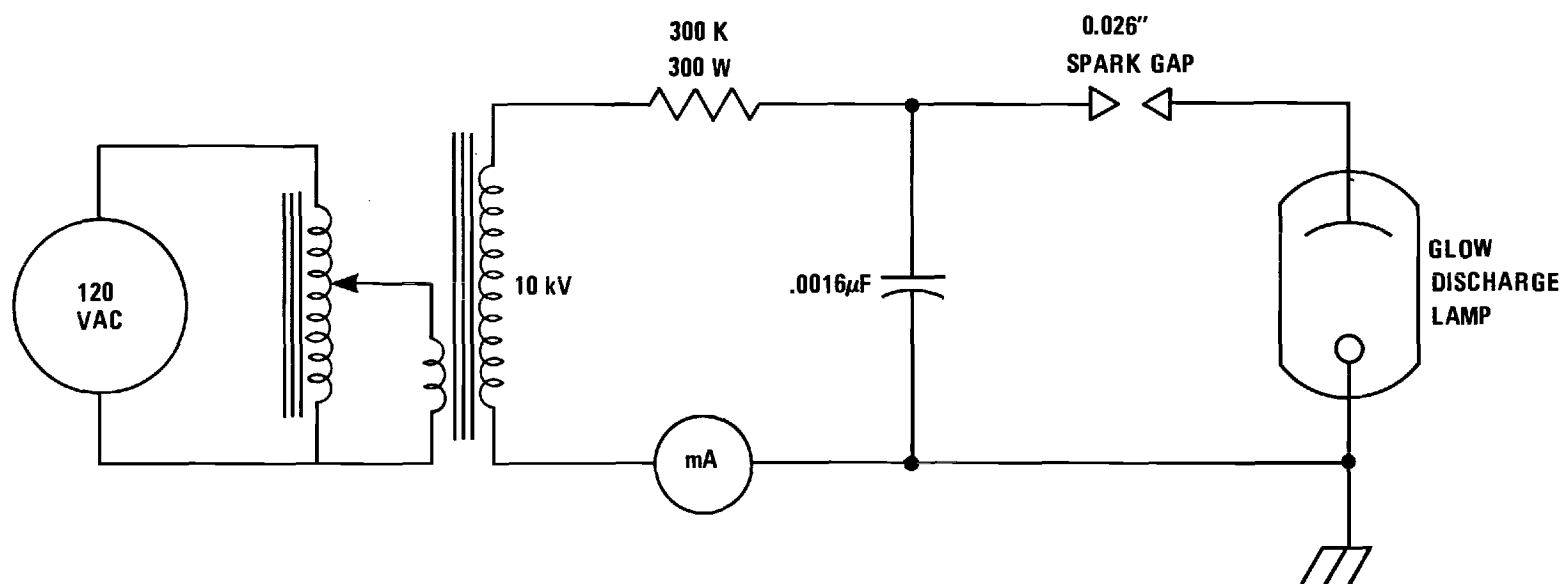


Figure 26. Parameters as Adjusted for the 720 Supply.

that fraction of the quarter cycle over which the spark-gap voltage was exceeded. The author failed to achieve a truly constant repetition rate above, say, 16 pulses per quarter cycle. A nominal repetition rate of 25 per quarter cycle was used.

The shaft-angle encoder for the drum reading of the monochromator is shown in Figure 27. The operational amplifiers were supplied by Burr-Brown Research Corporation; the ± 15 -V supply was a Burr-Brown model 508/16. The illustrated 9-V batteries were composed of 1.5-V telephone cells.

The 1552/16 op amps were used as voltage followers of high input impedance and low output impedance. Their outputs were summed by a unity-gain inverting amplifier, constructed from the 3021/15 op amp, which presented a 10-K input impedance to each of the follower outputs. The 10-K, 15-turn heli-pot which was fastened to the wavelength drum is shown connected to one of the non-inverting inputs. It was provided by Link Aviation Incorporated as Part No. 221003 and had a linearity tolerance of ± 0.025 percent. The 20-K heli-pot served to offset the voltage proportional to the drum reading, for the purpose of making recordings on an expanded scale; a horizontal recorder sensitivity of 10 mV/cm was usually used during wavelength calibration runs. The $\pm .5$ mA null meter was essential to avoid pegging of the recorder: its sensitivity was gradually decreased until the off-setting voltage was precisely set; only then could the recorder be safely connected.

Extreme Ultraviolet

The block diagram for this span is presented in Figure 28. A channel-electron multiplier, provided by the Bendix Corporation as

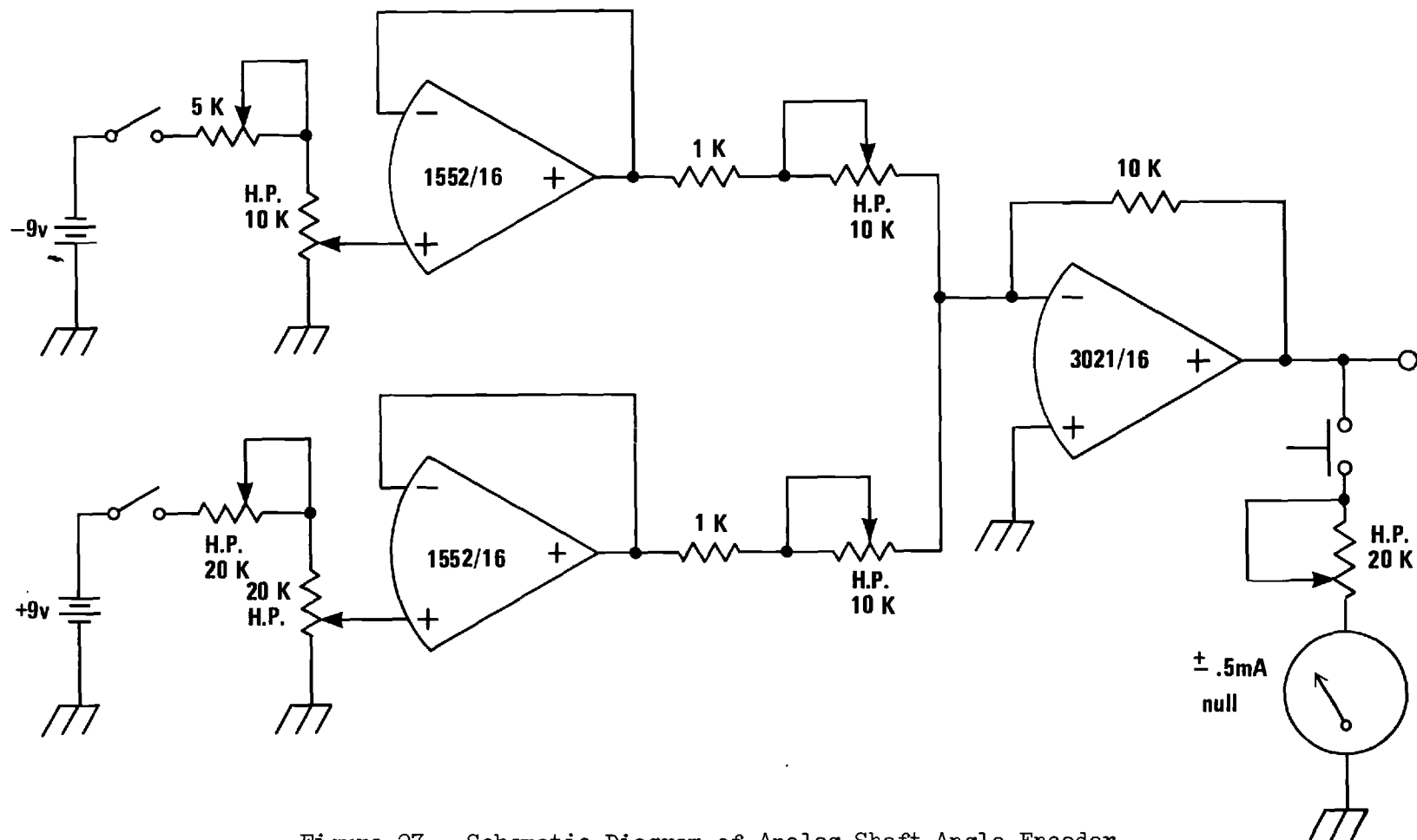


Figure 27. Schematic Diagram of Analog Shaft-Angle Encoder.

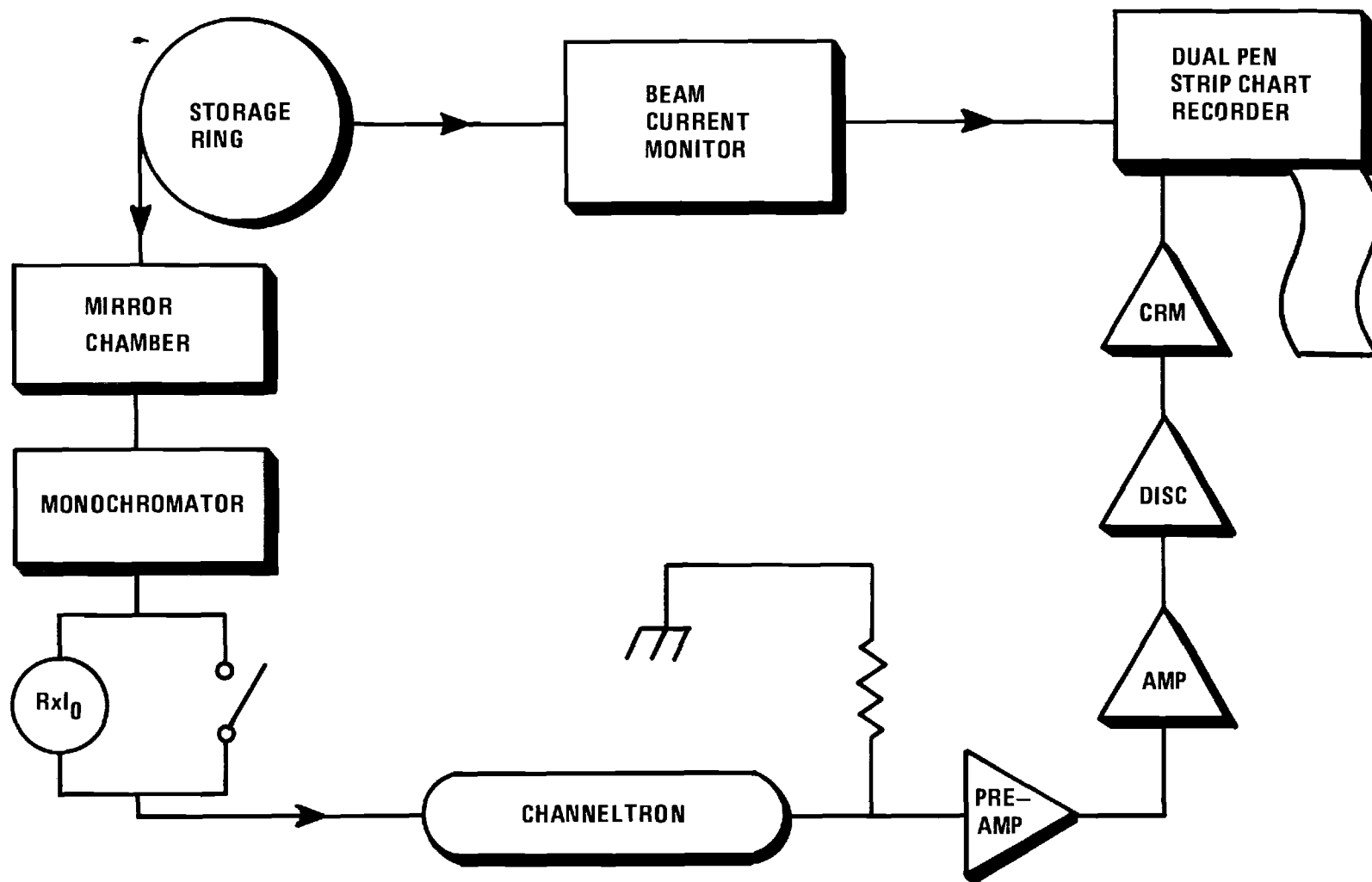


Figure 28. Block Diagram of Extreme UV Span.

CEM-4028, was used in the counting mode. The very narrow (~ 5 ns) current pulses were integrated over stray shunt capacitance and the input capacitance of the Ortec model 113 unity-gain preamplifier; the voltage on these capacitors then decayed with a time constant determined by this total capacitance and the parallel resistance of the load resistor and the input resistor selected by the preamp. The preamp output was series terminated and fed into an Ortec model 485 linear amplifier. An Ortec model 421 integral discriminator received the amplified-and-shaped pulses and accepted all pulses above a given threshold. The probability that two photons would contribute to a doubling of the pulse amplitude was very small but finite, so that the gain of the linear amplifier was correspondingly adjusted to allow the passage of the doubled pulses through the discriminator. The very narrow pulse-height distribution of the Channeltron facilitated adjustment of the discriminator setting.

An Ortec model 441 count-rate meter filtered the shot noise and provided a voltage output for one of the channels of a Varian dual-pen strip-chart recorder. The other channel of the recorder monitored a voltage proportional to the stored electron-beam current. This beam-current monitor was a secondary standard of measurement; the primary standard consisted of an electrostatic inductor. Figure 29 displays the salient features of this secondary standard. The ion sweep plates formed a nearly ideal current source. Residual ions were continuously removed from the electron-beam path. There existed a linear relationship between the swept ion current and the electron-beam current; the calibration of this beam current monitor was stated to be good to within ± 5 percent (88).

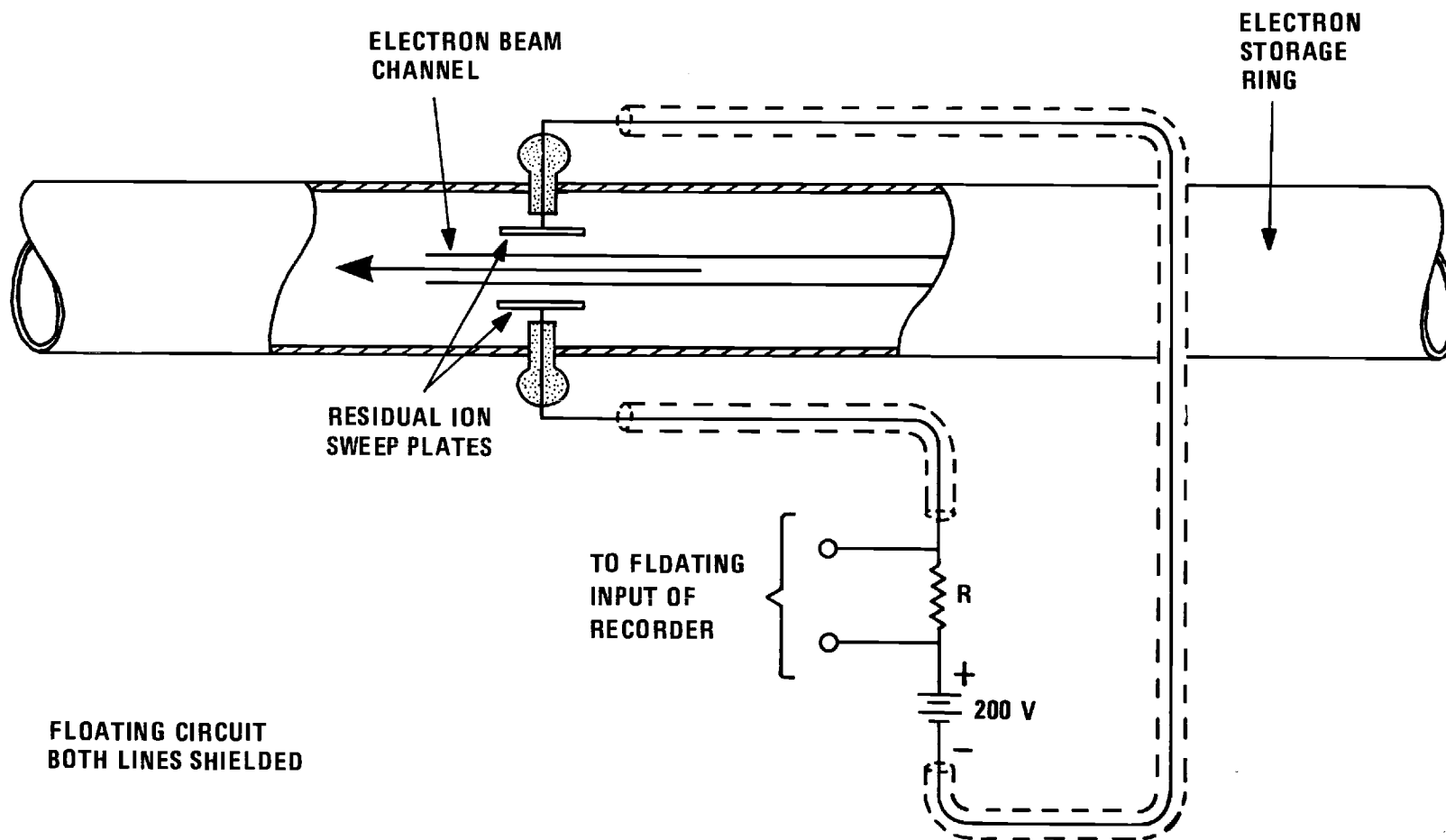


Figure 29. Electron Beam Current Monitor.

CHAPTER IV

EXPERIMENTAL PROCEDURE

Sample Preparation

A total of eight samples were obtained from the Naval Research Laboratory (N.R.L.) of Washington, D. C. and were 8-mm diameter discs sawed to 1-mm thicknesses. All the members were prepared by means of a modified Bridgman method (14). Wagner, Palik, and Swiggard (12) reported that the $\text{Cd}_3(\text{As}_{0.25}\text{P}_{0.75})_2$ and the $\text{Cd}_3(\text{As}_{0.12}\text{P}_{0.88})_2$ crystals were not physically strong. Radoff and Bishop (13) reported that for "x" greater than or equal to 0.25 the Bridgman-grown ingots show cracks associated with a solid-solid phase transition. See Chapter I for the phase diagram of this system. Table 3 summarizes the appearance of this set of samples.

The chemical analysis of the samples gave results which varied but slightly over the ingot length (89); the tabulated values of "x" in Table 3 are reliable to within ± 1 percent.

Mechanical-polishing and etching techniques were developed along lines suggested by the group at N.R.L. (89). The saw-cut samples were held to a 3-inch diameter, stainless-steel holder by Crystalbond 509, a cement stick of reasonable vacuum properties, manufactured by Aremco Products Inc. An 8-inch, polishing wheel was covered with Buehler AB Micro-cloth, Catalog No. 40-7208, at each stage of polishing. These samples were so soft as not to require "grinding". Polishing commenced with a

Table 3. Index of Samples and Qualitative Comment
on Crystalline Quality of Samples

Sample	End Member	(N.R.L.) Ingot Number	$\text{Cd}_3(\text{As}_x\text{P}_{1-x})_2$	Comment
1	✓	--	$x = 0.00$	cracked
2	--	8-151-3E	$x = 0.12$	good
3	--	8-149-8B	$x = 0.25$	badly cracked
4	--	8-111-7	$x = 0.50$	good
5	--	8-111-8	$x = 0.50$	very good
6	--	8-59-13B	$x = 0.75$	cracked
7	--	8-59-13C	$x = 0.75$	good
8	✓	--	$x = 1.00$	badly cracked

mixture of Union Carbide's 1- μ alumina powder and tap water, and it was continued until no scratches were visible except for those left by the powder. This was followed by polishing with a suspension of 0.25- μ diamond compound, provided by Buehler as AB Metadi with Catalog No. 40-6112, in a lapping oil provided by Buehler as AB Automet with Catalog No. 60-3250. Final polishing was performed with a mixture of Union Carbide's 0.05- μ (500 Å) alumina powder and distilled water.

The etching procedure lacked discernable trends. An etch consisting of a solution of bromine in methanol, 5 to 0.08 percent by volume, was used. This is a satisfactory etch for the removal of oxides from elemental arsenic. Polished samples were etched for 5 to 60 seconds in this solution; then they were quickly transferred to two successive rinses in acetone. If the etch was too concentrated and/or the exposure too long, then the results were deleterious: the sample surface appeared dull or had a strong bluish cast. The infrared reflectance of such a sample was still reasonable, but at 4000 Å the reflectance was down by a factor of three or four. Such samples were repolished with the 0.05- μ alumina powder and then re-etched. Several samples were recycled several times.

Alignment of Sample

Whereas the crystalline quality of the samples was not uniform and their fragility was accompanied with the fact that only a limited number of samples were available, little effort was expended toward orientation of the crystallographic axes: though cracked, the crystalline regions of several of the samples were sizable (~ 1 mm). Furthermore, the development of the instrumentation was not compatible in all wavelength regions with the attendant loss of signal strength that polarizers would have

introduced. Unmeasured instrumental polarization together with unspecified crystal orientation were assumed to generate a reflectance curve which mimicked a response to an isotropic sample.

Common to the IR, visible, and UV instruments was a simple alignment procedure. For each sample run, the three spring-loaded tilt and centering screws (see Figure 11) were adjusted with the sample holder positioned on the infrared reflectometer; this automatically aligned the sample for the visible and UV reflectometers, by means of earlier-made compatible adjustments on the respective tri-slotted pedestals for the sample holder. The IR reflectometer was chosen as the base for this procedure, as the optical paths were longer; this permitted a more sensitive adjustment.

The visible reflectometer's pedestal was machined such that it was angularly positioned by the presence of the cam surface of the sample raising and lowering mechanism; this cam wheel was oriented by the port supporting the rotary feedthrough. The UV reflectometer's pedestal was angularly positioned with the aid of the visible central image of the monochromator, when a tungsten lamp was substituted for the glow-discharge lamp (this procedure never required readjustment). As the angle of incidence was 20° , a polished stainless-steel bevel of 20° , whose surface was coincident with that of the axis of the chamber, was temporarily mounted to the sample holder. The pedestal, with sample holder and bevel in situ, was then rotated until the incident beam was reflected back onto itself. Once this angular position was located, a slotted cam allowed the pedestal to be lowered for the sample-out configuration and reproducibly positioned for the sample-in configuration.

Reflectance Measurements

Several monochromators (gratings, prism), light sources, and several sample chambers were combined in the effort to span the huge energy range of 0.083 to 21 eV. As mentioned in Chapter III, this range was extended to 30 eV for Cd_3As_2 . The normal sequence of data acquisition (exclusive of the extreme-UV data) was such that upon completion of the etching and alignment, a methanol-rinsed and air-blown-dry sample was placed in the ultrahigh-vacuum chamber (visible span); a run was executed and the sample was then emplaced in the UV chamber; finally, the sample was run in the IR reflectometer. This sequence was so chosen as within the IR region, the reflectance was the least sensitive to surface contamination; there was no in situ sample preparation. Table 4 gives an overview of the component spans that linked to form the entire region of interest.

With the exception of generated reflectance curves which proved unreasonable due to the action of the etch and the usual operational errors, there were no runs which were entirely duplicated for the purpose of averaging; however, many points were spot checked for consistency within a given span.

Determination of Backgrounds

Background or base-line corrections in the IR region were only of consequence near $15\ \mu$, where the data were poor for other reasons (see next chapter).

The use of quartz filters in the visible and UV regions singled-out long-wavelength scattered light as the major contributor to the background. This background manifested itself as a very slowly decreasing (versus

Table 4. Summary of Experimental Instrumentation and Conditions

Span No.	Light Source	Monochromator	Dispersing Element	Wavelength Span	Resolution $\sim \Delta\lambda$	Chamber Pressure [Torr]	Mode of Acquisition
0	Synchrotron	1-m Normal Incidence	800-Å Blaze Grating	400-1200 Å	5 Å	$\sim 1 \times 10^{-7}$	Repeated Scans
1	Glow Discharge HeI	1-m Normal Incidence	800-Å Blaze Grating	584 Å	4 Å	$\sim .6 \times 10^{-1}$	Point by Point
2	Condensed Discharge He ₂	1-m Normal Incidence	800-Å Blaze Grating	650- 950 Å	5 Å	$\sim .2 \times 10^1$	Point by Point
3	Glow Discharge H ₂	1-m Normal Incidence	800-Å Blaze Grating	950-1700 Å	10 Å	$\sim .6 \times 10^{-1}$	Point by Point
4	Glow Discharge H ₂	.3-m Czerny-Turner	1500-Å Blaze Grating	1700-3050 Å	5 Å	$\sim 1 \times 10^{-8}$	Repeated Scans
5	Glow Discharge H ₂	.3-m Czerny-Turner	5000-Å Blaze Grating	3050-3600 Å	5 Å	$\sim 1 \times 10^{-8}$	Repeated Scans
6	Tungsten Halogen Lamp	.3-m Czerny-Turner	5000-Å Blaze Grating	3600-6500 Å	5 Å	$\sim 1 \times 10^{-8}$	Repeated Scans
7	Tungsten Halogen Lamp	Littrow Mounting	NaCl Prism	0.65-1.4 μ	20 \rightarrow 160 Å	Atm.	Point by Point
8	Globar	Littrow Mounting	NaCl Prism	1.4-15 μ	.016 \rightarrow .9 μ	Atm.	Point by Point

wavelength) contribution from the central image. It was always assumed to be a constant within a given span. Two corrective terms were employed: at a short wavelength where no radiation should have reached the detector, an intensity measurement was taken for both sample-in and sample-out configurations. This was handled analytically by the replacements

$$R \equiv \frac{I_R}{I_O} + \frac{I'_R - B}{I'_O - A} \quad (172)$$

where "I" was respectively the incident and reflected intensity, and the primes denoted the measured intensities; "A" and "B" were the background corrections.

In the extreme-UV region, again the long-wavelength light was the greater contributor to the background. However, the use of a solar-blind channel-electron-multiplier eliminated the need for such corrections.

CHAPTER V

RESULTS AND DISCUSSION

The results of the hitherto unmeasured, reflectance spectra for these alloys will be presented below. In analogy to the III-V compounds, the strong structure in the reflectance will be interpreted as due to direct transitions. Probable assignments of interband transitions will be made on the basis of the available energy-band-structure calculations. An extensive comparison of our reflectance data with the limited (spectrally speaking) data of others will be made. This comparison serves as a check on the absolute and relative errors of our data and forms the basis for error estimates in our Kramers-Kronig unfolding of the optical constants. These optical constants have not been previously published for any of these alloys above the infrared region.

In the following presentation, samples will usually be denoted by the integer indices defined in Table 3 of Chapter IV. These indices are numbered one through eight and increase somewhat in proportion to the concentration of the arsenic constituent of these alloys. The index "1" denotes Cd_3P_2 . The index "8" denotes Cd_3As_2 .

Primary Data

The results of the near-normal-incidence reflectance measurements are presented in Figure 30. These measurements from 0.08 to 21.2 eV have been performed at the Georgia Institute of Technology. For several

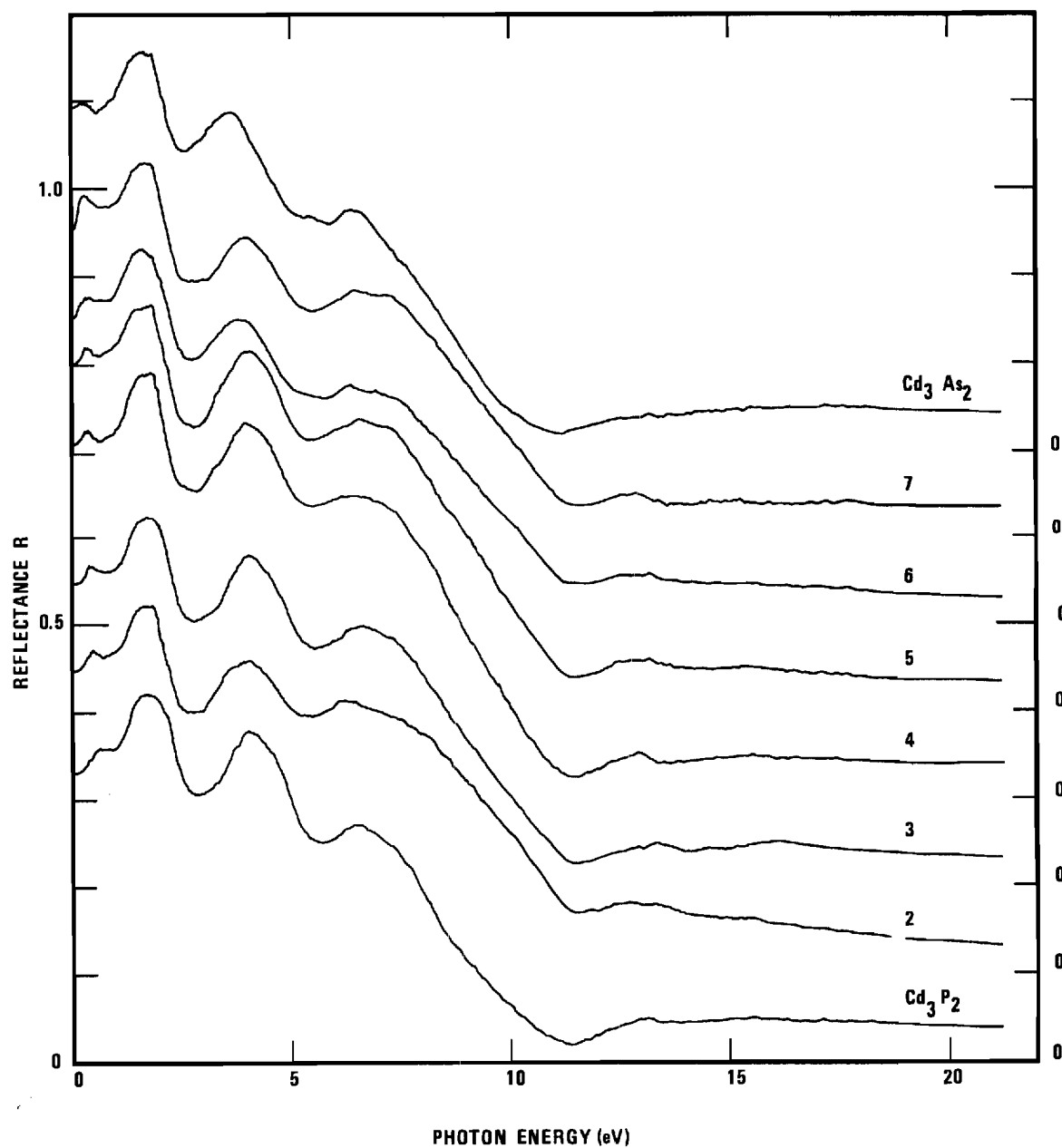


Figure 30. The Reflectance Spectra of the Cd_3As_2 - Cd_3P_2 Alloy System at 297°K (The curves are zero shifted as indicated to prevent overlap).

typical results, the nearly transparent or plasmon region is also shown on the enlarged scale of Figure 31. The results of similar measurements, performed at the Physical Sciences Laboratory of the University of Wisconsin, are presented in Figure 32. Included in this latter Figure 32 are the results of measurements on the related compound Zn_3As_2 (37).

In addition to the x-ray work of Masumoto and Isomura (2) and the low-temperature, transmission-edge work of Radoff and Bishop (13), we find that the roughly linear scaling of the strong structure of the reflectance, as a function of alloy composition, represents further evidence that these alloys form a continuous series of solid solutions. We note that the structure in the reflectance curves of the mid-members of this alloy system is as well defined as that for the end-members.

Interpretation of Reflectance Structure

The structure above the fundamental absorption edge (~ 0.6 eV) will be related to Lin-Chung's (37,43) band structure (B.S.) as calculated for the hypothetical structure (see Figure 5). Only that portion of our structure below say 0.7 eV is directly amenable to a discussion in terms of the joint density of states. This latter remark will be made clear when the optical constants are generated below.

First we redraw the primary data of Figure 30, as shown in Figure 33. These curves are zero-shifted in relation to the percentage of the anion concentration ("x" values of Table 3). We defer treatment of the sharp structure below 0.7 eV and begin with a discussion of the structure in the range of 2 eV. Our Figure 33 suggests a linear scaling of the

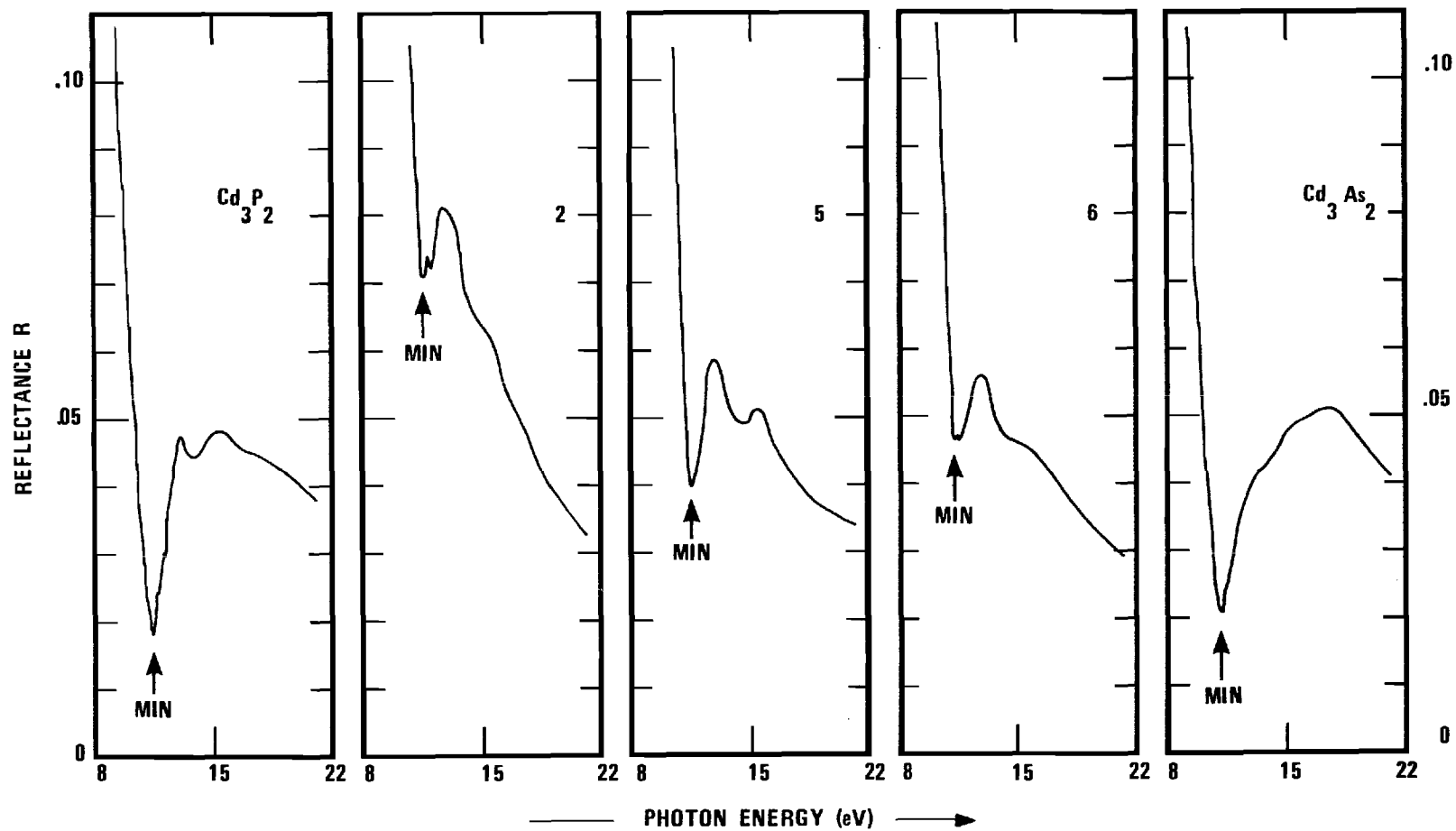


Figure 31. The Reflectance Spectra of the Cd_3As_2 - Cd_3P_2 Alloy System in the Plasmon Region.

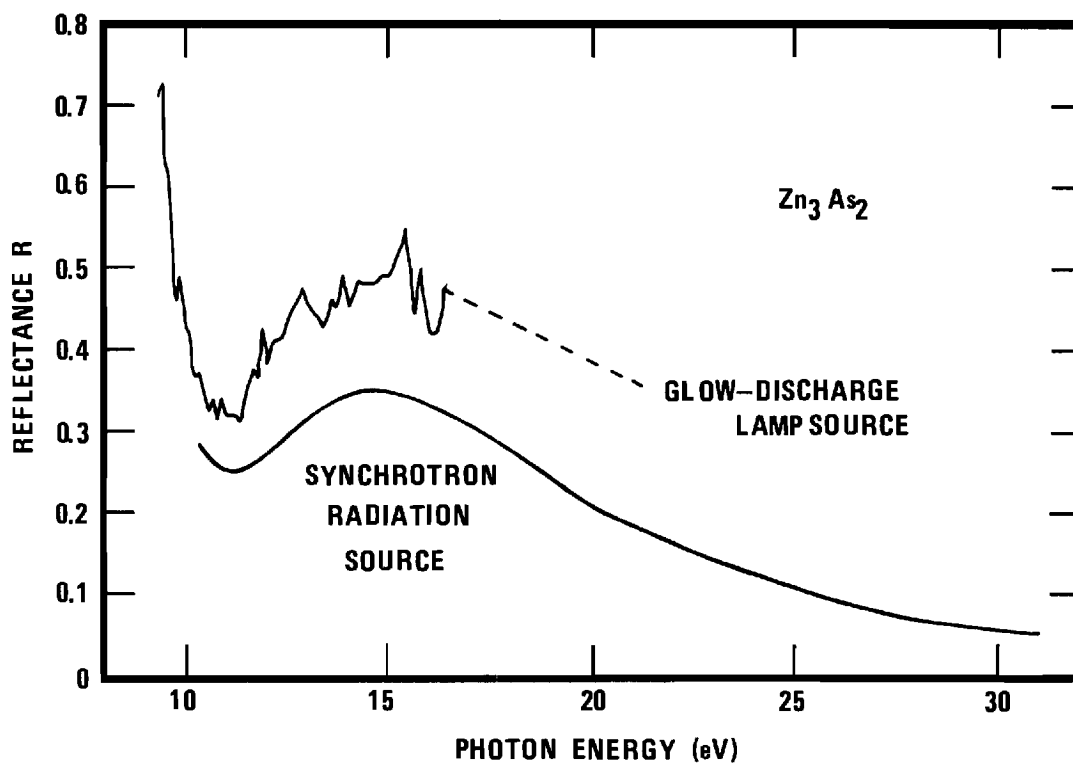
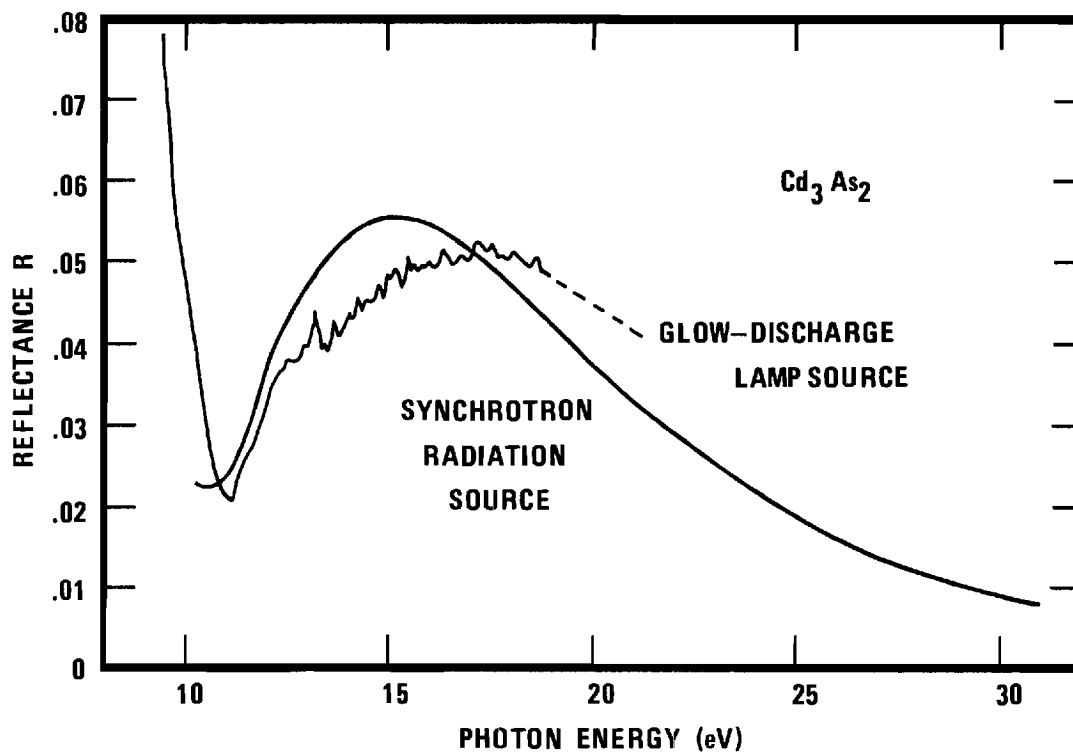


Figure 32. The Reflectance Spectra of Cd_3As_2 and of Zn_3As_2 .

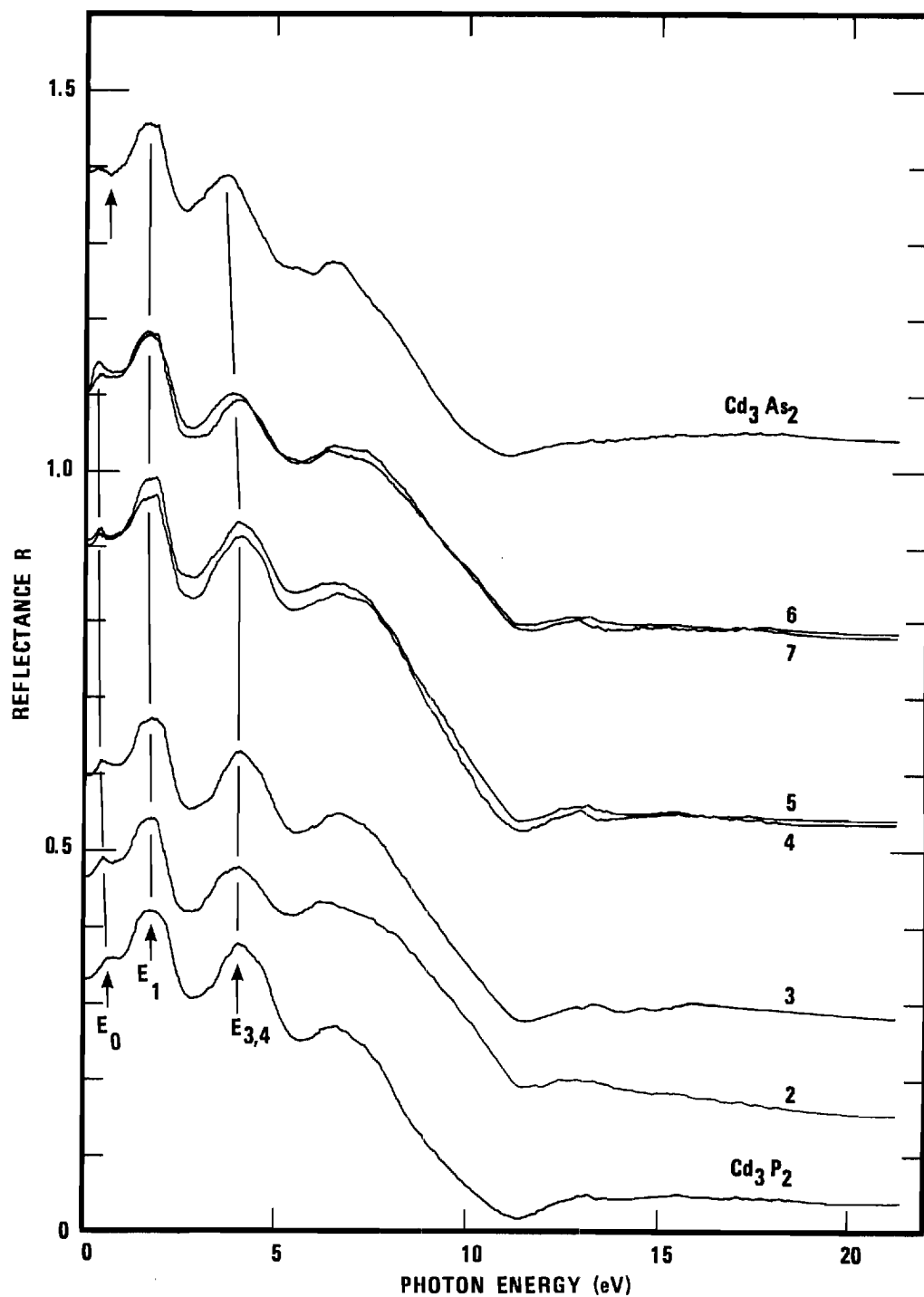


Figure 33. The Reflectance Spectra of the Cd_3As_2 - Cd_3P_2 Alloy System at 297°K (The curves are zero shifted as explained in the text).

position of this peak versus the alloy composition. In accordance with the work (40) of Sobolev et al. on Cd_3As_2 , we label this peak E_1 . The more refined data of Sobolev has shown this peak to be split by approximately 0.2 eV (see Figure 36). The center of gravity of our peak for Cd_3As_2 agrees well with Lin-Chung's B.S. calculation. The corresponding peak for Cd_3P_2 agrees poorly with the respective B.S. calculation. See Table 5 for a comparison of these observed peaks with the B.S. calculations. The probable assignments are made by analogy to the zinc-blende III-V compounds (for example, GaAs).

The doublet character of this peak in Cd_3As_2 is presumably due to the spin-orbit splitting of the upper valence band (Λ_3) along the Λ direction. (Recall that Lin-Chung's calculations were nonrelativistic when referring to Figure 5; only the single group notation is used herein.) This upper valence band is p-like about the As atoms. A good estimate of the spin-orbit splitting (90,91,92) of the upper valence band at the Γ point can be obtained from the spin-orbit splitting of the states of "p" character of the isolated anion atom (for example, the terms $^2P_{1/2}$ and $^2P_{3/2}$ of AsIII). In going from the isolated anion atom to the solid, the splitting is enhanced by the factor 29/20. Using Moore's tabulation (47) of atomic terms, we thereby obtain 0.10 eV and 0.53 eV for the spin-orbit splitting at Γ in Cd_3P_2 and Cd_3As_2 respectively.

The splitting observed in the reflectance structure (in analogy to III-V compounds) is along the Λ direction. Along this direction the upper valence band is presumably further spin-orbit split. The degree of the latter splitting is two-thirds of the splitting at the Γ point.

We therefore expect the observed splitting of the reflectance peak

Table 5. Probable Assignments, Between 0.7 and 6 eV,
of Interband Transitions

Ref (38)	Peaks	Cd_3As_2		B.S.	Probable
		293°K	77°K	Calculation	Location
	E_1	1.7	1.74	} 1.7 {	$\Lambda_3 \rightarrow \Lambda_1$
	E_1'	1.88	1.90		$\Lambda_3 \rightarrow \Lambda_1$
	E_2	2.86	2.86	2.7	$\Sigma_4 \rightarrow \Sigma_1$
	E_3	3.33	3.26	2.8	$X_5' \rightarrow X_3$
	E_4	3.7	3.7	3.9	$\Lambda_3 \rightarrow \Lambda_1$
	E_5	5.15	---	{ 4.7 5.2	$\Lambda_3 \rightarrow \Lambda_3$
					$X_4' \rightarrow X_i$
Present Results	Peaks	Cd_3As_2		B.S.	Probable
		297°K		Calculation	Location
	E_1	1.7		1.7	$\Lambda_3 \rightarrow \Lambda_1$
	$E_{3,4}$	3.6		{ 2.8 3.9	$X_5' \rightarrow X_3$
					$\Lambda_3 \rightarrow \Lambda_1$
Present Results	Peaks	Cd_3P_2		B.S.	Probable
		297°K		Calculation	Location
	E_1	1.9		2.4	$\Lambda_3 \rightarrow \Lambda_1$
	$E_{3,4}$	4.0		{ 3.9 5.1	$X_5' \rightarrow X_3$
					$\Lambda_3 \rightarrow \Lambda_1$

in the range of 2 eV to be 0.067 eV and 0.35 eV for Cd_3P_2 and Cd_3As_2 , respectively. This estimate of 0.35 eV is in qualitative agreement with the 0.2 eV splitting observed by Sobolev. Had we not encountered difficulties in this region (see below), we may also have been able to resolve this splitting in Cd_3As_2 . However, our estimated splitting of 0.067 eV for Cd_3P_2 would surely be obscured by lifetime broadening at room temperature. It is clear, at any rate, that the contribution to the joint density of states is large along a range of the line from Γ to L, since the bands Λ_1 and Λ_3 are nearly parallel in both Cd_3As_2 and Cd_3P_2 near the L point.

The peak in the range of 4 eV is labeled $E_{3,4}$, since it corresponds to an average of the locations of the peaks E_3 and E_4 found by Sobolev in single-crystal Cd_3As_2 (see Figure 36). In both end-members of this alloy system we assume that the peak E_3 corresponds to the transition $X_5' \rightarrow X_3$ and that E_4 corresponds to $\Lambda_3 \rightarrow \Lambda_1$. In Cd_3P_2 , the nearby transition $\Gamma_{15} \rightarrow \Gamma_{25}$ appears to be as likely an assignment as $\Lambda_3 \rightarrow \Lambda_1$ for peak E_4 . The peak E_2 of Sobolev is not resolved in our data. We assume, therefore, that the peak $E_{3,4}$ merely scales with the composition as shown in Figure 33. If the peak $E_{3,4}$ indeed scales as illustrated with the composition, then our results are in qualitative agreement with the B.S. calculations (see Table 5).

The structure of this peak $E_{3,4}$ represents a strong departure from the corresponding structure in the III-V compounds. In GaAs the similar peak, which is located around 5 eV, is largely associated with the transition $X_5 \rightarrow X_1$. A slightly higher (~ 0.5 eV) satellite is identified with

$X_5 \rightarrow X_3$ and a lower (~ 0.5 eV) energy shoulder is identified with $\Gamma_{15} \rightarrow \Gamma_{15}$ transitions. [We are using the representations which belong to GaAs (93)].

In sharp contrast to this distribution of oscillator strengths in GaAs, we associate vanishingly small oscillator strength with $X_5' \rightarrow X_1$. The B.S. calculations predict $X_5' \rightarrow X_1$ to be at 3.4 eV and 2.7 eV in Cd_3P_2 and Cd_3As_2 , respectively. The assignments of $\Lambda_3 \rightarrow \Lambda_1$ for a contribution to the peak $E_{3,4}$ are nearly zone centered and thus crudely correspond to $\Gamma_{15} \rightarrow \Gamma_{15}$ in GaAs. However in the $\text{Cd}_3\text{As}_2 - \text{Cd}_3\text{P}_2$ system, the transition $\Lambda_3 \rightarrow \Lambda_1$ lies above $X_5' \rightarrow X_3$ (at least in Cd_3As_2), and in GaAs the transition $\Gamma_{15} \rightarrow \Gamma_{15}$ lies below $X_5 \rightarrow X_1$.

We refrain from commenting at length on the structure, or rather our lack of it, between peak $E_{3,4}$ and the rise in reflectance at 11.0 eV. On a gross scale, this decrease in reflectance is similar to that found in the III-V compounds and corresponds to the near exhaustion of the f-sum rule for interband transitions (94). This overall decrease in reflectance typically signals the onset of the plasmon region. When the optical constants are generated below, we shall find a broad peak in the characteristic energy loss function in the range of 9.5 eV for all members of this alloy system.

Figure 31 clearly shows that all samples exhibit a sharp increase in the reflectance at approximately 11.0 eV. Since the bonding in these alloys appears to have a large ionic character, it is reasonable to assume that the cadmium 4d atomic levels generate a narrow band below the valence bands (see Figure 6). Lin-Chung has ignored these 4d levels in her B.S. calculations (in a tight-binding picture, charge transfer will lower these levels in the solid). This consideration of the relative position of the

"d" band in these alloys and the fact that this onset at 11.0 eV is independent of alloy composition [recall the formula $\text{Cd}_3(\text{As}_x\text{P}_{1-x})_2$] lead us to the conjecture that this threshold corresponds to the onset of real "d" band-to-conduction-band transitions. The data obtained for Cd_3As_2 and for the sister compound Zn_3As_2 at the University of Wisconsin storage ring provide convincing evidence that this increase in reflectance at 11.0 eV has not been due to an instrumental error (see Figure 32).

In the ionic II-VI compounds CdS, CdSe, and CdTe, Freeouf (95) has recently identified a doublet at about 13.5 eV with the spin-orbit-split transition from the Cd 4d level (the atomic terms are identified in Chapter 1). By way of contrast, rudimentary measurements (96) in this spectral region on elemental cadmium have revealed no semblance of structure.

Errors in the Reflectance Values

It is of singular importance that the absolute value of the reflectance "R" be reasonably known when the optical constants are computed from Equations (152) and (153); it can also be seen from Equation (160) that the phase shift θ is only dependent on the relative value of the reflectance. Consequently, a complete error analysis of the optical constants, which are simple functions of both "R" and θ , is based in principle on the absolute and relative errors of the reflectance values.

Since we have thus far chosen to interpret the reflectance structure directly, and since there exist practically no published values of the optical constants with which to compare results below, we find it convenient to compare our reflectance measurements with the results of others at this stage of the exposition. This comparison will enable a determination of the merit of the present work.

Before any comparative analysis is made, however, we first recount numerous sources of relative and absolute errors in our reflectance measurements. We refrain from making a global estimate of these errors for the reason that a total of four different optical systems have been employed in these measurements.

A graphic display of the relative error in these reflectance measurements is given in Figure 34. Spectral regions or "spans" are labeled in this figure according to Table 4. This particular result for Cd_3As_2 is typical of that for all the samples. The relative error is defined as the difference in two successive reflectance values divided by their arithmetic mean. This error is quite acceptable in spans numbered 4 through 8; however, the errors in spans 3 and 2 are almost as large as the structure which is usually reported for semiconductors in this region. It should be recalled that span 3 was essentially a line spectrum and that data were acquired at equal, wavelength spacing therein. Span 2 was a weak continuum, and the signals were at least an order of magnitude lower than those in span 3. The reflectance (sample-in) signals were usually below the dark current of the PM tube in span 2.

The most obvious source of absolute errors in the reflectance is the poor crystalline quality of the samples (see Table 3). The cracks which occur in these samples account for sizeable (5-15 percent) portions of the irradiated surfaces. Had the data been uniformly acquired in time, as discussed in Chapter IV, the compensation for this source of error would have been straight forward. However, there has been occasion to re-mount and re-run many of the samples for span 3. There has been simply no assurance that these samples were re-mounted as in the other spans.

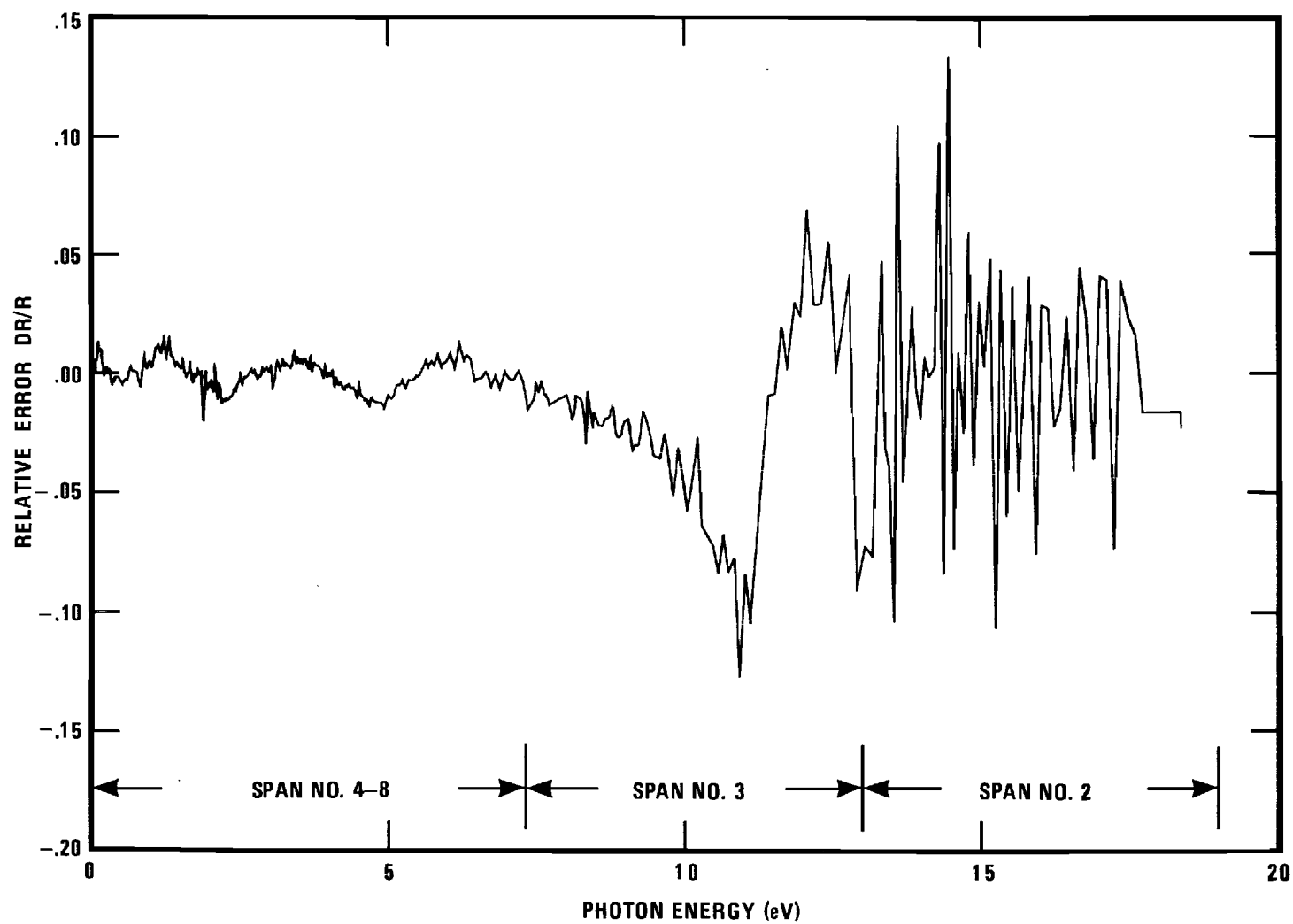


Figure 34. A Display of the Relative Error in the Reflectance Measurements (Spectral regions are labeled according to table 4).

A systematic error in the absolute value of the reflectance appears between spans 3 and 4 (1700 \AA). Table 4 shows that this wavelength corresponds to a change in monochromator and sample-chamber configurations. The shift in absolute value of the reflectance for these two spans is on the order of eight percent. Since the acceptance angle of the detector in span 3 is very much larger than that in span 4, the standard for compensation (forced matching of curves by a multiplicative term) has been taken to be span 3.

An unexpected, systematic, absolute error in the reflectance appears between spans 4 and 5 (3050 \AA), wherein the only alteration is a change of gratings in the monochromator. The shift in absolute value is 8 percent, 8 percent, 12 percent, 12 percent, and 12 percent for samples numbered 2, 3, 5, 6, and 8. Again, a forced matching of the reflectance curves has been performed. We note that samples numbered 4 and 5 are of the same chemical composition and that this artifice of forcing the curves to match in absolute value is such that the altered, reflectance curve for the sample number 5 closely resembles the unaltered curve for number 4. Since both samples numbered 4 and 5 had no cracks, this matching is presumably valid for the other samples.

At still longer wavelength (3600 \AA) between spans 5 and 6, another discontinuity in absolute value occurs. Span 6 marks that wavelength at which the high-vacuum chamber has been vented and the phosphor removed from the light pipe. On several occasions this span has been covered out of the usual sequence. This disruption has required the re-mounting of the sample, so that the absolute shifts which occur here could be taken as a measure of the absolute reproducibility of the reflectance data in

this spectral region. The shifts in the absolute reflectance are + 10 percent, + 8 percent, - 4 percent, - 4 percent, - 5 percent, - 4 percent, and + 15 percent for samples 1, 3, 4, 5, 6, 7, and 8 respectively. Since samples 4, 5, and 7 are of good quality (no visible cracks) and each has a reproducibility of 4 percent, it is therefore reasonable to assume that the larger shifts which have been incurred with the other samples are in part due to their cracks. In particular, two of the larger shifts (+ 8 percent and + 15 percent) have been incurred with the badly cracked samples 3 and 8.

A very large systematic error in the reflectance appears between spans 6 and 7 (6500 \AA), wherein the infrared measurements have commenced. These infrared measurements employ the configuration shown in Figure 7. Presumably this technique of preceding the monochromator with the reflectometer is much more sensitive to the errors of sample or reflectometer alignment, since the monochromator houses a large number of optical elements. The reflectance values uniformly undergo a downward shift of approximately 25 percent. Once again, the reflectance (of span 7) has been compensated to match that of a previous run (span 6).

Less well-defined errors occur in several spectral regions. We could identify these latter errors with "background" corrections. The finer structure (usually two bumps) which appears beyond the point labeled "MIN" in Figure 31 is attributed to such background corrections. These errors indicate a shortcoming of the simple correction terms given in Equation (172). A similar high-background region has been inadvertently created when oil back-streamed into the McPherson monochromator and damaged the 1700 \AA -blazed grating. This contaminated grating, which has

considerably increased the background correction, gives rise to the semblance of finer structure superposed on the broad structure at 7 eV (see Figure 30).

Just above 2 eV (6500 Å), background corrections again become considerable when the spectral response of the PM tube begins to drop rapidly. Also when the next span begins in the infrared region, it has been later found that a small quantity of the first-pass radiation of the two-pass I.R. monochromator persisted at the exit slit. There is no simple way to account for this error.

Finally, at both 0.15 and 0.20 eV strong, molecular-absorption lines obscure the data. These lines are superposed because the I.R. reflectometer has not been purged (inequality of the light paths for the sample-in and the sample-out configurations).

Returning to the Wisconsin data, we find that the scanning rates and counting rates have been so chosen that the relative accuracy of the curves of Figure 32 is approximately ± 5 percent. This Wisconsin data is plotted directly as it was generated, but there is little confidence in the absolute values of these reflectance curves.

We now continue with the error analysis of the reflectance values by direct comparison of our results with those of others (28,34,38,40). The infrared, plasma-edge, reflectance measurements of Turner *et al.* (34) and of Haidemenakis *et al.* (28) are given in Figure 35 along with the author's results for Cd_3As_2 . Better agreement in the absolute value of the reflectance is had with the data of Reference (34).

The shortcomings of the present results are readily apparent in the range of 0.1 eV (as discussed above). At 0.25 eV, the percentage error

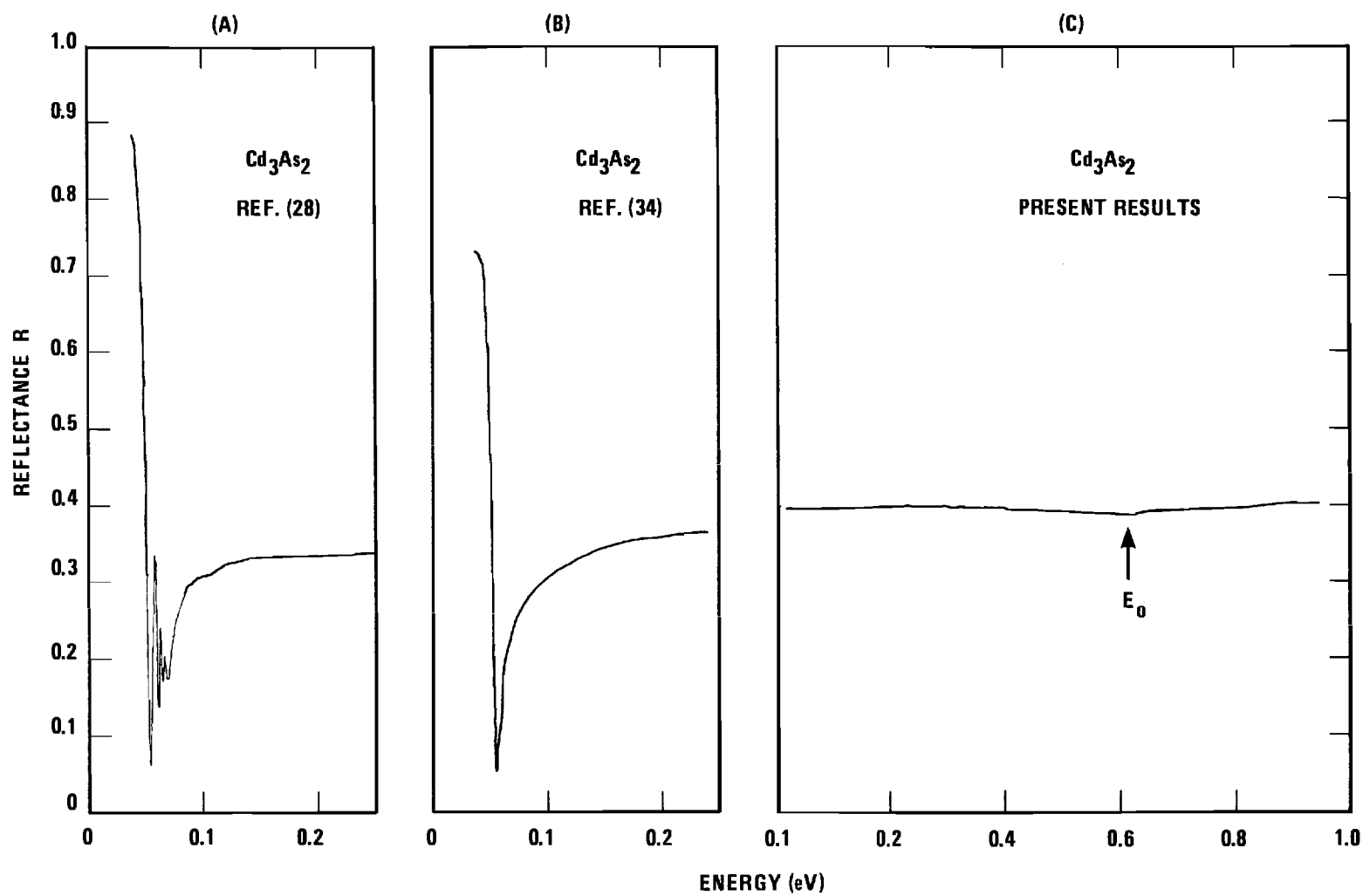


Figure 35. Relation of (C) the Infrared Results to the Plasma-Edge-Reflectance Measurements of (A) Reference (28) and of (B) Reference (34).

of the present results with respect to those of Reference (34), is + 8 percent. Note the strong similarity of this infrared plasma edge with the ultraviolet plasma edge of Figure 31.

It is convenient at this point to digress, in order to define the "optical" dielectric constant. If the assumptions be made that the room temperature gap of Cd_3As_2 is quite small (~ 0 eV), that the Reststrahlen absorption bands are energetically lower than the region of interest, and that the fundamental-absorption edge is not reached until say 0.6 eV (see Chapter I) then we may rewrite the classical Equation (215) of Appendix A as follows

$$\tilde{\kappa} = \kappa_{\infty} \left[1 - \frac{\omega_1^2}{\omega^2 + \omega\Gamma'} \right] \quad (173)$$

where

$$\omega_1 = \left[\frac{Ne^2}{m\kappa_{\infty}\epsilon_0} \right]^{1/2} \quad (174)$$

is the plasma frequency for a single group of degenerate carriers. Two asymptotic expressions for the reflectance can be immediately obtained by use of Equations (138), (139), (150), and (155); the alternate pairs of approximations to Equation (173) which yield the asymptotic expressions are

$$\omega \gg \omega_1, \Gamma' \quad (175)$$

and

$$\omega \ll \omega_1, \Gamma' . \quad (176)$$

The low-frequency approximation gives the Drude dependence for the reflectance. The high-frequency approximation is such that the asymptotic expression for the reflectance decreases with decreasing energy. So a minimum in the reflectance must exist in the range of angular frequency ω_1 . Figure 35 shows that both Reference (28) and (34) have found this minimum at 0.05 eV.

For all members of this alloy system, we shall subsequently define the "optical" dielectric constant $\kappa_1(0)$ to be the dielectric constant between the Reststrahlen bands or the infrared plasma edge and the fundamental-absorption edge. We have just seen that such a definition is compatible with the optical properties of Cd_3As_2 , since the photon-energy interval between the plasma edge and the fundamental edge is so large.

At higher photon energy we compare our reflectance measurements for Cd_3As_2 with those of Sobolev et al. (40) in Figure 36. The curves labeled "B" and "C" are equally zero-shifted as indicated to prevent overlap. The measurements of Reference (40) have been performed on single, unoriented crystals and no error estimates have been provided. His 293°K data is discontinuous not only in absolute magnitude, but also in shape. (Our data suffered background problems, as discussed above, in the encircled region of Figure 36.) At 1.6 eV our data has an absolute error of + 21 percent with respect to the reflectance data of Reference (40). It is difficult to account for an absolute error of that magnitude and sign, since Cd_3As_2 (sample number 8) was badly cracked. Presumably the data

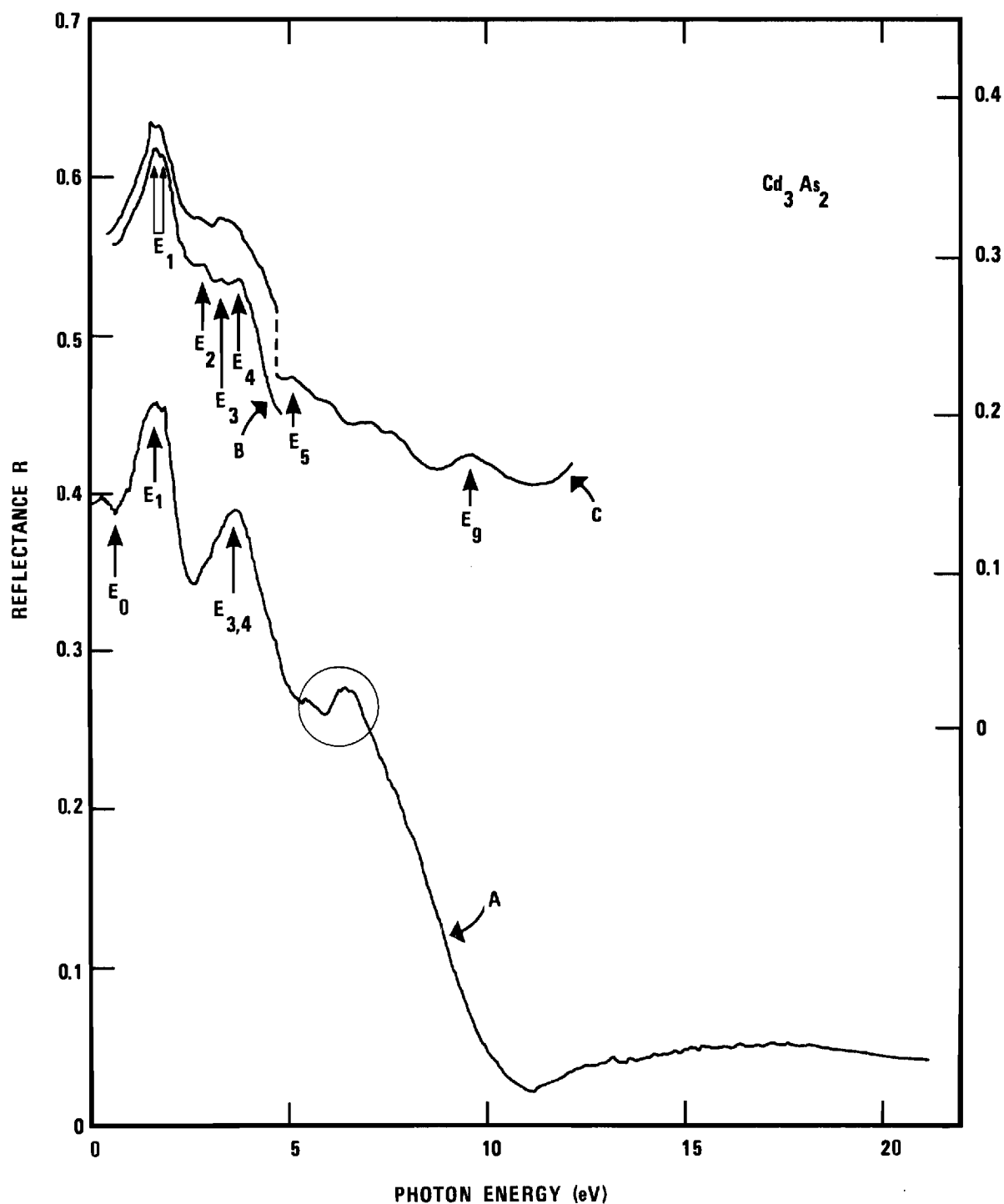


Figure 36. Relation of (A) the Present Results to (B) the 77°K Data and to (C) the 293°K Data of Reference (40) (The upper curves are zero shifted).

of Reference (40) is not well disposed to an absolute scale.

When the data of Figure 36 are inspected more closely, it is seen that our structure is poorly defined relative to that of Reference (40). We can only assume that this lack of definition is due to the poor crystalline quality or that the damaged layer incurred during the mechanical polishing has not been removed by the etchant. Between 5 and 12 eV, Reference (40) also obtained a series of peaks labeled E_5 through E_9 .

Sobolev et al. (38) has also performed rudimentary reflectance measurements on Cd_3P_2 . Figure 37 displays the present results for Cd_3P_2 and those of Reference (38), whose curve is given in arbitrary units. Their peak at approximately 4 eV is reasonable in view of our results. Note the strong similarity of this peak in our results for all members of this alloy system in Figure 27. The fact that Reference (38) has used a polycrystalline sample of Cd_3P_2 leads us to believe that the departure of our results from those (on single crystals) of Reference (40) in Figure 36 is attributable to a polycrystalline surface of our prepared samples. The remaining portion of their data on Cd_3P_2 is unreasonable.

Optical Constants and Further Interpretation

As described in Chapter II, we obtain the optical constants "n" and "k" from Equations (152) and (153), which are strictly correct for normal incidence. The errors introduced by the assumption of normal incidence are far less than the absolute error associated with our primary data (97). Furthermore, these Equations (152) and (153) do not account for anisotropy. Again we observe that our data appears to be representative of a polycrystalline surface so that the question of anisotropy becomes academic.

Usually when the Kramers-Kronig dispersion integral [see Equations (158-61)] is performed, an assumed form for the reflectance "R" must be used above the highest photon energy investigated. In semiconductors and insulators this assumed contribution to the calculated phase shift θ is then adjusted, by choosing the upper limit of the integral, so that the phase shift vanishes below the fundamental band gap \mathcal{E}_g . There are worthy alternatives (98,99) to this procedure; however, in large, we have adopted this more usual method.

Our assumed form for the reflectance above 21 eV, moreover, is not completely arbitrary. If indeed the absorption above 11 eV is due mostly to the Cd 4d levels, then the reflectance curve of Figure 32 for Cd_3As_2 provides an "assumed" form for all members of this alloy system. The analytic form which therefore describes the reflectance of all the alloys above 21 eV has been assumed to be

$$R(E) = R(21 \text{ eV}) \exp[-0.111(E - 21 \text{ eV})] . \quad (177)$$

That portion of the reflectance data below the adjusted, upper limit has been numerically integrated by means of a computer program kindly furnished by Shay (100). The integration is performed in such a manner that the only approximation involved is the assumption that the straight-line segments between data points accurately represent the true reflectance curve.

With the exception of samples numbers 6 and 7, the upper energy limit to the integral has been progressively decreased until the phase shift vanished. The practical "zero" for this vanishing has been

arbitrarily chosen to be 0.015 radians ($\sim 1^\circ$). The gap energies \mathcal{E}_g at which the phase shifts vanish are the room-temperature gaps 0.135, 0.175, 0.175, 0.233, 0.233, 0.37, 0.457, and 0.51 eV for samples numbers 8 through 1, respectively (12). The resultant values of the upper energy limits to the phase shift integral are 32.5, 22.5, 37.5, 62.5, 85.0, 75.0, 75.0, and 70 eV for samples numbers 1 through 8, respectively.

The energy limit of 22.5 eV for sample number 2 indicates the presence of a systematic error, since no sizeable extrapolation has been found acceptable. Figure 30 shows that in the plasmon region (~ 9 eV) the reflectance for sample number 2 is much higher than the reflectance of the other alloys. The upper energy limits of 75.0 eV for samples numbers 6 and 7 will be further discussed below. We merely remark here that the difficulty encountered with the choice of a limit has arisen since the relative error of the reflectance data in the range of their gap energies of 0.175 eV is large, as discussed above. This technique of forcing the phase shift to be zero below the fundamental gap \mathcal{E}_g is obviously very sensitive to the relative error of the reflectance in the range of the gap.

The results of the Kramers-Kronig dispersion integrals are conveniently displayed in the form of curves for the dual quantities "n" and "k". These curves are presented in Figure 38. The zero shifting for either family of curves is in the successive amount of one unit.

At this point of the discussion, it is convenient to compare our results for "n" and "k" with those of others for Cd_3As_2 . Haidemenakis et al. (28) obtained the value of 4.04 for "n", by fitting Equation (173) to their data of Figure 35 ($n_\infty = \kappa_\infty^{1/2}$). We have obtained at an energy

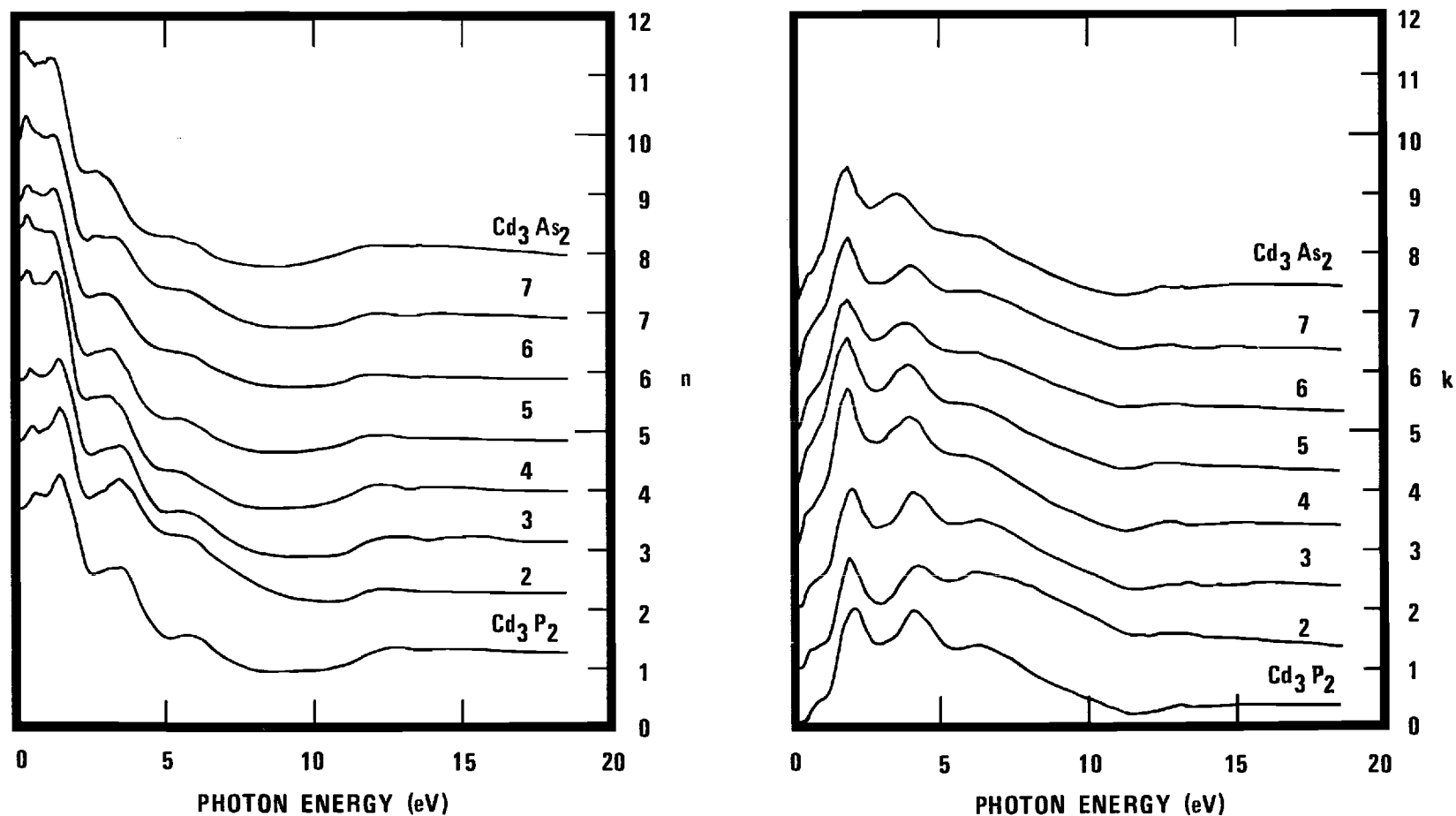


Figure 38. The Optical Constants "n" and "k" for the $\text{Cd}_3\text{As}_2\text{-Cd}_3\text{P}_2$ Alloy System (The curves are successively zero shifted in the amount of one unit).

above the IR plasma edge, say 0.4 eV, the value of 4.3 for "n" in Cd_3As_2 . More careful inspection of this same Figure 35 indicates a slight decrease in our reflectance for Cd_3As_2 as a function of increasing energy (below 0.6 eV). This decrease in reflectance manifests itself in Figure 38 as a decrease in "n" as a function of increasing energy in Cd_3As_2 (below 0.6 eV).

For further comparison, Zdanowicz (33) found values of 5.0 for "n" and 0.04 for "k" [$k = c\alpha/2\omega$, from Equation (123)] at 0.413 eV (3 microns). From Equations (150) and (155) these "n, k" values yield a normal-incidence reflectance of 0.44, which is even 10 percent greater than our value (recall that our reflectance was greater than that of References (28) and (34)). More importantly, this transmission work of Zdanowicz leads to an energy dependence for "n" that is opposite ours. In view of this result of Zdanowicz and the results of both References (28) and (34) in Figure 35, we therefore assume that our data for Cd_3As_2 is in error in this spectral region. The cause of the disagreement is unknown to the author.

Also Zdanowicz has found a sharp peak in "n" at about 0.6 eV. This peak has been associated (33,37) with the fundamental-absorption edge. The underlying transition is thought to be zone centered in the real crystal structure ($\Gamma_{15} \rightarrow \Gamma_1$). Our Cd_3As_2 data exhibit only a weak shoulder in "n" at 0.6 eV (see also the reflectance structure labeled E_0 in Figure 35).

Now use is made of the relations given by Equations (140) and (141) to obtain the dual quantities κ_1 and κ_2 , the components of the complex dielectric constant. The families of these quantities are given in Figure 39. As usual, the structure in the reflectance is seen to follow that in the corresponding κ_2 curve. This structure is sensitive to the

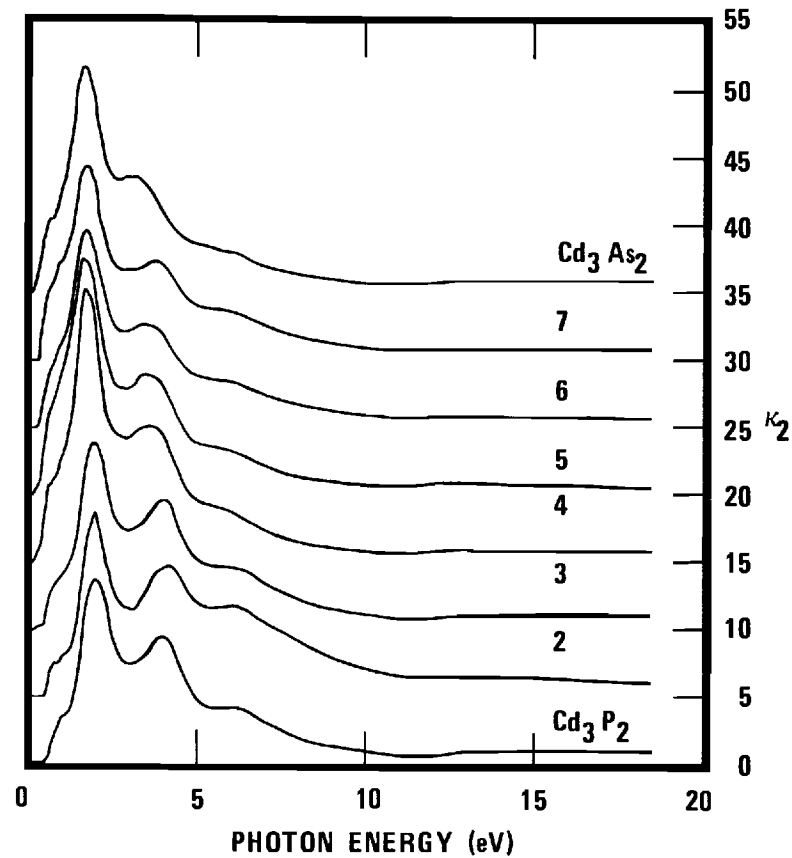
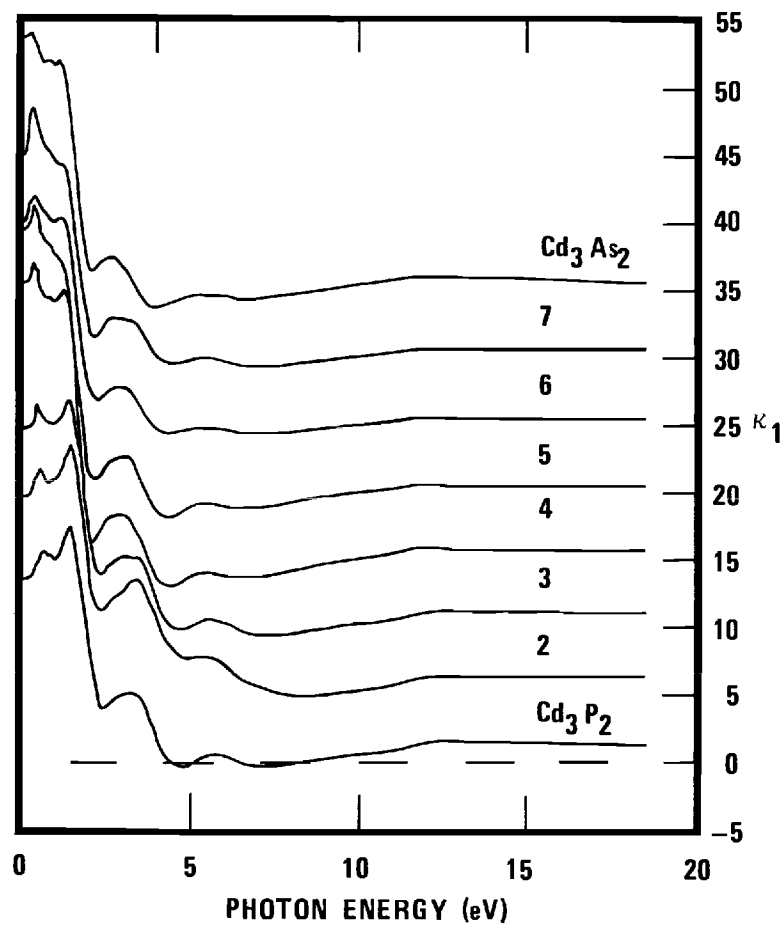


Figure 39. The Dielectric Constants κ_1 and κ_2 for the Cd_3As_2 - Cd_3P_2 Alloy System (The curves are successively zero shifted in the amount of five units).

relative value of reflectance, and precise values of absolute reflectance are not necessary for these correlations. Since κ_2 is the entity which relates directly to the theory of interband transitions, we now complete the justification for the above discussion of the transitions in terms of the primary reflectance data. We further note that the structural correlations given by Equations (146) and (147) are operative. For example, κ_1 is large where the slope of κ_2 is large; κ_2 is large where the slope of κ_1 is large and negative.

We now turn our attention to the structure below 0.7 eV. The structure in this particular region is sufficiently well defined as to be amenable to a description in terms of the joint density of states; that is, we believe that we recognize a couple of the characteristic shapes in κ_2 . As discussed in Chapter II, these characteristic shapes resemble four basic forms (M_0 , M_1 , M_2 , and M_4) of the joint density of states in the range of allowed transitions at critical points which are also symmetry points. This structure in κ_1 and κ_2 , along with the reflectance "R" is illustrated in both Figures 40 and 41.

With the exception of Cd_3As_2 , we have marked two discontinuities in the slopes of the κ_2 curves. The solid arrow locates what appears to be an M_0 critical point, and the dotted arrow locates what appears to be an M_1 critical point. In the case of Cd_3As_2 , the dotted line appears to locate an M_0 critical point; however, we recall, from above, that we have encountered serious relative errors in our Cd_3As_2 data in this region.

We have been aided in the determination of the location of the M_0 critical points by the room-temperature gaps \mathcal{E}_g of Wagner et al. (12). The underlying transition is $\Gamma_{15} \rightarrow \Gamma_1$, according to Lin-Chung's B.S.

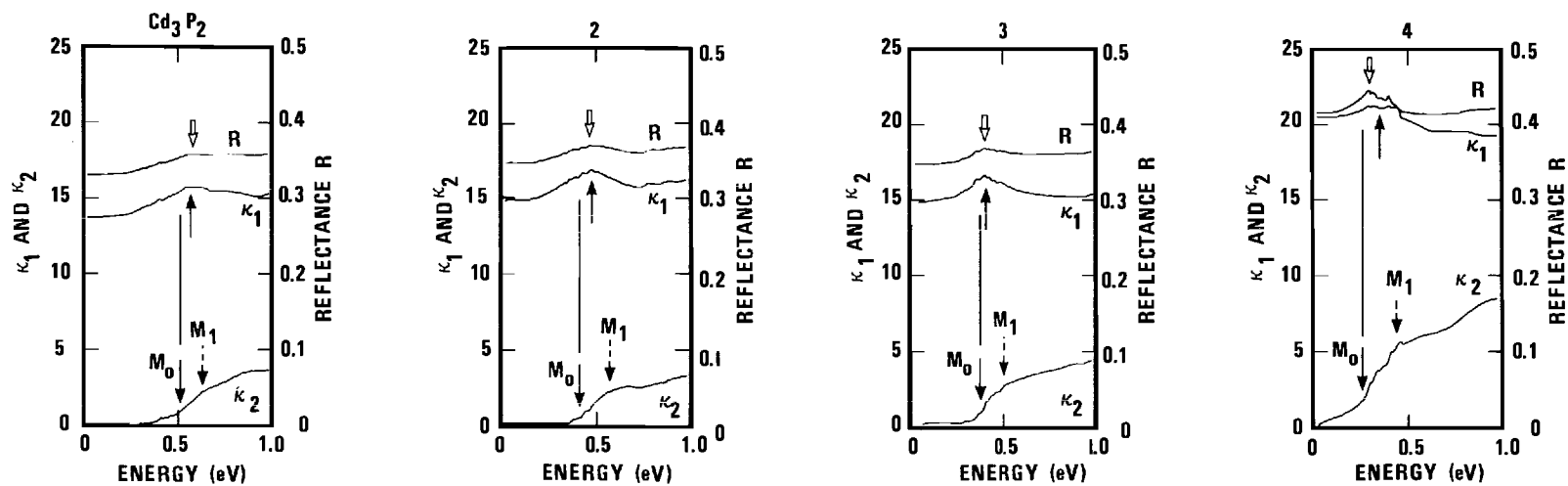


Figure 40. Dielectric Constants for Samples One through Four.

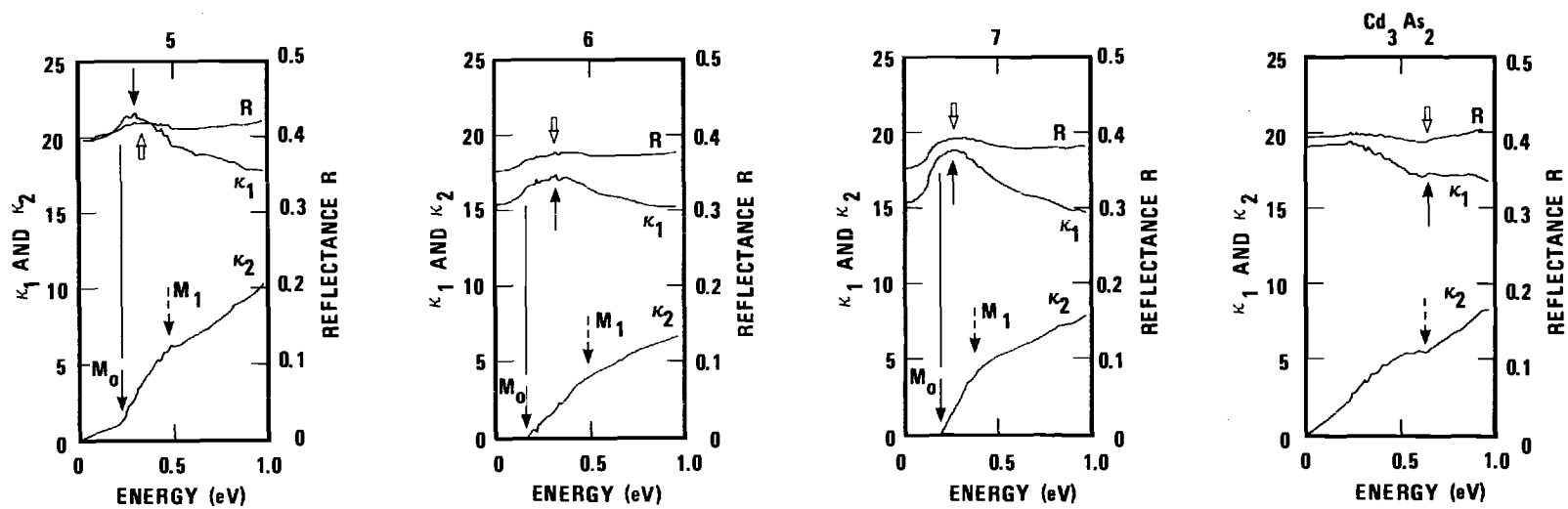


Figure 41. Dielectric Constants for Samples Five through Eight.

calculations. Figure 42 gives a plot of the location of this M_0 critical point as a function of the alloy composition. Note the good agreement with the transmission edges found by Reference (12). Our tentative location of the M_1 critical points may represent a new contribution to the knowledge of the band structure of these alloys.

These critical-point identifications are made in the following manner. The sharp rise in the κ_2 curves at the point located by the solid arrow is characteristic of an M_0 critical point (58). Were this M_0 critical point the only nearby contribution to the joint density of states, one would further expect κ_1 (and "R", since "k" is small here) to peak at the same location. We observe that in all cases, except for Cd_3As_2 , the κ_1 curve peaks above the location of the M_0 critical point. An explanation of this relative shift in structure is readily obtained if the change in slope of the κ_2 curves, located by the dotted lines, is due to an M_1 critical point. An M_1 critical point gives rise to peaking of the κ_1 curve slightly below the location of the M_1 critical point (101). Therefore, we find that our interpretation of two nearby critical points, M_0 and M_1 , contributing to a peaking of κ_1 (and "R") between the location of these critical points is quite consistent with our dielectric constants.

The location of the M_1 critical point is in qualitative agreement with Lin-Chung's B.S. calculations. The X point and the Γ point of the hypothetical structures are equivalent in the real crystal structure: the X point becomes a Γ point. We, therefore, envisage the direct transitions in the real structure giving rise to the M_1 critical point to be $\Gamma_{15} \rightarrow X_1$ in these alloys. We are unable to identify the exact type of critical point in Cd_3As_2 , but we assume the same transition is involved. Lin-Chung

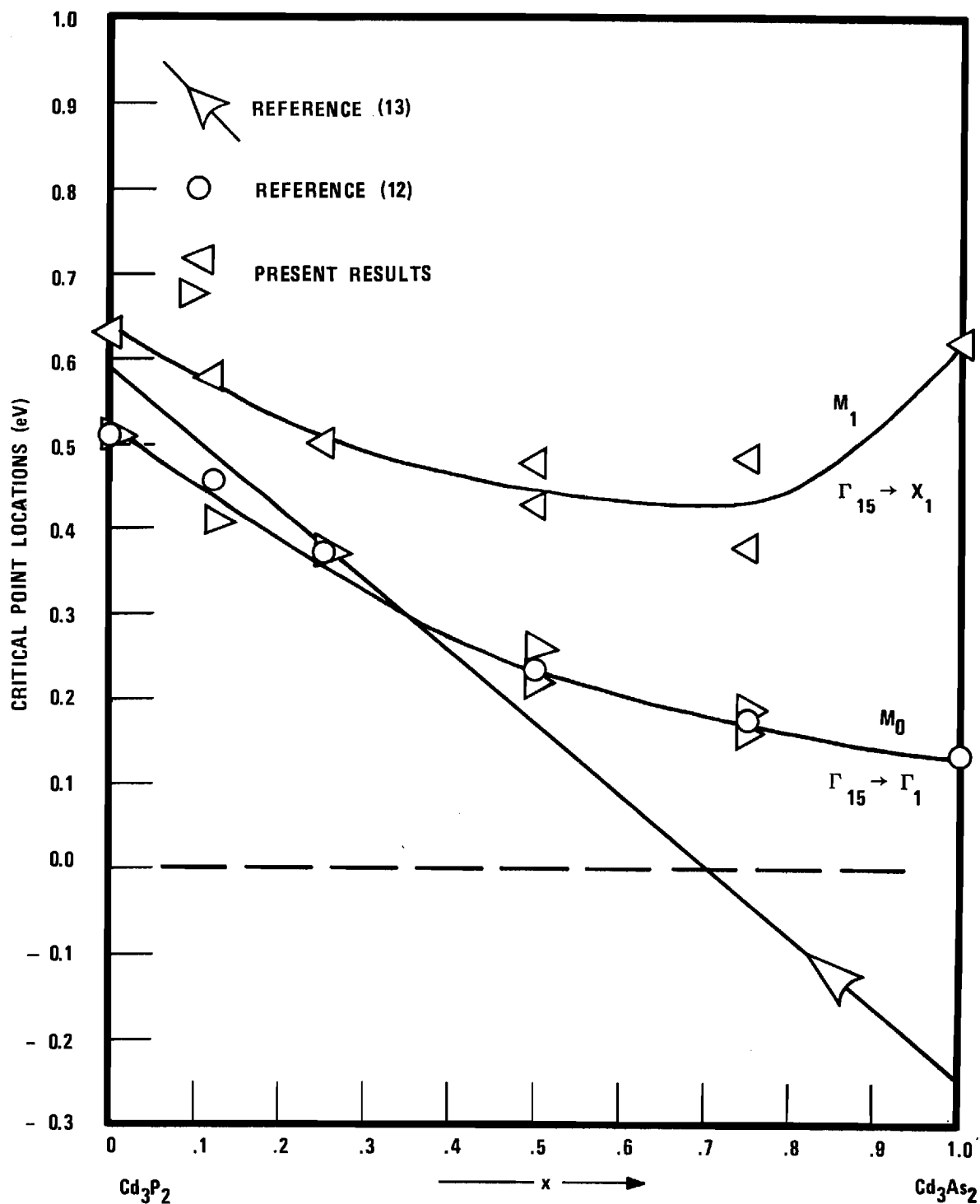


Figure 42. Location of the Band-Edge Critical Points as Determined by the Structure in κ_2 .

has calculated this transition $\Gamma_{15} \rightarrow X_1$ to be of energy 1.2 eV in Cd_3As_2 , and believes that it corresponds to the direct gap \mathcal{E}_g found by Zdanowicz (33) at 0.6 eV. In Cd_3P_2 , she calculated the transition $\Gamma_{15} \rightarrow X_1$ to be of energy 1.875 eV. We find this transition at 0.63 eV in Cd_3P_2 and therefore have the same qualitative agreement with the B.S. calculations as did Zdanowicz for Cd_3As_2 . Figure 42 also displays the composition dependence of this M_1 critical point, and includes, for reference, the low-temperature gaps given by Equation (16).

Errors in the Optical Constants

A minimum measure of the accuracy of the low-energy dielectric constants is obtained by comparing the optical (~ 0 eV) dielectric constant κ_1 from Figure 39 with $\kappa_1(0)$ of Equation (144). We have integrated this equation by means of the trapezoid rule, and the successive contributions to this integral are depicted in Figure 43, in which these curves are repeatedly zero-shifted in the amount of five units. The similarity to curves of the group IV and III-V compounds is apparent (102). The near saturation at photon energies below 5 eV is evidence that strong interband transitions at critical points below this energy are mainly responsible for the value of the low-energy dielectric constant. The total values of the integrals are taken, arbitrarily, to be the intercepts of the curves with the ordinate at 22 eV.

These total values of $\kappa_1(0)$ are now compared with the optical (~ 0 eV) dielectric constant κ_1 in Figure 44. For reference, the optical dielectric constant of germanium is 16.6. It is seen that the curves differ by approximately ± 10 percent, so we must consider this inconsistency to

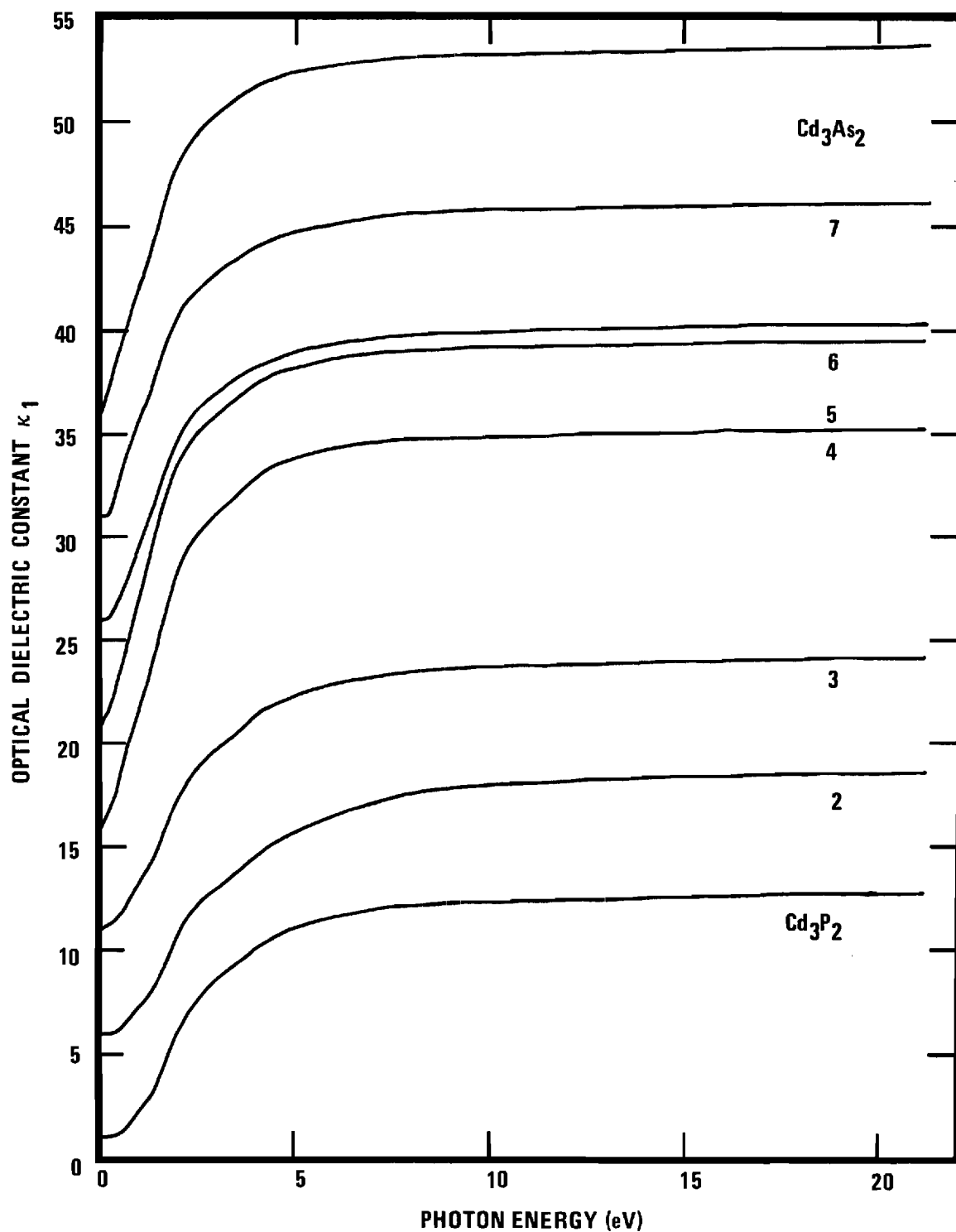


Figure 43. Successive Contributions to the Optical Dielectric Constant $\kappa_1(0)$ (The curves are repeatedly zero shifted in the amount of five units).

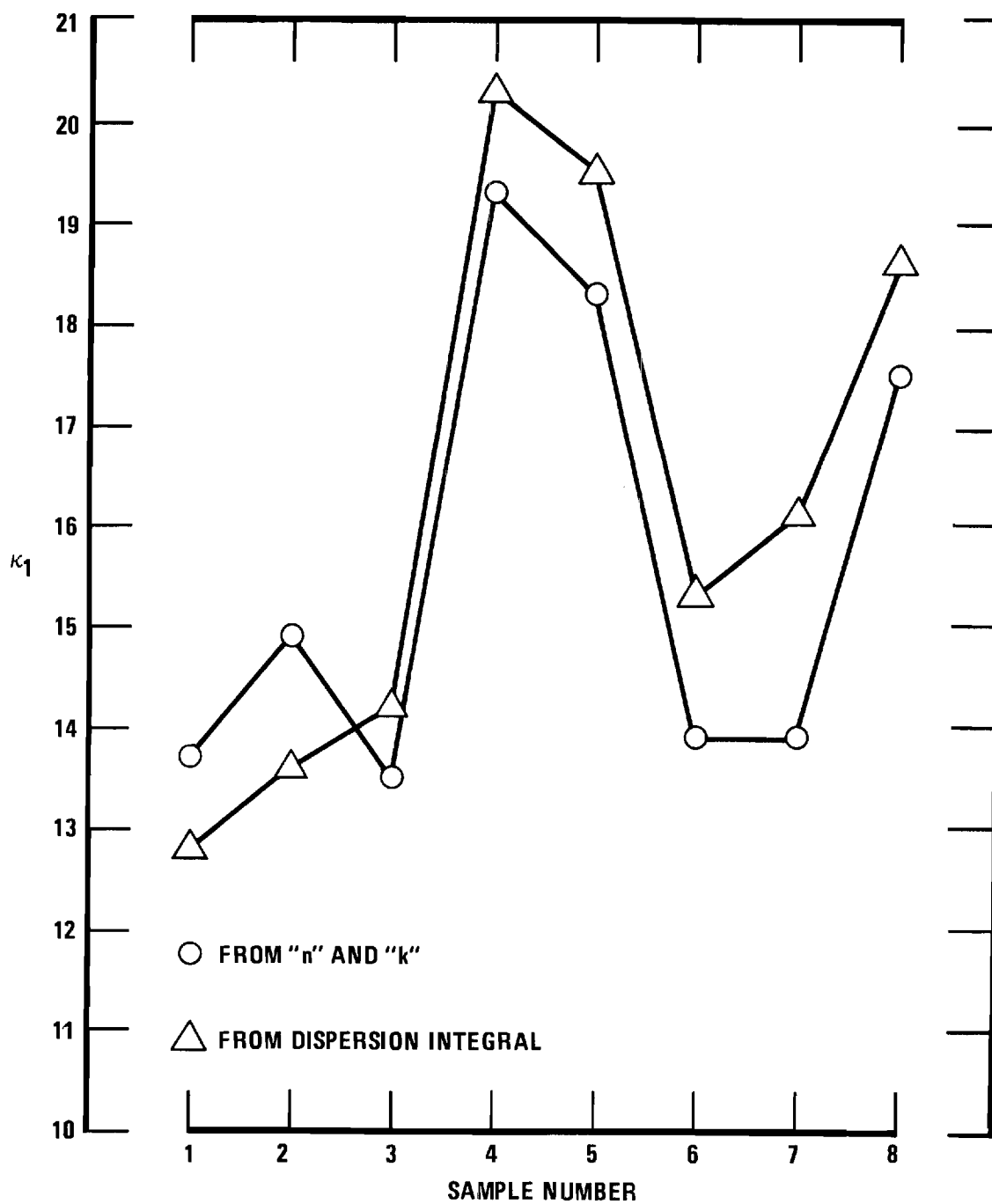


Figure 44. Consistency of the Optical Dielectric Constants.

be a minimum estimate of the error in the dielectric constants in the low-energy region. We further admit of possibly large absolute errors, ± 15 percent, in the reflectance "R" in this same region (see above). Since θ has been assumed to vanish here, Equation (152) yields a further average contribution of ± 15 percent to the error in κ_1 ($\kappa_1 = n^2$ in this case). This is an "average" contribution, since we have used the average value of the reflectance, 0.37, for these samples. By combining these two sources of error in κ_1 , we finally obtain the estimate of ± 18 percent for the percentage error in our optical dielectric constants.

Similar estimates could be made for higher-energy regions. Let it suffice to say that in view of the above comparison (see Figure 35) of our primary data with that of Reference (40) for Cd_3As_2 , particularly above 6 eV, we believe our optical constants are only qualitatively correct. At any rate, they are surely not representative of a single crystal.

The expression ("partial" sum rule)

$$n_{\text{EFF}} = \left[2m/N(\text{he})^2 \right] \int_0^{\mathcal{E}} \mathcal{E}' \kappa_2(\mathcal{E}') d\mathcal{E}' , \quad (178)$$

or in practical units

$$n_{\text{EFF}} = \left(0.04617 \times 10^{22} \text{ cm}^{-3}/N \right) \int_0^{\mathcal{E}} \mathcal{E}' \kappa_2(\mathcal{E}') d\mathcal{E}' , \quad (179)$$

yields an effective number of free electrons contributing to the optical properties over a finite range 0 to \mathcal{E} (102). "N" is the atomic density of the solid in units of cm^{-3} . If we again cavalierly disregard the

possible anisotropy of these samples, we may apply this expression to our results for κ_2 . The successive values of n_{EFF} which we have obtained are displayed in Figure 45. The atomic density "N" has been obtained by making use of the number of formula units "Z" ($Z = 32$) per unit cell and Equation (8).

Since there are exactly 3.2 valence electrons per atom, we are somewhat surprised to find that these curves nearly saturate (before the rise at 12 eV) at a value of approximately 2.2. In particular, since the cadmium d-band transitions are expected to overlap nearly the tail of the fundamental-absorption spectra in these alloys, we should look for an enhancement of n_{EFF} over the valence electron contribution of 3.2. This enhancement has not been found to be the case, and we attribute this fact to reflectance values which are low in the spectral region above 6 eV.

Sample number 2 appears to represent a favorable counter example to the failure of n_{EFF} to reach higher level; however, this sample was found to be inconsistent with our Kramers-Kronig extrapolation scheme (see above). It is appropriate to mention here that the high-energy limits to the phase-shift integral for samples numbers 6 and 7 were chosen so their respective values of n_{EFF} were consistent with the other members of this alloy system.

As mentioned above, the f-sum rule for interband transitions which involve the valence bands is nearly exhausted in the range of 9 eV. This remark is complimented by these curves of n_{EFF} . It is also usually the case that these valence electrons, in conjunction with d-band contributions, are able to participate in bulk plasmons (see Appendix A). Figure 46 in

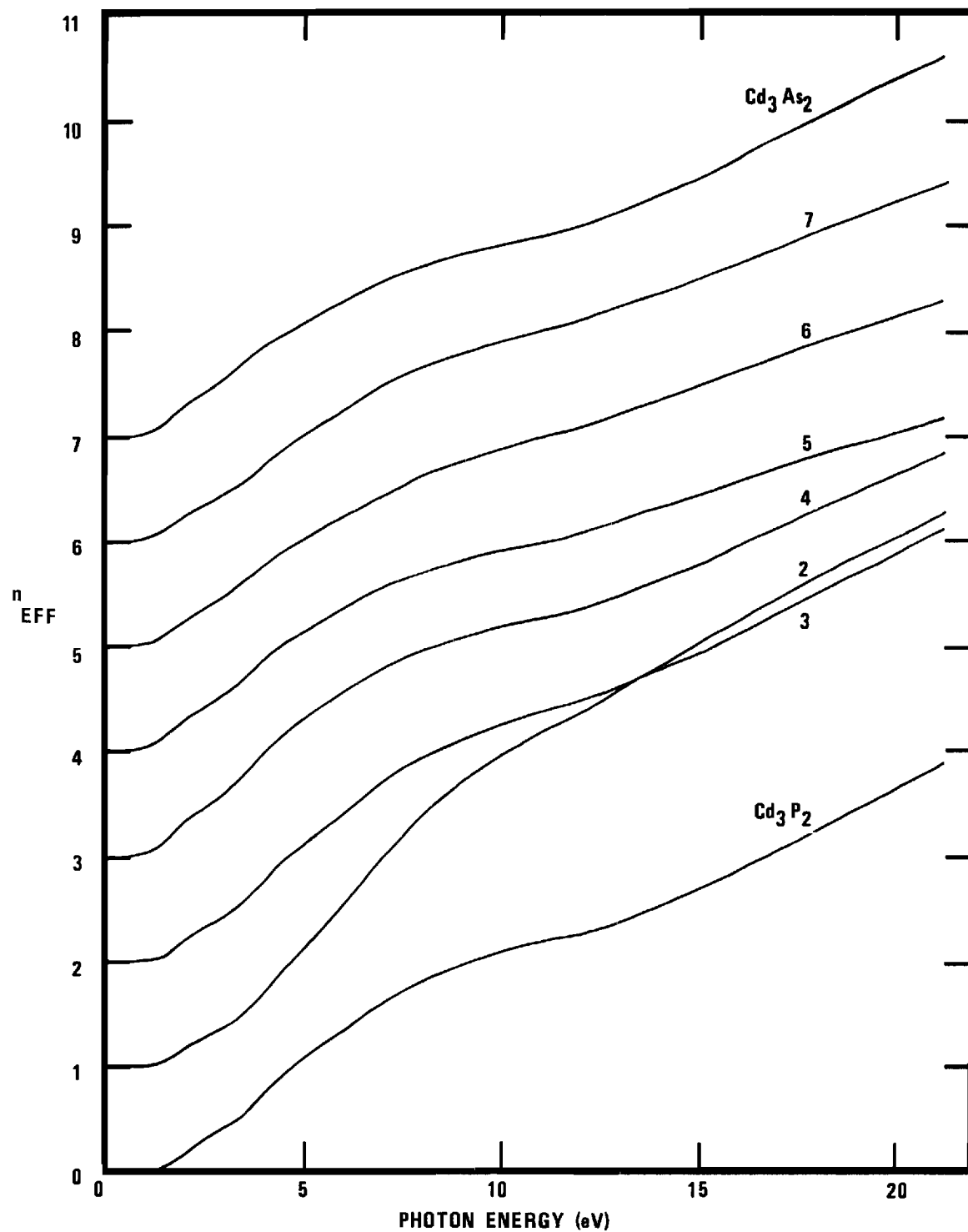


Figure 45. Successive Contributions to n_{EFF} (The curves are repeatedly zero shifted in the amount of one unit).

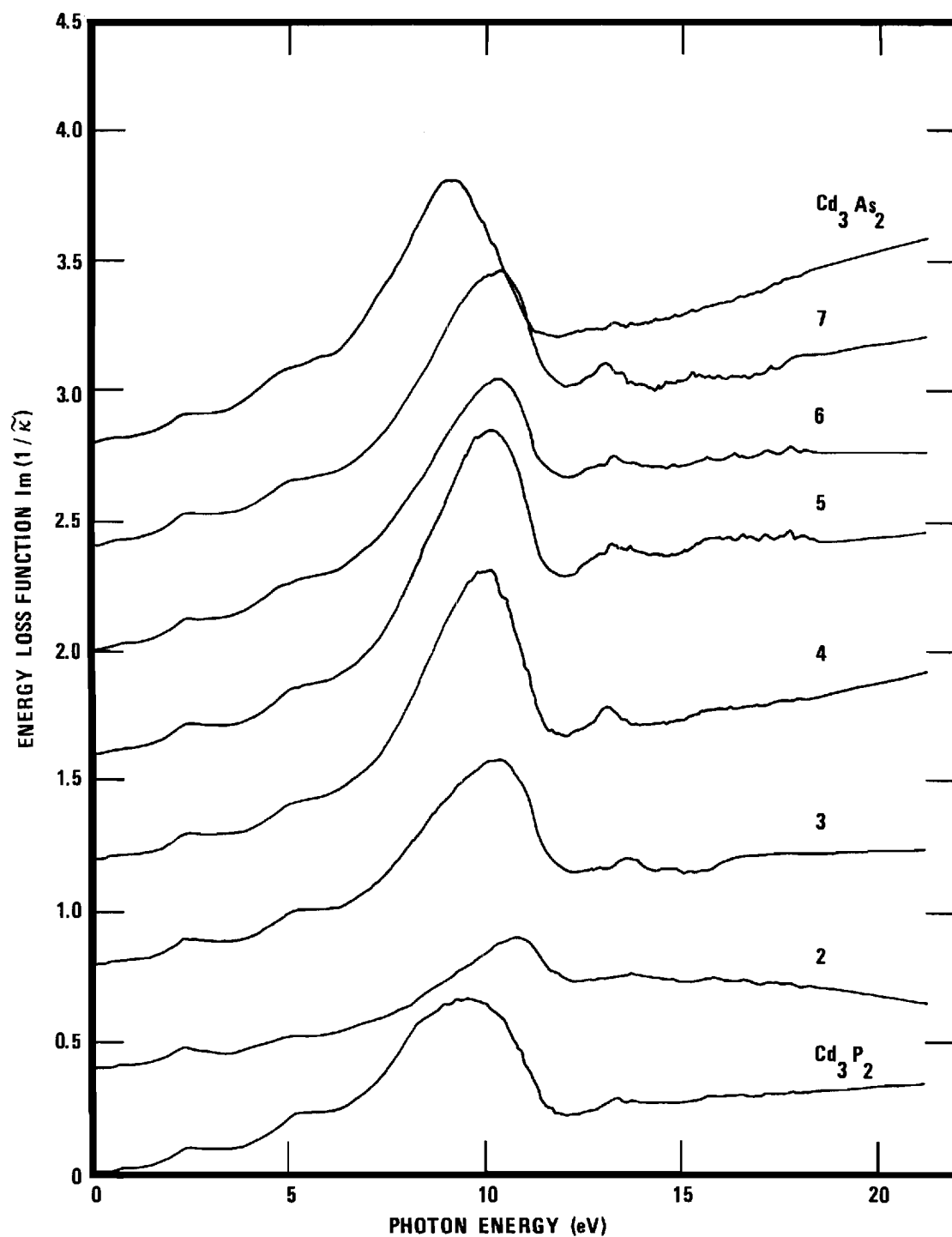


Figure 46. Characteristic Energy Loss Function as Derived from the Dielectric Constants (The curves are successively zero shifted in the amount of 0.4 units).

fact shows a broad peak in the characteristic-energy-loss function $\text{Im}(1/\tilde{\kappa})$. If our primary data indeed drop too fast in this photon-energy range, then these peaks provide a lower estimate of approximately 9.5 eV for the plasmon energy. For comparison, the free-electron plasmon energy, due to the valence electrons only, is 13.13 eV for Cd_3As_2 . This latter number is given for crude comparison only: it is well known that not only do the d-bands enhance the effective number of electrons available to contribute to a plasmon, but that the d-bands (electrons) provide a measure of shielding of the Coulomb interactions.

Furthermore, the dependence of the plasmon energy on the volume of the unit cells is weak ($E_p \sim V^{-1/2}$). Since the unit-cell volume change from Cd_3As_2 to Cd_3P_2 is small, we do not list the free-electron plasmon energies for the other alloys. The step-like structure around 2 and 4 eV corresponds to the single-electron excitations discussed above.

Summary

In this chapter several aspects of the optical properties, as related to the electronic structure, of these alloys have been discussed. We summarize here some of the main results that we have obtained.

The near-normal-incidence reflectance spectra were presented in Figure 30. The high-energy limit of our measurements was extended to 30 eV for the end-member Cd_3As_2 (see Figure 32). The relative error of data was large at the low-energy limit (~ 0.1 eV). Comparison with the work of Sobolev et al. on both the single-crystal Cd_3As_2 and poly-crystal Cd_3P_2 led us to the conclusion that our measurements were representative of poly-crystalline prepared surfaces.

Above the fundamental-absorption edge, we compared the reflectance structure directly with the band-structure calculations for Cd_3As_2 and Cd_3P_2 . This reflectance structure was similar to that of III-V compounds in the range of 2 eV. We obtained the estimates of 0.35 eV and 0.067 eV for the separation of the spin-orbit-split transitions near the L point, in Cd_3As_2 and Cd_3P_2 respectively. At 4 eV, the reflectance structure appeared to differ from that of III-V compounds.

The low-energy structure was discussed in terms of the "joint density of states." The joint density of states (actually κ_2) was obtained from the Kramers-Kronig generated optical constants. The optical dielectric constants ranged from 14 to 18 for Cd_3P_2 to Cd_3As_2 , respectively.

The application of Philipp and Ehrenreich's "partial" sum rule yielded values of n_{EFF} which appeared low; this inconsistency suggested that our absolute-reflectance values beyond 6 eV were low.

Although the values of the absolute reflectance effect the application of sum rules and a Kramers-Kronig analysis, the position of structure in the reflectance data remains relatively unchanged. As a consequence, the above results are presented in terms of the chemical shifts of the structure in κ_2 or "R". We present these findings in Figure 47. The upper two curves were obtained from the peaks in the reflectance data; the lower two curves, from the structure in κ_2 . The data presented in Figure 47 suggests a sharp change of transitions involved at an anion concentration of 50 percent in the energy range of 4 eV. Other interband transitions seem to change more gradually with anion concentration.

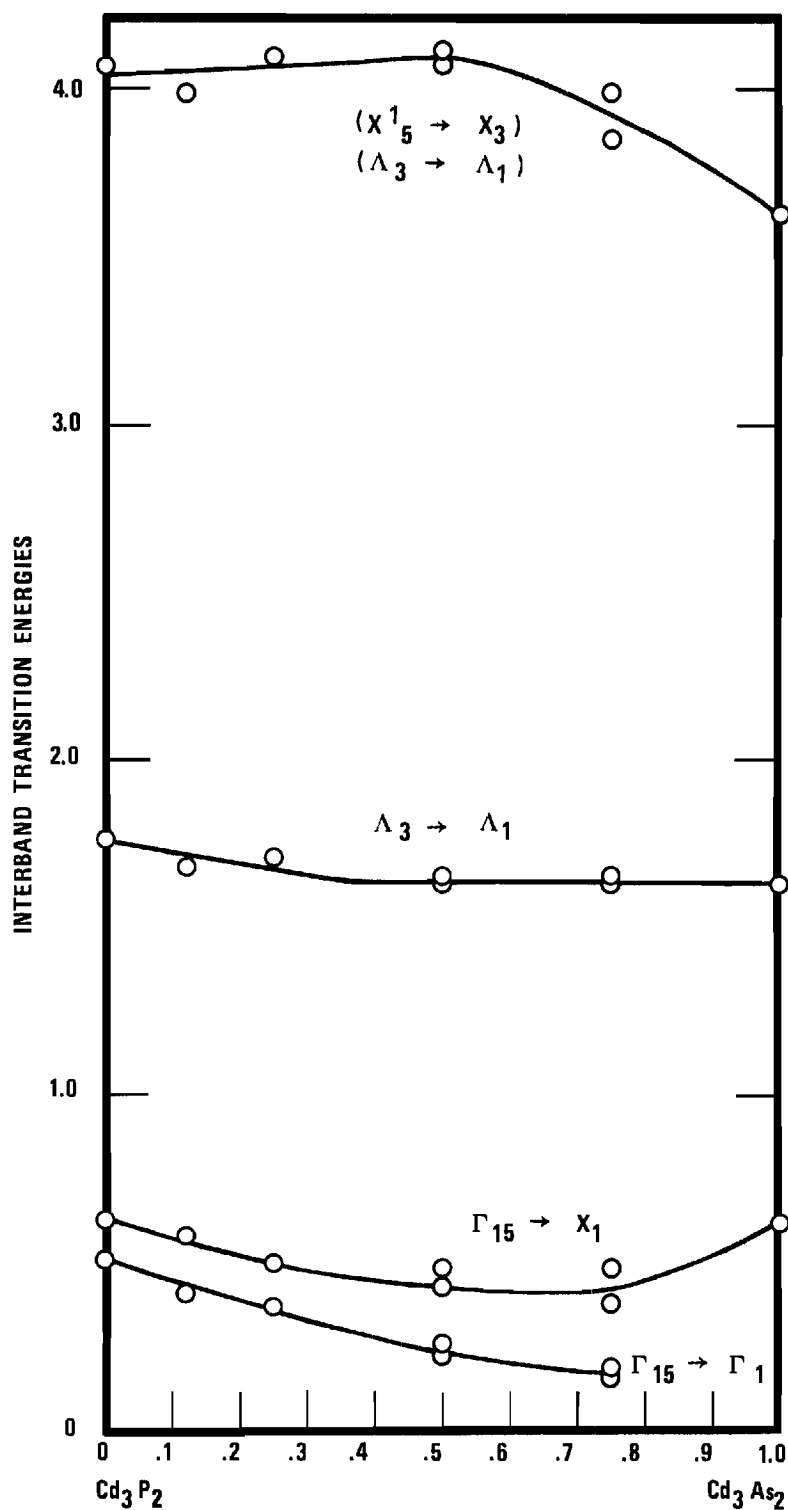


Figure 47. Probable Assignments of Direct Transitions in the Cd_3As_2 - Cd_3P_2 Alloy System.

Recommendations for Further Research

With Figure 47 clearly in mind, it is apparent that we have just begun to unfold the optical properties of these alloys. The infrared region needs more careful study; in particular, verification of our tentative assignment $\Gamma_{15} \rightarrow X_1$ is desirable. More refined data in the range of 2 eV would permit a following of the spin-orbit splitting as a function of composition. As we review the probable assignments in the range of 4 eV, it is clear that our results are limited by the absence of the availability of good crystalline surfaces. To permit a clearer understanding of the underlying transitions therein, much more attention has to be given to the subjects of crystal growth and sample preparation. Finally the elusive, photon-energy range beyond 5 eV requires a combination of improved sample-preparation techniques and a cleaner vacuum environment. Any one of these regions, if carefully investigated at low temperature (77°K), would prove a worthy subject of investigation.

APPENDICES

APPENDIX A

THEORETICAL CONSIDERATIONS

The Classical Oscillator Model for Dielectric Constants

The purpose of this treatment is to review a simple classical model for the interaction of radiation with a group of electronic oscillators as well as to precisely identify the terms which will enter into the equations of motion. We begin with a microscopic picture of a single nonrelativistic particle of mass "m" and charge "e" bound by a spherically symmetric, linear, restoring force $m\omega_0^2 \bar{x}$. Because we are considering steady-state oscillations, we use the Abraham-Lorentz (49) equation

$$m(-\tau \ddot{\bar{x}} + \ddot{\bar{x}} + \Gamma \dot{\bar{x}} + \omega_0^2 \bar{x}) = -e\bar{E}_m(t) \quad (180)$$

where

$$\bar{E}_m(t) = \bar{E}_0 \exp(-i\omega t) , \quad (181)$$

the incident, microscopic electric field in the dipole approximation, provides the driving force. This equation includes, in an average way, radiation damping; the characteristic time τ is given by

$$\tau = \left[1/6\pi\epsilon_0 \right] \left[e^2/(mc^3) \right] . \quad (182)$$

The resistive term $m\Gamma'\dot{\bar{x}}$ will be shown to measure the strength of non-electromagnetic dissipative effects (this is not known a priori). The steady-state (homogeneous) solution to Equation (180) is given by

$$\bar{x} = - (e/m)\bar{E}_0 \exp(-i\omega t) / (\omega_0^2 - \omega^2 - i\omega\Gamma_t) \quad (183)$$

where

$$\Gamma_t(\omega) = \Gamma' + (\omega/\omega_0)^2 \Gamma \quad (184)$$

is called the "total decay constant" or "total width"; the radiative decay constant $\Gamma(60)$ is given by

$$\Gamma = \omega_0^2 \tau. \quad (185)$$

We now introduce several total "cross sections". The accelerated motion described by Equation (183) gives rise to the radiation electric field

$$\bar{E}_{\text{rad}} = [(\mu_0/\epsilon_0)^{1/2}/4\pi] (-e/r) [\hat{n} \times (\hat{n} \times \ddot{\bar{x}})]_{\text{ret}} \quad (186)$$

where

$$\hat{n} = \bar{r}/r = (\bar{x}' - \bar{x}) / |\bar{x}' - \bar{x}| \quad (187)$$

is a unit vector directed from the position \bar{x} of the electron to the

observation point at \bar{x}' , and the bracket is to be evaluated at the retarded time

$$t' = t - r/c . \quad (188)$$

The magnetic induction is related to this radiation electric field by the relation

$$\bar{B} = (\mu_o \epsilon_o)^{1/2} \hat{n} \times \bar{E} . \quad (189)$$

The incident energy flux is given by Equation (121)

$$\langle S \rangle = (c\epsilon_o/2) \bar{E}_o^* \cdot \bar{E}_o \hat{k}_1 . \quad (190)$$

(Recall that we are presently using the microscopic fields.) It is convenient to describe this scattering of the incident radiation by the total scattering cross section

$$\sigma_{sc}(\omega) = \frac{\text{Energy radiated/unit time}}{\text{Incident energy flux}} \quad (191)$$

It follows from Equations (183) and (186) that this scattered radiation is of the same frequency as that of the incident radiation.

The next cross section we introduce is the absorption cross section. We begin with the expression

$$d\mathcal{E}/dt = \int_{-\infty}^{\infty} \bar{E} \cdot \bar{J}_m d^3x' \quad (192)$$

for the rate of doing work on our bound electron, and we use the representation

$$J_m = -ev \delta[\bar{x}' - \bar{x}(t)] \quad (193)$$

for the current density. The dipole approximation is again used for the microscopic field \bar{E}_m , which at this part of the derivation is generalized to the form

$$\bar{E}_m(t) = \int_{-\infty}^{\infty} \tilde{\bar{E}}_m(\omega) e^{-i\omega t} d\omega. \quad (194)$$

The total work done on the electron

$$\Delta\mathcal{E} = \int_{-\infty}^{\infty} dt \int \bar{E}_m \cdot \bar{J}_m d^3x' \quad (195)$$

becomes

$$\Delta\mathcal{E} = -e \int_{-\infty}^{\infty} \bar{v} \cdot \bar{E}_m dt \quad (196)$$

We now also Fourier analyze $\bar{x}(t)$, substitute into the Equation (180), and then obtain the solution

$$\tilde{\bar{x}}(\omega) = - (e/m) \tilde{\bar{E}}(\omega) / (\omega_o^2 - \omega^2 - i\omega\Gamma_t) \quad (197)$$

Compare this Equation with Equation (183). Jackson (49) shows that we finally obtain the result

$$\Delta \mathcal{E} = (e^2/m) \int_0^\infty \left\{ |\tilde{E}_m(\omega)|^2 2\omega^2 \Gamma_t / [(\omega_0^2 - \omega^2)^2 + \omega^2 \Gamma_t^2] \right\} d\omega. \quad (198)$$

We define the energy absorbed per unit frequency interval to be

$$d\mathcal{E}/d\omega = (e^2/m) |\tilde{E}_m(\omega)|^2 2\omega^2 \Gamma_t / [(\omega_0^2 - \omega^2)^2 + \omega^2 \Gamma_t^2], \quad (199)$$

where we now consider $\tilde{E}_m(t)$ to be essentially monochromatic; so we can rewrite this equation in the form

$$d\mathcal{E}/d\omega = (e^2/m) |\tilde{E}_0(\omega)|^2 2\omega^2 \Gamma_t / [(\omega_0^2 - \omega^2)^2 + \omega^2 \Gamma_t^2]. \quad (200)$$

This expression is now formulated in terms of the same incident electric field as used in Equation (181). We describe this absorption of the incident radiation by the absorption cross section

$$\sigma_{\text{abs}}(\omega) = \frac{\text{Energy absorbed/unit frequency}}{\text{Incident energy/unit area-frequency}} \quad (201)$$

The time-averaged incident energy per unit area per unit frequency is given by

$$\langle S \rangle' = 4[\text{sec}^2] \langle S \rangle \quad (202)$$

where $\langle S \rangle$ is given by Equation (190).

The evaluation of Equations (191) and (201) yields the results

$$\sigma_{sc}(\omega) \left\{ \begin{array}{l} = \frac{6\pi(\epsilon_o\mu_o)^{-1}(\omega/\omega_o)^2\Gamma}{(\omega_o^2 - \omega^2)^2 + \omega^2\Gamma_t^2} \end{array} \right\} (\omega/\omega_o)^2\Gamma. \quad (203)$$

$$\sigma_{abs}(\omega) \left\{ \begin{array}{l} \end{array} \right\} \Gamma_t. \quad (204)$$

By comparing Equation (184) with Equations (203) and (204), we are led to the following interpretation.

In the derivation of the cross section for absorption, we began with the microscopic Equation (192), which gave the mechanical energy absorbed by the oscillator; as of yet we have not answered the question of whether it was re-emitted as radiation or dissipated in some other way. The virtue of this derivation is that such questions are answerable; the radiative reaction force $m\tau\ddot{x}$ was introduced into Equation (180) such that field and mechanical energy are simultaneously conserved. These two cross sections have been defined, accordingly, so that their difference is a direct measure of radiation which has been absorbed, but not re-radiated. So we define the "reaction" cross section by the equation

$$\sigma_r(\omega) = \sigma_{abs}(\omega) - \sigma_{sc}(\omega). \quad (205)$$

When use is made of Equation (184), we can summarize the results as follows:

$$\left\{ \begin{array}{l} \sigma_{abs}(\omega) \\ \sigma_{sc}(\omega) \\ \sigma_r(\omega) \end{array} \right\} = 6\pi(\epsilon_o\mu_o)^{-1} \frac{(\omega/\omega_o)^2\Gamma}{(\omega_o^2 - \omega^2)^2 + \omega^2\Gamma_t^2} \left\{ \begin{array}{l} \Gamma_t \\ (\omega/\omega_o)^2\Gamma \\ \Gamma_t \end{array} \right\}. \quad (206)$$

The Classical Polarizability

We proceed to consider the electronic contribution to the induced, molecular polarizability of a solid (59,103). Since the contribution of the damping term $m\Gamma'\ddot{\bar{x}}$ in Equation (180) has been properly interpreted, we may ignore the radiation damping term $-\tau\ddot{\bar{x}}$ in the following discussion (49,104). The solution to Equation (180) becomes

$$\bar{x} = [- (e/m)/(\omega_0^2 - \omega^2 - i\omega\Gamma')] \bar{E}_m. \quad (207)$$

The induced dipole moment is

$$\bar{p}_m = - e\bar{x}, \quad (208)$$

so the molecular polarizability $\tilde{\alpha}$ is given by

$$\tilde{\alpha} = [(e^2/m)/(\omega_0^2 - \omega^2 - i\omega\Gamma')]. \quad (209)$$

To account for the total number of electrons "Z" per molecule, we introduce the oscillator strength f_j . We say there are f_j electrons with binding frequency ω_{oj} and damping constant Γ_j . We immediately have the f-sum rule

$$\sum_j f_j = Z \quad (210)$$

and the expression

$$\tilde{\alpha} = \sum_j \left[(f_j e^2 / m) / (\omega_{oj}^2 - \omega^2 - i\omega\Gamma_j') \right] \quad (211)$$

for the molecular polarizability. If we neglect "local-field" (internal-field) corrections (104) and define the macroscopic fields \bar{E} and \bar{P} by means of

$$\bar{E} \equiv \langle \bar{E}_m \rangle \quad (212)$$

and

$$\bar{P} \equiv N\bar{p}_m \quad (213)$$

where the bracket denotes a spacial average and "N" gives the number of identical molecules per unit volume, we will obtain the Sellmeyer formula (105)

$$\tilde{\kappa} = \tilde{\epsilon} / \epsilon_0 = 1 + \tilde{\chi}_b = 1 + (N\tilde{\alpha} / \epsilon_0) \quad (214)$$

for the complex dielectric constant.

We now regroup terms from Equations (211), (213), and (214) and write

$$\kappa = \left[1 + \sum_j \omega_{lj}^2 / (\omega_{oj}^2 - \omega^2 - i\omega\Gamma_j') \right] \quad (215)$$

and

$$\omega_{1j} = [N_j e^2 / m \epsilon_0]^{1/2} . \quad (216)$$

Here N_j ($N_j = N f_j$) is the concentration of electrons of the j th group. When free electrons (not external) are also present, the above derivation remains valid (48): merely replace ω_{0j} by zero. The complex dielectric constant of Equation (214) then becomes

$$\tilde{\kappa} = 1 + \tilde{\chi}_b + \tilde{\chi}_f \quad (217)$$

where the $\tilde{\chi}_b$ and $\tilde{\chi}_f$ are the bound and free electron contributions to the induced susceptibility, respectively.

We now make the observation that for sufficiently weak damping and sufficiently high frequency (if the electrons are bound) we may write Equation (215) as

$$\tilde{\kappa} = 1 - (\omega_p / \omega)^2 \quad (218)$$

where

$$\omega_p = \left[\sum_j \omega_{1j}^2 \right]^{1/2} \quad (219)$$

is the angular frequency for which the real part of the dielectric constant vanishes while the imaginary part is small; this frequency $\omega_p / 2\pi$ is generally called the plasma frequency. We explore the consequences of the vanishing of the complex dielectric constant in the next section.

Dielectric Energy-Loss Formulation

We remark that in the treatment, above, of the interaction of radiation with the solid we have assumed that it is legitimate to calculate the effect of the incident radiation on one electron in the molecule at a time, and then sum up incoherently the energy transfers to all the electrons in all the molecules. This same assumption underlies the discussion in Chapter II; therein, it was assumed that we could account for the interaction of the incident radiation with our valence (44) electrons, if we considered excitations of single electrons. Such "one-electron spectra" (54) accurately describe many optical properties of solids.

On the other hand, theoretical studies (106-9) and experimental studies first carried out by Watanabe (110) have demonstrated the existence of collective excitations in a solid. Experimental studies have involved measurement of the angular distribution of the inelastically scattered, fast (~ 10 keV) electrons, which have traversed thin foils. More recently (111-3) reradiation (following excitation by electron bombardment) associated these collective excitations in thin films has been detected.

We momentarily return to a microscopic picture of our "classical" solid and consider the energy transfer (49) which occurs in Coulomb collisions. The kinematics of energy and momentum conservation show that most of the energy loss of a fast, incident, charged particle is to the electrons, and we use the approximation (which is better for a massive particle) that the incident particle is negligibly deflected in a single collision. At small impact parameters, the effects of the binding force $m\omega_0^2 x$ are negligible. At large impact parameters, it is found that not

only must the effects of the binding force be considered, but that the Coulomb interaction becomes screened due to the polarization of the molecules between the incident particle and the electron at the given large impact parameter. An incoherent (one-electron) treatment, similar to that for the interaction of radiation with the electrons, is therefore found to give erroneously large contributions to the energy loss due to unscreened collisions at large impact parameters.

When we use a dielectric formulation for the energy loss suffered by our incident particle, it is clear that we are using macroscopic fields in the continuum approximation. This approximation will not be good for the impact parameters of the order of molecular dimensions, but will be valid for the great bulk of the collisions.

We seek here only the principal result of a dielectric formulation of the energy loss. It has been shown (114,115) that the maximum information obtainable is contained in the imaginary part of $[1/\tilde{\kappa}(k,\omega)]$. The arguments of the complex dielectric constant have the same quantum mechanical interpretation as in Chapter II (see Intraband Transitions): the momentum transfer $\hbar\vec{k}$ and the energy transfer $\hbar\omega$ are those involved in a single inelastic scattering event. We now outline a derivation of this important and revealing result.

A particle of charge Ze moves with velocity \vec{v} in a solid. The fields of the particle induce a polarization field which in turn gives rise to an electric field \vec{E} at the position of the incident particle; the field \vec{E} tends to oppose the motion of the incident particle. The power loss $-dE/dt$ can be written $-Ze\vec{E}\cdot\vec{v}$ and the stopping power, or energy loss per unit length, is given by

$$- \frac{1}{v} \frac{d\mathcal{E}}{dt} = - Ze \bar{\mathbf{E}} \cdot \bar{\mathbf{v}} / v. \quad (220)$$

If we represent the incident charge density $\rho(\mathbf{r}, t)$, which passes the origin with velocity $\bar{\mathbf{v}}$ at the zero of time, by $Ze\delta(\bar{\mathbf{r}} - \bar{\mathbf{v}}t)$, we obtain the Fourier components

$$\tilde{\rho}(\bar{\mathbf{k}}, \omega) = [Ze / (8\pi^3)] \delta(\omega - \bar{\mathbf{k}} \cdot \bar{\mathbf{v}}) \quad (221)$$

$$\tilde{\mathbf{J}}_{\text{ext}}(\bar{\mathbf{k}}, \omega) = [Ze\bar{\mathbf{v}} / (8\pi^3)] \delta(\omega - \bar{\mathbf{k}} \cdot \bar{\mathbf{v}}) \quad (222)$$

for the charge and current densities, respectively. For the choice of gauge in which the scalar potential $\tilde{\phi}$ vanishes, Equations (51) and (52) yield the longitudinal and transverse components of the vector potential as follows:

$$\tilde{A}_L(\bar{\mathbf{k}}, \omega) = - [Ze / (8\pi^3 \epsilon_0)] \{ \bar{\mathbf{k}} \delta(\omega - \bar{\mathbf{k}} \cdot \bar{\mathbf{v}}) / [\bar{\mathbf{k}}^2 \tilde{\kappa}(\bar{\mathbf{k}}, \omega)] \} \quad (223)$$

$$\tilde{A}_T(\bar{\mathbf{k}}, \omega) = [Ze\mu_0 / (8\pi^3)] [\bar{\mathbf{v}} - \hat{\mathbf{k}}(\hat{\mathbf{k}} \cdot \bar{\mathbf{v}})] \delta(\omega - \bar{\mathbf{k}} \cdot \bar{\mathbf{v}}) / [\bar{\mathbf{k}}^2 - (\omega/c)^2 \tilde{\kappa}^{\text{tr}}(\bar{\mathbf{k}}, \omega)] \quad (224)$$

This expression for $\tilde{A}_T(\bar{\mathbf{k}}, \omega)$ was obtained with the aid of Equations (36), (37), and (60); these other equations yield

$$\tilde{\kappa}^{\text{tr}} = \tilde{\kappa} + (c/\omega)^2 \bar{\mathbf{k}}^2 [1 - (1/\tilde{\kappa}_m)]. \quad (225)$$

The term $[\bar{\mathbf{v}} - \hat{\mathbf{k}}(\hat{\mathbf{k}} \cdot \bar{\mathbf{v}})]$ gives the transverse component of the velocity $\bar{\mathbf{v}}$.

The electric field is given by

$$\widetilde{\mathbf{E}}(\bar{\mathbf{r}}, t) = \widetilde{\mathbf{E}}_L + \widetilde{\mathbf{E}}_T; \quad (226)$$

for our choice of gauge ($\widetilde{\varphi} = 0$), the longitudinal component of the electric field is given by

$$\widetilde{\mathbf{E}}_L(\bar{\mathbf{r}}, t) = [-ie/(\partial\pi^3 \epsilon_0)] \int \{ \bar{\mathbf{k}} \exp[i\bar{\mathbf{k}} \cdot (\bar{\mathbf{r}} - \bar{\mathbf{v}}t)] / \bar{k}^2 \widetilde{\kappa}(\bar{\mathbf{k}}, \bar{\mathbf{k}} \cdot \bar{\mathbf{v}}) \} d^3k \quad (227)$$

A similar expression occurs for \mathbf{E}_T . Since we seek the electric field at the point $\bar{\mathbf{r}}$ equal to $\bar{\mathbf{v}}t$, Equation (227) simplifies to

$$\widetilde{\mathbf{E}}_L(\bar{\mathbf{v}}t, t) = [-ie/(\partial\pi^3 \epsilon_0)] \int [\bar{\mathbf{k}} / \bar{k}^2 \widetilde{\kappa}(\bar{\mathbf{k}}, \bar{\mathbf{k}} \cdot \bar{\mathbf{v}})] d^3k \quad (228)$$

The change of variable of integration and replacements

$$\bar{\mathbf{k}} \cdot \bar{\mathbf{v}} = kv\xi = \omega', \quad (229)$$

$$d^3k = 2\pi k^2 dk d\xi = 2\pi k dk d\omega' / v, \quad (230)$$

and

$$\bar{\mathbf{k}} \rightarrow \bar{\mathbf{v}}(\bar{\mathbf{k}} \cdot \bar{\mathbf{v}}) / v^2 = \omega' \bar{\mathbf{v}} / v^2 \quad (231)$$

lead to the form given by Linhard (114)

$$\tilde{E}_L(\nabla t, t) = [-iZe\nabla / (4\pi^2 \epsilon_0 v^3)] \int_0^\infty k^{-1} dk \int_{-kv}^{kv} [\omega' / \tilde{\kappa}(\bar{k}, \omega)] d\omega'. \quad (232)$$

From the reality of $\bar{E}(\bar{r}, t)$ and $\bar{D}(\bar{r}, t)$, and from Equation (42) we have

$$\tilde{\kappa}(-\bar{k}, -\omega) = \tilde{\kappa}^*(\bar{k}, \omega). \quad (233)$$

For a solid possessing inversion symmetry we have

$$\tilde{\kappa}(\bar{k}, \omega) = \tilde{\kappa}(-\bar{k}, \omega); \quad (234)$$

so that for such a solid we have the further relation

$$\kappa(\bar{k}, -\omega) = \tilde{\kappa}^*(\bar{k}, \omega). \quad (235)$$

Stern (48) shows that under these conditions κ_1 is an even function of ω and κ_2 is an odd function of ω . We therefore obtain the stopping power in the form

$$-v^{-1} d\mathcal{E}/dt = [-Z^2 e^2 / (2\pi^2 \epsilon_0 v^2)] \int_0^\infty k^{-1} dk \int_0^{kv} \omega' \text{Im}[1/\tilde{\kappa}(\bar{k}, \omega')] d\omega' \quad (236)$$

plus another term which comes from the contribution of the transverse component of the electric field \bar{E}_T . This latter contribution is usually much smaller and gives the energy loss to Cerenkov radiation. Equation (236) displays the principal result of a dielectric formulation of the stopping power. Large contributions to the stopping power come from those

regions of the spectrum where the imaginary part of the reciprocal of the dielectric constant is large; that is, from regions for which $\tilde{\kappa}(\bar{k}, \omega)$ approximately vanishes. In retrospect, we see that the charge-density fluctuation $\tilde{\rho}(\bar{k}, \omega)$ coupled with the longitudinal field, so that in a theoretical investigation of the normal modes of oscillation of the ideal electron gas, one calculates the "longitudinal" dielectric constant. The addition term in Equation (78) is retained in such investigations.

It is well known that quanta of long-wavelength oscillations (plasmons) exist in the free-electron gas; their angular frequency for infinite wavelength is given by

$$\omega_p = [Ne^2/m\epsilon_0]^{1/2}. \quad (237)$$

Compare this Equation (237) with Equations (216) and (219). Ehrenreich and Cohen (116) calculated the longitudinal dielectric constant for a real solid and claim that for vanishingly small wave vector, the longitudinal and transverse dielectric constants are equal. This equality, as pointed out by others (109) also, leads to the results that the plasma frequency of zero wave vector and the damping of these oscillations in the solid may be deduced from optical data.

Merit of the Transition Rate as Given by the Golden Rule

In Chapter II we obtained the following expressions for the inter-band contribution to the complex part of the dielectric constant:

$$\kappa_2 = [\pi e^2 / (m^2 \epsilon_0 \omega^2)] |M|^2 J_{mj} \quad (238)$$

$$M = (\bar{u}_{\bar{k}m} | \hat{a}_0 \cdot \bar{p} | \bar{u}_{\bar{k}j}) \quad (239)$$

$$J_{mj} = [2/(2\pi)^3] \int d\bar{S}_{\bar{k}} / |\nabla_{\bar{k}} [\epsilon_m(\bar{k}) - \epsilon_j(\bar{k})]| \quad (240)$$

Using a self-consistent field method, Ehrenreich et al. (42,116) found the expression

$$\begin{aligned} \tilde{\kappa} = \tilde{\kappa}(0, \omega) = 1 - [e^2 / (4\pi^3 m \epsilon_0)] \int d^3 K \sum_{jm} f[\epsilon_j(\bar{K})] f_{mj}^{\mu} \\ \times [\omega - \omega_{jm} + (i/\tau_{jm})]^{-1} [\omega + \omega_{jm} + (i/\tau_{jm})]^{-1} \end{aligned} \quad (241)$$

for the interband contribution to the complex dielectric constant; this expression was obtained as the limit (as $\bar{k} \rightarrow 0$) of the "exact" frequency- and wave-vector-dependent, longitudinal, complex dielectric constant $\tilde{\kappa}(\bar{k}, \omega)$. This limit (as $\bar{k} \rightarrow 0$) is equivalent to the approximation of Equation (94); this approximation gives rise to the descriptive name "vertical" transition. The term $f[\epsilon_j(\bar{K})]$ is the Fermi-Dirac distribution given by Equation (83). The angular frequency ω_{mj} is given by $\{[\epsilon_m(\bar{K}) - \epsilon_j(\bar{K})]/\hbar\}$. The oscillator strength is given by

$$f_{mj}^{\mu} = [(2/\hbar \omega_{mj})] |p_{mj}^{\mu}|^2 \quad (242)$$

and

$$p_{mj}^{\mu} = \Omega_D^{-1} (\bar{u}_{\bar{k}m} | p^{\mu} | \bar{u}_{\bar{k}j}) \quad (243)$$

where the Bloch functions are normalized to the volume Ω_D of a primitive cell of the direct lattice.

We note a strong similarity between this quantum mechanical result, Equation (241), and the classical result, Equation (215). What we seek now, however, is a detailed comparison of Equation (238) with Equation (241); the exercise is fruitful.

In the range of optical frequencies the phenomenological relaxation times τ_{jm} in Equation (241) are long; that is, we have

$$\omega_{jm} \tau_{jm} \gg 1. \quad (244)$$

If we introduce the variable η so that

$$\eta = 1/\tau_{jm} \quad (245)$$

is used in the prescription

$$\lim_{\eta \rightarrow 0} (x + i\eta) = (P/x) - i\pi\delta(x) \quad (246)$$

where "P" denotes the Cauchy principal value and " δ " denotes the Dirac delta function, we immediately obtain the expression

$$\kappa_2 = [e^2 / (4\pi^2 m \epsilon_0)] \int d^3K \sum_{jm}' f[\epsilon_j(\bar{K})] f_{mj}^\mu \delta(\omega_{jm} + \omega) / (\omega - \omega_{jm}) \quad (247)$$

$$= [e^2 / (8\pi^2 m \epsilon_0 \omega)] \int d^3K \sum_{jm} f[\epsilon_j(\bar{K})] f_{mj}^{\mu} \delta(\omega_{jm} + \omega)$$

for the complex part of the dielectric constant.

An interchange of indices "j" and "m" changes the sign of f_{mj}^{μ} according to the denominator of Equation (242); otherwise, the terms j,m and m,j in Equation (247) only differ by their occupancies $f[\epsilon_j(\bar{K})]$ and $f[\epsilon_m(\bar{K})]$. Equation (84) provides a simple interpretation of this relationship between the occupancies. We can now rewrite Equation (247) as a single sum over initial states

$$\kappa_2 = - [e^2 / (8\pi^2 m \epsilon_0 \omega)] \int d^3K \sum_j \{F.D.\} f_{mj}^{\mu} \delta(\omega_{jm} + \omega). \quad (248)$$

In addition, we now restrict our attention to the contribution of a single pair of states "m" and "j"; the integral over the Brillouin zone widens the scope of our attention to a single pair of bands. We further assume that the lower band is full and the upper band is empty. Equation (248) becomes

$$\begin{aligned} \kappa_2 &= [e^2 / (8\pi^2 m \epsilon_0 \omega)] \int d^3K f_{mj}^{\mu} \delta(\omega_{jm} + \omega) \\ &= [e^2 \hbar / (8\pi^2 m \epsilon_0 \omega)] \int d^3K f_{mj}^{\mu} \delta[\epsilon_m(\bar{K}) - \epsilon_j(\bar{K}) - \hbar \omega]. \end{aligned} \quad (249)$$

The property of the Dirac delta function

$$\int_a^b g(x) \delta[f(x)] dx = \sum_{x_0} g(x_0) \left| \partial f / \partial x \right|_{x=x_0}^{-1} \quad (250)$$

where $f(x_0)$ vanishes, when generalized to three dimensions, allows us to rewrite Equation (249) in the form

$$\kappa_2 = [e^2 \hbar / (8\pi^2 m \epsilon_0 \omega)] \int dS_{\bar{K}} f_{mj}^{\mu} / |\nabla_{\bar{K}} [\mathcal{E}_m(\bar{K}) - \mathcal{E}_j(\bar{K})]|. \quad (251)$$

The sum in Equation (250) becomes an integral over that surface, in \bar{K} -space, on which energy is conserved; that is, that surface on which the term $[\mathcal{E}_m(\bar{K}) - \mathcal{E}_j(\bar{K}) - \hbar\omega]$ vanishes. As was done in Chapter II, we assume that f_{mj}^{μ} is a constant over the Brillouin zone. We may now replace ω_{mj} by ω in Equation (242) and regroup terms in Equations (242), (243), and (251) as follows:

$$\kappa_2 = [\pi e^2 / (m^2 \epsilon_0 \omega)] |p_{mj}|^2 J_{mj} \quad (252)$$

$$p_{mj} = \Omega_D^{-1} (u_{Km}^{\mu} | p^{\mu} | u_{Kj}^{\mu}) \quad (253)$$

$$J_{mj} = [2 / (2\pi)^3] \int dS_{\bar{K}} / |\nabla_{\bar{K}} [\mathcal{E}_m(\bar{K}) - \mathcal{E}_j(\bar{K})]| \quad (254)$$

We have introduced the joint density of states J_{mj} by regrouping terms. At this stage of the analysis of Ehrenreich's result, it is convenient to compare Equations (238), (239), and (240) with Equations (252), (253), and (254). Only the matrix elements "M" and p_{mj}^{μ} have yet to be shown to be equivalent. The momentum operator p^{μ} was chosen parallel to the direction \bar{k} of the propagation of the longitudinal wave in Ehrenreich's treatment. We are at liberty to choose our unit vector \hat{a}_0 of Equation (239) parallel

to any direction; in particular, the μ -direction of Equation (253).

A remaining detail in this comparison is that of the choice of normalization in Equation (239)

$$M = (\bar{u}_{K_m} | p^\mu | \bar{u}_{K_j})_V \quad (255)$$

and Equation (253)

$$p_{mj} = \Omega_D^{-1} (\bar{u}_{K_m} | p^\mu | \bar{u}_{K_j})_{\text{cell}}. \quad (256)$$

The normalization to the total volume "V" of the solid may be shown explicitly in Equation (255) by writing

$$|V^{-1/2} \bar{u}_{K_m}) \leftarrow | \bar{u}_{K_m}) \quad (257)$$

so that Equation (255) becomes

$$M = [1/V] (\bar{u}_{K_m} | p^\mu | \bar{u}_{K_j})_V. \quad (258)$$

If we recall that the Bloch functions are periodic in the direct lattice, then it is seen that we obtain a large number of identical contributions to this integral (Matrix element). When the total number of primitive cells is given by the parameter "N", we obtain

$$M = [N/V] (\bar{u}_{K_m} | p^\mu | \bar{u}_{K_j})_{\text{cell}} \quad (259)$$

where the integration is now to be performed over the volume of a single primitive cell. Since $[N/V]$ is Ω_D , by definition, we have demonstrated the equivalence of Equations (255) and (256).

APPENDIX B

EXACT GEOMETRY OF THE GRATING DRIVE

As seen in Figure 13, the grating holder is directly supported by a horizontal yoke which permits tilt adjustment; the combination of horizontal yoke and grating holder rotates through angle θ by means of a vertical yoke support and a drive screw which is spring loaded against an arm attached to the horizontal yoke. The rotation of the grating is about its vertical tangent (the Rowland circle defines the horizontal plane). The radius of the rounded rod, against which the end of the screw is in contact, is much smaller than that of the arm.

Figure 48 gives a simplified view of the drive; the rounded stock is drawn oversized for clarity. The grating rotates about point "O". The screw translates along the line "X" and makes contact with the enlarged rounded stock of radius "r" at the intersection of lines "X" and "L". Now, from Figure 48 we have

$$P = (L^2 - X^2)^{1/2}, \quad (260)$$

$$Z^2 = R^2 + r^2, \quad (261)$$

and

$$L^2 = Z^2 + r^2 - 2Zr \cos\phi. \quad (262)$$

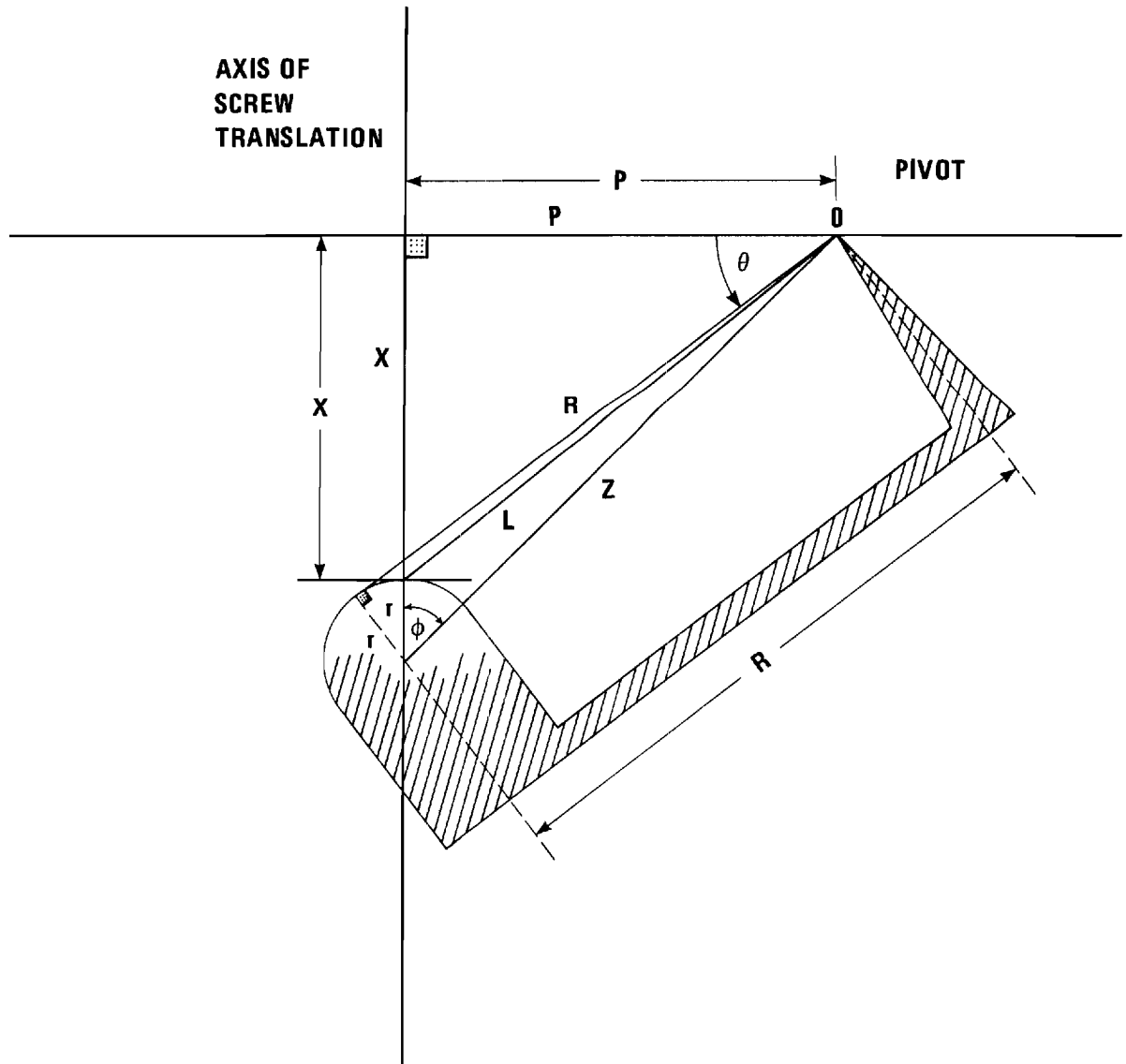


Figure 48. Schematic of the Grating Drive.

Also we have the relationship

$$\cos\varphi = \frac{X + r}{Z} . \quad (263)$$

Substituting Equations (263) and (261) into Equation (262), one finds

$$L^2 = R^2 - 2rX. \quad (264)$$

Finally, since we may write

$$\sin\theta = \frac{X}{L} , \quad (265)$$

and by substituting Equations (264) into Equation (265) one obtains the desired expression

$$\sin\theta = \frac{X}{R} [1 - (2rX/R^2)]^{-1/2}. \quad (266)$$

We now make the following valued assignments:

$$R = 3.00", \quad (267)$$

$$r = 0.0625", \quad (268)$$

and

$$X = DR/2800. \quad (269)$$

(The radii "R" and "r" were not precisely measured.) This last equality

follows from the two relations (1) the pitch of the drive screw is 28 turns per inch and (2) there are 100 drum readings, DR, per revolution. Since DR never exceeds 850, it is seen that a Maclaurin-series expansion is in order; that is, Equation (266) becomes

$$\sin\theta = \frac{X}{R} \left[1 + \frac{rX}{R^2} . . . \right]. \quad (270)$$

Employing the grating Equation (165), wherein "d" equals mm/(1200 lines) and substituting Equations (267-270) therein, we have the result

$$\lambda \approx 1.983 \text{ DR} + 0.00000492 (\text{DR})^2. \quad (271)$$

APPENDIX C

ZERO-VOLTAGE SWITCHING

The device that was constructed fell into the category of zero-voltage switches. These devices used triacs (two complementary SCR's, back to back) which had to be derated or not used at all for purely inductive loads. Some of these devices had minimum-load requirements; others had unknown characteristics due to compensation which the vendor claimed allowed the use of their device on purely inductive loads. There were even integrated circuits which triggered triacs at the zero-voltage crossing. Armed with the above, a discrete-component zero-voltage switch was constructed. Use was made of several commercial triacs, with varying degrees of success.

A block diagram of the circuitry is given in Figure 49. The schematics, including the unregulated dc supplies, are reproduced in Figures 50 through 52.

Two General Electric triacs were tried; both made use of a switch closure (relay) for triggering. The GE S200A3 internally generated its trigger pulses, which enforced zero-voltage switching, as a result of an imbalance in a resistance bridge which incorporated the relay; it promptly ceased to work. The GE S100F5 did not generate internal trigger pulses. The firing angle of this triac was simply determined by the resistance of the relay contacts in shunt with a 500-K resistor; with the contacts closed, it fired full cycle and vice versa. This latter triac performed well until it was destroyed by operator error.

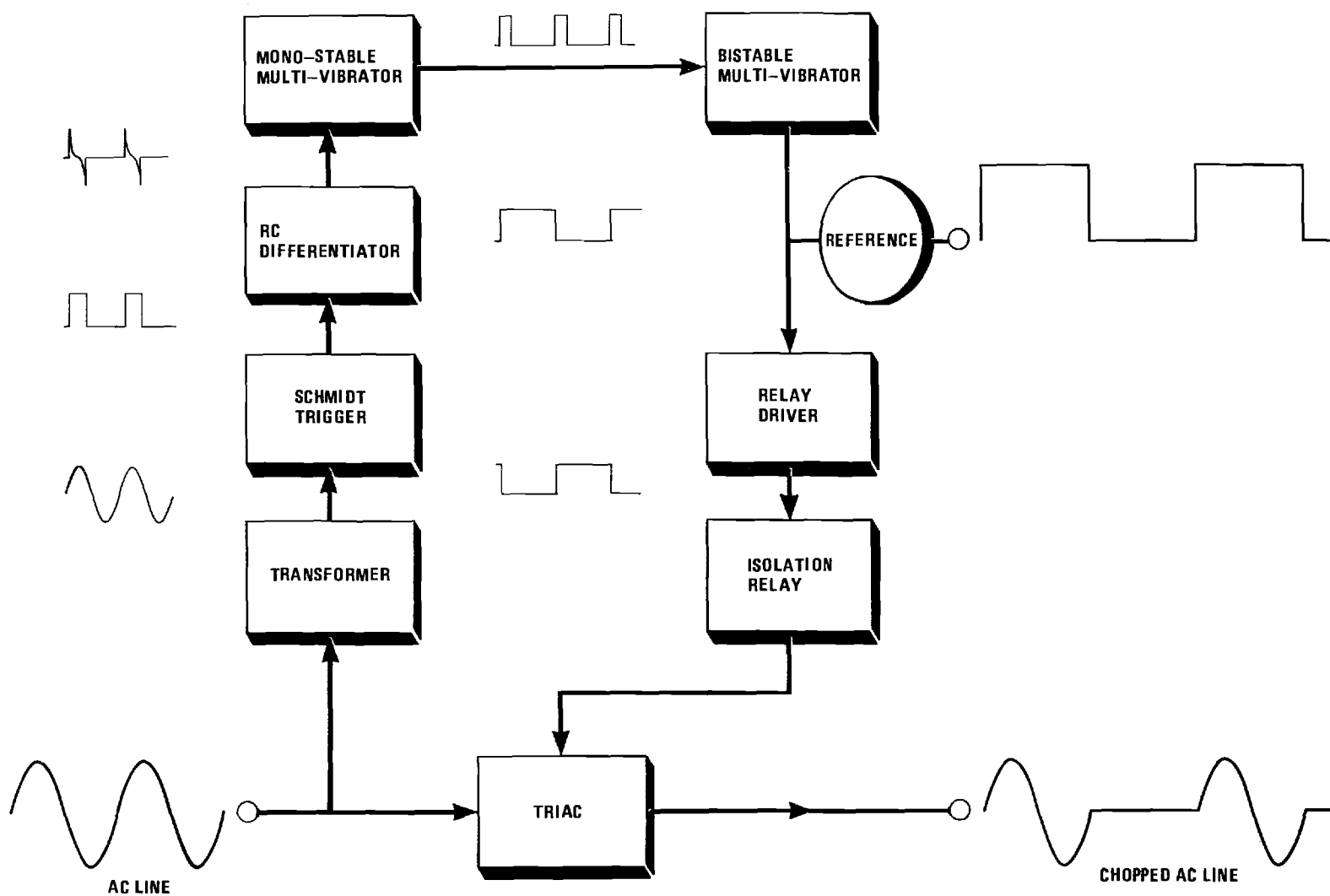


Figure 49. Block Diagram of the 30-Hz Chopper Circuitry.

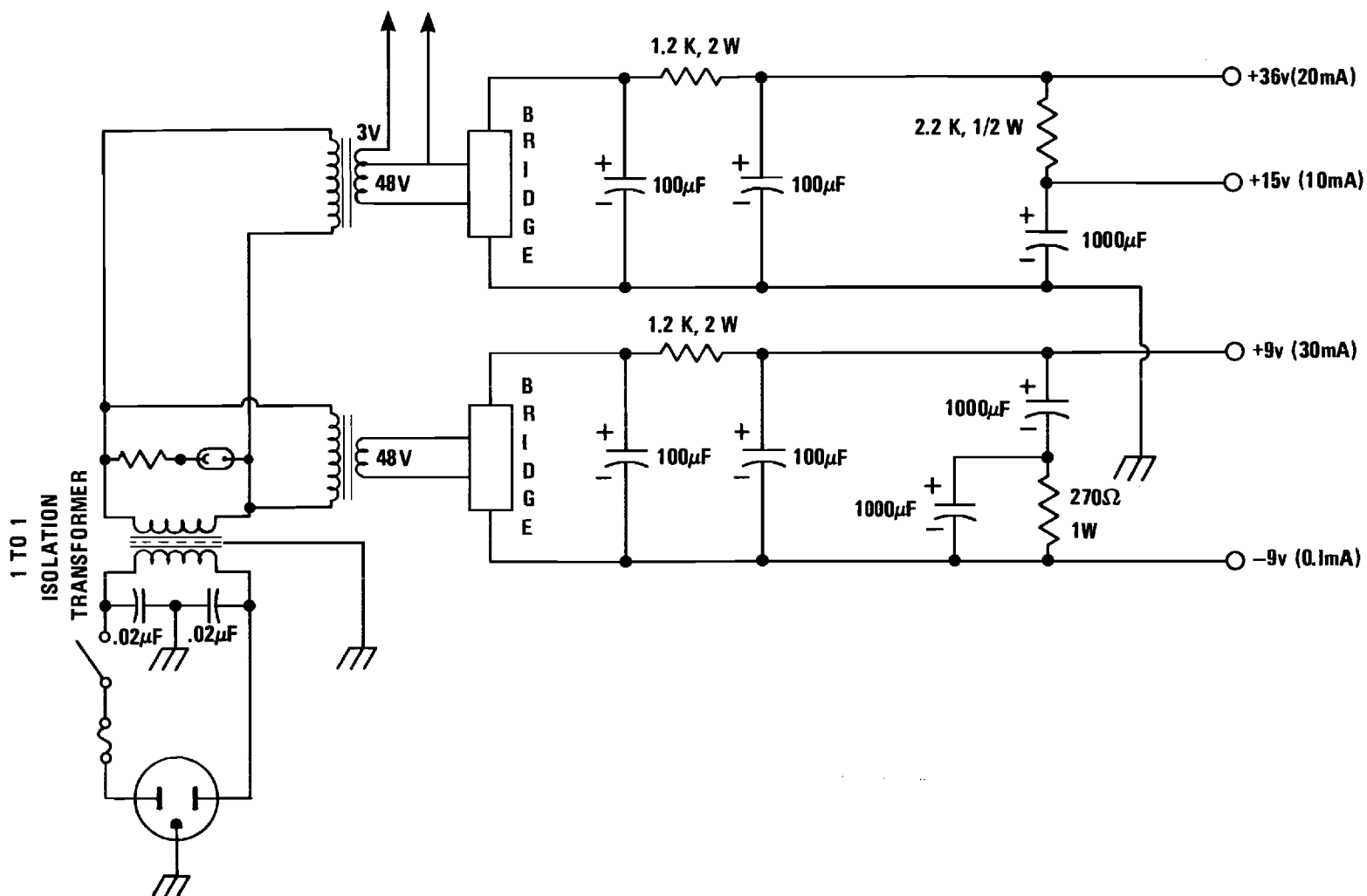


Figure 50. Isolation Transformer and Power Supplies.

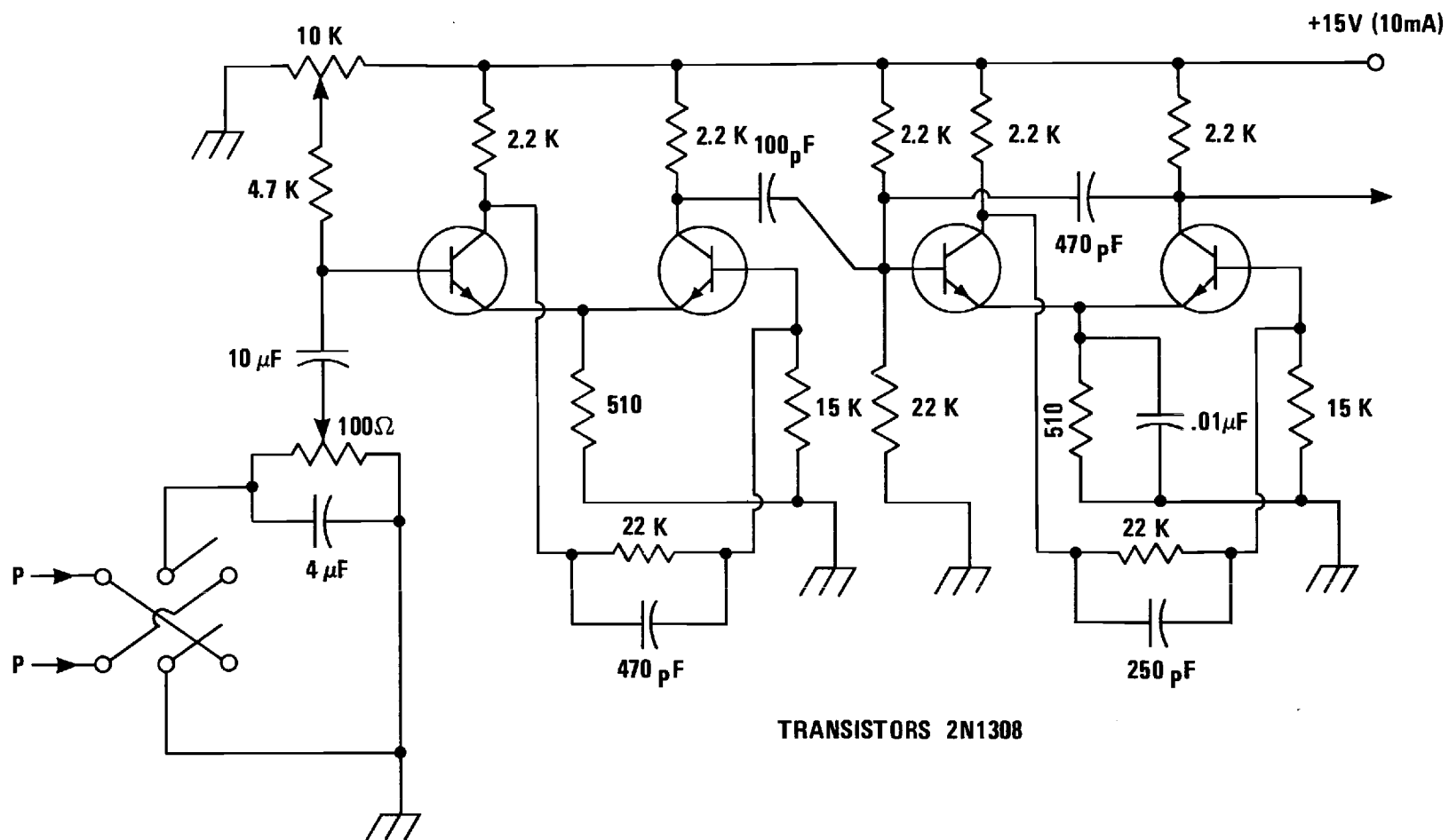


Figure 51. Line Sense, Schmidt Trigger, and Monostable Multivibrator.

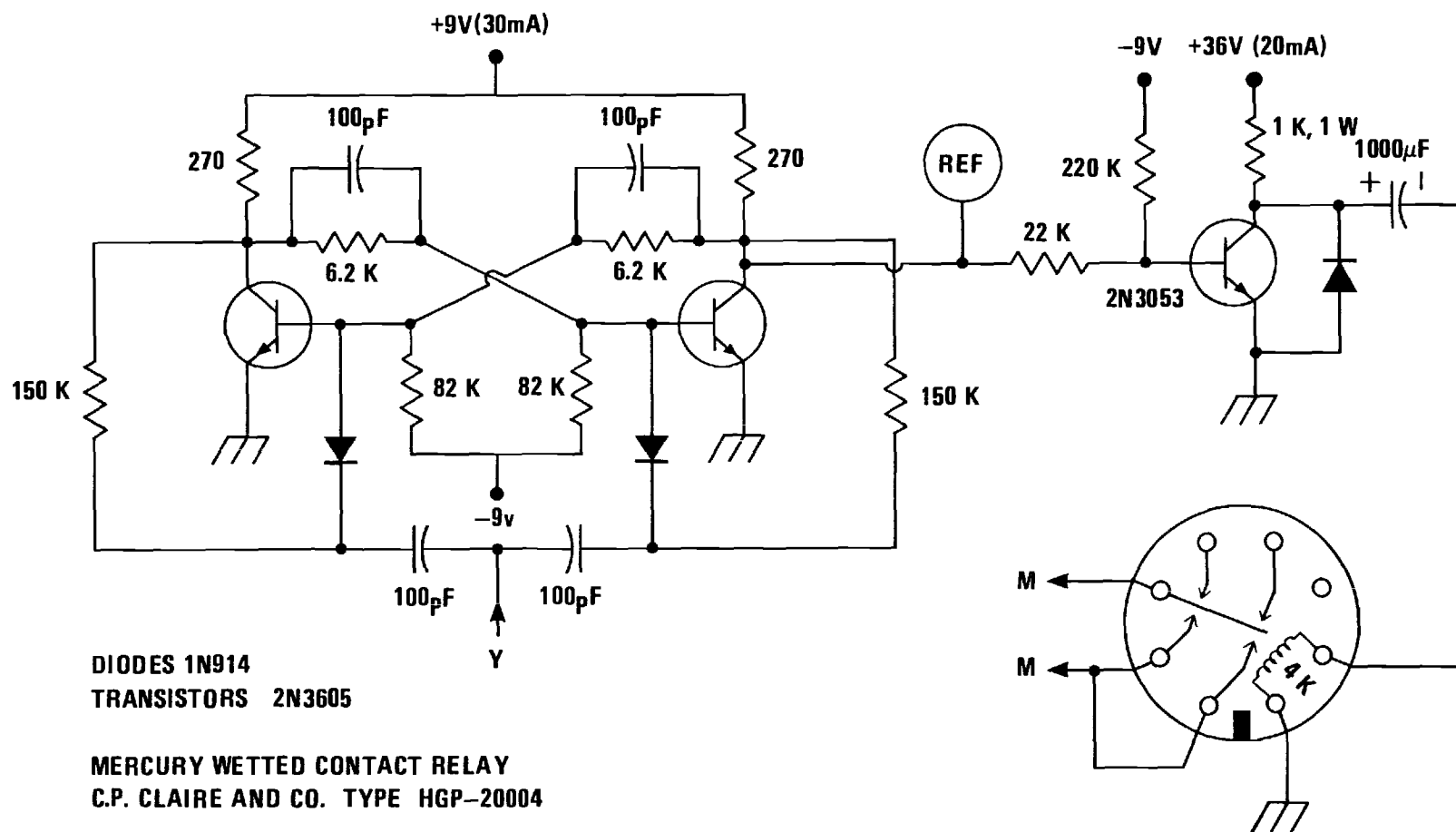


Figure 52. Bistable Multivibrator, Relay Driver, and Relay.

A "Synchro-Reedac," manufactured by Grigsby-Barton, Incorporated and provided with part no. GB 7200-0700-3-QS, almost met the desired "no minimum-load" requirements. The GE triacs required large (10 Amp) resistive loads in shunt with an inductive load, whereas the Barton unit only required a 0.5-A load in shunt with the McPherson spark-gap supply. There was one early failure with the Barton unit; since then, several hundred successful hours have elapsed.

Figure 53 displays the waveforms related to this chopper. The "Chopped Line Voltage" was typical of the waveform obtained with the GE units. The capacitor voltage was monitored by a resistance chain which is not illustrated in Figure 26, for the sake of clarity. It is seen that the RC time constant (see Figure 26) was small (0.5 ms) compared to 1/60 s. The overshoot which appeared on the capacitor was not permitted to become so large as to cause an additional breakdown of the gap: there was attendant gross instability if that occurred. This consideration usually limited the dc current through the gap to approximately 12 mA when the chopper was operative. The PM-tube anode pulses are seen to be coincident with the gap breakdowns. Careful measurement has shown that the radiation is emitted as an after glow which reaches a maximum intensity of 1.4 μ s after the spark discharge. This picture of the anode pulses could be obscured by the addition of dark-current pulses when the ratio of signal to dark current was poor.

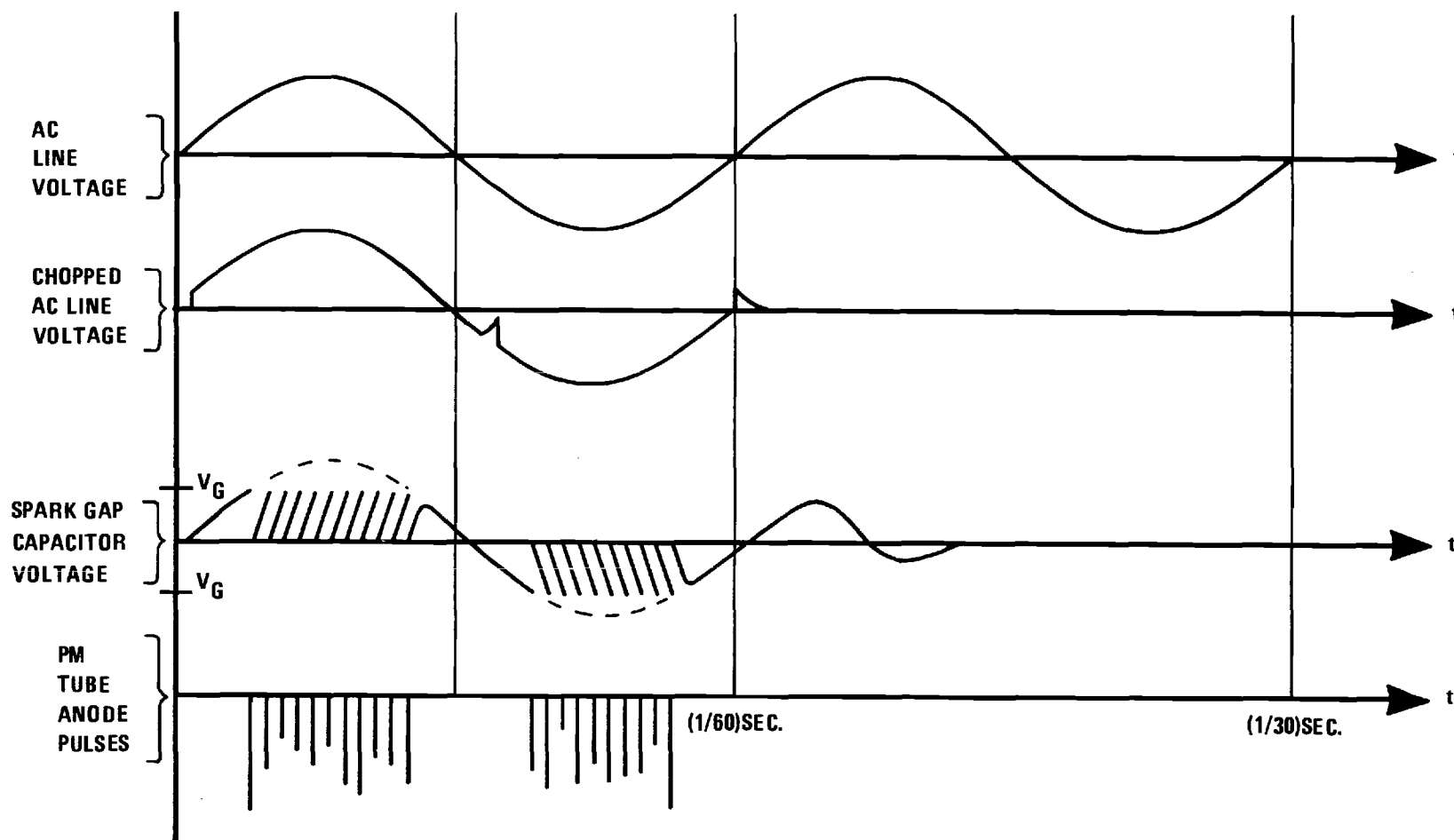


Figure 53. Waveforms Related to 30-Hz ac Line.

BIBLIOGRAPHY

1. H. J. Naake and S. C. Belcher, J. Appl. Phys. 35, 3064-5 (1964).
2. K. Masumoto and S. Isomura, Energy Convers. 10, 129 (1970).
3. W. Zdanowicz, F. Krolicki, P. Plenkiewicz, Acta Phys. Polon. A 41, 27 (1972).
4. G. Natta and L. Passerini, Gazz. chim. Ital. 58, 541 (1928).
5. M. V. Stackelberg and R. Paulus, Z. Phys. Chem. B28, 427 (1935).
6. H. Cole, F. W. Chambers, and H. M. Dunn, Acta Cryst. 9, 685 (1956).
7. W. Zdanowicz, K. Lukaszewicz, and W. Trzebiatowski, Bull. Acad. Polon. Sci., Ser. sci. chim. 12, 169 (1964).
8. W. Zdanowicz and A. Wojakowski, Phys. Stat. Sol. 8, 569 (1965).
9. G. A. Steigmann and J. Goodyear, Acta Cryst. B24, 1062 (1968).
10. S. F. Zemczuzny, Intern. Z. Metallog 4, 228 (1913).
11. G. Haacke and G. A. Castellion, J. Appl. Phys. 35, 2484 (1964).
12. R. J. Wagner, E. D. Palik, and E. M. Swiggard, J. Phys. Chem. Solids Suppl. 1, 471 (1971).
13. P. L. Radoff and S. G. Bishop, Phys. Rev. B 5, 442 (1972).
14. R. A. Smith, Semiconductors (Cambridge University Press, Cambridge, U. K., 1968) General Reference.
15. F. C. Brown, The Physics of Solids (W. A. Benjamin, Inc., 1967), Chapters 10 and 11.
16. J. P. Suchet, J. Phys. Chem. Solids 16, 265 (1960).
17. S. G. Bishop and P. L. Radoff, Solid State Communications 9, 133 (1971).
18. Y. A. Ugai and T. A. Zyubina, Izvest. Akad. Nauk SSSR, Neorgan. Mater 1, 860 (1965). [Sov. Phys. - Inorg. Mater. 1, 790 (1965)].

BIBLIOGRAPHY (Continued)

19. Smith, pp 114-116.
20. D. P. Spitzer, G. A. Castellion, and G. Haacke, J. Appl. Phys. 37, 3795 (1966). Appendix.
21. L. M. Rogers, R. M. Jenkins, and A. J. Crocker, J. Phys. D. Appl. Phys., 793 (1971). Appendices.
22. W. J. Turner, A. S. Fischler, and W. E. Reese, Phys. Rev. 121, 759 (1961).
23. J. Tauc, Photo and Thermoelectric Effects in Semiconductors (Pergamon Press, New York, 1962). pp 145-50.
24. R. J. Wagner, E. D. Palik, and E. M. Swiggard, Phys. Letters 30A, 175 (1969).
25. E. O. Kane, Semiconductors and Semimetals, edited by R. K. Willardson and A. C. Beer (Academic Press, New York, 1966), Vol. 1, p. 75.
26. D. Armitage and H. J. Goldsmid, Phys. Letters 28A, 149 (1968).
27. F. A. P. Blom and J. T. Schrama, Phys. Letters 30A, 245 (1969).
28. E. D. Haidemenakis, M. Balkanski, E. D. Palik, and J. Tavernier, J. Phys. Soc. Japan Suppl. 21, 189 (1966).
29. N. Sexter, Phys. Stat. Sol. 21, 225 (1967).
30. I. Rosenman, J. Phys. Chem. Solids 30, 1385 (1969).
31. M. W. Heller, J. Babiskin, and P. L. Radoff, Phys. Letters 36A, 363 (1971).
32. T. S. Moss, Proc. Phys. Soc. (London) B63, 167 (1950).
33. L. Zdanowicz, Phys. Stat. Sol. 20, 473 (1967).
34. W. J. Turner, A. S. Fischler, and W. E. Reese, J. Appl. Phys. Suppl. 32, 2241 (1961).
35. S. G. Bishop, W. J. Moore, and E. M. Swiggard, Proc. Third Int. Conf. on Photoconductivity, Stanford University, 1969, edited by F. M. Pell (Pergamon Press, Oxford, 1971), p. 205.
36. S. G. Bishop, W. J. Moore, and E. M. Swiggard, Appl. Phys. Letters 16, 459 (1970).

BIBLIOGRAPHY (Continued)

37. P. J. Lin-Chung, Phys. Rev. 188, 1272 (1969).
38. V. V. Sobolev, N. N. Syrbu, and S. D. Shutov, Chemical Bonds in Semiconductors and Thermodynamics, edited by N. N. Sirota (Consultants Bureau, New York, 1968), p. 165.
39. M. Zivitz, R. J. Bartlett, and J. R. Stevenson, Bull. Am. Phys. Soc. 15, 1343 (1970).
40. V. V. Sobolev, N. N. Syrbu, T. A. Zyubina, and Y. A. Ugai, Fiz. Tekh. Poluprov. 5, 327 (1971). [Sov. Phys.-Semicond. 5, 279 (1971)].
41. J. R. Stevenson, M. Zivitz, H. Ellis, and R. J. Bartlett, Third Int. Conf. on Vacuum Ultraviolet Radiation Physics, Tokyo, Japan, 30 Aug.-2 Sept. 1971.
42. H. Ehrenreich and H. R. Philipp, Proc. Int. Conf. on Semiconductor Physics, Exeter 367 (1962). pp 367-74.
43. P. J. Lin-Chung, Phys. Stat. Sol. 47, 33 (1971).
44. W. A. Harrison, Solid State Theory (McGraw-Hill, New York, 1970).
45. J. C. Slater, Phys. Rev. 98, 1039 (1955).
46. H. Harrison, J. Chem. Phys. 901 (1970).
47. C. E. Moore, Atomic Energy Levels [Nat. Stand. Ref. Data Ser., Nat. Bur. Stand. (U.S.), 35, 1971] Vols. 1-3.
48. F. Stern, Solid State Physics 15, 299-408 (1963).
49. J. D. Jackson, Classical Electrodynamics (J. Wiley & Sons, Inc., 1962). Appendix.
50. A. B. Pippard, Proc. Roy. Soc. (London) A191, 385 (1947).
51. J. A. Stratton, Electromagnetic Theory (McGraw-Hill, New York, 1941). p. 284.
52. H. Goldstein, Classical Mechanics (Addison-Wesley, Mass., 1950).
53. L. I. Schiff, Quantum Mechanics (McGraw-Hill, New York, 1955), 2nd ed. p. 252.
54. J. C. Phillips, Solid State Physics 18, 55-164 (1966).
55. J. C. Woolley and K. W. Blazey, J. Phys. Chem. Solids 25, 713 (1964).

BIBLIOGRAPHY (Continued)

56. C. Kittel, Introduction to Solid State Physics (John Wiley & Sons, Inc., New York, 1966).
57. M. Cardona, "Electronic Density of States," L. H. Bennett, ed. (National Bureau of Standards Special Publication 323, 1972) pp. 77-89.
58. D. L. Greenaway and G. Harbeke, Optical Properties and Band Structure of Semiconductors (Pergamon Press, Oxford, 1968).
59. F. Seitz, The Modern Theory of Solids (McGraw-Hill, New York, 1940).
60. E. Fermi, Rev. Mod. Phys. 4, 87 (1932).
61. W. Heisenberg, The Physical Principles of the Quantum Theory (Dover, New York, 1930).
62. J. C. Slater, Rev. Mod. Phys. 37, 68 (1965).
63. A. R. Downie, M. C. Magoon, T. Purcell, and B. Crawford, Jr., J. Opt. Soc. Am. 43, 941 (1953).
64. E. K. Plyler and C. W. Peters, Journal of Research of the National Bureau of Standards 45, 462 (1950).
65. I. S. Sokolnikoff and R. M. Redheffer, Mathematics of Physics and Modern Engineering (McGraw-Hill, New York, 1958), p. 699.
66. Model 99 Monochromator Instruction Manual, Volume 3A (The Perkin-Elmer Corporation, Norwalk, 1956).
67. E. D. Palik and J. R. Stevenson, Naval Research Laboratory Report 6177 (1964).
68. A. Smith, J. Opt. Soc. Am. 50, 862 (1960).
69. D. C. Hinson, Doctoral Thesis, Georgia Institute of Technology (1967).
70. J. A. R. Samson, Techniques of Vacuum Ultraviolet Spectroscopy (John Wiley & Sons, New York, 1967), p. 212.
71. H. E. Bennett and W. F. Koehler, J. Opt. Soc. Am. 50, 1 (1950).
72. Diffraction Grating Handbook (Bausch & Lomb, Rochester, 1970).
73. Samson, pp. 5-25.
74. P. D. Johnson, Phys. Rev. Letters 42, 278 (1952).

BIBLIOGRAPHY (Continued)

75. R. P. Godwin, Springer Tracts Mod. Phys. 51, 1 (1969).
76. E. M. Rowe, R. A. Otte, C. H. Pruett, and J. D. Steben, Trans. IEEE Nucl. Sci. NS-16, 159 (1969).
77. C. Gahwiller, F. C. Brown, and H. Fujita, Rev. Sci. Instrum. 41, 1275 (1970).
78. J. D. Jackson, Chap. 14.
79. Notes on the Synchrotron Radiation Users Group Meeting, 1970, unpublished.
80. G. W. Rubloff, H. Fritzsche, U. Gerhardt, and J. Freeouf, Rev. Sci. Instrum. 42, 1507 (1971).
81. R. P. Madden, D. L. Ederer, and K. Codling, Appl. Opt. 6, 31 (1967).
82. Notes on the Synchrotron Radiation Users Group Meeting, 1969, unpublished.
83. W. R. Hunter, J. Opt. Soc. Am. 55, 1197 (1965).
84. R. Haensel and C. Kunz, Z. Agew. Physik 23, 276 (1967).
85. R. L. Fitzwilson, private communication.
86. Samson, pp. 98-100.
87. L. K. Jordan, Doctoral Thesis, Georgia Institute of Technology (1969).
88. C. H. Pruett, private communication.
89. E. D. Palik and E. M. Swiggard, private communication.
90. E. O. Kane, J. Phys. Chem. Solids 1, 249 (1957).
91. H. Ehrenreich, J. Appl. Phys., Suppl. 32, 2155 (1961).
92. F. Herman, C. D. Kuglin, K. F. Cuff, and R. L. Kortum, Phys. Rev. Letters 11, 541 (1963).
93. M. L. Cohen and T. K. Bergstresser, Phys. Rev. 141, 789 (1966).
94. H. R. Philipp and H. Ehrenreich, Phys. Rev. 129, 1550 (1963).
95. J. L. Freeouf, Phys. Rev. B 7, 3810 (1973).

BIBLIOGRAPHY (Concluded)

96. R. J. Bartlett, D. W. Lynch, and R. Rosei, Phys. Rev. B 3, 4074 (1971).
97. W. R. Hunter, J. Opt. Soc. Am. 55, 1197 (1965).
98. D. M. Roessler, Brit. J. Appl. Phys. 16, 1119 (1965).
99. D. M. Roessler, Brit. J. Appl. Phys. 17, 1313 (1966).
100. J. L. Shay, private communication.
101. M. Cardona, Phys. Rev. 129, 69 (1963).
102. H. R. Philipp and H. Ehrenreich, Phys. Rev. 129, 1550 (1963).
103. S. A. Korff and G. Breit, Rev. Mod. Phys. 4, 471 (1932).
104. H. A. Lorentz, The Theory of Electrons (Dover, New York, 1952), 2nd ed.
105. P. Nozieres and D. Pines, Phys. Rev. 109, 762 (1958).
106. D. Pines, Rev. Mod. Phys. 28, 184 (1956).
107. R. H. Ritchie, Phys. Rev. 106, 874 (1957).
108. P. Nozieres and D. Pines, Phys. Rev. 113, 1254 (1959).
109. D. Pines, Elementary Excitations (W. A. Benjamin, New York, 1963).
110. H. Watanabe, J. Phys. Soc. Japan 11, 112 (1956).
111. W. Steinmann, Phys. Rev. Letters 5, 470 (1960).
112. R. W. Brown, P. Wessel, and E. P. Trownson, Phys. Rev. Letters 5, 472 (1960).
113. E. T. Arakawa, R. J. Herickhoff, and R. D. Birkhoff, Phys. Rev. Letters 12, 319 (1964).
114. J. Lindhard, Kgl. Danske Videnskab, Mat. Fys. Medd 28, 8 (1954).
115. U. Fano, Phys. Rev. 103, 1202 (1956).
116. H. Ehrenreich and M. H. Cohen, Phys. Rev. 115, 786 (1959).

VITA

Maury Zivitz was born September 5, 1943 in Mobile, Alabama. He received his elementary and high school educations in the public schools of Mobile.

In 1965, Mr. Zivitz was awarded by Spring Hill College the degree of Bachelor of Science in Physics. He received the Master of Science in Physics from the Georgia Institute of Technology in 1967.

While an undergraduate, Mr. Zivitz was a Student Laboratory Assistant. In 1965, he became a Graduate Teaching Assistant. In the summer of 1966, he was employed as an Aerospace Technologist by NASA at the George C. Marshall Space Flight Center in Huntsville, Alabama. Since 1967, he has been a Graduate Research Assistant under Dr. Stevenson in reflectance studies of semiconductor alloy systems. In the summer of 1968, however, he was the recipient of a National Science Foundation Teaching Traineeship.

Mr. Zivitz was married to the former Elizabeth June Smith of Mobile on August 8, 1967. They have a daughter, Ellen Prince, born on January 14, 1972.

UNCLASSIFIED

Security Classification

G-41-606

DOCUMENT CONTROL DATA - R & D

(Security classification of title, body of abstract and indexing annotation must be entered when the overall report is classified)

1. ORIGINATING ACTIVITY (Corporate author)

Georgia Institute of Technology
School of Physics
Atlanta, Georgia 30332

2a. REPORT SECURITY CLASSIFICATION

UNCLASSIFIED

2b. GROUP

3. REPORT TITLE

OPTICAL INTERACTIONS IN SOLIDS RELATING TO SOLID STATE DETECTORS AND CORROSION
CONTROL

4. DESCRIPTIVE NOTES (Type of report and inclusive dates)

SCIENTIFIC INTERIM

5. AUTHOR(S) (First name, middle initial, last name)

JAMES R. STEVENSON

6. REPORT DATE

January 23, 1974

7a. TOTAL NO. OF PAGES

7b. NO. OF REFS

8a. CONTRACT OR GRANT NO.

AFOSR 70-1892

b. PROJECT NO.

c.

d.

9a. ORIGINATOR'S REPORT NUMBER(S)

NONE

9b. OTHER REPORT NO(S) (Any other numbers that may be assigned this report)

NONE

10. DISTRIBUTION STATEMENT

Approved for public release; distribution unlimited.

11. SUPPLEMENTARY NOTES

TECH, OTHER

12. SPONSORING MILITARY ACTIVITY

AFOSR-NE
1400 WILSON BLVD.
Arlington, Virginia 22209

13. ABSTRACT

Optical Properties of the Cd_3As_2 - Cd_3P_2 alloy system have been completed in the form of a thesis. - Appendix A. The convergence of sum rules as a test of the reliability of Kramers-Kronig analysis of optical data have been investigated. Auger and optical data have been obtained on some semiconductive alloys.

14.

KEY WORDS

LINK A

LINK B

LINK C

ROLE

WT

ROLE

WT

ROLE

WT

Reflectivity, Semiconductors, Alloys,

Kramers-Kronig, Synchrotron